

EXPERIMENTAL AND ANALYTICAL STUDY OF AXIAL TURBULENT
FLOWS IN AN INTERIOR SUBCHANNEL OF A BARE ROD BUNDLE

by

Pedro Carajilescov

M.E., Instituto Tecnologico de Aeronautica, Brazil, (1968)

M.S., Massachusetts Institute of Technology, U.S.A., (1972)

SUBMITTED IN PARTIAL FULFILLMENT OF THE
REQUIREMENTS FOR THE
DEGREE OF
DOCTOR OF PHILOSOPHY

at the

MASSACHUSETTS INSTITUTE OF TECHNOLOGY

March 1975

Signature of Author

Department of Nuclear Engineering

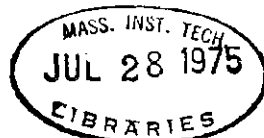
Certified by

Thesis Supervisor

Accepted by

Chairman, Department Committee on
Graduate Students

ARCHIVES



Title of Thesis: Experimental and Analytical Study of Axial Turbulent Flows in an Interior Subchannel of a Bare Rod Bundle

Name of Author: Pedro Carajilescov

Submitted to the Department of Nuclear Engineering, March 1975, in partial fulfillment of the requirements for the Degree of Doctor of Philosophy.

ABSTRACT

Reactor fuel elements generally consist of rod bundles with the coolant flowing axially through the bundles in the space between the rods. Heat transfer calculations form an important part in the design of such elements, which can only be carried out if information of the velocity field is available. A one-equation statistical model of turbulence is applied to compute the detailed description of velocity field (axial and secondary flows), the wall shear stress distribution and the friction factor of steady, fully developed, turbulent flows with incompressible, temperature-independent fluid, flowing through triangular arrays of rods with different aspect ratios (P/D). Also experimental measurements of the distributions of the axial velocity, turbulence kinetic energy and Reynolds stresses were performed using a laser Doppler anemometer (LDA), operating in a "fringe" mode with forward scattering, in a simulated interior subchannel of a triangular rod array with $P/D=1.123$ and $L/D_H=77$. From the experimental results, a new mixing length distribution is proposed. Comparisons between the analytical results and the results of this experiment as well as other experimental data available in the literature are presented. The results are in good agreement.

Thesis Supervisor: Neil E. Todreas
Title: Associate Professor of Nuclear Engineering

Thesis Reader: Michael W. Golay
Title: Assistant Professor of Nuclear Engineering

To my daughter

Tatiana

ACKNOWLEDGEMENTS

The author wishes to express his gratitude to Dr. Neil E. Todreas for his encouragement and guidance throughout this work.

This research was conducted as part of the "Coolant Mixing in LMFBR Rod Bundles Project", contract AT(11-1)-224 sponsored by the AEC. The author gratefully acknowledges this support.

The author wishes to thank the FAPESP - Fundação de Amparo a Pesquisa do Estado de São Paulo, Brazil, for granting him a fellowship during the preparation of this work.

The author wishes to thank the ITA - Instituto Tecnológico de Aeronáutica, for granting him a leave of absence during which this work was performed.

The author is grateful to Mr. David Gwinn, Mr. Francis L. Woodworth and Mr. Albert T. Supple, Jr., members of the MIT Reactor staff, for the useful discussions during the design of the test section.

Thanks are also due to Mrs. Carmen S.G. Aranha, who drafted the figures and to Mrs. Shirley Okun and Mrs. Virginia O'Keefe, who performed most of the typing of this thesis.

The author wishes to express his sincere appreciation to his wife Terezinha, for her patience and encouragement during this research effort.

TABLE OF CONTENTS

SECTIONS	PAGE NO.
TITLE	1
ABSTRACT.	2
ACKNOWLEDGEMENTS	4
TABLE OF CONTENTS	5
LIST OF TABLES	10
LIST OF FIGURES	11
NOMENCLATURE	15
CHAPTER I INTRODUCTION	
1. Foreword	18
2. Theoretical Background Information	19
3. Summary of Present Work	22
REFERENCES	25
CHAPTER II REVIEW OF LITERATURE	
1. Introduction	26
2. Analytical Methods Applied to Rod Bundles.	28
2.a Deissler and Taylor Method	28
2.b Bender, Switick and Field Method	29
2.c Method of Ibragimov and Co-workers	30
2.d Eifler and Nijsing Method	33
2.e Buleev's Model	36
3. Statistical Turbulence Models	38
3.a One-equation Models	38
3.b Two-equation Models	40
3.c Many-equation Models	41

4. Experimental Measurements Performed in Rod Bundles	44
CHAPTER III DESCRIPTION OF ANALYTICAL MODEL	
1. General Consideration	55
2. Detailed Description of Model	60
3. Boundary Conditions	65
a. Boundaries I and II	66
b. Boundary II	66
c. Boundary IV	69
c.1 Wall Functions for Axial Velocity and Turbulence Kinetic Energy . .	69
c.2 Vorticity Boundary Conditions at Wall	72
4. Source Term for Axial Momentum Equation .	75
5. Constants of the Model	77
6. Summary of Equations of the Model	80
References	85
CHAPTER IV NUMERICAL PROCEDURE	
1. Convection Terms	89
2. Diffusion Terms	94
3. Complete Finite Difference Equation . . .	96
4. Source Terms for Transport Equations . . .	98
4.1 Source Term of the Axial Momentum Equation	98
4.2 Vorticity Equation Source Term . . .	99
4.3 Stream Function Source Term	101
4.4 Source Term for TKE Equation	102
5. Grid for Numerical Procedure	104
6. Boundary Conditions	106
7. Iterative Method	111
8. Convergence Criterion	112

	Page No.
9. Initial Conditions for Parameters	113
References	117
 CHAPTER V DESIGN OF EXPERIMENTAL APPARATUS	
1. Introduction	118
2. Experimental Apparatus	118
2.1 Test Section	118
2.2 Hydraulic Loop	122
2.3 The Laser Doppler Anemometer (LDA)	122
2.3.1 Optics	122
2.3.2 Traverse Mechanism	126
2.3.3 Signal Processing Electronics.	126
3. Mesh Grid Used in Measurements	129
4. Measured Parameters	129
4.1 Axial Velocity	130
4.2 Turbulence Kinetic Energy	130
4.3 Reynolds Stresses $\overline{v'_r v'_z}$ and $\overline{v'_\theta v'_z}$	130
4.4 Pressure Drop Around Windows	133
5. General Aspects of Error Analysis	134
5.1 Flow Fluctuations	134
5.2 Electronics Error	134
5.2.1 Uncertainty in the Analog Voltage Readout	135
5.2.2 Uncertainty in the RMS Voltage	135
5.3 Finite Integration Time	136
6. Expression for Error Analyses	138
6.1 Axial Velocity	138
6.2 Turbulence Kinetic Energy	138
6.3 Cross Correlations $\overline{v'_r v'_z}$ and $\overline{v'_\theta v'_z}$	139
References	152

CHAPTER VI DISCUSSION OF RESULTS

1.	Introduction	153
2.	Experimental Data Obtained in the Present Work	156
3.	Error Analysis	158
3.1	Axial Velocity Distribution	158
3.2	Turbulence Kinetic <u>Energy</u>	159
3.3	Cross Correlations $v'_r v'_z$ and $v'_\theta v'_z$	160
4.	Secondary Flow Search	161
5.	Determination of Mixing Length and Constants of the Model	161
6.	Comparison of Experimental and Analytical Results	163
6.1	First Case: $\frac{P}{D} = 1.123$	164
6.2	Second Case: $\frac{P}{D} = 1.217$	165
7.	Applications of the Theory	167
7.1	Wall Shear Stress Distribution	167
7.2	Friction Factor	167
7.3	Effect of Reynolds Number	168
7.4	Prediction of Eddy Diffusivities	168
8.	Final Note	169
	References	203

CHAPTER VII CONCLUSIONS AND RECOMMENDATIONS FOR FUTURE WORK

1.	Conclusions	205
2.	Recommendations for Future Work	206
3.	Concluding Remarks	208

APPENDICES

A.	Transport Equations for Computation of Velocity Field	210
B.	Transport Equation for the Turbulence Kinetic Energy (TKE)	218

	Page No.
C. Analytical Approach for Vorticity Source Term Based on the Algebraic Stress Model	225
D. Numerical Procedure to Compute Mixing Length Using Buleev's Equation	238
E. Comment on the Turbulent Intensity Correlations as Proposed by Bobkov and Co-workers	244
F. Laser Doppler Anemometer Theory	247
G. Effect of Different Refractive Indices on the Crossing Point of the Two Beams	266
H. Preliminary Test of Test Section	275
I. Tabulation of Experimental Data	286
J. Description and Listing of Computer Code "HYBBAC"	290
References for Appendices	331
Biographical Note	333

LIST OF TABLES

	Page No.
II.1. Summary Table of Measurements in Rod Bundles	47
IV.1. Parameters ϕ , a_ϕ , b_ϕ and S_ϕ for the Differential Equations	88
V.1. Selected and Actual Parameters of Test Section	120
V.2. Design Elements of the LDA	124
VI.1. Operational Conditions for Measurements Performed in Rod Bundle with $P/D=1.123$.	155
VI.2. Order of Magnitude of Turbulent Intensities and Errors	160
VI.3. Comparison of Present Values of Constants with Values in the Literature	170
I.1. Pressure Drop Measurements	286
I.2. Measured Distribution of Parameters	287

LIST OF FIGURES

	Page No.
I.1. Fuel Bundle Geometry with Triangular Array of Rods	24
II.1. Procedure for Calculation of Velocity Distribution by Deissler and Taylor Method	48
II.2. Schematic Representation of Secondary Flow Pattern Proposed by Eifler and Nijsing	48
II.3. Cross-Section of Test Section Used by Eifler and Nijsing for Velocity Field Measurements	49
II.4. Cross-Section of Test Section Used by Kjellstrom	49
II.5. Cross-Section of Test Section Used by Trupp and Azad	50
IV.1. Finite-Difference Grid	115
IV.2. Points Near East Boundary of Subchannel	115
IV.3. Grid for Numerical Procedure	116
V.1. Cross-Section Shape of Test Section	140
V.2. Variation of the Half-Gap Size with Rod Diameter for Different Values of P/D	141
V.3. Variation of Length of Test Section for $100 D_H$ with Rod Diameter for Different Values of P/D.	142
V.4. Cross-Section View of Test Section	143
V.5. Test Section: Overall View	144
V.6. Design of Test Section Windows	145
V.7. The Hydraulic Loop	146
V.8. Laser Doppler Anemometer Set-up	147
V.9. Sequential Method for Cross-Correlation Measurements	148
V.10. Experimental Set-up	149
V.11. Signal Processing Electronics	150
V.12. Mesh Grid for Experimental Measurements	151
VI.1.(a,b,c). Comparison of Experimental Results for Axial Velocity	171

VI.2.(a,b).	Isovel Plot for $\frac{L}{D_H} = 77$ and	
	$\frac{P}{D} = 1.123$	174
VI.3.	Lines of Constant $\frac{K}{2} \times 10^3$ for $Re = 2.7 \times 10^4$ and $\frac{P}{D} = 1.123$	176
VI.4.	Distribution of $-\left[\frac{v'_r v'_z}{\bar{v}_r^2} \right]$	177
VI.5.	Distribution of $-\left[\frac{v'_\theta v'_z}{\bar{v}_\tau^2} \right]$	178
VI.6.	Mixing Length Distribution	179
VI.7.	The TKE Distribution	180
VI.8.	Effect of the Value of C_D in the TKE Distribution	181
VI.9.(a,b,c)	Comparison Between Experimental and Analytical Axial Velocity Distributions	182
VI.10.(a,b,c).	Comparison Between Experimental and Analytical TKE Distributions	185
VI.11.	Predicted Normalized Streamlines $\left(\frac{\psi}{\psi_{\max}} \right)$ for $\frac{P}{D} = 1.123$ and $Re = 2.7 \times 10^4$	188
VI.12.(a,b,c).	Comparison Between Experimental and Analytical Axial Velocity Distributions	189
VI.13.(a,b,c).	Comparison Between Experimental and Analytical TKE Distributions	192
VI.14.	Predicted Normalized Streamlines $\left(\frac{\psi}{\psi_{\max}} \right)$ for $\frac{P}{D} = 1.217$ and $Re = 1.49 \times 10^5$	195
VI.15.	Comparison of Predicted Secondary Flow with Experimental Data for $\frac{P}{D} = 1.217$	196
VI.16.	Wall Shear Stress Distribution	197
VI.17.	Wall Shear Stress Distribution	198
VI.18.	Friction Factor vs Re	199

	Page No.
VI.19. Predicted Normalized Streamlines ($\frac{\psi}{\psi_{\max}}$) for $\frac{P}{D} = 1.123$ and $Re = 2 \times 10^5$	200
VI.20. Effect of Reynolds Number on Secondary Flow Distribution ($\frac{P}{D} = 1.123$)	201
VI.21. Effect of Reynolds Number on the Wall Shear Stress Distribution	202
VI.22. Radial Eddy Diffusivity Distribution for $\frac{P}{D} = 1.123$ and $Re = 2.7 \times 10^4$	202
D.1. Computational Procedure of Buleev's Mixing Length	242
D.2. "Shadow" of Rod 1 over Rod 3 Relative to Point P	243
F.1. Basic LDA Set-ups	263
F.2. Enlarged View of Probe Volume	264
F.3. Light Intensity Radial Distribution in the Probe Volume	265
F.4. Typical Time and Frequency Signals Generated by Particles Crossing Probe Volume	265
G.1. Laser Beam Path Through Mediums with Different Refractive Indices when Focused by an Integrated Optical Unit Lens	273
G.2. Determination of Measuring Region Based on Crossing Point at Beam Waists	274
H.1. Test Section Symmetry Test	277
H.2. Symmetry Test of Test Section: line A_1	278
H.3. Symmetry Test of Test Section: lines A_2 and A_3	279
H.4. Symmetry Test of Test Section: lines A_4 and A_5	280
H.5. Symmetry Test of Test Section: line B_1	281
H.6. Symmetry Test of Test Section: lines B_2 and B_3	282

	Page No.
H.7. Isovel Plot for $\frac{L}{D_H} = 15$ and $\frac{P}{D} = 1.123$. . .	283
H.8. Isovel Plot for $\frac{L}{D_H} = 46$ and $\frac{P}{D} = 1.123$. . .	284
H.9. Developing Region Test	285
J.1. Block Diagram of Main Program	293
J.2. Block Diagram of Subroutine Core	294

NOMENCLATURE

1. Fluid Flow Parameters

A_t	subchannel area;
c_1	constant in pressure-velocity gradient correlation;
c_2	constant in main rate of strain-turbulence correlation;
C_D	constant in the dissipation rate of TKE;
C_v	constant in turbulent viscosity;
D	rod diameter;
D_H	hydraulic diameter of subchannel;
E	constant in "law of the wall";
f	friction factor;
K	turbulence kinetic energy;
l	mixing length;
L	length of test section from inlet to measuring station;
m	mass flow rate;
p	instantaneous pressure;
\bar{p}	timeaveraged pressure;
p'	fluctuating component of pressure;
P	pitch of rod array;
P_w	wetted perimeter of subchannel;
r	radial coordinate;
R	rod radius;
Re	Reynolds number;
v_b	bulk velocity of the flow;
v_i	instantaneous velocity component in the direction i , where i is (a) cylindrical coordinates: r , θ or z (b) cartesian coordinates: x , y or z ;

\bar{v}_i	time averaged velocity component in the direction i ;
v_i'	fluctuating component of velocity in the direction i ;
v^+	normalized axial velocity ($\equiv \frac{\bar{v}_z}{v_\tau}$);
v_τ	local friction velocity ($\equiv \sqrt{\tau_\omega/\rho}$);
\bar{v}_τ	average friction velocity ($\equiv \sqrt{\bar{\tau}_\omega/\rho}$);
x	cartesian coordinate in plane of cross section;
y	distance from rod wall to point of interest in the radial direction; also, cartesian coordinate in plane of cross section;
\hat{y}	distance from rod wall to MVL;
y^+	non-dimensional distance from wall ($\equiv \hat{y} v_\tau / \nu$);
z	axial direction of flow (cartesian or cylindrical coordinate);
Δ_ω	$\equiv (v_\theta'^2 - v_r'^2)$;
ϵ	dissipation rate of turbulence kinetic energy;
$\epsilon_{m,r}$	radial eddy diffusivity of momentum;
$\epsilon_{m,\theta}$	tangential eddy diffusivity of momentum;
ψ	stream function;
κ	constant in "law of the wall";
ν	kinematic viscosity;
ν_T	turbulent viscosity;
ρ	fluid density;
θ	angular coordinate;
τ_ω	wall shear stress;
$\bar{\tau}_\omega$	average wall shear stress;
ω	vorticity.

2. Laser Doppler Anemometer Parameters

a	distance from beams to optical axis;
b_o	beam radius at waist;
d_f	distance between two consecutive fringes in probe volume;
D_o	beam diameter at laser exit;
D_{ph}	pin hole diameter in front of photomultiplier tube;
f_L	focal length of lens;
h_v	probe volume height;
l_v	probe volume length;
N_f	number of fringes within probe volume;
n_o	air refractive index;
n_p	plexiglas refractive index;
n_w	water refractive index;
x_o	distance from inside surface of window wall to focal point of lens;
x_M	distance from inside surface of window wall to probe volume;
t	plexiglas wall thickness;
w_v	probe volume width;
β	half-angle between beams in water;
λ_i	laser beam wavelength;
ν_D	Doppler frequency shift;
θ	half-angle between beams in air.

CHAPTER I

INTRODUCTION

1. FOREWORD

Nuclear reactor fuel elements generally consist of rod bundles, in which each rod represents fissile material clad by a suitable casing. In the space between the rods, the coolant flows axially through the bundle.

Present methods of thermal design of such fuel elements are lumped parameter methods which deal only with subchannel flow and enthalpy averages. However, in many cases, the surface temperature of the fuel rods limits the thermal power that can be generated by the reactor. Such temperatures can only be calculated by present methods if heat transfer coefficients are provided as input. Also exchange coefficients for mixing, diffusion and convection processes are essential for lumped parameter calculations. To date, all information required by those methods is obtained through expensive experimental measurements. However, principally because of the existence of fuel element spacers, lumped parameter techniques are presently the only practical means of analysis. Nevertheless the study of distributed parameter methods can lead to insight of the functional dependence of the required input parameters on geometric and

operating conditions and in some cases to reliable prediction of the required information. Eventually, when more understanding about the exchange processes is obtained, distributed parameter methods may be used in place of lumped parameter methods in the thermal design of reactors.

2. THEORETICAL BACKGROUND INFORMATION

The fundamental equations, for the computation of the velocity field in any geometry, are the Navier-Stokes and continuity equations. For a steady, fully developed, turbulent flow with incompressible, temperature-independent property fluid and neglecting body forces, these equations can be reduced to the axial momentum, vorticity and stream function equations, as shown in appendix A. In cylindrical coordinates, with the main flow in the axial direction, they are:

(a) Axial momentum equation:

$$\frac{1}{r} \frac{\partial}{\partial r} \left(r \bar{v}_z \frac{\partial \psi}{\partial \theta} \right) - \frac{\partial}{\partial \theta} \left(\bar{v}_z \frac{\partial \psi}{\partial r} \right) - \frac{1}{r} \frac{\partial}{\partial r} \left(r \frac{\partial \bar{v}_z}{\partial r} - \frac{\overline{v'_r v'_z}}{\nu} \right) - \frac{\partial}{\partial \theta} \left(\frac{\partial \bar{v}_z}{\partial \theta} - \frac{\overline{v'_\theta v'_z}}{\nu} \right) = - \frac{1}{\rho \nu} \frac{\partial \bar{p}}{\partial z} ; \quad (I.1)$$

(b) Vorticity equation:

$$\begin{aligned} & \frac{1}{r} \frac{\partial}{\partial r} r \omega \left(\frac{\partial \psi}{r \partial \theta} \right) - \frac{\partial}{r \partial \theta} \omega \left(\frac{\partial \psi}{\partial r} \right) - \frac{1}{r} \frac{\partial}{\partial r} r \left(\frac{\partial \omega}{\partial r} \right) - \frac{\partial}{r \partial \theta} \left(\frac{\partial \omega}{r \partial \theta} \right) = \\ & - \frac{1}{\nu r} \left\{ \frac{\partial}{\partial \theta} \left[\frac{1}{r} \frac{\partial}{\partial r} r (\overline{v'_\theta{}^2} - \overline{v'_r{}^2}) \right] - \left[\frac{\partial}{\partial r} \frac{1}{r} \frac{\partial}{\partial r} r - \frac{\partial^2}{r^2 \partial \theta^2} \right] (r \overline{v'_r v'_\theta}) \right\} \quad (I.2) \end{aligned}$$

(c) Stream function equation:

$$- \frac{1}{r} \frac{\partial}{\partial r} r \left(\frac{\partial \psi}{\partial r} \right) - \frac{\partial}{r \partial \theta} \left(\frac{\partial \psi}{r \partial \theta} \right) = \frac{\omega}{\nu} \quad (I.3)$$

with vorticity defined as

$$\omega \equiv \frac{1}{r} \frac{\partial}{\partial r} r \overline{v_\theta} - \frac{\partial \overline{v_r}}{r \partial \theta} \quad (I.4)$$

and the stream function, as given by the expressions:

$$\overline{v_\theta} \equiv - \nu \frac{\partial \psi}{\partial r} \quad (I.5.a)$$

$$\overline{v_r} \equiv \nu \frac{\partial \psi}{r \partial \theta} \quad (I.5.b)$$

and $\frac{\overline{p}}{z} = \text{constant}$.

Equation (I.4) includes only velocities and gradients in the radial and angular directions. Thus the vorticity can only exist when they are not zero. So, the vorticity is directly connected with the existence of secondary flow in the channel. Take equation (I.2). The first two terms on the left represent convection of vorticity by the secondary flow. This process tends to make the

vorticity constant along the secondary flow streamlines. The last two terms on the left represent diffusion of vorticity by viscosity and tend to make the vorticity uniform over the duct cross-section by diffusing it from high intensity to low intensity regions. In a laminar flow, these are the only processes present, since the Reynolds stresses, on the right hand side of eq. (I.2) do not exist. So, in a straight duct in laminar flow, no generation of vorticity takes place and the existence of secondary flow is not possible, as pointed out in ref. 1. In a turbulent flow, in a straight axisymmetrical channel, the term $\overline{v'_r v'_\theta}$ is zero because an instantaneous value of $v'_r v'_\theta$ is equally probable in time as its negative, $-v'_r v'_\theta$, both cancelling each other out when the term is integrated over a long period of time. The first term on the right hand side of equation (I.2) is also zero because angular gradients of all parameters in the flow are zero. In this case, therefore, no generation of vorticity takes place and no secondary flow existence is possible. Such axisymmetry, however, does not exist in flows parallel to rod bundles (Fig. I.1). In this geometry the effect of the vorticity generation terms is expected to increase as the aspect ratio, P/D , approaches 1.

With this last consideration, it is shown that no complete description of the velocity field (axial and

secondary flows) can be obtained that does not involve either the solution of equations (I,1-3) or any other equivalent form. The accomplishment of this goal, however, is not a simple task since it requires information about the Reynolds stresses which is not available in analytical grounds. So, the engineer has to make assumptions about their behavior, usually, based on experimental observation. In many cases this assumption can be to disregard terms that he senses do not have any appreciable contribution to the velocity field being sought.

A review of the different approaches that have been used throughout the years for rod bundle geometries is presented and discussed in chapter II. Additionally discussed are more recent turbulence models which, although, they have not been applied to rod bundles, look very promising for a larger variety of applications.

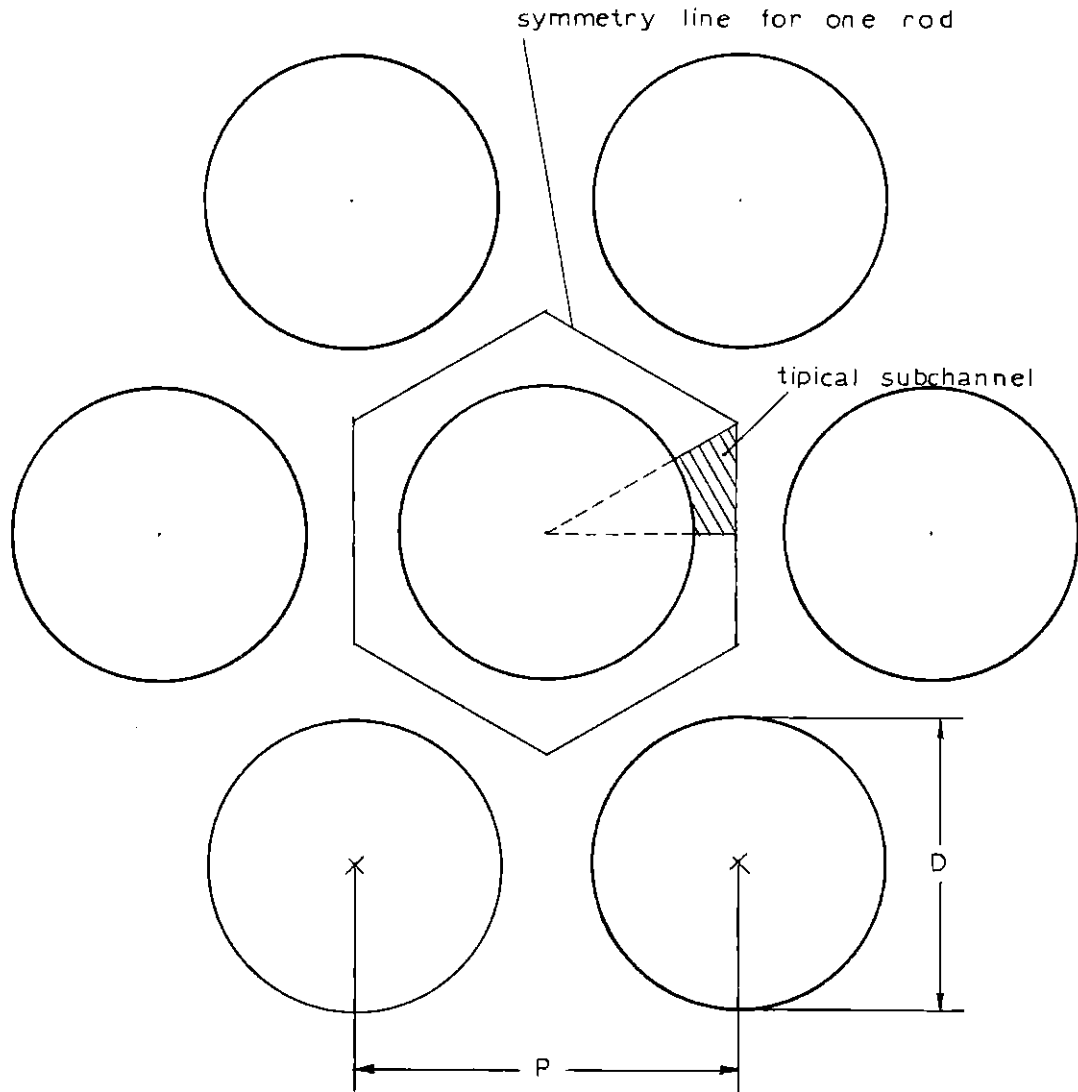
3. SUMMARY OF PRESENT WORK

In the present work, the hydrodynamic structure of the flow in a typical channel of a rod bundle with triangular array (see Fig. I.1) is examined analytical and experimentally. The simplified One-equation Statistical Stress Model for turbulent flows, used by Launder and Ying⁽²⁾ for square duct geometries, is modified for rod bundle applications. A new

mixing length distribution based on analysis of experimental data, obtained in this work, is used instead of the distribution suggested by Buleev⁽³⁾.

In the experimental task, a Laser Doppler Anemometer (LDA) was set up for measurements of the hydrodynamic parameters (axial velocity, turbulence kinetic energy and Reynolds stresses) of a flow of water within a test section designed to simulate a typical interior channel of a triangular cluster of rods with aspect ratio P/D equal to 1.123 and L/D_H equal to 77. The test section was designed to reduce to a negligible level the refractions of the laser beams on curved surfaces. A closed loop was used to circulate the water. The experimental results were, then, analysed to produce the constants needed to complete and optimize the analytical model.

Finally, the analytical and experimental results were compared to those obtained by other methods currently available.



$$\frac{P}{D} = \text{Aspect Ratio}$$

Fig. I.1. Fuel Bundle Geometry with Triangular Array of Rods

REFERENCES

1. Brundrett, E. and Baines, W.D., The Production and Diffusion of Vorticity in Duct Flow, J.Fluid Mech., Vol. 19,(1964).
2. Launder, B.E. and Ying, W.M., Prediction of Flow and Heat Transfer in Ducts of Square Cross-Section, The Institution of Mechanical Engineers, Proceedings 1973, Vol. 187 37/73, pp.455-461.
3. Buleev, N.I., Theoretical Model of the Mechanism of Turbulent Exchange in Fluid Flow, AERE Trans. 957, (1963).

CHAPTER II

REVIEW OF LITERATURE

1. Introduction

The solution of equations (I.1-3) for flows in any geometry requires information about the Reynolds stress tensor. It has become usual to classify the various different approaches designed to provide such information into three categories:

a. The phenomenological turbulence models.

A turbulence model is assumed to explain the behavior of turbulent eddies and how turbulent shear stresses are created. An example of this group is the mixing-length theory proposed by Prandtl, in 1925, in analogy with the kinetic theory of gases. Schlichting⁽²⁾ describes in detail this model. More recently, Buleev⁽¹⁾ proposed a model assuming two mechanisms of momentum exchange of the eddies with the medium: first, momentum exchange by molecular mechanisms and second, the disintegration of part of large eddies into small ones by the effect of surface friction forces.

b. The eddy diffusivity methods.

Here, the turbulent shear stresses are related to

a velocity gradient by a coefficient defined as the "eddy diffusivity" of momentum, i.e.

$$\overline{v'_z v'_r} = -\epsilon_{mr} \frac{\partial \bar{v}_z}{\partial r} \quad . \quad (\text{II.1})$$

Many expressions have been proposed for the variation of ϵ_{mr} over the cross section of the flow channel. Such expressions can be derived on theoretical grounds or they can be calculated from either measurements of velocity distribution, using equation (I.1) and (II.1) or from measurements of the cross correlation $\overline{v'_z v'_r}$ and the velocity distribution, utilizing equation (II.1) directly.

c. The statistical turbulence models.

This group of models assumes that the turbulent fluctuations are random in nature and that a few of the statistical properties of turbulence are supposed to obey laws of generation, dissipation and transport. For the prediction of the velocity field utilizing one of these models, the fundamental equations (I.1-3), a set of differential transport equations that describes the behavior of the statistical properties, and associated algebraic equations that provide closure to the model have to be solved altogether.

Another way of classifying the different methods that is becoming usual lately is by the number of additional differential transport equations necessary to solve the basic equations. So, in this classification, the phenomenological and eddy diffusivity approaches would be roughly classified as zero-equation turbulence models and the different statistical turbulence models would be one-, two-, or many-equation turbulence models, depending on the number of turbulence properties whose behavior is assumed to obey differential transport equations.

Until now, all methods applied to rod bundle geometries have been of the phenomenological and eddy diffusivity types. Even more empirical methods have been suggested throughout the years. Some of them are reviewed briefly in the next section.

2. Analytical Methods Applied to Rod Bundles

2.a. Deissler and Taylor Method⁽³⁾

This seems to be the pioneer work, for rod bundle geometries and represents an empirical approach to the problem. The first step is to draw assumed velocity gradient lines using best judgment (Fig. II.1). These are lines with normal velocity gradients equal

to zero. The universal velocity profile, obtained by circular tubes, is assumed to be obeyed along those lines. With such a velocity distribution, new velocity gradient lines are drawn and the procedure is repeated, iteratively.

The tedious graphic-iterative procedure, the assumption of analogy to circular tube velocity distribution, the impossibility of accounting for secondary flow effects and the difficulty of adapting this method for computer calculation are some of the drawbacks of this method.

2.b Bender, Switick and Field Method^(4,5)

This method represents an application of the mixing length theory proposed by Prandtl to rod bundles. Secondary flows are neglected. The Reynolds shear stresses are written in the form

$$\overline{v_r v_z} = -\epsilon_{m,r} \frac{\partial \bar{v}_z}{\partial r} \quad (\text{II.2})$$

and

$$\overline{v_\theta v_z} = -\epsilon_{m,\theta} \frac{\partial \bar{v}_z}{r \partial \theta} \quad , \quad (\text{II.3})$$

where the coefficients $\epsilon_{m,r}$ and $\epsilon_{m,\theta}$, called radial and tangential eddy diffusivities of momentum, respectively, are given by

$$\epsilon_{m,r} = c \ell_c^2 \left| \frac{\partial \bar{v}_z}{\partial r} \right| \quad (\text{II.4})$$

and

$$\epsilon_{m,\theta} = c \ell_c^2 \left| \frac{\partial \bar{v}_z}{r \partial \theta} \right| \quad (\text{II.5})$$

In these equations, ℓ_c is the turbulent characteristic mixing length, assumed given by Buleev's formula (see Appendix D), and c is a constant.

Among the criticisms of this method, are the fact that the eddy diffusivities are forced to zero, wherever the respective velocity gradients go to zero and the lack of inclusion of secondary flows. Also the resulting variations of the wall shear stress distribution are unrealistically high.

2.c. Method of Ibragimov and Co-workers⁽⁷⁾

Since the total transfer of momentum is due to two processes (see, for example, Ref. 8, pp. 288): a gradient (or diffusion) transfer of momentum due to molecular friction and small-scale turbulent eddies, and a convective (or secondary flow) transfer of momentum due to the large scale motion of eddies. Ibragimov and co-workers suggested that convective transport of momentum should become important for channels with sharply varying

cross-sectional shapes where exchange between eddies of considerably different velocities may occur. For those cases, neglect of the convective transfer may lead to considerable errors. Based on these presumptions they concluded that the effect of the large eddies will be most important circumferentially along the perimeter, in the direction in which the velocity varies slowly. Normal to the channel walls, such effects can be neglected because the velocity gradient and the diffusive transfer are high.

This reasoning led them to propose a semi-empirical relation for the wall shear stress distribution, determined only by geometric parameters of the channel, that, for a rod bundle subchannel, can be written as

$$\frac{\tau_w(\theta)}{\bar{\tau}_w} = c \left[1 - \exp \left[-\frac{7.7}{\phi^{0.8}} \cdot \frac{\hat{y}(\theta)}{y_{av}} \right] \right], \quad (\text{II.6})$$

where

$$\phi = \frac{A_c}{\bar{y}_{av}^2}$$

A_c = subchannel flow area;

$\hat{y}(\theta)$ = distance from wall to maximum velocity line along normal;

\hat{y}_{av} = average value of $\hat{y}(\theta)$;

and c is a normalization constant given by

$$\frac{1}{\theta_{\max}} \int_0^{\theta_{\max}} \frac{\tau_w(\theta)}{\bar{\tau}_w} d\theta = 1 \quad . \quad (\text{II.7})$$

With this wall shear stress distribution and the friction factor given by the Blasius formula for circular tubes

$$f_c = \frac{0.0791}{\text{Re}^{0.25}} \quad , \quad (\text{II.8})$$

the universal velocity distribution was assumed to hold normal to the channel walls. In their next paper⁽⁹⁾, they suggested an expression for the ratio between the friction factor for the specific geometry being analysed and that for circular tube, i.e.,

$$\frac{f}{f_c} = [0.58 + 0.42 \exp(-0.021 K_e^3)] \left[1 + 0.1 \left(\frac{\hat{y}_{\text{av}}}{R_c} + 1 \right)^{4/3} \right] \quad , \quad (\text{II.9})$$

where

$$K_e = \phi^{0.25} \left(\frac{\hat{y}_{\max} - \hat{y}_{\min}}{\hat{y}_{\text{av}}} \right) \quad ,$$

$R_c \equiv$ radius of curvature of surface.

This method was proposed for any geometry and it was applied to rod bundles by Bender and Magee⁽⁶⁾ in the code VELVET-II, developed for computation of temperature field in rod bundles cooled by liquid metal coolant.

The generality of this method makes it very attractive but the method does not provide any information about the magnitude of the secondary flows that is desirable for turbulent heat transfer calculations. Also, the assumption of the universal velocity profile along lines normal to the wall is not valid for all cases. Finally the assumption that the wall shear stress distribution is only a function of geometric parameters and independent of the Reynolds number should not be expected on theoretical grounds since different turbulent parameters have different behavior with the Reynolds number.

2.d. Eifler and Nijsing Method⁽¹⁰⁾

These authors, initially, proposed a method⁽¹⁸⁾ to overcome the shortcoming of the Deissler and Taylor⁽³⁾ model which assumed that turbulent diffusion of momentum around the rod periphery is neglected. Later the effect of secondary flows was included as follows.

Based on the explanation proposed by Hinze⁽¹¹⁾ that secondary flows must transport turbulence-rich fluid away from regions where turbulence production exceeds dissipation, they observed that the lateral variation of wall shear stress must be considered the prime cause for the existence of secondary flow. Along with the experimental observation that the rate of fluid ejection away from the wall⁽¹²⁾ is directly related to the local wall shear stress, Eifler and Nijsing concluded that in the presence of a lateral wall shear stress gradient, this will induce a circular motion tending to transport high momentum fluid through the mainflow in the direction of decreasing wall shear stress. This reasoning led to the proposition of an expression for the secondary flow component v_θ as follows:

$$v_\theta = F \left[\sqrt{\frac{\tau_w}{\rho}}, \Delta\theta_e \right] \cdot F \left(\frac{\hat{y}}{\bar{y}} \right), \quad (\text{II.10})$$

where $\Delta\theta_e$ is the circumferential extent of the characteristic domain. This secondary flow can be represented as shown in Fig. II.2. The following shapes were suggested for the functions shown in eq. (II.10):

$$F \left[\sqrt{\frac{\tau_w}{\rho}}, \Delta\theta_e \right] = 2C_{\text{sec}} \sqrt{\frac{\tau_w}{\rho}} \cdot \frac{d \left(\frac{\tau_w}{\tau_w} \right)^{1/2}}{d\theta} \cdot \Delta\theta_e, \quad (\text{II.11})$$

$$F \left(\frac{y}{\hat{y}} \right) = \cos \left(\frac{y}{\hat{y}} \pi \right) \quad (\text{II.12})$$

where $C_{\text{sec}} = 0.6$.

For the eddy diffusivities, they used;

$$\epsilon_{m,\theta} = 0.154 \hat{y} \sqrt{\frac{\tau_w}{\rho}}, \quad (\text{II.13})$$

$$\epsilon_{m,r} = C_r \hat{y} \sqrt{\frac{\tau_w}{\rho}} \quad (\text{II.14})$$

where C_r , in this case is taken as a function of the aspect ratio $\left(\frac{P}{D}\right)$ and the Reynolds number.

Since no reliable secondary flow measurements have yet been obtained, for rod bundle geometries, the proposed shape of the peripheral velocity distribution is not based on experimental evidence. In fact, measurements of the wall shear stress distribution obtained by several workers (13,14,15,16) showed the maximum value of the wall shear stresses for $\frac{P}{D} \geq 1.2$ does not occur at the symmetry line of the subchannel connecting the center of the channel to the rod center ($\theta = 30^\circ$). This distribution of wall shear stress would induce secondary currents in disagreement with the description suggested by Eifler

and Nijsing. Furthermore, Rowe⁽¹⁷⁾, analysing the fluctuating velocity contours obtained for both triangular and square arrays with a laser Doppler anemometer, concluded that, in certain cases, the deformation of the isovels could only be explained by the presence of more than one loop of secondary flow in a subchannel.

2.e. Buleev's⁽¹⁹⁾ Model

The model proposed by Buleev is intended to describe the interaction of a turbulent eddy with the medium strictly from the phenomenological point of view. Two mechanisms of momentum exchange are assumed. The first mechanism states that the eddy exchanges momentum with the medium by molecular interaction. The second one considers that, due to the effect of surface friction forces, a portion of the eddy disintegrates into small eddies and is transferred to the surrounding medium. With these two hypotheses in mind and describing the probability that an eddy, starting at a certain point, will reach the point where the Reynolds stresses are being sought, Buleev was able to construct the tensor of turbulent stresses by integrating over all points that can contribute to the turbulent behavior of the fluid at the point in question. Buleev and his co-workers

applied this approach to several different geometries⁽²¹⁾
(22) such as rod bundles and rectangular ducts.

In order to match the experimental results available for rod bundles, Ramm and Johannsen⁽²⁰⁾ made several minor changes in the above method. Artificial boundaries were introduced to limit the flow area that contributes to the turbulent properties prevailing at a certain point. Anisotropy of the turbulence was introduced by taking different scales of turbulence for different directions. The momentum transfer in the circumferential direction was arbitrarily increased to examine the degree of compensation obtained for the lack of inclusion of secondary flows in the model.

Although having the attraction of attempting to explain the nature of the momentum exchanging mechanisms, this model lacks of experimental evidence of the proposed exchange mechanisms. Also, when the physical mechanisms are mathematically expressed, many assumption become necessary which certainly will affect the predicted results. The proof of the utility of the model will lie in its future comparison with experimental data. Here again the impossibility of predicting secondary flows is observed. The compensation of the secondary flows by increasing the tangential diffusional momentum transfer cannot be expected to produce accurate results in a detailed

velocity distribution, since momentum transfer by convection near the wall and near the maximum velocity line are expected to occur at opposite directions for continuity reasons.

3. STATISTICAL TURBULENCE MODELS

As mentioned before, these models attempt to describe certain turbulence parameters of the flow by laws of diffusion, convection, generation and dissipation. Transport equations are proposed for the parameters to be described according to such laws. The other necessary parameters are approximated by algebraic equations. These statistical methods are usually classified by the number of extra transport equations necessary to provide closure for the Reynolds equations. In the presentation that follows, these methods will not be reviewed in chronological order, but instead, by the number of equations, simplicity of approach and the relevance of the contribution.

3.a. One-equation models

In 1945, Prandtl suggested that the turbulent viscosity could be described by a relation involving the turbulent kinetic energy (K) and a length scale, ℓ , that is,

$$v_T = K^{1/2} \ell \quad (\text{II.15})$$

In this model, K is obtained by the solution of a transport equation, such as that presented in Appendix B, and the length scale l was to be proportional to the distance from the wall.

Launder and Ying⁽²³⁾ applied the above method to predict the secondary flow distribution in a square duct. For the normal and shear stresses involved in the vorticity equation source terms, algebraic equations were obtained from the transport equations for the second order moments, after a series of approximations. The results obtained were very encouraging when compared to the experimental results obtained by the same authors⁽²⁴⁾, that had been published previously.

Bradshaw and co-workers⁽²⁵⁾, studying a two-dimensional boundary layer development, converted the turbulent energy equation into a differential equation for the turbulent shear stress by defining three empirical functions relating the turbulent intensity, diffusion and dissipation to the shear stress profile. This approach eliminates the restriction imposed by the association of the shear stress to the velocity gradient that they should be zero at the same position. This method, however, as one-equation model can not be applied to three dimensional flows since transport equation for only one turbulent

shear stress is provided,

3.b. Two-equation models

All two-equation models use the definition of turbulent viscosity, eq. (II.15) as proposed by Kolmogorov and Prandtl separately. Of the two transport equations, one is used to describe the behavior of the turbulence kinetic energy, K , and the other one is for a quantity from which the length scale ℓ can be obtained. The different approaches differ with respect to the selection of this latter quantity and the procedure to obtain a transport equation for it.

The first two-equation model was proposed by Kolmogorov⁽²⁶⁾ in 1942. He proposed an equation for the mean frequency of turbulence, f , that is defined as

$$f \equiv \frac{\sqrt{K}}{\ell} \quad . \quad (II.16)$$

Harlow and Nakayama⁽²⁷⁾ constructed a transport equation for ℓ , on semi-empirical grounds. Three source terms were added. The first one represented a source term for non-steady flows. The second source term which would be the only term for a completely homogeneous flow, represented contribution to the growth of mean eddy size. Finally, the last term described the breakdown of eddy size in regions of shear. In a following paper⁽²⁸⁾, they derived

on rigorous grounds a transport equation, but this time for the turbulent energy decay rate, assumed to be equal to K/ℓ^2 .

Spalding⁽²⁹⁾ proposed a model that deals with the same parameter K/ℓ^2 but gave a different interpretation for it. It was assumed to be a characteristic turbulence parameter or vorticity decay parameter. The source terms of the equation were obtained by analogy to the source term of the turbulence kinetic energy equation.

Another two-equation statistical model was proposed by Jones and Launder⁽³¹⁾. This model involved a transport equation for the turbulent energy dissipation rate, following the line proposed by Harlow and Nakayama⁽²⁸⁾ including molecular viscosity effects on the turbulence when the turbulent Reynolds number is low.

3.c. Many-equation models

Several different approaches have been suggested to avoid, primarily, the concept of turbulent viscosity involved in the simpler models. The basic idea is to construct separate transport equations for second, third, etc. order correlations of the turbulent intensities.

In 1945, Chou⁽³⁰⁾ observed that double and triple correlation equations are necessary to describe a flow field when walls are present. Quadruple correlations

can be approximated by algebraic expressions. For free turbulence cases, only double correlations are required. Also, an extra equation for the vorticity decay is required. So, this procedure, in its most general form, would require 17 equations. Davydov^(32,33) also described a method involving transport equations for second and third moments of turbulent intensities and finally the turbulent energy dissipation. In a following paper⁽³⁴⁾, he argued the necessity of including equations for the "dissipation flow parameter C_1 ", defined as

$$C_1 \equiv \overline{v v'_1 \left[\frac{\partial v'_k}{\partial x_l} \right]^2} \quad . \quad (\text{II.17})$$

These methods just described are some of the most general methods proposed to date. Due to the complexity involved in the numerical solution of such a large number of equations and the proportionally high number of empirical constants involved which require estimation from experimental information, they have not been tested to date. Many uncertainties remain about the degree of improvement they would provide over some of the simpler models. However, to overcome some of the shortcomings associated with one- and two-equation models and while still not being as complicated as the models with equations for the second and third moments of the velocity fluctuations,

several models were proposed where only equations for the double correlations are present. This type of model has the potential for treating highly anisotropic flows or flows with low turbulent intensities, when diffusive effects significantly modify the transport of turbulent properties.

Hanjalić and Launder⁽³⁵⁾ developed a model involving approximate transport equations to the Reynolds stress tensor and for the turbulence energy dissipation rate, in a total of seven equations. For boundary-layer flows a simpler version is suggested involving only transport equations for the shear stress - $\overline{v_1' v_2'}$, the turbulence kinetic energy and the turbulence energy dissipation rate. Harlow and Hirt^(36,37) also developed a seven-equation model along the same lines as the previous one, but where the unknown correlations are approximated by expressions containing mean velocity gradients, Reynolds stresses and length scales. Gosse and co-workers⁽⁴²⁾ recently proposed a three-equation model where transport equations were derived for the turbulence kinetic energy and for two independent turbulence scales: one connected with the turbulent diffusion, and the other related to the viscous dissipation process.

The statistical turbulence models described are going

through a period of intensive tests in a wide range of applications. Summaries of details and applications can be found in references (38),(39),(40) and (41).

Until now, there is no general criterion to select the method that would yield best results for a certain flow. This is left to the designer to decide which method would combine accuracy with economy and simplicity for his specific case of interest.

4. EXPERIMENTAL MEASUREMENTS PERFORMED IN ROD BUNDLES

Published experimental data of distributed turbulent parameters such as axial velocity, turbulence kinetic energy, Reynolds stresses, are very limited.

Eifler and Nijsing^(43,44), using a Pitot tube, measured the velocity distribution of water flowing through a test section with a cross-section as shown in fig.II.3, for $\frac{P}{D} = 1.05, 1.10$ and 1.15 and Reynolds number in the range $(15-50) \times 10^3$. Eifler⁽⁴⁵⁾ extended the measurements for $\frac{P}{D} = 1.08$. Subbotin and co-workers⁽¹⁵⁾ also used the same type of cross section for their measurements of velocity field and wall shear stress distribution in air for $\frac{P}{D} = 1.05, 1.10$ and 1.20 with Reynolds number in the range $(18.8-81) \times 10^3$. They also utilized a Pitot tube for the velocity measurements. It was observed from the data of both investigations that the proximity of the

wall blocking the gap of the subchannel adjoining the subchannel where measurements were being performed in fact distorted the velocity distribution in a way that should not be expected by symmetry considerations. In his experiment, Kjellström⁽¹³⁾ tried to eliminate such perturbations by placing his subchannel being analysed (Fig.II.4) as far as possible of blocking walls. He used $\frac{P}{D} = 1.217$ and air flow. With the utilization of a Preston tube, wall shear stress distribution were measured for $Re = 2.74 \times 10^5$. He also measured, using a hot-wire anemometer, velocity distributions, turbulent intensity distributions in axial, tangential and radial directions, as well as the Reynolds stress $-\overline{v'_r v'_z}$ distribution, for a few angular directions. He also attempted to measure secondary flows but obtained only very scattered results. Hall and Svenningsson⁽¹⁴⁾ using the same experimental techniques and test section as Kjellström also attempted to measure secondary flows, with no better results. Rowe⁽¹⁷⁾ used a laser doppler anemometer to measure velocity distribution and turbulent intensities along a few specific lines of several different geometries, typical of rod clusters. However, the most complete experimental work on rod bundle hydrodynamics has been performed by Trupp and Azad⁽¹⁶⁾ using a hot wire anemometer. Pitch-to-diameter

ratios were 1.20, 1.35 and 1.50, and the Reynolds number was in the range $(12-84) \times 10^3$. Measurements were made of axial velocity, turbulent intensities, shear stress $-\overline{v_r v_z}$ as well as power spectra of the axial turbulence. Also wall shear stress distributions were obtained by a Preston tube. Measurements of the tangential shear stress $-\overline{v_\theta v_z}$ were very scattered so that no information could be obtained about the relative value of the peripheral eddy diffusivity $\epsilon_{m,\theta}$ compared to the radial eddy diffusivity $\epsilon_{m,r}$. The cross-section of the test section used by Trupp and Azad is shown in figure II.5. Table II.1 shows a summary of the measurements performed in rod bundles as discussed in this section.

TABLE II.1. SUMMARY TABLE OF MEASUREMENTS IN ROD BUNDLES

INVESTIGATOR	$\frac{P}{D}$ (#)	$\frac{L}{D_H}$	$Re \times 10^{-3}$	Velocity		Turb. Intensity			Cross-correlations		$\frac{\tau_w}{\bar{\tau}_w}$
				Axial	Second.	z	r	θ	$\overline{v'_r v'_z}$	$\overline{v'_\theta v'_z}$	
Eifler, Nijsing ^(43,44)	1.05	139	15, 30, 50	✓							
	1.10	90	15, 30, 50	✓							
	1.15	65	15, 30, 50	✓							
Eifler ⁽⁴⁵⁾	1.08	137	10-152	✓							
Subbotin et al ⁽¹⁵⁾	1.05	154	18.8-81	✓							✓
	1.10	100	18.8-81	✓							✓
	1.20	72	18.8-81	✓							✓
Kjellström ⁽¹³⁾	1.217	81	149-373	✓	✓	✓	✓	✓	✓		✓
Hall and Svenningsson ⁽¹⁴⁾	1.217	81	270		✓						✓
Trupp and Azad ⁽¹⁶⁾	1.20	51	12-84	✓		✓	✓	✓	✓	✓	✓
	1.35	30	12-84	✓		✓	✓	✓	✓	✓	✓
	1.50	20	12-84	✓		✓	✓	✓	✓	✓	✓
Rowe ⁽¹⁷⁾	1.25 ^(*)	85 ^(o)	50-200	✓		✓					
	1.11 ^(*)	117	50-200	✓		✓					
	1.25 ^(*)	90	50-200	✓		✓					
	1.25 ^(**)	105	50-200	✓		✓					
	1.25	138	50-200	✓		✓					
	1.25	122	50-200	✓		✓					

(#) All data for triangular array except where mentioned otherwise.

(*) Square array

(**) Square and triangular channels in same test section

(o) Based on cross section hydraulic diameter instead of subchannel's.

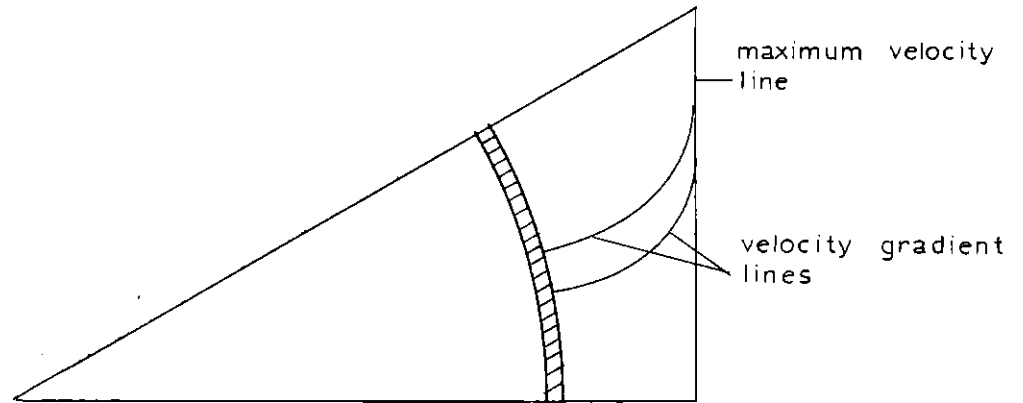


Fig. II.1. Procedure for Calculation of Velocity Distribution by Deissler and Taylor Method

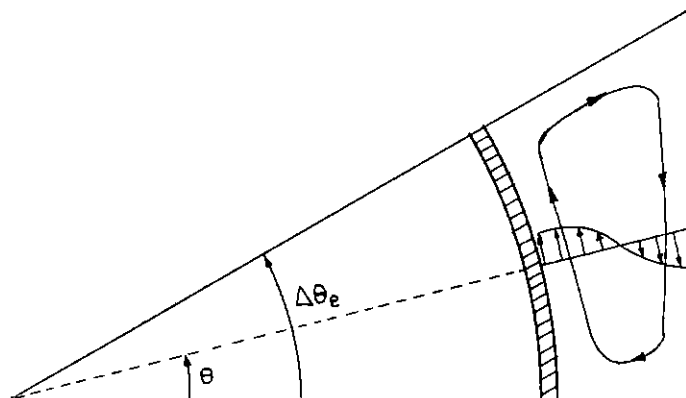


Fig. II.2. Schematic Representation of Secondary Flow Pattern proposed by Eifler and Nijssing

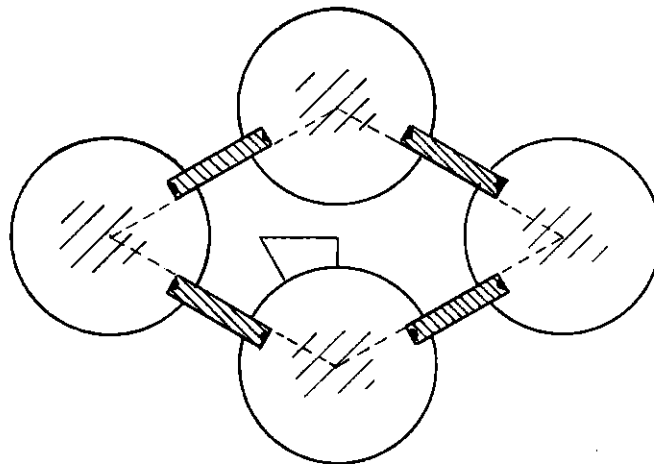


Fig. II.3. Cross-Section of Test Section used by Eifler and Nijssing for Velocity Field Measurements

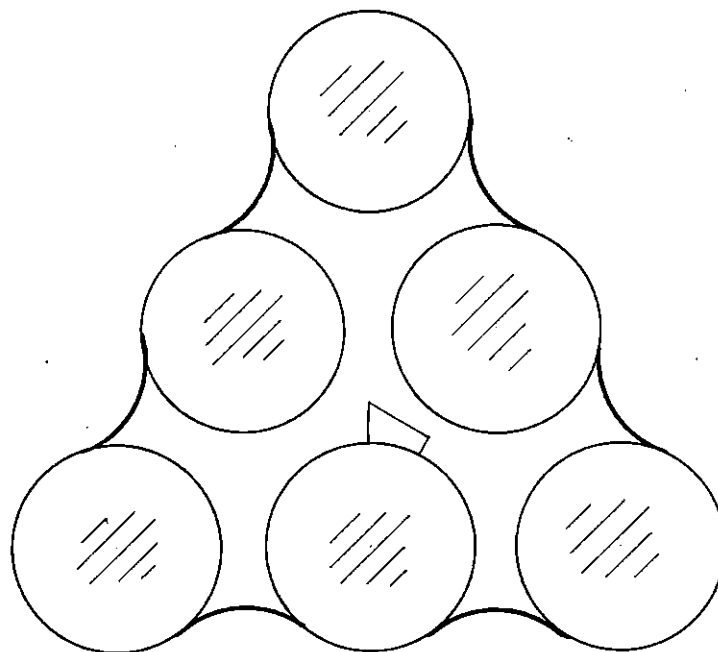


Fig. II.4. Cross-Section of Test Section used by Kjellström

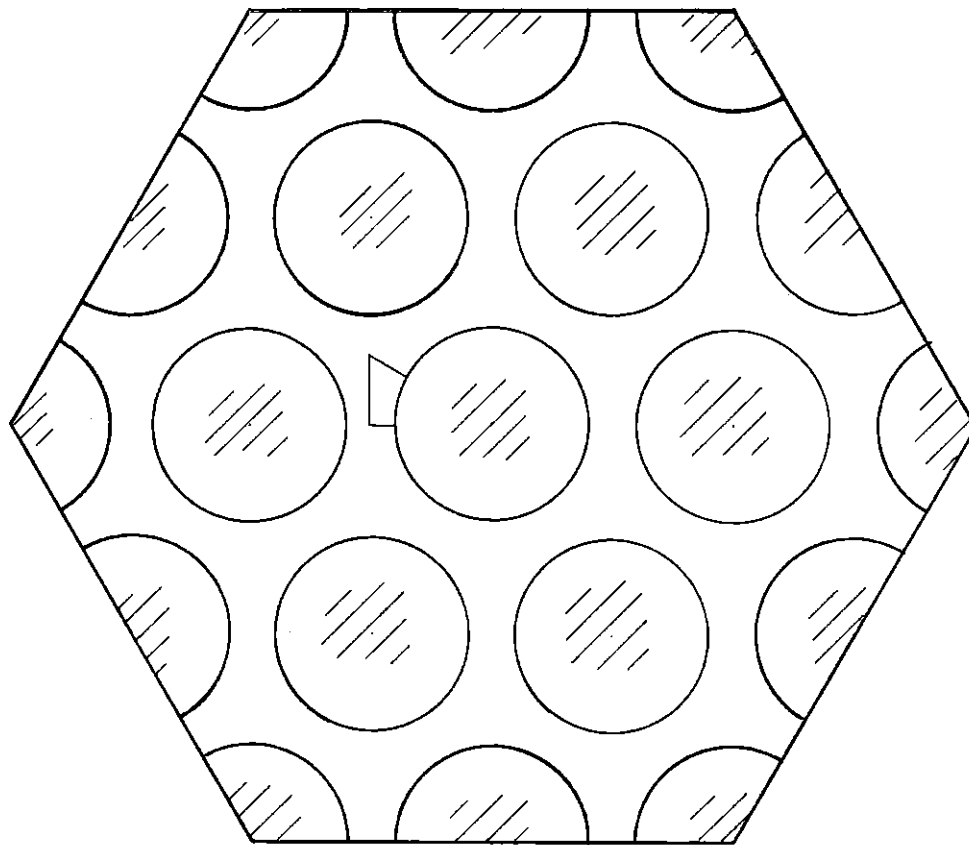


Fig. II.5. Cross-Section of Test Section used by Trupp and Azad

REFERENCES

1. Buleev, N.I., Theoretical Model for Turbulent Transfer in Three-Dimensional Fluid Flow, 3rd UN Intern. Conf. Peaceful Uses At. Energy, Geneva, (1964), paper No.329.
2. Schlichting, H., Boundary-Layer Theory, 6th ed., McGraw-Hill, (1968), Ch. XIX.
3. Deissler, G.R. and Taylor, M.F., "Analysis of Axial Turbulent Flow and Heat Transfer Through Banks of Rods or Tubes," Reactor Heat Transfer Conference of 1956, TID-7529 (pt.1), Vol. 2, Cleveland (issued in Nov.1957).
4. Bender, D.J., Switick, D.M. and Field, T.H., Turbulent Velocity Distribution in a Rod Bundle, GEAP-5411, (Oct. 1967).
5. Bender, D.J. and Switick, D.M., Turbulent Velocity Distribution in a Rod Bundle, ASME 68-WA/HT-36 (1969).
6. Bender, D.J. and Magee, P.M., Turbulent Heat Transfer in a Rod Bundle with Liquid Metal Coolant, GEAP-10052, (July 1969).
7. Ibragimov, M.Kh. et al., Calculation of the Tangential Stresses at the Wall of a Channel and the Velocity Distribution in a Turbulent Flow of Liquid, Soviet Atomic Energy, Vol. 21, No. 2, (Aug. 1966), pp.731-739.
8. Hinze, J.O., Turbulence, McGraw-Hill, (1959).
9. Ibragimov, M.Kh. et al., Calculation of Hydraulic Resistivity Coefficients for Turbulent Fluid Flow in Channels of Noncircular Cross Section, Soviet Atomic Energy, Vol. 23, No. 4, (Oct. 1967), pp. 1042-47.
10. Nijssing, R., Heat Exchange and Heat Exchanger with Liquid Metals, Agard-LS-57-72 (ed. by J.J. Ginoux), (1972).
11. Hinze, J.O., Secondary Currents in Wall Turbulence, The Phys. Fluids Supplement, (1967) p. S 122-125.
12. Kline, S.J., et al., The Structure of Turbulent Boundary Layer, J. Fluid Mechanics, 30 (1967), p.741-773.

13. Kjellström, B., Studies of Turbulent Flow Parallel to a Rod Bundle of Triangular Array, Report AE-RV-196 AB Atomenergi, Sweden (1971),
14. Hall, Ch. and Svenningsson, P.J., Secondary Flow Velocities in a Rod Bundle of Triangular Array, Report AE-RL-1326, AB Atomenergi, Sweden (1971).
15. Subbotin, V.I. et al., Velocity Field of Turbulent Fluid Flow in a Longitudinal Streamline of Clusters of Rods, AEC-tr-7189 (1971)
16. Trupp, A.C. and Azad, R.S., The Structure of Turbulent Flow in Triangular Array Rod Bundles, Dpt. of Mech. Eng., Univers. of Manitoba, Winnipeg, Canada (1973)
17. Rowe, D.S., Measurement of Turbulent Velocity Intensity and Scale in Rod Bundle Flow Channels, BNWL-1736, UC-80, Battelle, (May 1973).
18. Nijssing, R. et al., Analysis of Fluid Flow and Heat Transfer in a Triangular Array of Parallel Heat Generating Rods., Nucl. Eng. Design 4, (1966) pp. 375-398.
19. Buleev, N.I., Theoretical Model of the Mechanism of Turbulent Exchange in Fluid Flow, AERE Translation 957, 1963.
20. Ramm, H. and Johannsen, K., Hydrodynamics and Heat Transfer in Regular Arrays of Circular Tubes, 1972 International Seminar on Recent Developments in Heat Exchangers of the International Centre for Heat and Mass Transfer, Trogir, Yugoslavia, (Aug. 30-Sept. 6, 1972).
21. Buleev, N.I. et al., Turbulent Flows of a Liquid in Annular and Plane Channels, High Temperature, Vol. 5, (1967), pp. 566-573.
22. Buleev, N.I. and Biryukova, G.P., Calculation of the Velocity Field in Turbulent Flow of a Liquid in a Channel of Rectangular Cross Section, High Temperature, Vol. 5, (1967), pp. 753-760.
23. Launder, B.E. and Ying, W.M., Prediction of Flow and Heat Transfer in Ducts of Square Cross-Section, The Institution of Mech. Eng., Proceedings 1972, Vol. 187 37/73, pp. 455-461.

24. Launder, B.E. and Ying, W.M., Secondary Flows in Ducts of Square Cross Section, *J. Fluid Mech.* 54(1972),pp.289-29
25. Bradshaw, P., Ferriss, D.H. and Atwell, N.P., Calculation of Boundary-Layer Development Using the Turbulent Energy Equation *J. Fluid Mech.* 28, part 3, (1967),pp.593-616.
26. Kolmogorov, A.M., "Equations of Turbulent Motions of the Incompressible Turbulent Fluid," *Izv, Akad. Nauk. SSSR, Ser. Phys. VI, no. 1-2 (1942), p.56.*
27. Harlow, F.H. and Nakayama, P.I., Turbulence Transport Equations, *The Phys. of Fluids, Vol. 10, No. 11, (Nov. 1967).*
28. Harlow, F.H. and Nakayama, P.I., Transport of Turbulence Energy Decay Rate, Report LA-3854, (1968).
29. Spalding, D.B., A Two-equation Model of Turbulence, Report VDI-Forsch.-Heft 549 (1971)
30. Chou, P.Y., On Velocity Correlations and the Solutions of the Equations of Turbulent Fluctuations, *Quart. Appl. Math.* 3, 31 (1945), pp. 38-54.
31. Jones, W.P. and Launder, B.E., The Prediction of Laminarization with a Two-equation Model of Turbulence, *Int. J. Heat and Mass Transfer, Vol. 15, (1972) pp.301-314.*
32. Davydov, B.I., On the Statistical Dynamics of an Incompressible Turbulent Fluid, *Soviet Physics-Doklady, Vol. 4, (1960) pp. 769-772.*
33. Davydov, B.I., On the Statistical Theory of Turbulence, *Soviet Physics-Doklady, Vol. 4, (1960) pp. 779-781.*
34. Davydov, B.I., On Statistical Dynamics of an Incompressible Turbulent Fluid, *Soviet Physics-Doklady, Vol. 6 (1961), pp. 10-12.*
35. Hanjalić, K. and Launder, B.E., A Reynolds Stress Model of Turbulence and its Application to Thin Shear Flows, *J. Fluid Mech.* 52, part 4, (1972), pp. 609-638.
36. Harlow, F.H., Transport of Anisotropic or Low-Intensity Turbulence, Report LA-3947, (1968).

37. Harlow, F.H. and Hirt, C.W., Generalized Transport Theory of Anisotropic Turbulence, Report LA-4086, (1969).
38. Launder, B.E. and Spalding, D.B., Turbulence Models and Their Application to the Prediction of Internal Flows, Imperial College Report TM/TN/A/18, (April 1971). Also, Symposium on Internal Flows, Paper 1, Salford, (1971).
39. Launder, B.E. and Singham, J.R., The prediction of fully developed flow in non-circular ducts, Symposium on Internal Flows, Paper 12, Salford, (1971).
40. Spalding, D.B. et al, Turbulence Model and their Experimental Verification, Notes of short course presented at the Penn. State Univ., (1974).
41. Launder, B.E. and Spalding, D.B., Lectures on Mathematical Models of Turbulence, Academic Press, London, (1972).
42. Gosse, J., Schiestel, R. and Robin, M.G., A New Model of Turbulence Applied to Prediction of Liquid Metal Heat Transfer, Internal Report, Laboratoire de Mecanique, Nancy, Cedex, France, (1973).
43. Eifler, W. and Nijsing, R., Fundamentals Studies of Fluid Flow and Heat Transfer in Fuel Element Geometries, Report EUR 2193.e, part II, (1965).
44. Eifler, W. and Nijsing, R., Experimental Investigation of Velocity Distribution and Flow Resistance in a Triangular Array of Parallel Rods, Nucl. Eng. Des.5, (1967), pp. 22-42.
45. Eifler, W., Uber die Turbulente Geschwindigkeitsverteilung und Wandreibung in Stromungskanalen verschiedener Querschnitte, Ph.D., Technische Hochschule, Darmstadt (1968).

CHAPTER III
DESCRIPTION OF ANALYTICAL MODEL

1. General Consideration

As observed in Chapter II, none of the models that have been applied to rod bundles can give a detailed description of the complete velocity field in a typical subchannel. Description of axial and secondary flows can only be obtained through the solution of the Reynolds' equations for all three directions (axial, tangential and radial) along with the continuity equation. Obviously, information about the Reynolds stress tensor is necessary to accomplish such goal.

In the present work, the velocity field will be sought for an incompressible flow with temperature-independent properties, in steady state and fully developed conditions with body forces neglected. The subchannel selected will be one from a very large (infinite) array of rods. For such situation, the Reynolds and continuity equations can be reduced to a set of three transport equations for the axial momentum, vorticity and stream function, as shown in Appendix A. They are presented below, in cylindrical coordinates.

(a) Axial momentum equation:

$$\begin{aligned} \frac{1}{r} \frac{\partial}{\partial r} r v_z \left(\frac{\partial \psi}{r \partial \theta} \right) - \frac{\partial}{r \partial \theta} v_z \left(\frac{\partial \psi}{\partial r} \right) - \frac{1}{r} \frac{\partial}{\partial r} r \left(\frac{\partial v_z}{2r} - \frac{v_r v_z}{v} \right) \\ = \frac{\partial}{r \partial \theta} \left(\frac{\partial v_z}{r \partial \theta} - \frac{v_\theta v_z}{v} \right) = -\frac{1}{v \rho} \frac{\partial p}{\partial z} \quad ; \quad (\text{III.1}) \end{aligned}$$

(b) Stream function equation:

$$-\frac{1}{r} \frac{\partial}{\partial r} r \left(\frac{\partial \psi}{\partial r} \right) - \frac{\partial}{r \partial \theta} \left(\frac{\partial \psi}{r \partial \theta} \right) = \frac{\omega}{v} \quad ; \quad (\text{III.2})$$

(c) Vorticity equation

$$\begin{aligned} \frac{1}{r} \frac{\partial}{\partial r} r \omega \left(\frac{\partial \psi}{r \partial \theta} \right) - \frac{\partial}{r \partial \theta} \omega \left(\frac{\partial \psi}{\partial r} \right) - \frac{1}{r} \frac{\partial}{\partial r} r \left(\frac{\partial \omega}{\partial r} \right) - \frac{\partial}{r \partial \theta} \left(\frac{\partial \omega}{r \partial \theta} \right) \\ = -\frac{1}{v r} \left[\frac{\partial}{\partial \theta} \frac{1}{r} \frac{\partial}{\partial r} r \left(v_\theta^2 - v_r^2 \right) + \left[\frac{\partial}{\partial r} \frac{1}{r} \frac{\partial}{\partial r} r - \frac{\partial^2}{r^2 \partial \theta^2} \right] r \frac{v_r v_\theta}{v} \right] \quad (\text{III.3}) \end{aligned}$$

where the vorticity was defined as

$$\omega \equiv \frac{1}{r} \frac{\partial}{\partial r} r \bar{v}_\theta - \frac{\partial \bar{v}_r}{r \partial \theta} \quad , \quad (\text{III.4})$$

and the stream function, by the relations

$$\bar{v}_\theta \equiv -v \frac{\partial \psi}{\partial r} \quad , \quad (\text{III.5})$$

$$\bar{v}_r \equiv v \frac{\partial \psi}{r \partial \theta} \quad . \quad (\text{III.6})$$

In equation (III.1), the bars over v_z and p , meaning time-averaged values, were dropped since, from now on, instantaneous values of those quantities will not appear in the development of the model.

To solve equations (III.1,2 and 3), only statistical turbulence models were considered in view of the limitations of the other models. Statistical models with more than two equations which were considered still in the development stage were ruled out because of their added complexity and due to the fact that, until now, they have not proved to produce more accurate results than simpler one- and two-equation models. So, the choice was between one- and two-equation models.

These two types of models assume the Reynolds stresses as being proportional to axial velocity gradients, for example $\overline{v_r v_z} \propto \frac{\partial v_z}{\partial r}$. For the proportionality parameter or turbulent viscosity, it is assumed the expression prepared by Kolmogorov and Prandtl, independently,

$$v_T = K^{1/2} L_v, \quad \text{or}$$

$$v_T = C_v K^{1/2} \ell, \quad (\text{III.7})$$

where C_v is a constant, K is the turbulence kinetic energy, ℓ is the mixing or mixture length, and L_v is the actual

diffusion length of momentum. Both types of models compute K through a transport equation.

With equation (III.7) in mind, the selection of a model is reduced to the consideration of whether or not to express λ (or related parameter) also in terms of a transport equation. A few intensive arguments are presented below to substantiate the decision of using a one-equation model; that is, expressing λ by an algebraic expression.

Since, in rod bundle subchannels with $\frac{P}{D} > 1.0$, the absence of corners rules out the presence of strong vorticity-generating regions, as observed in square ducts⁽¹⁾, the generation and dissipation of vorticity are expected to be more uniformly distributed along the surface of the rods, with secondary flows being established due to imbalances of these two processes⁽²⁾. Based on this reasoning secondary flows in rod bundle subchannels should not be expected to be as strong as in ducts with corners, and they should decrease with the increase of $\frac{P}{D}$, since the asymmetry of the channel, that can be mathematically expressed by

$$\alpha \equiv \frac{\hat{y}_{\max} - \hat{y}_{\min}}{\hat{y}_{\text{av}}} \quad , \quad (\text{III.8})$$

decreases as $\frac{P}{D}$ increases. In the range of values for $\frac{P}{D}$

where secondary flows can be considered important, say $\frac{P}{D} < 1.25$ ⁽³⁾ the wetted perimeter is usually much larger than \hat{y}_{av} , because of the elongated shape of the subchannel. So, the wall region plays an important role in the calculations. However, it is expected that for points close to the wall the mixing length should be proportional to distance from the wall.

With the two heuristic arguments above, it was inferred that, in rod bundles, secondary flows are not very strong and that the wall region can be considered dominant in the description of turbulent parameters. It is known that, in the wall region of any turbulent flow without secondary flows such as flows in circular ducts or over flat plates, that the mixing length can be taken as proportional to the distance from the wall, to the point being analysed. In the region near the maximum velocity line (MVL), small errors in the values of the mixing length ℓ , consequently in v_T , will not affect the final velocity field computation considerably, since, over that region velocity gradients are very small.

In the following sections which present a detailed description of the model, selection of many input parameters and constants is described based on existing experimental data. For the mixing length, ℓ , and constants

C_D and C_v in particular, experimental data from this study were used to deduce optimum representations or numerical values. As pointed out in the discussion of results, Chapter VI, however, alternate representations or numerical values for these functions based on existing data in the literature would demonstrate the general success of the one-equation model utilized here for predicting the hydrodynamic parameters of turbulent flows in rod bundle geometry.

2. DETAILED DESCRIPTION OF MODEL

The first step in the application of the one-equation statistical model of turbulence is to relate the Reynolds shear stresses to main velocity gradients in terms of the turbulent viscosity ν_T , that is,

$$\overline{v'_r v'_z} = -\nu_T \left(\frac{\partial v_z}{\partial r} \right) , \quad (\text{III.9})$$

$$\overline{v'_\theta v'_z} = -\nu_T \left(\frac{\partial v_z}{r \partial \theta} \right) , \quad (\text{III.10})$$

where the turbulent viscosity is given by the Prandtl-Kolmogorov formula (III.7), repeated here,

$$\nu_T = C_v K^{1/2} \ell . \quad (\text{III.11})$$

The turbulence kinetic energy, K , will be calculated

by the transport equation (obtained in Appendix B):

$$\begin{aligned} & \frac{1}{r} \frac{\partial}{\partial r} r K \left(\frac{\partial \psi}{r \partial \theta} \right) - \frac{\partial}{r \partial \theta} K \left(\frac{\partial \psi}{\partial r} \right) - \frac{1}{r} \frac{\partial}{\partial r} r \left(\frac{\partial K}{\partial r} - \frac{\overline{v_r' K'}}{v} \right) - \frac{\partial}{r \partial \theta} \left(\frac{\partial K}{r \partial \theta} - \frac{\overline{v_\theta' K'}}{v} \right) \\ & = -C_D \frac{K^{3/2}}{v \ell} - \frac{1}{v} \left[\overline{v_r' v_z'} \left(\frac{\partial v_z}{\partial r} \right) + \overline{v_\theta' v_z'} \left(\frac{\partial v_z}{r \partial \theta} \right) \right] \end{aligned} \quad (\text{III.12})$$

Here again K is the time-averaged value of the turbulence kinetic energy, the bar over its symbol being dropped for simplicity.

Assume, by analogy with (III.9) and (III.10),

$$\overline{v_r' K'} \approx -\Gamma_K \frac{\partial K}{\partial r}, \quad (\text{III.13})$$

$$\overline{v_\theta' K'} \approx -\Gamma_K \frac{\partial K}{r \partial \theta}, \quad (\text{III.14})$$

where Γ_K is an exchange coefficient of the kinetic energy of the fluctuating motion. Assuming that the diffusion of turbulence kinetic energy is produced by eddies with approximately the same scales of motion of those which promote momentum transfer, Γ_K can be approximated as

$$\Gamma_K \approx \frac{v_T}{\sigma_K}, \quad (\text{III.15})$$

where Γ_K can be understood as an effective Prandtl number,

which is taken as constant.

Regarding the mixing length distribution, there is no information available about its distribution in rod arrays based on experimental data. Buleev⁽⁴⁾ proposed a semi-empirical expression,

$$\frac{l}{\ell} = \frac{1}{2} \int_0^{2\pi} \frac{d\phi}{s} \quad , \quad (III.16)$$

where s represents the distance from the point in question to the solid wall in the direction ϕ . Based on analysis of rod bundle subchannel experimental data obtained in this present work, as will be discussed later, it is proposed the mixing length distribution be expressed as

$$\frac{l}{\ell} = \frac{y}{\hat{y}} \quad , \quad \text{for } 0 \leq \frac{y}{\hat{y}} \leq 0.44 \quad , \quad (III.17)$$

$$\frac{l}{\ell} = 0.44 + 0.066 \sin \left[\frac{\pi}{0.38} \left(\frac{y}{\hat{y}} - 0.44 \right) \right] \quad ,$$

$$\text{for } 0.44 < \frac{y}{\hat{y}} \leq 1.0 \quad , \quad (III.18)$$

where \hat{y} is distance from the wall to the maximum velocity line, along a radial line.

Both expressions will be compared to experimental data in Chapter IV, for different angular positions.

In order to obtain a closed system of equations,

the vorticity source term in equation III.3 has to be determined. This term (see Appendix A) is:

$$I_{\omega} = -\frac{1}{vr}(I_1 + I_2) \quad , \quad (\text{III.19})$$

where

$$I_1 \equiv \frac{\partial}{\partial \theta} \frac{1}{r} \frac{\partial}{\partial r} r \left[v_{\theta}^{\prime 2} - v_r^{\prime 2} \right] \quad , \quad (\text{III.20})$$

$$I_2 \equiv \left[\frac{\partial}{\partial r} \frac{1}{r} \frac{\partial}{\partial r} r - \frac{\partial^2}{r^2 \partial \theta^2} \right] r \overline{v_r v_{\theta}} \quad . \quad (\text{III.21})$$

Brundrett and Baines⁽¹⁾ observed that, for square ducts, $I_1 \gg I_2$. This is assumed, here, to be true also for rod bundle subchannels. Then,

$$I_{\omega} \approx -\frac{1}{vr} \frac{\partial}{\partial \theta} \frac{1}{r} \frac{\partial}{\partial r} r \left[v_{\theta}^{\prime 2} - v_r^{\prime 2} \right] \quad . \quad (\text{III.22})$$

Define the term $\Delta_{\omega} \equiv \left[v_{\theta}^{\prime 2} - v_r^{\prime 2} \right]$. Three possibilities were analysed to obtain the term Δ_{ω} as follows:

i. from empirical correlation of experimental data in the literature;

ii. by associating Δ_{ω} to the turbulence kinetic energy, through a geometric function, that is,

$$\Delta_{\omega} \approx K \cdot f(r, \theta) \quad , \quad (\text{III.23})$$

iii. from algebraic approximations of the transport equations for the turbulent intensities.

In the first approach the procedure examined to correlate turbulent intensities was that proposed by Bobkov et al⁽⁵⁾ and applied by Ibragimov et al⁽⁶⁾ for square ducts. The difficulty associated with this procedure arises from the fact that the experimental error associated with Δ_w is very large, since it represents a small quantity obtained by the difference of large quantities each having an experimental error. This precludes any effort to obtain gradients of Δ_w accurately, particularly in the tangential direction.

The second possibility was also explored for applications in square ducts, this time by Ying as described in Ref. 7. The difficulty lays in obtaining the geometric function $f(r,\theta)$. This would have to be accomplished by examining experimental data related to the behavior of Δ_w based on heuristic considerations. The major setback of such approach is its lack of universality. For rod bundles, there is no reason to believe that the same function would represent well Δ_w for very different values of P/D .

The third approach comes from the assumption that, close to the wall, all turbulent intensity is produced in the axial direction and part of it is redistributed into the tangential and radial directions by pressure fluctuations.

So, since convection and diffusion are negligible near the wall, the pressure redistribution of v_θ or v_r is made equal to its dissipation (see Appendix C for details).

From these assumptions, one obtains:

$$\overline{v_\theta}^2 - \overline{v_r}^2 \approx -c\ell^2 \left| \left(\frac{\partial v_z}{r \partial \theta} \right)^2 - \left(\frac{\partial v_z}{\partial r} \right)^2 \right|, \quad (\text{III.24})$$

where

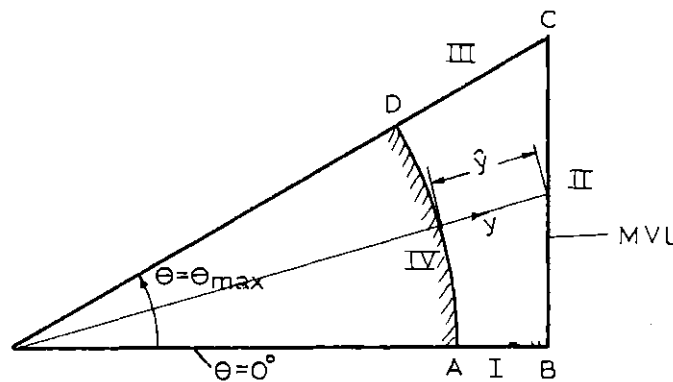
$$c = \frac{c_v}{c_D} \cdot \frac{2[6c_2 - 2]}{11[c_1 - 2c_2]}, \quad (\text{III.25})$$

with c_1 and c_2 , constants.

Expression (III.24) will be adopted in the present work.

3. Boundary Conditions

The sketch below shows the subchannel boundaries where conditions are being sought.



a. Boundaries I and III ($\theta = 0^\circ$ and $\theta = \theta_{\max}$, respectively)

For the axial velocity and turbulence kinetic energy, by symmetry considerations,

$$\left(\frac{\partial v_z}{\partial \theta} \right)_{I, III} = 0 \quad , \quad (III.26)$$

$$\left(\frac{\partial K}{\partial \theta} \right)_{I, III} = 0 \quad . \quad (III.27)$$

Since no net flow crosses lines AB or CD, the stream function must be constant along boundaries I and III, which can be observed from equation (III.5) by imposing \bar{v}_θ equal to zero. Since the value of this constant is arbitrary, it is taken as zero. So,

$$\psi_{I, III} = 0 \quad . \quad (III.28)$$

The boundary condition for the vorticity along these boundaries is obtained from equation (III.4), observing that $\bar{v}_\theta = 0$ and $\frac{\partial \bar{v}_r}{\partial \theta} = 0$ by symmetry. Then

$$\omega_{I, III} = 0 \quad . \quad (III.29)$$

b. Boundary II (maximum velocity line, MVL)

By symmetry, the gradients of the axial velocity and

turbulence kinetic energy are zero along the normal to MVL, that is,

$$\left(\frac{\partial v_z}{\partial n} \right)_{MVL} = 0 \quad ,$$

$$\left(\frac{\partial K}{\partial n} \right)_{MVL} = 0 \quad .$$

These expressions can be written in the form:

$$\left(\frac{\partial v_z}{\partial r} \right)_{MVL} = \left(\frac{\partial v_z}{r \partial \theta} \right)_{MVL} \tan \theta \quad , \quad (III.30)$$

$$\left(\frac{\partial K}{\partial r} \right)_{MVL} = \left(\frac{\partial K}{r \partial \theta} \right)_{MVL} \tan \theta \quad . \quad (III.31)$$

Since no net flow crosses MVL, the stream function is constant along BC and the constant is set to zero, that is,

$$\psi_{MVL} = 0.$$

Since no net flow crosses MVL, the direction of the secondary flow velocity, v , is along that line. Expressing \bar{v}_θ and \bar{v}_r in terms of v , obtain:

$$\bar{v}_\theta = v \cdot \cos \theta \quad ,$$

$$\bar{v}_r = v \cdot \sin \theta \quad .$$

Substituting these two expressions into equation

(III.4), one gets:

$$\omega_{MVL} = \frac{v \cos \theta}{r} + \cos \theta \frac{\partial v}{\partial r} - \frac{\sin \theta}{r} \frac{\partial v}{\partial \theta} - \frac{v \cos \theta}{r} ,$$

or

$$\omega_{MVL} = \left(\frac{\partial v}{\partial n} \right)_{MVL} .$$

By symmetry, the normal gradient of v along MVL is zero. Then

$$\omega_{MVL} = 0, \quad (\text{III.32}).$$

By symmetry, the gradients of the axial velocity and turbulence kinetic energy are zero along the normal to MVL, that is,

$$\left(\frac{\partial v_z}{\partial n} \right)_{MVL} = 0 ,$$

$$\left(\frac{\partial K}{\partial n} \right)_{MVL} = 0 .$$

These expressions can be written in the form:

$$\left(\frac{\partial v_z}{\partial r} \right)_{MVL} = \left(\frac{\partial v_z}{r \partial \theta} \right)_{MVL} \tan \theta , \quad (\text{III.30})$$

$$\left(\frac{\partial K}{\partial r} \right)_{MVL} = \left(\frac{\partial K}{r \partial \theta} \right)_{MVL} \tan \theta . \quad (\text{III.31})$$

Since no net flow crosses MVL, the stream function is constant along BC and the constant is set to zero, that is,

C. Boundary IV (solid wall)

Since the wall is non-porous, that is, no flow crosses its surface, and applying the non-slip condition, one finds:

$$(v_z)_\omega = 0 \quad , \quad (\text{III.33})$$

$$K_\omega = 0 \quad , \quad (\text{III.34})$$

$$\psi_\omega = 0 \quad , \quad (\text{III.35})$$

$$\text{and } \left(\frac{\partial \psi}{\partial r}\right)_\omega = 0 \quad . \quad (\text{III.36})$$

C.1. Wall Functions for Axial Velocity and Turbulence Kinetic Energy

Near solid walls, the radial gradients of the velocity and turbulence kinetic energy are very large. So, a numerical procedure based on linear approximations would not be valid for large mesh space in that region. Also, the coefficients C_D and C_v , introduced in the analytical model, can only be assumed as constant, with the mixing length given by either eq. (III.16) or the set of equations (III.17) and (III.18) for large turbulent Reynolds number, defined as

$$R_t \equiv \frac{K^{1/2} y}{\nu} \quad , \quad (\text{III.37})$$

where y is the distance of the point being analysed to the wall. The coefficients C_D and C_ν are chosen in such way that, just outside the wall sublayers, in the fully turbulent region, the diffusion length L_ν , associated with ν_T ($\equiv K^{1/2} L_\nu$), multiplied by $1/C_\nu$ is equal the dissipation length L_D , associated with the dissipation rate of turbulence kinetic energy ϵ ($\equiv \frac{K^{3/2}}{L_D}$), multiplied by C_D . Also each product is equal to the distance from the wall to the point being studied, that is,

$$\frac{L_\nu}{C_\nu} = C_D L_D = \ell = y \quad . \quad (\text{III.38})$$

However this does not happen close to the wall or in the so-called laminar and buffer sublayers. Distributions of the mixing length, as a function of the turbulent Reynolds number, have been proposed^(8,9) for the wall sublayers.

In general, they can be written in the form:

(a) laminar sublayer:

$$\ell_\nu = A_\nu R_t y \quad , \quad (\text{III.39})$$

$$\ell_D = A_D R_t y \quad , \quad (\text{III.40})$$

(b) buffer or transition sublayer

$$\ell_\nu = y \left[1 - \exp(-A_\nu R_t) \right] \quad , \quad (\text{III.41})$$

$$\ell_D = y \left[1 - \exp(-A_D R_t) \right] , \quad (\text{III.42})$$

where A_v and A_D are constant. Distinction was made between the diffusion and dissipation length scales since they are not proportional to each other inside the wall sublayers.

Utilization of the mixing scales as given by expressions (III.39-42) in a numerical procedure would require a very fine mesh space in the radial direction, near solid walls, which would make the numerical solution very expensive. Since, inside the laminar and transition sublayers, convection of momentum is small, it is expected that the velocity profile in the region close to the wall could be accurately represented by a law-of-the-wall function (see, for example, Ref. 10, p. 554) of the type:

$$v_z = \frac{v_t}{K} \log \frac{E v_t y}{\nu} , \quad (\text{III.43})$$

where v_t is the friction velocity and K and E are constants. This distribution will be assumed in this work.

For the turbulence kinetic energy, assuming that diffusion and convection are negligible compared to generation and dissipation near the wall, its equation (III.12) is reduced to

$$c_D \frac{K^{3/2}}{\ell_D} = - \frac{v_r v_z}{v_r v_z} \left(\frac{\partial v_z}{\partial r} \right) - \frac{v_\theta v_z}{v_\theta v_z} \left(\frac{\partial v_z}{r \partial \theta} \right) \quad (\text{III.44})$$

The velocity gradient in the tangential direction is very small compared to its radial gradient, so, it can be neglected. Using equations (III.9) and (III.7), equation (III.44) is further reduced to

$$C_D \frac{K^{3/2}}{l_D} = C_v K^{1/2} l_v \left(\frac{\partial v_z}{\partial r} \right)^2 \quad . \quad (\text{III.45})$$

Now, from eq. (III.43), assuming negligible curvature effects near the wall,

$$\left(\frac{\partial v_z}{\partial r} \right) = \left(\frac{\partial v_z}{\partial y} \right) = \frac{v_\tau}{\kappa y} \quad .$$

Plugging this result into (III.45)

$$\frac{C_D K^{3/2}}{l_D} = C_v K^{1/2} l_v \cdot \frac{v_\tau^2}{\kappa^2 y^2} \quad .$$

Since, it can be assumed that, at the edge of the buffer sublayer (call it point B), $l_D = l_v = y$, one obtains

$$K_B \approx \frac{C_v}{C_D \kappa^2} v_\tau^2 \quad . \quad (\text{III.46})$$

The value of K given by eq. (III.46) will be used as the wall boundary condition for the turbulence kinetic energy equation.

C.2. Vorticity boundary condition at wall⁽¹¹⁾

Since neither the vorticity nor its gradient normal

to the wall are known, its wall boundary condition has to be deduced from the non-slip condition between the wall and the fluid. Assume, then, that in a very thin layer close to the wall, the vorticity source term is negligible. Usually, in this region, gradients in the peripheral direction are much smaller than gradients in the direction normal to the wall. With this assumption; equation (III.3) is reduced to

$$\frac{\partial}{\partial r} \omega \left(\frac{\partial \psi}{\partial \theta} \right) - \frac{\partial}{\partial r} r \left(\frac{\partial \omega}{\partial r} \right) \approx 0 \quad (\text{III.47})$$

Integrating this equation from the wall to a radial position r , one obtains::

$$\omega \frac{\partial \psi}{\partial \theta} - r \left(\frac{\partial \omega}{\partial r} \right) + \bar{A} = 0 \quad ,$$

where \bar{A} is an integration constant. For a domain very close to the wall r can be taken as the radius of the rod, R . Then

$$\frac{\partial \omega}{\partial r} - \frac{\omega}{R} \frac{\partial \psi}{\partial \theta} = \frac{\bar{A}}{R} = A \quad ,$$

The solution of this equation is

$$\omega = \frac{A \int_R^r dr' \left\{ \exp \left[-\frac{1}{R} \int_R^{r'} \left(\frac{\partial \psi}{\partial \theta} \right) dr'' \right] + B \right.}{\exp \left[-\frac{1}{R} \int_R^r \left(\frac{\partial \psi}{\partial \theta} \right) dr' \right]} \quad (\text{III.48})$$

where B is another integration constant.

Since, at the wall, $(\frac{\partial \psi}{\partial \theta})_{\omega} = 0$, take $(\frac{\partial \psi}{\partial \theta}) \approx 0$ in the thin layer close to the wall considered. Then equation (III.48) is reduced to

$$\omega \approx A(r - R) + B$$

or

$$\omega \approx Ay + B \quad . \quad (III.49)$$

This expression represents a linear approximation of the vorticity near the wall. A and B are the radial gradient and value of the vorticity at wall respectively.

With the approximation expressed by (III.49), neglecting tangential gradients and curvature effects in the wall region, equation (III.2) yields:

$$\frac{\partial}{\partial y^2} \psi \approx \frac{1}{\nu}(Ay + B) \quad . \quad (III.50)$$

Integrating twice with the conditions $\psi_{\omega} = 0$ and $(\frac{\partial \psi}{\partial y})_{\omega} = 0$,

$$\psi = -\frac{1}{\nu} \left[\frac{Ay^3}{6} + \frac{By^2}{2} \right] \quad (III.51)$$

Equations (III.49) and (III.51) define the boundary

condition for the vorticity at the wall. Taking P as the point at the wall and F as the first mesh point inside the flow, A can be written as

$$A = \frac{\omega_F - \omega_P}{r_F - R} ,$$

and $B = \omega_P$.

Equations (III.49) and (III.51) are reduced to

$$\omega_P = -\frac{\omega_F}{2} - \frac{3\nu}{(r_F - R)^2} \psi_F . \quad (\text{III.52})$$

This equation represents the numerical approximation adopted for the vorticity boundary condition at a solid wall.

4. SOURCE TERM FOR AXIAL MOMENTUM EQUATION

The source term for the axial momentum equation is

$$I_{v_z} = -\frac{1}{\rho\nu} \frac{\partial p}{\partial z} , \quad (\text{III.53})$$

where $\frac{\partial p}{\partial z}$ is constant since only fully developed flow is being treated.

A balance of force between two positions 1 and 2 in

the downstream direction, one gets

$$(p_1 - p_2) \cdot A_t = \bar{\tau}_w \cdot P_w \cdot (z_2 - z_1) \quad , (III.54)$$

where

$A_t \equiv$ subchannel flow area,

$P_w \equiv$ subchannel wet perimeter,

$\bar{\tau}_w \equiv$ average wall shear stress.

From (III.54) obtain

$$-\frac{1}{\rho} \frac{\partial p}{\partial z} = \frac{\bar{\tau}_w}{\rho} \cdot \left(\frac{4}{D_H} \right) \quad , \quad (III.55)$$

where D_H is the subchannel hydraulic diameter, defined as

$$D_H \equiv \frac{4A_t}{P_w} \quad . \quad (III.56)$$

Defining the friction factor, f , as

$$f \equiv \frac{\bar{\tau}_w / \rho}{\frac{v_b^2}{2}} \quad , \quad (III.57)$$

where v_b is the flow bulk velocity, equation (III.55)

is reduced to

$$I_{v_z} \equiv -\frac{1}{\rho} \frac{dp}{dz} = f \left(\frac{2}{D_H} \right) \cdot \frac{v_b^2}{2} \quad . \quad (III.58)$$

This equation represents the source term for the axial momentum equation,

Recalling that

$$v_{\tau}(\theta) = \left[\frac{\tau_{\omega}(\theta)}{\rho} \right]^{1/2}, \quad (\text{III.59})$$

the required friction factor f is obtained directly from equation (III.57) with $\bar{\tau}_{\omega}/\rho$ given by

$$\frac{\bar{\tau}_{\omega}}{\rho} = \frac{1}{\theta_{\max}} \int_0^{\theta_{\max}} v_{\tau}^2(\theta) d\theta. \quad (\text{III.60})$$

The distribution of the friction velocity v_{τ} with the angular position is obtained (see Chapter IV, section 6.3.1) from application of the wall function, equation (III.43).

5. CONSTANTS OF THE MODEL

Several constants were introduced during the description of the model. They are:

(a) C_v , introduced through the definition of the turbulent viscosity, equation (III.7);

(b) C_D , from the approximation of the dissipation rate of turbulence kinetic energy, ϵ , equation (B.7);

(c) σ_K , effective Prandtl number defined by equation (III.15);

(d) c_1 and c_2 , from the vorticity source term as deduced in Appendix C and shown in equation (III.25);

(e) κ and E introduced in the axial velocity distribution near the wall, equation (III.43).

The procedure adopted to obtain these constants will be described, here, not in the sequence above, but in the sequence that they were obtained.

5.1 κ and E

They can be obtained from the plot of v^+ $\left[\equiv \frac{v_z}{v_\tau} \right]$ as a function of y^+ $\left[\equiv \frac{v_\tau y}{\nu} \right]$

by approximating its distribution by the function

$$v^+ = \frac{1}{\kappa} \log E y^+ \quad . \quad (\text{III.61})$$

Since, in the present work, no experimental measurements of the wall shear stress distribution were carried out, necessary to obtain $v_\tau = v_\tau(\theta) = \left[\frac{\tau_w(\theta)}{\rho} \right]^{1/2}$, the values of κ and E given by Patel⁽¹²⁾, were adopted

$$\kappa = 0.4186 \quad ,$$

$$E = 9.8 \quad .$$

5.2 C_v

The constant C_v is obtained from the expression

$$C_v \ell = \frac{1}{K^{1/2}} \frac{\left[\overline{v_r' v_z'} \right]}{\left[\frac{\partial v_z}{\partial r} \right]}, \quad (\text{III.62})$$

which is obtained directly from (III.7) and (III.9). The parameter $C_v \ell$ can be calculated directly from the experimental measurements of $\overline{v_r' v_z'}$, v_z and K . Taking ℓ to be equal to the distance from the point under study to the wall along the radial line, for points close to the wall, C_v is, then calculated considering all angular positions in the subchannel. The value obtained was 0.180.

5.3 C_D

C_D can be calculated from (III.46), by estimating v_τ from pressure drop measurements. The value obtained for K/v_τ^2 near the wall was approximately 3.5. From this value, $C_D = 0.30$. However, better agreement between analytical predictions and measurements of this thesis for the TKE distribution were obtained using C_D equal to 0.38. So, this later value was adopted in all subsequent computations.

5.4 σ_K

Since the measurements of $\overline{v_r'K'}$ and $\overline{v_\theta'K'}$ would require triple correlation measurements, this was not carried out. These measurements are necessary for a correct estimate of the value of σ_K . It has been suggested in the literature (see, for example, Ref. 9) that σ_K should be in the range (0.9 - 2.5). This constant was arbitrarily taken as 1.3 although no sensible difference predictions of all parameters were observed utilizing a value 1.5.

5.5 c_1 and c_2

The constant c_1 was discussed in Appendix C. Its value is expected to be between 2.5 and 3.0. In this work, $c_1 = 3.0$.

Hanjalic⁽¹³⁾, analysing the experimental work performed by Champagne and co-workers⁽¹⁴⁾ on nearly homogeneous turbulent shear flows, concluded that c_2 was approximately 0.4. This value was readjusted to 0.37 based on analogy to square duct results of Launder and Ying.⁽¹⁵⁾

6. SUMMARY OF EQUATIONS OF THE MODEL

This section presents a summary of the relevant equations of the model.

6.1 Transport equations

(a) Axial momentum equation

$$\begin{aligned} \frac{1}{r} \frac{\partial}{\partial r} r v_z \left(\frac{\partial \psi}{r \partial \theta} \right) - \frac{\partial}{r \partial \theta} v_z \left(\frac{\partial \psi}{\partial r} \right) - \frac{1}{r} \frac{\partial}{\partial r} r \left(1 + \frac{v_T}{v} \right) \frac{\partial v_z}{\partial r} \\ - \frac{\partial}{r \partial \theta} \left(1 + \frac{v_T}{v} \right) \frac{\partial v_z}{r \partial \theta} = - \frac{1}{\nu \rho} \frac{\partial p}{\partial z} \end{aligned} \quad . \quad (\text{III.63})$$

(b) Stream function equation

$$- \frac{1}{r} \frac{\partial}{\partial r} r \left(\frac{\partial \psi}{\partial r} \right) - \frac{\partial}{r \partial \theta} \left(\frac{\partial \psi}{r \partial \theta} \right) = \frac{\omega}{\nu} \quad . \quad (\text{III.64})$$

(c) Vorticity equation

$$\begin{aligned} \frac{1}{r} \frac{\partial}{\partial r} r \omega \left(\frac{\partial \psi}{r \partial \theta} \right) - \frac{\partial}{r \partial \theta} \omega \left(\frac{\partial \psi}{\partial r} \right) - \frac{1}{r} \frac{\partial}{\partial r} r \left(\frac{\partial \omega}{\partial r} \right) - \frac{\partial}{r \partial \theta} \left(\frac{\partial \omega}{r \partial \theta} \right) \\ = - \frac{1}{\nu} \frac{\partial}{r \partial \theta} \frac{1}{r} \frac{\partial}{\partial r} r \left[v_\theta^2 - v_r^2 \right] \end{aligned} \quad . \quad (\text{III.65})$$

(d) Turbulence kinetic energy equation

$$\begin{aligned} \frac{1}{r} \frac{\partial}{\partial r} r K \left(\frac{\partial \psi}{r \partial \theta} \right) - \frac{\partial}{r \partial \theta} K \left(\frac{\partial \psi}{\partial r} \right) - \frac{1}{r} \frac{\partial}{\partial r} r \left[1 + \frac{v_T}{\nu \sigma_K} \right] \frac{\partial K}{\partial r} \\ = \frac{\partial}{r \partial \theta} \left[1 + \frac{v_T}{\nu \sigma_K} \right] \frac{\partial K}{r \partial \theta} + \frac{C_D K^{3/2}}{\nu l} + \frac{v_T}{\nu} \left[\left(\frac{\partial v_z}{\partial r} \right)^2 + \left(\frac{\partial v_z}{r \partial \theta} \right)^2 \right] \end{aligned} \quad . \quad (\text{III.66})$$

6.2 Algebraic equations

(a) Turbulent viscosity

$$\nu_T = C_v K^{1/2} \ell \quad , \quad (\text{III.67})$$

(b) Mixing length distribution

$$\frac{\ell}{\hat{y}} = \frac{y}{\hat{y}} \quad , \quad \text{for } 0 \leq \frac{y}{\hat{y}} \leq 0.44 \quad , \quad (\text{III.68})$$

$$\frac{\ell}{\hat{y}} = 0.44 + 0.066 \sin \left[\frac{\pi}{0.38} \left(\frac{y}{\hat{y}} - 0.44 \right) \right] \quad , \quad \text{for } 0.44 < \frac{y}{\hat{y}} \leq 1.0 \quad .$$

(c) Expression for $\Delta_\omega \equiv v_\theta'^2 - v_r'^2$

$$\Delta_\omega = -c\ell^2 \left[\left(\frac{\partial v_z}{r \partial \theta} \right)^2 - \left(\frac{\partial v_z}{\partial r} \right)^2 \right] \quad , \quad (\text{III.69})$$

where

$$c = \frac{C_v}{C_D} \cdot \frac{2(6c_2 - 2)}{11(c_1 - 2c_2)} \quad . \quad (\text{III.70})$$

(d) Source term for axial momentum equation

$$I_{v_z} = f \left(\frac{2}{D_H} \right) \cdot \frac{v_b^2}{v} \quad . \quad (\text{III.71})$$

(e) Friction factor

$$f \equiv \frac{\frac{\bar{\tau}_\omega}{\rho}}{\frac{v_b^2}{2}} \quad . \quad (\text{III.72})$$

(f) Average value of wall shear stress

$$\frac{\bar{\tau}_w}{\rho} = \frac{1}{\theta_{\max}} \int_0^{\theta_{\max}} v_{\tau}^2(\theta) d\theta \quad . \quad (\text{III.73})$$

6.3 Boundary conditions

(a) Wall boundary conditions

$$v_z = \frac{v_{\tau}}{\kappa} \log \frac{Ev_{\tau}y}{\nu} \quad ,$$

$$K = \frac{C_v}{C_D \kappa^2} v_{\tau}^2 \quad ,$$

$$\psi = 0 \quad ,$$

$$\omega_p = -\frac{\omega_F}{2} - \frac{3\nu}{(r_F - R)^2} \psi_F \quad .$$

(b) $\theta = 0^\circ$ and $\theta = \theta_{\max}$

$$\frac{\partial v_z}{\partial \theta} = \frac{\partial K}{\partial \theta} = 0 \quad ,$$

$$\psi = \omega = 0 \quad .$$

(c) MVL

$$\frac{\partial v_z}{\partial r} = \left(\frac{\partial v_z}{r \partial \theta} \right) \tan \theta \quad ,$$

$$\frac{\partial K}{\partial r} = \left(\frac{\partial K}{r \partial \theta} \right) \tan \theta \quad ,$$

$$\frac{\partial K}{\partial r} = \left(\frac{\partial K}{r \partial \theta} \right) \tan \theta \quad ,$$

$$\psi = \omega = 0 \quad .$$

6.4 Constants of the model

$$c_v = 0.180 \quad ,$$

$$c_D = 0.38 \quad ,$$

$$\sigma_K = 1.3 \quad ,$$

$$\kappa = 0.4186 \quad ,$$

$$E = 9.8 \quad ,$$

$$c_1 = 3.0 \quad ,$$

$$c_2 = 0.37 \quad .$$

REFERENCES

1. Brundrett, E. and Baines, W.D., The Production and Diffusion of Vorticity in Duct Flow, *J.Fluid Mech.*, Vol. 19 (1964), pp.375-394.
2. Hinze, J.O., Secondary Currents in Wall Turbulence, *The Phys.of Fluid Suppl.*, (1967), pp.S122-S125.
3. Ramm, H. and Johannsen, K., Hydrodynamics and Heat Transfer in Regular Arrays of Circular Tubes, 1972 Intern.Seminar on Recent Develop.in Heat Exchangers of the Intern.Centre for Heat and Mass Transfer, Trogir, Yugoslavia, (Aug.30-Sept.6, 1972).
4. Buleev, N.I., Theoretical Model of the Mechanism of Turbulent Exchange in Fluid Flow, *AERE Trans.*957, (1963).
5. Bobkov, V.P. et al., Correlation of Experimental Data on the Pulsation Velocity Intensity for Turbulent Fluid Flow in Channels of Different Form, *Fluid Dynamics*, Vol.3, No.3, (1968), pp.111-113.
6. Ibragimov, M.Kh. et al., Calculation of Secondary Flow in a Turbulent Fluid Stream, *Fluid Dynamics*, Vol.4, No.4 (1969), pp.114-116.
7. Launder, B.E. and Singham, J.R., The Prediction of Fully Developed Flow in Non-circular Ducts, *Symposium on Internal Flows*, paper 12, Salford, (1971).
8. Driest, E.R.van, On Turbulent Flow near a Wall, *J. Aerospace Sci.* 23, (1956), pp.1007-1011.
9. Wolfshtein, M., The Velocity and Temperature Distribution in One-dimensional Flow with Turbulence Augmentation and Pressure Gradient, *Int.J.Heat Mass Transfer*, Vol.12 (1969),pp.301-318.
10. Schlichting, H., *Boundary-Layer Theory*, McGraw-Hill Book Co.,6th.ed.,(1968).
11. Gosman,A.D. et al., *Heat and Mass Transfer in Recirculating Flows*, Academic Press (1969).

12. Patel, V.C., Calibration of the Preston Tube and Limitations on its Use in Pressure Gradients, J.Fluid Mech., vol.23,part 1,(1965),pp.185-208.
13. Hanjalić,K. and Launder,B.E., A Reynolds Stress Model of Turbulence and its Application to Thin Stress Flows, J.Fluid.Mech.,Vol.52,part 4,(1972),pp.609-638.
14. Champagne,F.H.et al., Experiments on Nearly Homogeneous Turbulent Shear Flow, J.Fluid Mech.,Vol.41,part 1,(1970), pp.81-139.
15. Launder, B.E. and Ying, W.M., Prediction of Flow and Heat Transfer in Ducts of Square Cross-Section, The Inst.Mech.Eng.,Proceedings 1972, Vol.187 37/73, pp.455-461.

CHAPTER IV

NUMERICAL PROCEDURE

To derive finite-difference equations from those differential ones described in the previous chapter, the procedure selected was that of integrating the equations over finite areas, making assumptions regarding the distribution of the variables between the nodes of the grid. This procedure ensures that the conservation laws are obeyed over arbitrarily large or small areas, within the accuracy of assumptions made.

It can be observed that the differential equations for the axial momentum, vorticity, stream function and turbulence kinetic energy can be put into a generic form

$$a_{\phi} \left\{ \frac{1}{r} \frac{\partial}{\partial r} \phi \frac{\partial \psi}{\partial \theta} - \frac{\partial}{r \partial \theta} \phi \frac{\partial \psi}{\partial r} \right\} - \left\{ \frac{1}{r} \frac{\partial}{\partial r} r b_{\phi} \frac{\partial \phi}{\partial r} + \frac{\partial}{r \partial \theta} b_{\phi} \frac{\partial \phi}{r \partial \theta} \right\} = S_{\phi} , \quad (\text{IV.1})$$

with the parameters given in the table IV.1.

Table IV.1, Parameters ϕ , a_ϕ , b_ϕ and S_ϕ for the
Differential Equations

ϕ	a_ϕ	b_ϕ	S_ϕ
v_z	1	ϵ	$-\frac{1}{\rho v} \frac{\partial p}{\partial z}$
ω	1	1	$-\frac{1}{v} \frac{\partial}{r \partial \theta} \left[\frac{1}{r} \frac{\partial}{\partial r} r (\overline{v'_\theta{}^2} - \overline{v'_r{}^2}) \right]$
ψ	0	1	$\frac{\omega}{v}$
K	1	ϵ_K	$\frac{v_T}{v} \left[\left(\frac{\partial v_z}{\partial r} \right)^2 + \left(\frac{\partial v_z}{r \partial \theta} \right)^2 \right] - C_D \frac{K^{3/2}}{l}$

where $\epsilon = 1 + \frac{v_T}{v}$, (IV.2)

$\epsilon_K = 1 + \frac{v_T}{v \sigma_K}$.

Figure IV.1 represents the finite difference grid. The dashed lines limit the integration area and they are placed half way between two consecutive grid lines, that is,

$$\begin{aligned}
 r_{i+1/2} &= \frac{1}{2} (r_{i+1} + r_i) , \\
 r_{i-1/2} &= \frac{1}{2} (r_i + r_{i-1}) , \\
 \theta_{j+1/2} &= \frac{1}{2} (\theta_{j+1} + \theta_j) , \\
 \theta_{j-1/2} &= \frac{1}{2} (\theta_j + \theta_{j-1}) .
 \end{aligned}
 \tag{IV.3}$$

The element of area, in cylindrical coordinates, is

$$dA = r dr d\theta ,$$

Integrate, now, equation (IV.1) over the dashed area:

$$a_{\phi} \underbrace{\int_{r_{i-1/2}}^{r_{i+1/2}} \int_{\theta_{j-1/2}}^{\theta_{j+1/2}} \left[\frac{\partial}{\partial r} \phi \frac{\partial \psi}{\partial \theta} - \frac{\partial}{\partial \theta} \phi \frac{\partial \psi}{\partial r} \right] dr d\theta}_{\text{Convection Terms} \equiv I_C} -$$

$$\underbrace{\int_{r_{i-1/2}}^{r_{i+1/2}} \int_{\theta_{j-1/2}}^{\theta_{j+1/2}} \left[\frac{\partial}{\partial r} r b_{\phi} \frac{\partial \phi}{\partial r} + \frac{\partial}{\partial \theta} r b_{\phi} \frac{\partial \phi}{\partial \theta} \right] dr d\theta}_{\text{Diffusion Terms} \equiv I_D} =$$

$$\underbrace{\int_{r_{i-1/2}}^{r_{i+1/2}} \int_{\theta_{j-1/2}}^{\theta_{j+1/2}} r S_{\phi} dr d\theta}_{\text{Source Terms} \equiv I_{\text{sor}}^{\phi}} . \quad (\text{IV.4})$$

So, the equation assumes the form

$$a_{\phi} I_C - I_D = I_{\text{sor}}^{\phi} . \quad (\text{IV.5})$$

1. CONVECTION TERMS

The convection terms can be broken down into four integrals:

$$I_C = \int_{\theta_{j-1/2}}^{\theta_{j+1/2}} d\theta \left(\phi \frac{\partial \Psi}{\partial \theta} \right)_{r_{i+1/2}} - \int_{\theta_{j-1/2}}^{\theta_{j+1/2}} d\theta \left(\phi \frac{\partial \Psi}{\partial \theta} \right)_{r_{i-1/2}} - \int_{r_{i-1/2}}^{r_{i+1/2}} dr \left(\phi \frac{\partial \Psi}{\partial r} \right)_{\theta_{j+1/2}} + \int_{r_{i-1/2}}^{r_{i+1/2}} dr \left(\phi \frac{\partial \Psi}{\partial r} \right)_{\theta_{j-1/2}} \quad (IV.6)$$

Consider the first of the integrals

$$I_{C,1} = \int_{\theta_{j-1/2}}^{\theta_{j+1/2}} d\theta \left(\phi \frac{\partial \Psi}{\partial \theta} \right)_{r_{i+1/2}} \quad (IV.7)$$

For regions away from the wall, it is assumed that ϕ and Ψ are well-behaved functions, so an average value $\bar{\phi}_{i+1/2,j}$ is defined⁽¹⁾ for the parameter ϕ , such that

$$\bar{\phi}_{i+1/2,j} = \frac{\int_{\theta_{j-1/2}}^{\theta_{j+1/2}} d\theta \left(\phi \frac{\partial \Psi}{\partial \theta} \right)_{r_{i+1/2}}}{\int_{\theta_{j-1/2}}^{\theta_{j+1/2}} d\theta \left(\frac{\partial \Psi}{\partial \theta} \right)_{r_{i+1/2}}} \quad (IV.8)$$

So, $I_{C,1}$ can be written in the form:

$$I_{C,1} = \bar{\phi}_{i+1/2,j} (\Psi_{i+1/2,j+1/2} - \Psi_{i+1/2,j-1/2}), \quad (\text{IV.9})$$

At this point, "upwind differences" are introduced⁽¹⁾ into equation (IV.9), which means that if the difference $(\Psi_{i+1/2,j+1/2} - \Psi_{i+1/2,j-1/2})$ is positive, the direction of the flow is from the point (i,j) to the point $(i+1,j)$, and so the property $\phi_{i,j}$ has predominance at point $(i+1/2,j)$, and $\bar{\phi}_{i+1/2,j}$ is assumed to be equal to $\phi_{i,j}$. On the other hand, if that difference is negative, the flow is from $(i+1,j)$ to (i,j) , and the property $\phi_{i+1,j}$ is predominant at $(i+1/2,j)$, and $\bar{\phi}_{i+1/2,j}$ is taken as $\phi_{i+1,j}$. Mathematically, one can write

$$I_{C,1} = \phi_{i+1,j} \left\{ \frac{(\Psi_{i+1/2,j+1/2} - \Psi_{i+1/2,j-1/2})_-}{2} \right. \\ \left. \frac{|\Psi_{i+1/2,j+1/2} - \Psi_{i+1/2,j-1/2}|}{2} \right\} \\ \phi_{i,j} \left\{ \frac{(\Psi_{i+1/2,j+1/2} - \Psi_{i+1/2,j-1/2})_+}{2} \right. \\ \left. \frac{|\Psi_{i+1/2,j+1/2} - \Psi_{i+1/2,j-1/2}|}{2} \right\}. \quad (\text{IV.10})$$

Another approximation is introduced by taking the value of the stream function at a particular corner of the integration area as being equal to the average of the values

at the four neighbouring nodes. Hence, typically

$$\Psi_{i+1/2,j+1/2} = \frac{1}{4} [\Psi_{i+1,j+1} + \Psi_{i+1,j} + \Psi_{i,j+1} + \Psi_{i,j}]. \quad (\text{IV.11})$$

The other terms are obtained the same way and the total convection term can be written as, after rearranging,

$$\begin{aligned} I_C = & A_{i+1,j} (\phi_{i,j} - \phi_{i+1,j}) + A_{i-1,j} (\phi_{i,j} - \phi_{i-1,j}) + \\ & A_{i,j+1} (\phi_{i,j} - \phi_{i,j+1}) + A_{i,j-1} (\phi_{i,j} - \phi_{i,j-1}), \quad (\text{IV.12}) \end{aligned}$$

where the coefficients A, using (IV.11), are:

$$\begin{aligned} A_{i+1,j} & \equiv \frac{1}{8} \left\{ (\Psi_{i+1,j-1} - \Psi_{i+1,j+1} + \Psi_{i,j-1} - \Psi_{i,j+1}) + \right. \\ & \quad \left. |\Psi_{i+1,j-1} - \Psi_{i+1,j+1} + \Psi_{i,j-1} - \Psi_{i,j+1}| \right\}, \\ A_{i-1,j} & \equiv \frac{1}{8} \left\{ (\Psi_{i-1,j+1} - \Psi_{i-1,j-1} + \Psi_{i,j+1} - \Psi_{i,j-1}) + \right. \\ & \quad \left. |\Psi_{i-1,j+1} - \Psi_{i-1,j-1} + \Psi_{i,j+1} - \Psi_{i,j-1}| \right\}, \\ A_{i,j+1} & \equiv \frac{1}{8} \left\{ (\Psi_{i+1,j+1} - \Psi_{i-1,j+1} + \Psi_{i+1,j} - \Psi_{i-1,j}) + \right. \\ & \quad \left. |\Psi_{i+1,j+1} - \Psi_{i-1,j+1} + \Psi_{i+1,j} - \Psi_{i-1,j}| \right\}, \\ A_{i,j-1} & \equiv \frac{1}{8} \left\{ (\Psi_{i-1,j-1} - \Psi_{i+1,j-1} + \Psi_{i-1,j} - \Psi_{i+1,j}) + \right. \\ & \quad \left. |\Psi_{i-1,j-1} - \Psi_{i+1,j-1} + \Psi_{i-1,j} - \Psi_{i+1,j}| \right\}. \end{aligned} \quad (\text{IV.13.a})$$

The approximation given by equation (IV,11) can be applied only if the stream function is known at the four nodes around the corner of the rectangle. This means that such an approximation cannot be applied to points near the east boundary (MVL) of the subchannel (see Fig. IV.2). For points at boundary, it can be written that

$$\psi_{i+1,j} = 0,$$

$$\psi_{i,j-1} = 0.$$

Since the mesh spacing is small, point $(i+1/2, j-1/2)$ is very close to the MVL and therefore it can be assumed that

$$\psi_{i+1/2, j-1/2} = 0.$$

This would be exact if the lines for $r=\text{constant}$ were straight lines. Due to their curvature, it is only an approximation. However since $r_i \gg (r_{i+1} - r_i)$, this should be expected to be a reasonable approximation.

Following the procedure already described, the coefficients A of the convection terms for those points are given by

$$A_{i+1,j} = \frac{1}{8} \left\{ - (\psi_{i+1,j+1} + \psi_{i,j+1} + \psi_{i,j}) + \right. \\ \left. - |\psi_{i+1,j+1} + \psi_{i,j+1} + \psi_{i,j}| \right\},$$

$$A_{i-1,j} \equiv \frac{1}{8} \left\{ (\psi_{i-1,j+1} - \psi_{i-1,j-1} + \psi_{i,j+1}) + \right. \\ \left. |\psi_{i-1,j+1} - \psi_{i-1,j-1} + \psi_{i,j+1}| \right\}, \quad (\text{IV.13.b})$$

$$A_{i,j+1} \equiv \frac{1}{8} \left\{ (\psi_{i+1,j+1} - \psi_{i-1,j+1} - \psi_{i-1,j}) + \right. \\ \left. |\psi_{i+1,j+1} - \psi_{i-1,j+1} - \psi_{i-1,j}| \right\},$$

$$A_{i,j-1} \equiv \frac{1}{8} \left\{ (\psi_{i-1,j-1} + \psi_{i-1,j} + \psi_{i,j}) + \right. \\ \left. |\psi_{i-1,j-1} + \psi_{i-1,j} + \psi_{i,j}| \right\}.$$

2. DIFFUSION TERMS

Here again, the diffusion terms can be separated into four terms:

$$I_D = \int_{\theta_{j-1/2}}^{\theta_{j+1/2}} d\theta \left(r b_\phi \frac{\partial \phi}{\partial r} \right)_{r_{i+1/2}} - \int_{\theta_{j-1/2}}^{\theta_{j+1/2}} d\theta \left(r b_\phi \frac{\partial \phi}{\partial r} \right)_{r_{i-1/2}} + \\ \int_{r_{i-1/2}}^{r_{i+1/2}} dr \left(b_\phi \frac{\partial \phi}{r \partial \theta} \right)_{\theta_{j+1/2}} - \int_{r_{i-1/2}}^{r_{i+1/2}} dr \left(b_\phi \frac{\partial \phi}{r \partial \theta} \right)_{\theta_{j-1/2}}. \quad (\text{IV.14})$$

Call $I_{D,1}$, the first term of I_D . $I_{D,1}$ is given by

$$I_{D,1} = \int_{\theta_{j-1/2}}^{\theta_{j+1/2}} d\theta (r b_\phi)_{r_{i+1/2}} \left(\frac{\partial \phi}{\partial r} \right)_{r_{i+1/2}} \quad (IV.15)$$

Now, both b_ϕ and ϕ are linearly approximated along the line $r = r_{i+1/2}$ which gives

$$(b_\phi)_{r_{i+1/2}} = \frac{b_{\phi_{i+1,j}} + b_{\phi_{i,j}}}{2} \quad \text{and} \quad (IV.16)$$

$$\left(\frac{\partial \phi}{\partial r} \right)_{r_{i+1/2}} = \frac{\phi_{i+1,j} - \phi_{i,j}}{r_{i+1} - r_i}$$

This way, $I_{D,1}$ is reduced to

$$I_{D,1} = \frac{1}{8} \frac{r_{i+1} + r_i}{r_{i+1} - r_i} (\theta_{j+1} - \theta_{j-1}) (b_{\phi_{i+1,j}} + b_{\phi_{i,j}}) (\phi_{i+1,j} - \phi_{i,j}) \quad (IV.17)$$

Analogous considerations lead to similar terms for the other parts of the diffusion integral, which can be written in the form:

$$I_D = - B_{i+1,j} (b_{\phi_{i+1,j}} + b_{\phi_{i,j}}) (\phi_{i,j} - \phi_{i+1,j})$$

$$- B_{i-1,j} (b_{\phi_{i-1,j}} + b_{\phi_{i,j}}) (\phi_{i,j} - \phi_{i-1,j})$$

$$- B_{i,j+1} (b_{\phi_{i,j+1}} + b_{\phi_{i,j}}) (\phi_{i,j} - \phi_{i,j+1})$$

$$- B_{i,j-1} (b_{\phi_{i,j-1}} + b_{\phi_{i,j}}) (\phi_{i,j} - \phi_{i,j-1}) \quad (\text{IV.18})$$

with the coefficients given by the expression below

$$\begin{aligned} B_{i+1,j} &\equiv \frac{1}{8} \frac{r_{i+1} + r_i}{r_{i+1} - r_i} (\theta_{j+1} - \theta_{j-1}) , \\ B_{i-1,j} &\equiv \frac{1}{8} \frac{r_i + r_{i-1}}{r_i - r_{i-1}} (\theta_{j+1} - \theta_{j-1}) , \\ B_{i,j+1} &\equiv \frac{1}{4} \frac{1}{r_i} \frac{r_{i+1} - r_{i-1}}{\theta_{j+1} - \theta_j} , \\ B_{i,j-1} &\equiv \frac{1}{4} \frac{1}{r_i} \frac{r_{i+1} - r_{i-1}}{\theta_j - \theta_{j-1}} . \end{aligned} \quad (\text{IV.19})$$

Although the procedure was not the same of Gosman's⁽¹⁾, the obtained expression for the diffusion terms was the same.

3. COMPLETE FINITE DIFFERENCE EQUATION

The source term is

$$I_{\text{sor},i,j}^{\phi} = \int_{r_{i-1/2}}^{r_{i+1/2}} \int_{\theta_{j-1/2}}^{\theta_{j+1/2}} r S_{\phi} dr d\theta . \quad (\text{IV.20})$$

The finite difference expressions for the source term for each transport equation will be treated separately in section 4, along with the finite difference formulas for

the boundary conditions.

At this point, however, the complete finite-difference equation can be written assembling equations (IV.12), (IV.18) and (IV.20):

$$\phi_{i,j} = C_{i+1,j} \phi_{i+1,j} + C_{i-1,j} \phi_{i-1,j} + C_{i,j+1} \phi_{i,j+1} + C_{i,j-1} \phi_{i,j-1} + \frac{I_{\text{SOR},i,j}^{\phi}}{\Sigma_{i,j}}, \quad (\text{IV.21})$$

where

$$\begin{aligned} C_{i+1,j} &\equiv \left[a_{\phi} A_{i+1,j} + (b_{\phi_{i+1,j}} + b_{\phi_{i,j}}) B_{i+1,j} \right] / \Sigma_{i,j}, \\ C_{i-1,j} &\equiv \left[a_{\phi} A_{i-1,j} + (b_{\phi_{i-1,j}} + b_{\phi_{i,j}}) B_{i-1,j} \right] / \Sigma_{i,j}, \\ C_{i,j+1} &\equiv \left[a_{\phi} A_{i,j+1} + (b_{\phi_{i,j+1}} + b_{\phi_{i,j}}) B_{i,j+1} \right] / \Sigma_{i,j}, \\ C_{i,j-1} &\equiv \left[a_{\phi} A_{i,j-1} + (b_{\phi_{i,j-1}} + b_{\phi_{i,j}}) B_{i,j-1} \right] / \Sigma_{i,j} \end{aligned} \quad (\text{IV.22})$$

and

$$\begin{aligned} \Sigma_{i,j} &\equiv a_{\phi} (A_{i+1,j} + A_{i-1,j} + A_{i,j+1} + A_{i,j-1}) \\ &\quad + (b_{\phi_{i+1,j}} + b_{\phi_{i,j}}) B_{i+1,j} + (b_{\phi_{i-1,j}} + b_{\phi_{i,j}}) B_{i-1,j} \\ &\quad + (b_{\phi_{i,j+1}} + b_{\phi_{i,j}}) B_{i,j+1} + (b_{\phi_{i,j-1}} + b_{\phi_{i,j}}) B_{i,j-1}. \end{aligned} \quad (\text{IV.23})$$

4. SOURCE TERMS FOR TRANSPORT EQUATIONS

Due to the different mathematical form of the source terms, they will be treated separately.

4.1. Source term of the axial momentum equation.

This term is

$$I_{\text{sor},i,j}^v = - \frac{1}{\rho v} \frac{\partial p}{\partial z} \int_{r_{i-1/2}}^{r_{i+1/2}} \int_{\theta_{j-1/2}}^{\theta_{j+1/2}} r \, dr \, d\theta, \quad (\text{IV.24})$$

since $\frac{\partial p}{\partial z} = \text{constant}$, for fully developed flow.

Defining $V_{i,j}$ as

$$V_{i,j} \equiv \int_{r_{i-1/2}}^{r_{i+1/2}} \int_{\theta_{j-1/2}}^{\theta_{j+1/2}} r \, dr \, d\theta, \quad (\text{IV.25})$$

the axial momentum equation source term is reduced to

$$I_{\text{sor},i,j}^v = I_{v_z} \cdot V_{i,j}, \quad (\text{IV.26})$$

with I_{v_z} defined by equation (III.53) and calculated using equation (III.71).

Equation (IV.25) can be integrated to yield

$$V_{i,j} = \frac{1}{16} (\theta_{j+1} - \theta_{j-1}) \left[(r_{i+1} + r_i)^2 - (r_i + r_{i-1})^2 \right]. \quad (\text{IV.27})$$

4.2. Vorticity equation source term

The vorticity source term is

$$I_{\text{sor},i,j}^{\omega} = -\frac{1}{v} \int_{r_{i-1/2}}^{r_{i+1/2}} \int_{\theta_{j-1/2}}^{\theta_{j+1/2}} \left[\frac{\partial}{r \partial \theta} \left[\frac{1}{r} \frac{\partial}{\partial r} r \Delta_{\omega} \right] \right] r \, dr \, d\theta, \quad (\text{IV.28})$$

with the term $\Delta_{\omega} \equiv \overline{v'_{\theta}} - \overline{v'_r}$. This term can be written as

$$I_{\text{sor},i,j}^{\omega} = -\frac{1}{v} \int_{r_{i-1/2}}^{r_{i+1/2}} \int_{\theta_{j-1/2}}^{\theta_{j+1/2}} \left[\frac{\partial}{\partial \theta} \frac{\partial}{\partial r} \Delta_{\omega} + \frac{\partial}{r \partial \theta} \Delta_{\omega} \right] dr \, d\theta. \quad (\text{IV.29})$$

The first part of equation (IV.29) is then integrated to give

$$-\frac{1}{v} \left[(\Delta_{\omega})_{i+1/2,j+1/2} - (\Delta_{\omega})_{i+1/2,j-1/2} - (\Delta_{\omega})_{i-1/2,j+1/2} + (\Delta_{\omega})_{i-1/2,j-1/2} \right]. \quad (\text{IV.30})$$

Assuming that, inside the integration area around a mesh point, the radial distance r does not change very much, the second term of (IV.29) is reduced to

$$-\frac{1}{vr_i} \left[\int_{r_{i-1/2}}^{r_{i+1/2}} (\Delta_{\omega})_{j+1/2} \, dr - \int_{r_{i-1/2}}^{r_{i+1/2}} (\Delta_{\omega})_{j-1/2} \, dr \right]. \quad (\text{IV.31})$$

The term Δ_ω will now be assumed to be approximately constant along the radial line between the points $r_{i-1/2}$ and $r_{i+1/2}$, with a value equal its value at point i . So, equation (IV.31) is finally reduced to

$$-\frac{(r_{i+1} - 2r_i + r_{i-1})}{4 \nu r_i} \left[(\Delta_\omega)_{i,j+1} - 2(\Delta_\omega)_{i,j} + 2(\Delta_\omega)_{i,j-1} \right]. \quad (\text{IV.32})$$

From equation (III.24), one has

$$\Delta_\omega = -c \ell^2 \left[\left(\frac{\partial v_z}{r \partial \theta} \right)^2 - \left(\frac{\partial v_z}{\partial r} \right)^2 \right]. \quad (\text{IV.33})$$

When this expression is applied into equations (IV.30) and (IV.32), the mixing length ℓ is taken as constant and equal to its value at point (i,j) . So, from equation (IV.33), one obtains

$$(\Delta_\omega)_{i+1/2,j+1/2} = -c \ell_{i,j}^2 \left[\left(\frac{\partial v_z}{r \partial \theta} \right)_{i+1/2,j+1/2}^2 - \left(\frac{\partial v_z}{\partial r} \right)_{i+1/2,j+1/2}^2 \right]. \quad (\text{IV.34})$$

The velocity gradient in the tangential direction is then calculated by

$$\left(\frac{\partial v_z}{r \partial \theta} \right)_{i+1/2,j+1/2} = \frac{(v_z)_{i+1,j+1} + (v_z)_{i,j+1} - (v_z)_{i+1,j} - (v_z)_{i,j}}{(r_{i+1} + r_i)(\theta_{j+1} - \theta_j)}, \quad (\text{IV.35})$$

and the radial gradient,

$$\left(\frac{\partial v_z}{\partial r}\right)_{i+1/2, j+1/2} = \frac{(v_z)_{i+1, j+1} + (v_z)_{i+1, j} - (v_z)_{i, j+1} - (v_z)_{i, j}}{(r_{i+1} - r_i)} \quad (\text{IV.36})$$

These two expressions are plugged into equations (IV.34) to obtain the term $(\Delta_\omega)_{i+1/2, j+1/2}$. A similar approach is used to compute the other terms of equations (IV.30) and (IV.32), determining then the finite difference expressions for the vorticity source term.

4.3. Stream function source term.

From the stream function transport equation,

$$I_{\text{sor}, i, j}^\psi = \frac{1}{v} \int_{r_{i-1/2}}^{r_{i+1/2}} \int_{\theta_{j-1/2}}^{\theta_{j+1/2}} \omega r dr d\theta \quad (\text{IV.37})$$

This integral can be divided into four integrals:

$$I_{\text{sor}, i, j}^\psi = \frac{1}{v} \left\{ \int_{r_{i-1/2}}^{r_i} \int_{\theta_{j-1/2}}^{\theta_j} \omega r dr d\theta + \int_{r_{i-1/2}}^{r_i} \int_{\theta_j}^{\theta_{j+1/2}} \omega r dr d\theta \right. \\ \left. + \int_{r_i}^{r_{i+1/2}} \int_{\theta_{j-1/2}}^{\theta_j} \omega r dr d\theta + \int_{r_i}^{r_{i+1/2}} \int_{\theta_j}^{\theta_{j+1/2}} \omega r dr d\theta \right\} \quad (\text{IV.38})$$

Take, for example, the integral

$$I_1 = \int_{r_i}^{r_{i+1/2}} \int_{\theta_j}^{\theta_{j+1/2}} \omega r dr d\theta .$$

Assume now a linear approximation for ω of the kind:

$$\omega = \omega_{i,j} + \frac{\omega_{i+1,j} - \omega_{i,j}}{r_{i+1} - r_i} (r - r_i) + \frac{\omega_{i,j+1} - \omega_{i,j}}{\theta_{j+1} - \theta_j} (\theta - \theta_j) , \quad (\text{IV.39})$$

then, the integral I_1 can be written, after assuming that

$$3 r_i + r_{i+1} = 4 r_i ,$$

$$2 r_i + r_{i+1} = 3 r_i ,$$

in the form:

$$I_1 = \frac{r_i (r_{i+1} - r_i) (\theta_{j+1} - \theta_j)}{16} (2\omega_{i,j+1} + \omega_{i+1,j} + \omega_{i,j}) .$$

Analogous expressions can be derived for the other integrals of (IV.38). Assuming $\Delta\theta = \theta_{j+1} - \theta_j = \theta_j - \theta_{j-1}$, one writes:

$$I_{\text{sor},i,j}^{\psi} = \frac{r_i \Delta\theta}{8\nu} \left[(r_{i+1} - r_{i-1}) (\omega_{i,j} + \omega_{i,j+1} + \omega_{i,j-1}) + (r_{i+1} - r_i) \omega_{i+1,j} + (r_i - r_{i-1}) \omega_{i-1,j} \right] . \quad (\text{IV.40})$$

4.4. Source term for turbulence kinetic energy equation.

This source term is

$$I_{\text{sor},i,j}^K = I_{\text{sor},i,j}^1 - I_{\text{sor},i,j}^2, \quad (\text{IV.41})$$

where

$$I_{\text{sor},i,j}^1 = \int_{r_{i-1/2}}^{r_{i+1/2}} \int_{\theta_{j-1/2}}^{\theta_{j+1/2}} \left[\frac{v_T}{v} \left[\left(\frac{\partial v_z}{\partial r} \right)^2 + \left(\frac{\partial v_z}{r \partial \theta} \right)^2 \right] \right] r \, dr \, d\theta, \quad (\text{IV.42})$$

$$I_{\text{sor},i,j}^2 = C_D \int_{r_{i-1/2}}^{r_{i+1/2}} \int_{\theta_{j-1/2}}^{\theta_{j+1/2}} \frac{K^{3/2}}{\ell} r \, dr \, d\theta. \quad (\text{IV.43})$$

Selecting a mesh space such that the velocity gradients do not change much over the integration area, expression (IV.42) can be approximated to

$$I_{\text{sor},i,j}^1 = \left[\left(\frac{\partial v_z}{\partial r} \right)_{i,j}^2 + \left(\frac{\partial v_z}{r \partial \theta} \right)_{i,j}^2 \right] \int_{r_{i-1/2}}^{r_{i+1/2}} \int_{\theta_{j-1/2}}^{\theta_{j+1/2}} \frac{v_T}{v} r \, dr \, d\theta. \quad (\text{IV.44})$$

The integral that appears in the term above was then treated in a similar manner as the vorticity in the stream function source term, yielding an expression similar to (IV.40) substituting ω by v_T/v . Same treatment was performed on $K^{3/2}/\ell$ in equation (IV.43). The velocity gradients of equation (IV.44) were written as

$$\left(\frac{\partial v_z}{\partial r}\right)_{i,j} \approx \frac{1}{2} \left[\frac{(v_z)_{i+1,j} - (v_z)_{i,j}}{r_{i+1} - r_i} + \frac{(v_z)_{i,j} - (v_z)_{i-1,j}}{r_i - r_{i-1}} \right],$$

$$\left(\frac{\partial v_z}{r \partial \theta}\right)_{i,j} = \frac{(v_z)_{i,j+1} - (v_z)_{i,j-1}}{r_i (\theta_{j+1} - \theta_{j-1})}.$$

5. Grid for numerical procedure.

Since large gradients of any properties in the tangential direction are not expected, an uniform angular separation was selected in this direction, that is,

$$\Delta\theta = \theta_{j+1} - \theta_j = \text{constant}. \quad (\text{IV.45})$$

Also, in order to simplify writing boundary conditions for the MVL, mesh points were taken on that line, (see Fig. IV.3), that is, if r_G is equal $P/2$, then,

$$r_{G+1} = \frac{P/2}{\cos \theta_1}.$$

In general,

$$r_{G+m} = \frac{P}{2 \cos \theta_m}. \quad (\text{IV.46})$$

In the gap region, an approximately uniform grid was used. The distance between the two first line is

$$r_2 - r_1 = \Delta . \quad (\text{IV.47})$$

The next,

$$\begin{aligned} r_3 - r_2 &= \Delta + \delta , \\ r_4 - r_3 &= \Delta + 2\delta , \dots \\ r_i - r_{i-1} &= \Delta + (i-2)\delta , \end{aligned} \quad (\text{IV.48})$$

with Δ selected in a way that the edge of the wall sublayer, taken as $y^+ = 30$, falls right in the middle of two mesh spaces. Since the friction velocity and hence the spacial position corresponding to $y^+ = 30$ changes from one iteration to the next, the edge of the wall sublayer does not remain in its initially prescribed position in the middle of two mesh spaces. The change in spacial position is insignificant. That is, Δ corresponds to

$$y^+ = \frac{30}{n + 0.5} , \quad (n \geq 1) \quad (\text{IV.49})$$

where n is the smallest integer such that

$$(G - 1)\Delta < \frac{P}{2} - R , \quad (\text{IV.50})$$

where G is the radial mesh point at $r = \frac{P}{2}$ (see Fig. IV.3).

δ is given by

$$\delta = \frac{2 \left[\left(\frac{P}{2} - R \right) - (G-1)\Delta \right]}{(G-1)(G-2)} . \quad (\text{IV.51})$$

In the computer program developed, the following

notation was used:

- (a) for $r = R$, $i = 1$;
- (b) for $r = r_{G+m}$, $i = i_{lim}^{(m)}$, $i-1 = i_{max}^{(m)}$;
- (c) for $\theta = 0^0$, $j=1$;
- (d) for $\theta = \theta_{max}$, $j = J_n$;
- (e) $i_{lim}^{(J_n)} = I_n$;
- (f) for $(r_i - R)$ corresponding to $y^+ > 30$, such that
 $(r_{i-1} - R)$ corresponds to $y^+ < 30$, $i = i_{min}$.

This notation will be followed from now on.

6. Boundary conditions

6.1. Boundary conditions for $\theta = 0^0$ and $\theta = \theta_{max}$.

For $\theta = 0^0$, expanding the velocity in a Taylor series in the angular direction, following the notation just introduced,

$$(v_z)_{i,2} = (v_z)_{i,1} + (\theta_2 - \theta_1) \left(\frac{\partial v_z}{\partial \theta} \right)_{i,1} + \frac{(\theta_2 - \theta_1)^2}{2} \left(\frac{\partial^2 v_z}{\partial \theta^2} \right)_{i,1} + \dots$$

and

$$(v_z)_{i,3} = (v_z)_{i,1} + (\theta_3 - \theta_1) \left(\frac{\partial v_z}{\partial \theta} \right)_{i,1} + \frac{(\theta_3 - \theta_1)^2}{2} \left(\frac{\partial^2 v_z}{\partial \theta^2} \right)_{i,1} + \dots$$

Since it has been assumed that $\theta_2 - \theta_1 = \theta_3 - \theta_2$, and neglecting terms of the order of $(\theta_2 - \theta_1)^3$, taking into account eq. (III.26), then

$$(v_z)_{i,1} \approx \frac{4}{3}(v_z)_{i,2} - \frac{1}{3}(v_z)_{i,3} . \quad (\text{IV.52})$$

Analogously for K,

$$K_{i,1} \approx \frac{4}{3} K_{i,2} - \frac{1}{3} K_{i,3} . \quad (\text{IV.53})$$

For vorticity and stream function,

$$\omega_{i,1} = \psi_{i,1} = 0 . \quad (\text{IV.54})$$

Analogous expressions apply to $\theta = \theta_{\max}$.

6.2. Boundary conditions for MVL.

For the velocity equation, from equation (III.30), one writes, taking $i = i_{\text{lim}}(j)$,

$$\frac{(v_z)_{i,j} - (v_z)_{i-1,j}}{r_i - r_{i-1}} \approx \frac{(v_z)_{i,j+1} - (v_z)_{i,j}}{r_i(\theta_{j+1} - \theta_j)} \tan \theta_j ,$$

or

$$(v_z)_{i,j} \approx \frac{\eta_j (v_z)_{i,j+1} + (v_z)_{i-1,j}}{\eta_j + 1} , \quad (\text{IV.55})$$

where

$$\eta_j \equiv \frac{r_i - r_{i-1}}{r_i(\theta_{j+1} - \theta_j)} \tan \theta_j . \quad (\text{IV.56})$$

An expression analogous to (IV.55) is written for K,

$$K_{i,j} \approx \frac{\eta_j K_{i,j+1} + K_{i-1,j}}{\eta_j + 1} . \quad (\text{IV.57})$$

Again the vorticity and stream functions are

$$\omega_{i,j} = \psi_{i,j} = 0. \quad (\text{IV.58})$$

6.3. Boundary conditions at wall.

Starting with the vorticity and stream function, it can be written, directly from equations (III.52) and (III.35),

$$\psi_{i,j} = 0, \quad \text{and} \quad (\text{IV.59})$$

$$\omega_{1,j} = - \frac{\omega_{2,j}}{2} - \frac{3\nu}{(r_2 - R)^2} \psi_{2,j}. \quad (\text{IV.60})$$

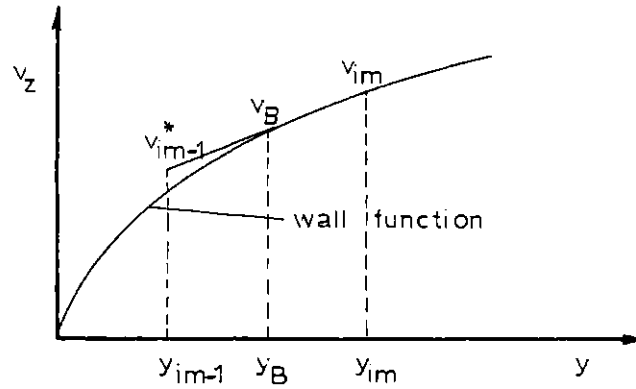
6.3.1. Boundary condition at wall for axial momentum equation.

The wall function for the axial velocity is given by equation (III.43),

$$v_z = \frac{v_\tau}{\kappa} \log E \frac{v_\tau y}{\nu} . \quad (\text{IV.61})$$

Taking $y = y_B$ when $y^+ = 30$, and $i_m = i_{\min}$,

continuity of the velocity and its radial gradient is imposed at point $y = y_B$, that is, (see Sketch)



$$v_B = \frac{v_\tau}{\kappa} \log 30 E, \quad (\text{IV.62})$$

$$y_B = \frac{30 \nu}{v_\tau}. \quad (\text{IV.63})$$

From (IV.61), differentiating at point y_B , one has

$$\left(\frac{\partial v_z}{\partial y} \right)_B = \frac{v_\tau}{y_B} = \frac{v_\tau^2}{30 \nu \kappa}. \quad (\text{IV.64})$$

Now, one writes

$$\frac{v_{im} - v_B}{y_{im} - y_B} = \frac{v_\tau}{\kappa y_B}. \quad (\text{IV.65})$$

From (IV.62), (IV.63) and (IV.64),

$$\frac{v_{im} - v_\tau \frac{\log 30 E}{\kappa}}{y_{im} - \frac{30 \nu}{v_\tau}} = \frac{v_\tau^2}{30 \nu \kappa}. \quad (\text{IV.66})$$

Solving this equation for v_τ yields

$$v_\tau = \sqrt{\chi^2 + \eta v_{im}} - \chi, \quad (\text{IV.67})$$

with

$$\chi \equiv \frac{30\nu(\log 30E - 1)}{2 y_{im}} , \quad (\text{IV.67})$$

$$\eta \equiv \frac{30\nu\kappa}{y_{im}} . \quad (\text{IV.69})$$

A fictitious value of \bar{v}_z , at point i_{m-1} is then defined such that, for the numerical procedure, a linear approximation between points y_{im-1} and y_{im} becomes a reasonable assumption, regardless of the magnitude of the actual steep gradient existing in that region. Mathematically, it is imposed

$$\frac{v_{im} - v_{im-1}^*}{y_{im} - y_{im-1}} = \frac{v_\tau^2}{30\nu\kappa} , \quad (\text{IV.70})$$

hence

$$v_{im-1}^* = v_{im} - \left(\frac{y_{im} - y_{im-1}}{30 \nu \kappa} \right) v_\tau^2 . \quad (\text{IV.71})$$

This fictitious value of the velocity is, then, used as the wall boundary condition for the axial momentum equation.

6.3.2. Boundary condition at wall for the turbulence kinetic energy equation.

Knowing v_τ from equation (IV.67), the value of K at point y_B can be calculated using (III.46)

$$K_B = \frac{C_v}{C_D \kappa^2} v_\tau^2. \quad (\text{IV.72})$$

Defining here, also, a fictitious value for K at point i_{m-1} , one has

$$\frac{K_{im} - K_{im-1}^*}{y_{im} - y_{im-1}} = \frac{K_{im} - K_B}{y_{im} - y_B}, \quad (\text{IV.73})$$

or

$$K_{im-1}^* = K_{im} - \left(\frac{y_{im} - y_{im-1}}{y_{im} - \frac{30v}{v_\tau}} \right) \left(K_{im} - \frac{C_v}{C_D \kappa^2} v_\tau^2 \right). \quad (\text{IV.74})$$

So, this value K_{im-1}^* represents the wall boundary conditions for the turbulence kinetic energy equation.

7. ITERATIVE METHOD

The procedure selected to solve the finite difference equation (IV.21) is the method of successive displacements⁽²⁾ also known as the Gauss-Siedel method, which is a point iterative method, where each new value of the parameters is used in the finite difference equation as soon as it becomes available. For simplicity, however, the coefficients of equation (IV.21) and the source term were assumed to be given only by the values of the parameters from the previous cycle. For a certain value of j (angular position), the method proceeds to iterate from $i = 2$ to $i = i_{\max}(j)$, sweeping,

this way, one radial line, then proceeding to the next value of j . Based on the above, equation (IV.21) becomes, for the n^{th} iteration:

$$\begin{aligned} \phi_{i,j}^{(n)} = & C_{i+1,j}^{(n-1)} \phi_{i+1,j}^{(n-1)} + C_{i-1,j}^{(n-1)} \phi_{i-1,j}^{(n-1)} + C_{i,j+1}^{(n-1)} \phi_{i,j+1}^{(n-1)} + \\ & C_{i,j-1}^{(n-1)} \phi_{i,j-1}^{(n-1)} + \left[\frac{I\phi_{\text{sor},i,j}}{\Sigma_{i,j}} \right]^{(n-1)}. \end{aligned} \quad (\text{IV.75})$$

Included in the procedure is provision for under- or over-relaxation in order to compensate for variations of the coefficients $C_{i,j}$, that, in certain cases, can lead to divergence of the numerical iteration. So, it was taken

$$\phi_{i,j}^{(n)} = \alpha_R \phi_{i,j}^{(n)*} + (1-\alpha_R) \phi_{i,j}^{(n-1)}, \quad (\text{IV.76})$$

where, now, $\phi_{i,j}^{(n)*}$ is the value of $\phi_{i,j}$ as given by equation (IV.75) and α_R is the relaxation parameter, with $\alpha_R < 1$ or $\alpha_R > 1$ for under- or over-relaxation, respectively.

8. CONVERGENCE CRITERION

The first idea was to impose as convergence criterion that the maximum fractional change of the parameter ϕ , in the field, from one cycle to the next, should not exceed a prescribed value, i.e.:

$$\left| \frac{\phi_{i,j}^{(n)} - \phi_{i,j}^{(n-1)}}{\phi_{i,j}^{(n-1)}} \right|_{\max} \leq \lambda. \quad (\text{IV.77})$$

However, Gosman et al⁽¹⁾ pointed out that, when it happens that the value of a variable at a particular node is much smaller than the values at the surrounding nodes, fluctuations in the small value will occur which is not acceptable by the above criterion. This happens, particularly, to the vorticity. So, it was suggested to base the criterion on the rate of the change of the variable to the maximum previous value in the field, $\phi_{\max}^{(n-1)}$, that is,

$$\left| \frac{\phi_{i,j}^{(n)} - \phi_{i,j}^{(n-1)}}{\phi_{\max}^{(n-1)}} \right|_{\max} \leq \lambda. \quad (\text{IV.78})$$

This later approach was adopted here.

9. INITIAL CONDITIONS FOR PARAMETERS

The initial conditions for the axial velocity distribution are given by the method of Ibragimov and co-workers (see Chapter II, section 2.c.).

The turbulence kinetic energy initial conditions are determined by

$$K_{i,j} = \frac{1}{2} \left[\overline{(v_z')^2}_{i,j} + \overline{(v_\theta')^2}_{i,j} + \overline{(v_r')^2}_{i,j} \right] \quad (\text{IV.79})$$

with the turbulent intensities obtained using Bobkov's empirical correlations (see appendix E).

The vorticity is taken as zero in the field.

The stream function is initially assumed as given by its definition

$$\bar{v}_\theta \equiv -v \frac{\partial \psi}{\partial r}, \quad (\text{IV.80})$$

with \bar{v}_θ given by Nijssing's assumptions, equation (II.10), i.e.,

$$\psi = -\frac{2}{\bar{v}} C_{\text{sec}} \sqrt{\frac{\bar{\tau}_w}{\rho}} \frac{d\left(\frac{\bar{\tau}_w}{\tau_w}\right)^{1/2}}{d\theta} \Delta\theta_e \int_0^y \cos\left(\frac{y}{\hat{y}} \pi\right) dy. \quad (\text{IV.81})$$

The computer code "HYBBAC" was developed to solve the equations just described. This code is presented in appendix J.

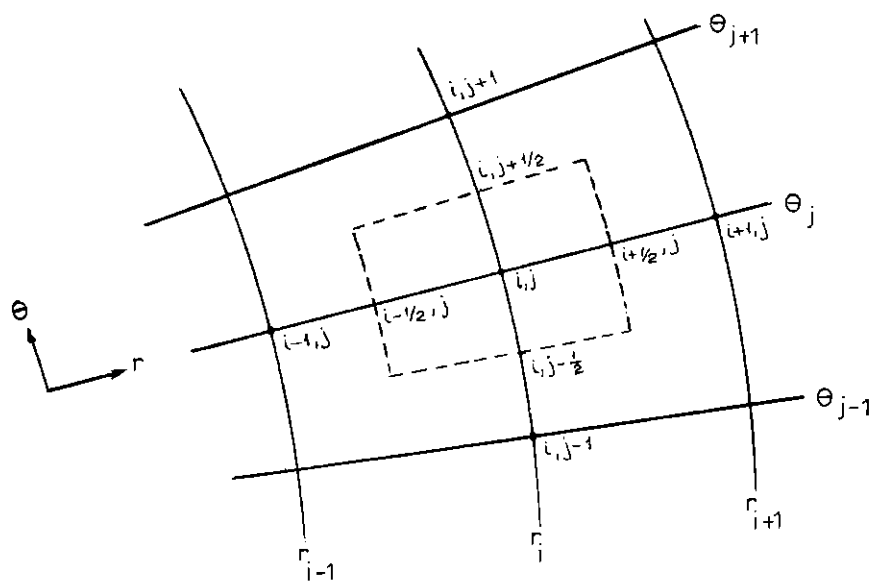


Fig. IV.1. Finite-Difference Grid

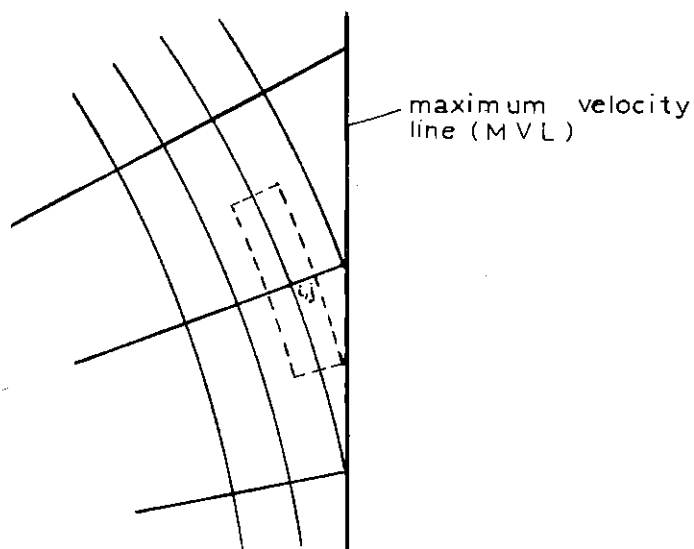


Fig. IV.2. Points Near East Boundary of Subchannel

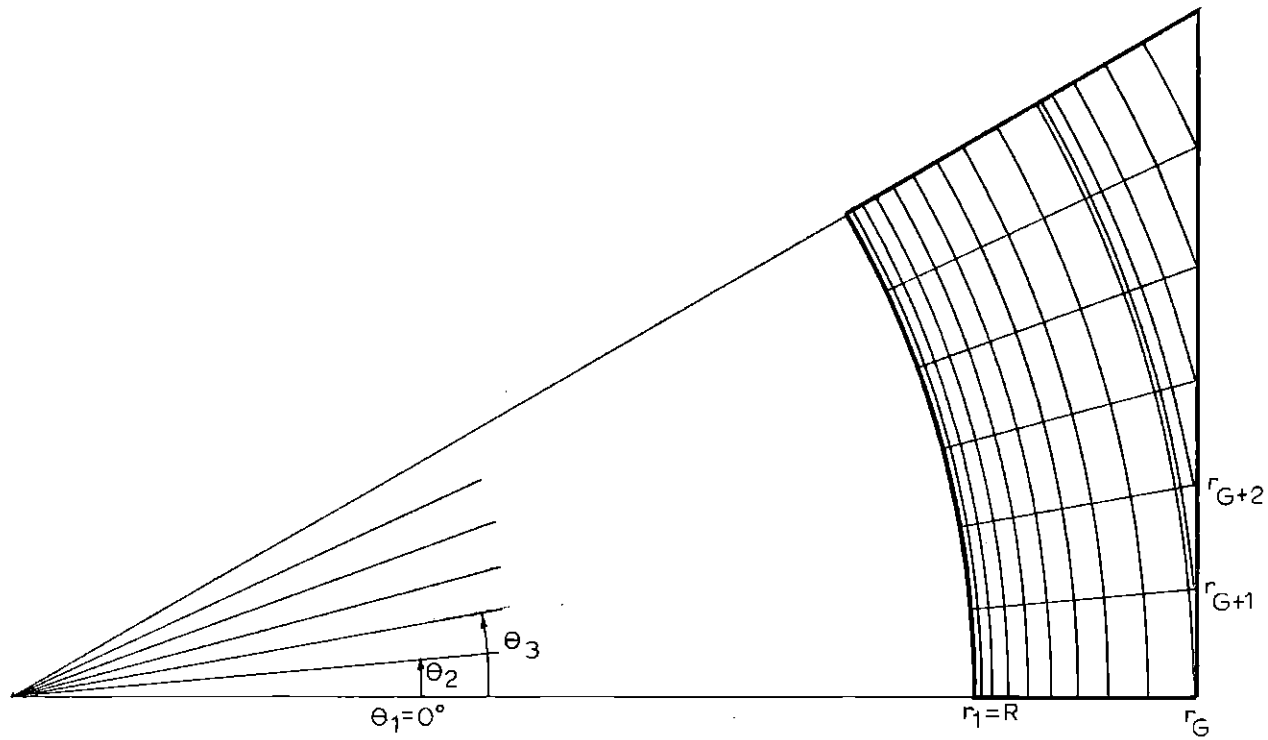


Fig. IV.3. Grid for Numerical Procedure

REFERENCES

1. Gosman, A.D. et al., Heat and Mass Transfer in Recirculating Flows, Academic Press, London, (1969).
2. Clark, M.Jr. and Hansen, K.F., Numerical Methods of Reactor Analysis, Nuclear Science and Tech.Serie, Vol.3, Academic Press, (1964).

CHAPTER V

DESIGN OF EXPERIMENTAL APPARATUS

1. INTRODUCTION

Measurements were made in water flowing within a test section using a laser Doppler anemometer (LDA) operating in the fringe mode with forward scattering. The cross section of the test section was designed to simulate an interior, undisturbed subchannel of a triangular array rod cluster. The following sections describe the test section, the hydraulic loop, the laser Doppler anemometer and traversing mechanism.

2. EXPERIMENTAL APPARATUS

2.1. Test section

It was observed in Chapter II that the cross section shape adopted by Subbotin and Eifler and Nijssing introduced perturbation in the subchannels where measurements were performed. Also, the use of a full scale bundle scaled up to allow distributed parameter measurements would be very expensive and require the LDA to operate in a back-scattering mode which would decrease the scattered light intensity drastically. The shape adopted for the

cross section is shown in Fig. V.1.

Four constraints were adopted in the selection of the dimensions of the test section: (1) the aspect ratio P/D should be as small as possible, preferably below 1.1, since it is expected that the influence of secondary flows increases as P/D decreases; (2) the half-gap size, $g \equiv \frac{P - D}{2}$, should be large compared to the probe volume length, l_v , (see Appendix F); (3) the number of hydraulic diameters of the length, L/D_H , should be as large as possible to insure fully developed conditions; (4) fabrication cost should be minimized.

Figs. V.2 and V.3 show variations of the half-gap dimension, g , and the length of test section required for $L/D_H = 100$, with the rod diameter for different values of D . A typical value for the probe volume length, l_v , is 0.5 mm.

Table V.1 shows the selected values of test section dimensions and the values measured in the test section after fabrication.

TABLE V.I. SELECTED AND ACTUAL PARAMETERS OF TEST SECTION

PARAMETER	$\frac{P}{D}$	D (in)	D_H (in)	L (ft)	$\frac{L}{D_H}$	g (mm)	$A_f \times 10^2$ (in ²)
SELECTED	1.10	2.0	0.668	5	90	2.54	8.75
AFTER FABRICATION	1.123	2.014	0.787	5	77	3.15	10.37

In this table, D_H and A_f represent the hydraulic diameter and flow area of a typical interior subchannel.

They are

$$A_f = \frac{D^2}{8} \left[\frac{1}{\sqrt{3}} \left(\frac{P}{D} \right)^2 - \frac{\pi}{6} \right] , \quad (V.1)$$

and

$$D_H = \frac{4A_f}{P_\omega} \quad (V.2)$$

where P_ω is the wetted perimeter of the subchannel given

by

$$P_{\omega} = \frac{\pi D}{12} \quad . \quad (V.3)$$

The length L represents the distance from the flow inlet to the measuring station (windows).

Fig. V.4 shows the cross section view of test section with assembly details. Fig. V.5 is an overall view of the test section with description of components and dimensions. The test section is composed of three sections, each 2 feet long and, to reduce costs, only one of the sections is provided with windows. However, since the sections are the same, the section with window can be relocated to permit observations into the developing region. Two tap holes, 19" apart, symmetrically located around the windows were used for pressure drop measurements to estimate the average friction velocity and friction factor. It was fabricated with a low-copper aluminum alloy AA-6061 T6, for better corrosion resistance.

At the measuring station, windows were provided on the four sides of the test section to permit the laser beams to reach the flowing water. Due to refraction of the beams on curved surfaces of materials with different refraction indices, hollow rods were used at the measuring station, with apertures 1/2" wide. The hollow rods were, then

covered by a thin plastic film, 0.010" thick, with water on both sides of the film, as shown in Fig. V.6. This way, an optically homogeneous region was obtained with refraction reduced to a negligible level. Distances from the plexiglas wall inside surface to the flowing water are in the range from 1.1 to 2.0 in.

2.2 Hydraulic loop

A closed circuit hydraulic loop was used as shown in Fig. V.7. In order to minimize corrosion of the test section and to have control over the size and concentration of the seeding particles, distilled water was used to fill the loop

2.3 The laser Doppler anemometer (LDA)

Principles of the LDA are discussed in Appendix F. The dual scattered beam mode, also called fringe mode, is used due to the simplicity in aligning the beams and its suitability for low seeding particle concentrations.

2.3.1 Optics

Fig. V.8 shows the optics components used in the set-up. The green line beam ($\lambda_1 = 0.5145\mu$) of a Spectra Physics model 164 Argon laser is split into two beams by a Disa model 55L01 optical unit. The two beams are focused by a single lens into the flow region and the scattered light is received by a light collecting system

composed of two lens. Finally the scattered light is focused at the pin hole located in front of a RCA-7265 photo multiplier tube. The current signal generated by the PMT is then fed to the electronics. Table V.2 shows the design elements of the LDA used in the present work, following the discussion of Appendix F.

In all measurements of turbulent intensities, a DISA flow direction adapter (Bragg cell), model 55L02, was used. The frequency difference used between the two beams was 250 KHz.

For cross correlation measurements, a sequential method was used as will be discussed later in this chapter. The laser beam was split into two beams. A supplementary optical unit was attached to the original one. The four resultant beams, in perpendicular planes, were focused at the same point. The measurements of the turbulent intensities were then obtained by blocking each of the original two beams one at a time. So, the measurements were made sequential with this set-up and the data were obtained exactly at the same point. Fig. V.9 shows, schematically, this set-up.

TABLE V.2. DESIGN ELEMENTS OF THE LDA

PARAMETER	SYMBOL	DATA
A. Refractive indices		
Air	n_o	1.00
Water	n_w	1.33
Plexiglas	n_p	1.50
B. Laser		
Wavelength	λ_l	0.5145 μ
Beam diameter ($1/e^2$)	D_o	1.5 mm
C. Integrated optical unit		
Distance from beams to optical axis	a	25 mm
Focal length of lens	f_L	130 mm
Half angle between beams in air	θ	10° 50'
Half angle between beams in water	β	8° 10'
D. Light collecting system		
Focal length of lens 1	f_s	200 mm
Focal length of lens 2	f_p	105 mm
Diameter of pin hole	D_{ph}	0.1 mm
E. Probe volume		
Diameter of beams at waist	b_o	0.054 mm
Length	l_v	0.541 mm
Height	h_v	0.078 mm

TABLE V.2.(cont.)

Depth	w_v	0.108 mm
Distance between fringes	d_f	1.362 μ
F. Seeding particles		
Material		Polystyrene
Density relative to water		1.0
Shape		Spherical
Diameter		0.234 μ

2.3.2. Traversal mechanism,

All optics components were mounted on a milling machine table and were distributed on a two-level bed (see Fig. IV. 10). The test section was assembled horizontally on a fixed table. So, the positioning of the measuring point was done by moving the optics. A unit movement of the optics changes the position of the measurement point in air, x_0 , and the location of the measuring point in water, x_M , is related to x_0 as shown in Appendix G.

2.3.3. Signal processing electronics

The pedestal of the signal generated by the PMT (RCA-7265, S-20 Spectral response) was removed by a TSI 10095 high pass filter and then processed by the TSI model 1090 frequency tracker. The frequency signal ν_D , is then transformed into an analog voltage signal, v_D ,

$$v_D = \frac{\nu_D}{\nu_{\max}} v_{\max}, \quad (V.4)$$

where

ν_{\max} \equiv upper limit of tracker frequency range being used

v_{\max} \equiv maximum output voltage

For the TSI tracker, $v_{\max} = 10$ V.

To obtain the time-average of v_D , the voltage given by eq. (V.4) is integrated by a RC integrating circuit and fed to a digital voltmeter (Keithley model 160). The time averaged value \bar{v}_D is proportional to the velocity of the fluid normal to the interference fringes at the point under study, that is, \bar{v}_1 .

The RMS of the analog voltage v_D is given by a DISA model 55D35, RMS voltmeter. Call it

$$\sqrt{v_D'^2}.$$

The turbulent fluctuation of v_1 is obtained by removing the broadening resulting from finite transit time and velocity gradient making use of eqs. (F.24) and (F.27). (See Appendix F, section 3.1.c), that is

$$\frac{\overline{v_1'^2}}{\bar{v}_1^2} = \frac{\overline{v_D'^2}}{\bar{v}_D^2} - \left(\frac{2}{\pi N_f} \right)^2 - \left[\frac{l_v}{2\bar{v}_D} \left(\frac{\partial \bar{v}_D}{\partial y} \right) \right]^2, \quad (V.5)$$

From eqs. (V.4) and (F.17)

$$\bar{v}_1 = \frac{\lambda_\omega}{2 \sin \beta} \cdot \frac{v_{\max}}{v_{\max}} \bar{v}_D. \quad (V.6)$$

Since $\lambda_\omega = \left(\frac{n_o}{n_\omega}\right) \lambda_1$ and $\sin \theta = \left(\frac{n_\omega}{n_o}\right) \sin \beta$,

$$\bar{v}_i = \frac{\lambda_1}{2 \sin \beta} \frac{v_{\max}}{v_{\max}} \bar{v}_D \quad . \quad (V.7)$$

The value of v_{\max} used in all measurements was 5.0 MHz.
So, numerically,

$$\bar{v}_i = 0.681 \bar{v}_D \text{ m/s} \quad , \quad (V.8)$$

with \bar{v}_D given in volts.

Since the velocity gradients were not very large in the region where measurements were made, the velocity gradient broadening was neglected. Then, from eq.(V.5) since $N_f = \underline{57}$

$$\sqrt{\frac{v_i'^2}{v_i^2}} = \left[\frac{\frac{v_D'^2}{v_D^2} - 0.00012}{\frac{v_D^2}{v_D^2}} \right]^{1/2} \cdot \bar{v}_i \quad . \quad (V.9)$$

However, the smallest value observed for the ratio $\sqrt{\frac{v_i'^2}{v_i^2}} / \bar{v}_i$ was, for the axial velocity, 0.053, at the center of the subchannel. At that position $\frac{v_D'^2}{v_D^2} / \frac{v_D^2}{v_D^2}$ was equal to 0.0028, which is much larger than 0.00012. Then

$$\sqrt{\frac{v_i'^2}{v_i^2}} = 0.053 \bar{v}_i \quad , \text{ or}$$

$$\sqrt{\frac{v_i'^2}{v_i^2}} = 0.681 \sqrt{\frac{v_i'^2}{v_D^2}} \text{ m/s} \quad . \quad (V.10)$$

with $\sqrt{\frac{v_i'^2}{v_D^2}}$ given in volts.

In the case of turbulent intensities of the secondary flow components, a frequency shift unit (DISA model 55L02 was used). When a frequency shift is used, the interference fringes move with a velocity equivalent to the shifting. The number of fringes crossed by a particle is much larger than it would be if the fringes were still, that is, the effective number $(N_f)_{\text{eff}}$ in this case is much larger than N_f . Based on this argument, the finite transit time broadening, in measurements of the turbulent intensities of secondary flow, can also be neglected. So, equation (V.10) applies to all cases.

3. MESH GRID USED IN MEASUREMENTS

Measurements were performed along 11 radial lines, 3° apart, within one typical subchannel as shown in Fig. V.12. In the plane of the cross section, measurements were made in the directions x and y , instead of r and θ as desired. Only measurements of velocity components parallel to the walls were possible in order to avoid beams with different paths within the test section and ensure correct probe volume positioning.

4. MEASURED PARAMETERS

Measurements of the parameters described below were performed.

4.1 Axial velocity.

4.2 Turbulence kinetic energy.

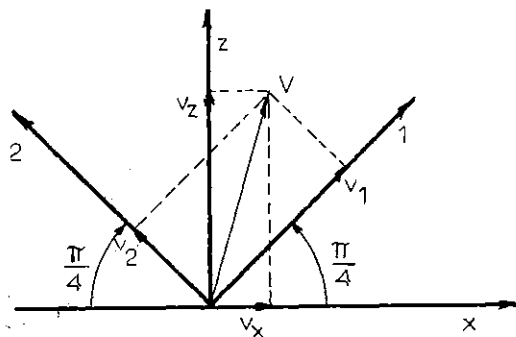
Measurements of the turbulent intensities in the directions x, y and z were performed. The turbulence kinetic energy was calculated by the expression:

$$k = \frac{1}{2} \left[\overline{v_x'^2} + \overline{v_y'^2} + \overline{v_z'^2} \right] \quad (V.11)$$

4.3 Reynolds stresses $\overline{v_r'v_z'}$ and $\overline{v_\theta'v_z'}$.

The Reynolds stresses $\overline{v_r'v_z'}$ and $\overline{v_\theta'v_z'}$ were calculated from sequential measurements of turbulent intensities along axes 45° from the coordinates x, y and x, z as discussed next.

Take the plane x-z, see sketch below:



One writes

$$v_x = v \cos\left(\frac{\pi}{4} + \alpha\right) = \frac{\sqrt{2}}{2} v (\cos \alpha - \sin \alpha) \quad , \quad (\text{V.12})$$

$$v_z = v \sin\left(\frac{\pi}{4} + \alpha\right) = \frac{\sqrt{2}}{2} v (\cos \alpha + \sin \alpha) \quad . \quad (\text{V.13})$$

Also

$$v_1 = v \cos \alpha \quad , \quad (\text{V.14})$$

$$v_2 = v \sin \alpha \quad (\text{V.15})$$

Taking the time-average of equations (V.12-15) and subtracting them from the above equations, they are reduced to

$$v_x' = \frac{\sqrt{2}}{2} (v_1' - v_2') \quad , \quad (\text{V.16})$$

$$v_z' = \frac{\sqrt{2}}{2} (v_1' + v_2') \quad . \quad (\text{V.17})$$

Multiplying,

$$v_x' v_z' = \frac{1}{2} (v_1'^2 - v_2'^2) \quad . \quad (\text{V.18})$$

The time-average of this equation is

$$\overline{v'_x v'_z} = \frac{1}{2} \left(\overline{v_1'^2} - \overline{v_2'^2} \right) \quad (V.19)$$

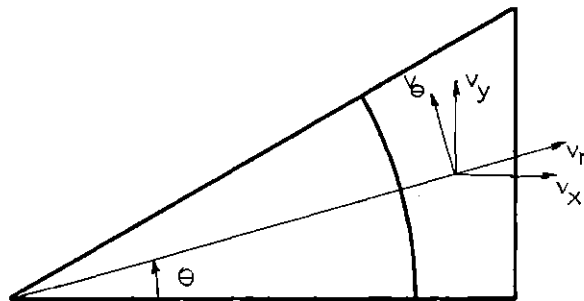
From equation (V.19), it can be observed that measurement of turbulent intensities at directions making 45° with the axis can be used to measure the cross correlation

$$\overline{v'_x v'_z}$$

Analogously,

$$\overline{v'_y v'_z} = \frac{1}{2} \left(\overline{v_3'^2} - \overline{v_4'^2} \right) \quad (V.20)$$

The cross correlations $\overline{v'_r v'_z}$ and $\overline{v'_\theta v'_z}$ can be calculated from the values of $\overline{v'_x v'_z}$ and $\overline{v'_y v'_z}$, by observing that (see sketch)



$$v_r = v_x \cos \theta + v_y \sin \theta \quad , \quad (V.21)$$

$$v_\theta = v_y \cos \theta - v_x \sin \theta \quad . \quad (V.22)$$

Taking the time averages of (V.21) and (V.22) and subtracting them from equations (V.21) and (V.22), multiplying by v_z' and again taking the time-average:

$$\overline{v_r v_z'} = \overline{v_x v_z'} \cos \theta + \overline{v_y v_z'} \sin \theta \quad , \quad (V.23)$$

$$\overline{v_\theta v_z'} = \overline{v_y v_z'} \cos \theta - \overline{v_x v_z'} \sin \theta \quad . \quad (V.24)$$

Measurements of $v_1'^2$, $v_2'^2$, $v_3'^2$ and $v_4'^2$ were performed. From equations (V.19) and (V.20), $\overline{v_x v_z'}$ and $\overline{v_y v_z'}$ were then calculated. Finally, plugging those values into (V.23) and (V.24), the Reynolds stress $\overline{v_r v_z'}$ and $\overline{v_\theta v_z'}$ were obtained.

4.4. Pressure drop around windows

The pressure drop were measured by an inclined gage using a gage oil with specific density $\rho_o = 2.95$. The average wall shear stress was calculated by

$$\frac{\overline{\tau_w}}{\rho} = \frac{1}{\rho} \left(\frac{D_H}{4L} \right) \Delta p \quad , \quad (V.25)$$

with $\Delta p = (\rho_o - \rho) g \Delta H$

where $L \equiv$ distance between tap holes,
 $\Delta H \equiv$ inclined gage reading.

The friction factor is given by

$$f = \frac{\frac{\tau_w}{\rho}}{\frac{1}{2} v_b^2}, \quad (V.26)$$

5. GENERAL ASPECTS OF ERROR ANALYSIS.

The following sources of error in the measurements were identified.

1. flow fluctuations
2. electronics error
3. finite integration time.

5.1. Flow fluctuations

The flow fluctuation was estimated to be 1/4 of division of the flowmeter scale. This scale is divided into 100 parts with the full scale corresponding to 30 gpm. This fluctuation is then given by $\sigma_f = \frac{30}{m} \frac{v_1}{400}$, (V.27) where m is the operational flow rate (in gpm) and v_1 is the measured velocity.

5.2 Electronics error

It can be divided into two different sources:

- a. uncertainty in the analog voltage readout,

b. uncertainty in the RMS voltage.

5.2.1 Uncertainty in the analog voltage readout

The error introduced in the analog voltage is 1% f.s.d. of range in use. In volts, the error is 0.1 V. Transforming into m/s, utilizing equation (V.8)

$$\overline{\Delta v_i} \approx 0.07 \text{ m/s} .$$

This error is uniformly distributed. The standard deviation is, then, given by

$$\sigma_A \approx \frac{\Delta v_i}{\sqrt{3}} = 0.04 \text{ m/s} . \quad (\text{V.28})$$

This is the error for the time-averaged velocity. For the turbulent intensity, it was assumed that it had the same percentual error as the time-averaged velocity, that is

$$\frac{\sigma_{A'}}{\left[\overline{v_i'^2} \right]^{1/2}} \approx \frac{\sigma_A}{v_1} . \quad (\text{V.29})$$

5.2.2. Uncertainty in the RMS voltage

This uncertainty affects only the turbulent intensity measurements. It is 1% of the RMS range in use.

5.3. Finite integration time

This error occurs only in the measurement of the time-averaged velocities and it is due to turbulent fluctuations of the flow (see ref.1, p.211).

The measured time-averaged velocity, \bar{v}_T , is given by

$$\bar{v}_T = \frac{1}{T} \int_0^T v(t) dt, \quad (V.30)$$

where the instantaneous velocity is given by

$$v(t) = \bar{v} + v'(t). \quad (V.31)$$

T is the integration time and \bar{v} is the actual time averaged velocity. The difference between the measured and true values is

$$\bar{v}_T - \bar{v} = \frac{1}{T} \int_0^T v'(t) dt, \quad (V.32)$$

and the variance is

$$\sigma_T^2 = \overline{(\bar{v}_T - \bar{v})^2} = \frac{1}{T^2} \int_0^T \int_0^T \overline{v'(t)v'(t')} dt dt'. \quad (V.33)$$

Defining the autocorrelation coefficient $\rho(t'-t)$ as

$$\rho(t'-t) \equiv \frac{\overline{v'(t)v'(t')}}{\overline{v'^2}}, \quad (V.34)$$

and taking $\tau = t-t'$, equation (V.33) can be reduced to

$$\begin{aligned}\sigma_T^2 &= \frac{\overline{2v'^2}}{T^2} \int_0^T dt \int_0^t \rho(\tau) d\tau \\ &= \frac{\overline{2v'^2}}{T} \int_0^T \left(1 - \frac{\tau}{T}\right) \rho(\tau) d\tau .\end{aligned}\quad (\text{V.35})$$

The integral defined by

$$\Gamma \equiv \int_0^\infty \rho(\tau) d\tau \quad (\text{V.36})$$

represents the integral time scale of the fluctuation $v'(t)$ and provides a rough measure of the time interval over which $v'(t)$ is related to itself. Taking $T \gg \Gamma$, $\tau/T \ll 1$, then

$$\sigma_T^2 \approx \frac{\overline{2v'^2}}{T} \Gamma . \quad (\text{V.37})$$

For isotropic turbulence,

$$\Gamma \approx \frac{\nu_T}{\overline{v'^2}} \quad (\text{V.38})$$

where ν_T is the eddy viscosity. Hence

$$\begin{aligned}\sigma_T^2 &\approx \frac{2\nu_T}{T} , \text{ or} \\ \sigma_T &\approx \left(\frac{2\nu_T}{T}\right)^{1/2} .\end{aligned}\quad (\text{V.39})$$

To calculate σ_T , v_T is estimated from the measurements of $\overline{v'_r v'_z}$ and $\overline{v'_z}$ through the expression

$$v_T = - \frac{\overline{v'_r v'_z}}{\left(\frac{\partial \overline{v'_z}}{\partial r} \right)} . \quad (\text{V.40})$$

The integration time, T , used in the experiment was 10 s.

The total error is estimated by

$$\sigma = \left[\sum_i \sigma_i^2 \right]^{1/2} , \quad (\text{V.41})$$

where the sum is over all error causes of the particular parameter.

6. EXPRESSIONS FOR ERROR ANALYSIS

6.1. Axial velocity

$$\sigma_{\overline{v'_z}} = \left[\sigma_F^2 + \sigma_A^2 + \sigma_T^2 \right]^{1/2} . \quad (\text{V.42})$$

6.2. Turbulence kinetic energy

The turbulence kinetic energy is

$$K = \frac{1}{2} \left(\overline{v'_x{}^2} + \overline{v'_y{}^2} + \overline{v'_z{}^2} \right) . \quad (\text{V.43})$$

Differentiating

$$\Delta K = \frac{\partial K}{\partial v'_x} \Delta v'_x + \frac{\partial K}{\partial v'_y} \Delta v'_y + \frac{\partial K}{\partial v'_z} \Delta v'_z ,$$

where $v_i' \equiv \left[\overline{v_i'^2} \right]^{1/2}$.

Now $\frac{\partial K}{\partial v_i'} = v_i'$, then follows:

$$\Delta K = v_x' \Delta v_x' + v_y' \Delta v_y' + v_z' \Delta v_z'$$

or, in terms of standard deviations,

$$\sigma_K = v_x' \sigma_x + v_y' \sigma_y + v_z' \sigma_z. \quad (V.44)$$

6.3. Cross correlations $\overline{v_r' v_z'}$ and $\overline{v_\theta' v_z'}$

From equations (V.23) and (V.24), one writes the standard deviations of the errors introduced in the cross correlations $\overline{v_r' v_z'}$ and $\overline{v_\theta' v_z'}$ as:

$$\sigma_{rz} = \sigma_{xz} \cos \theta + \sigma_{yz} \sin \theta, \quad (V.45)$$

$$\sigma_{\theta z} = \sigma_{yz} \cos \theta + \sigma_{xz} \sin \theta. \quad (V.46)$$

The subscripts represent the cross correlation.

Analogously to eq. (V.44), from eqs. (V.19) and (V.20), one obtains

$$\sigma_{xz} = v_1' \sigma_1 + v_2' \sigma_2, \quad (V.47)$$

$$\sigma_{yz} = v_3' \sigma_3 + v_4' \sigma_4. \quad (V.48)$$

With the values of σ_{xz} and σ_{yz} given by (V.47) and (V.48) plugged into eqs. (V.45) and (V.46), the errors of $\overline{v_r' v_z'}$ and $\overline{v_\theta' v_z'}$ are found.

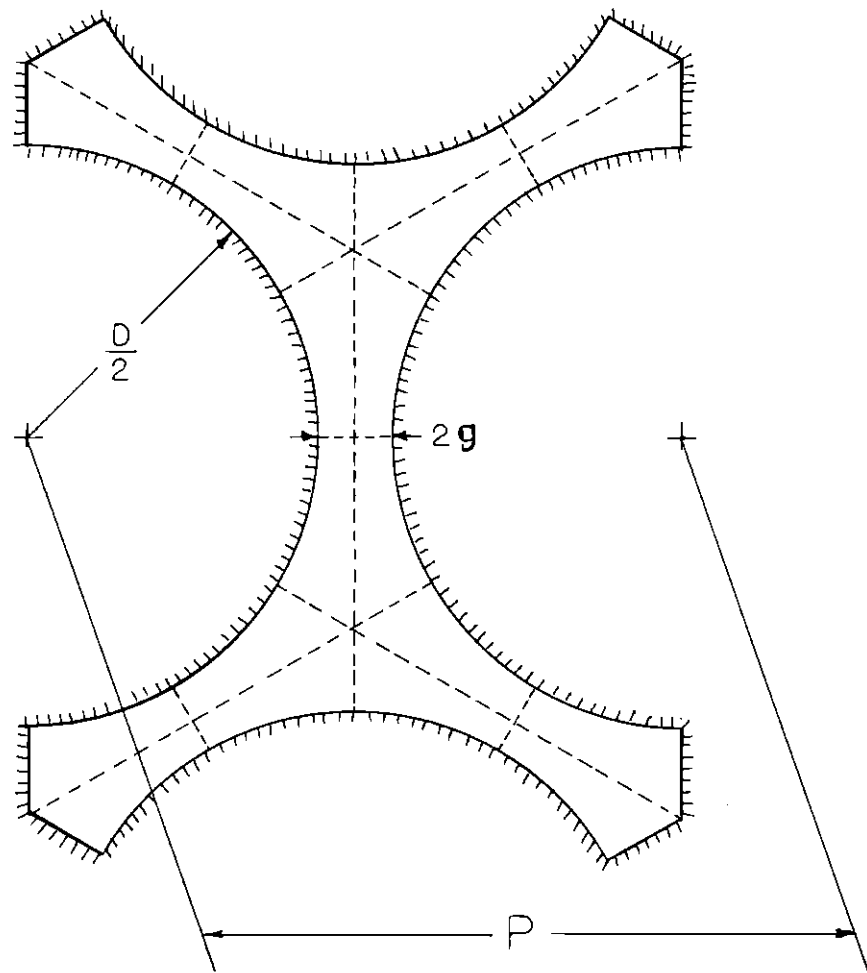


Fig. V.1. Cross-Section Shape of Test Section

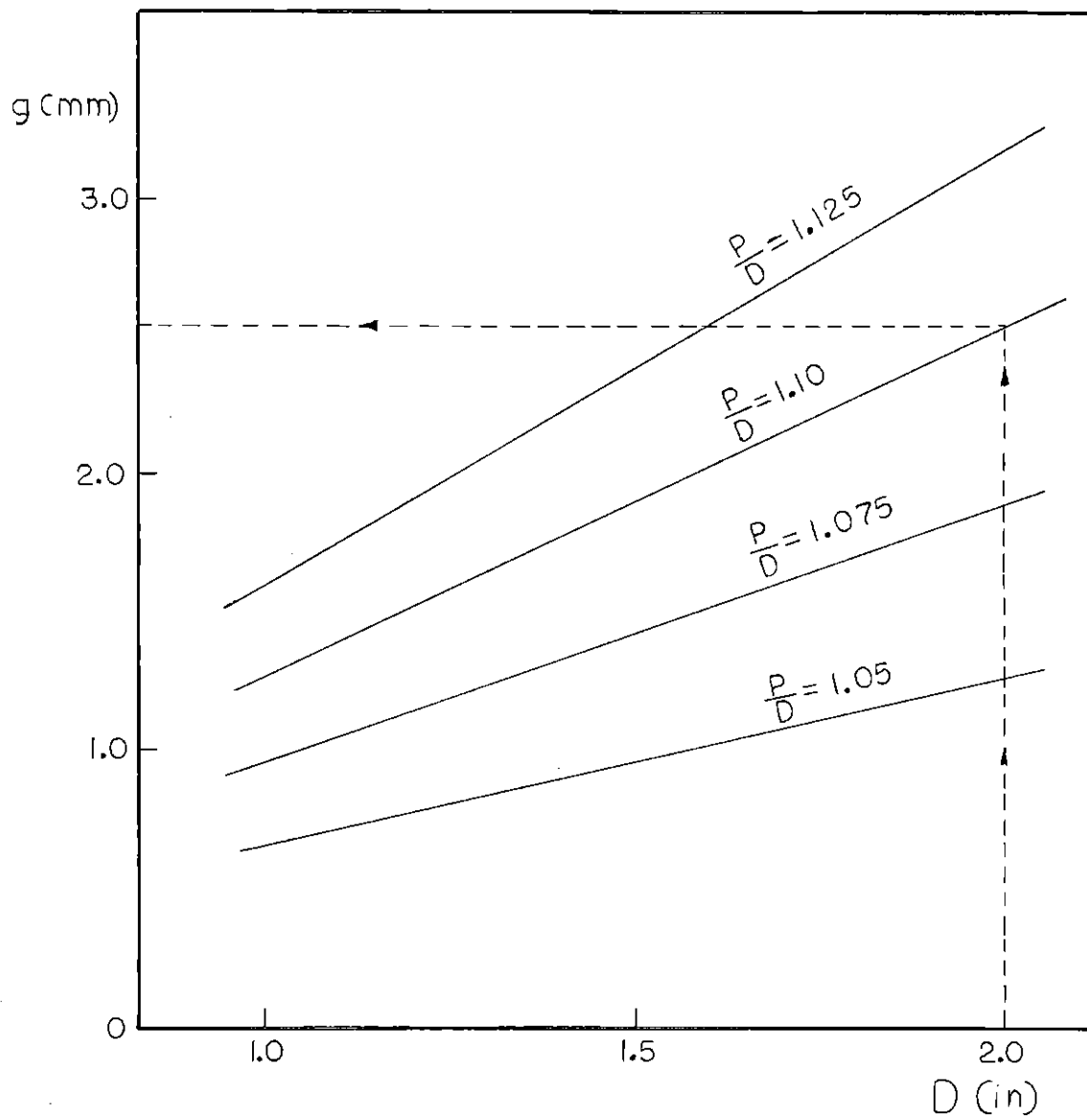


Fig. V.2. Variation of the Half-Gap Size with Rod Diameter for Different Values of P/D

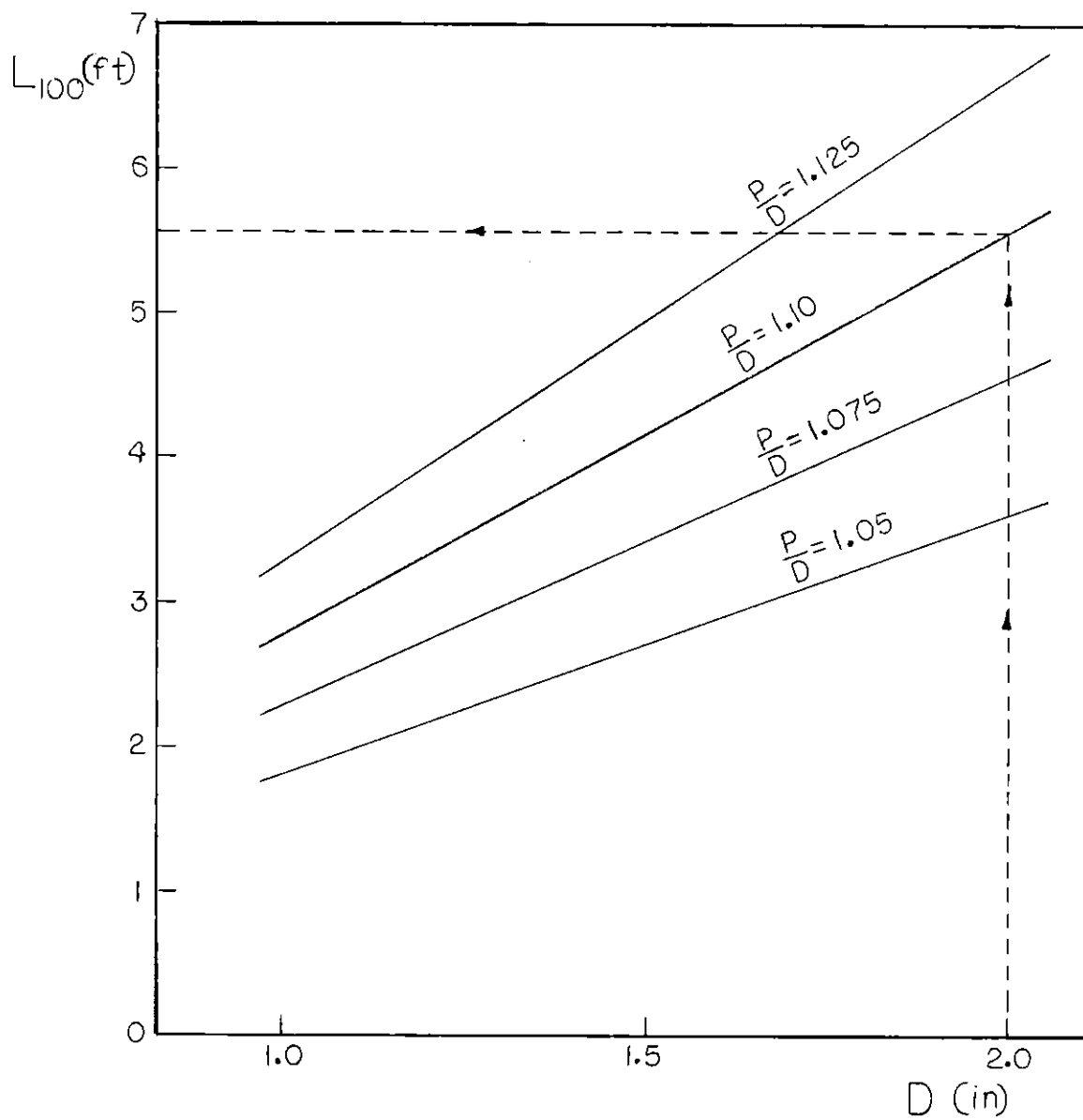


Fig. V.3. Variation of Length of Test Section for 100 D_H with Rod Diameter for Different Values of P/D

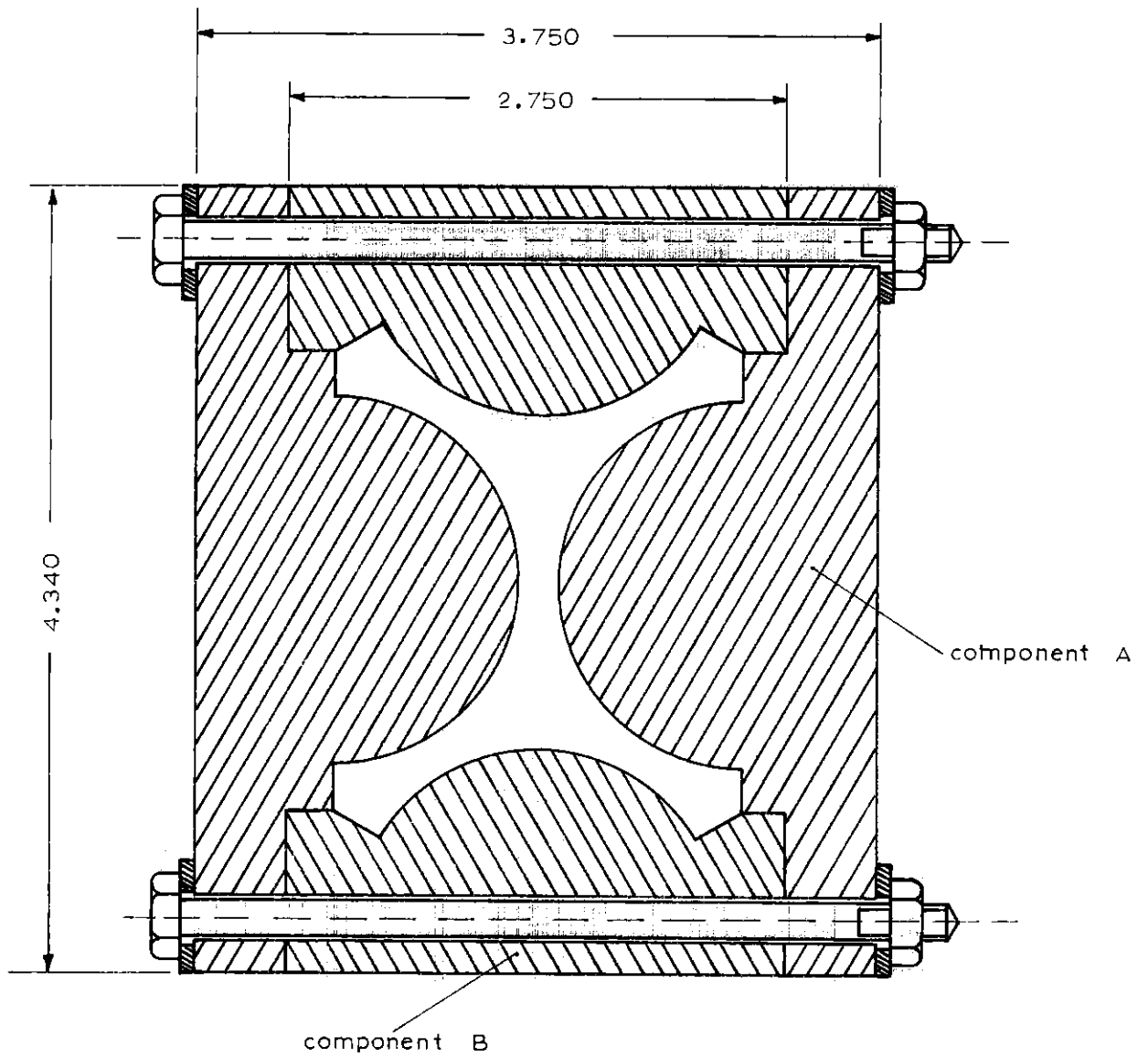


Fig. V.4. Cross-Section View of Test Section

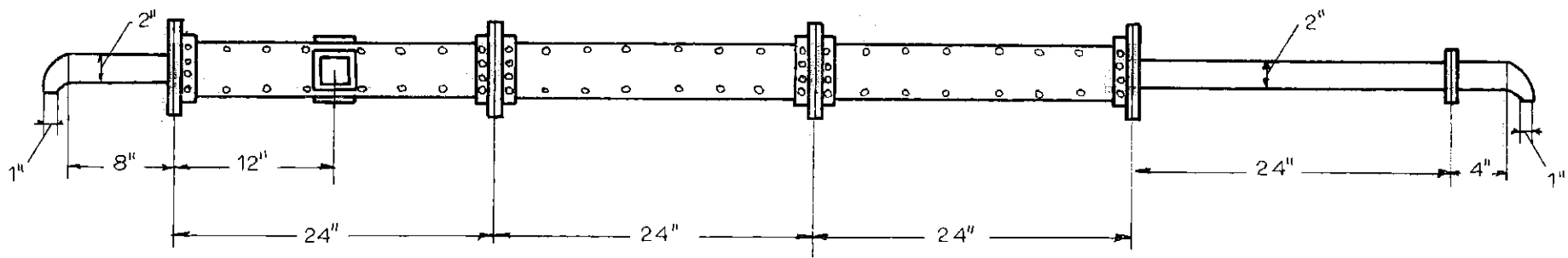


Fig. V.5. Test Section: Overall View

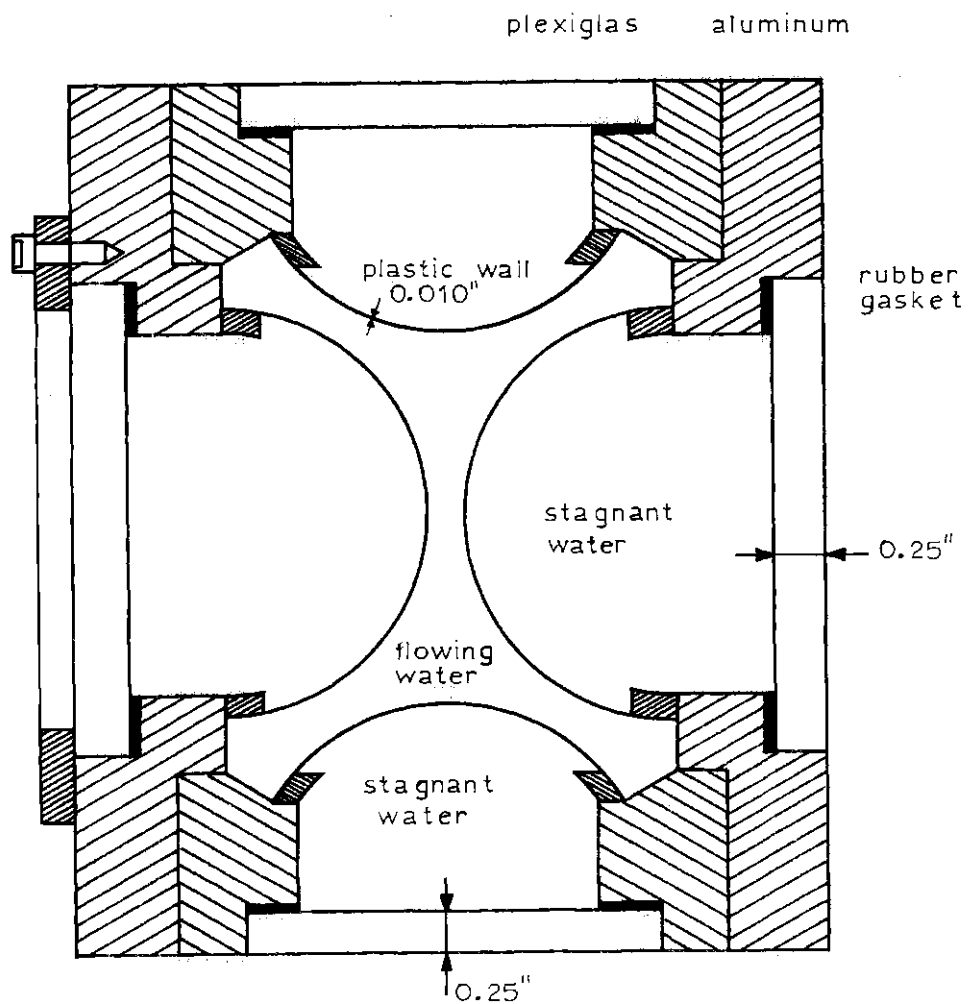


Fig. V.6. Design of Test Section Windows

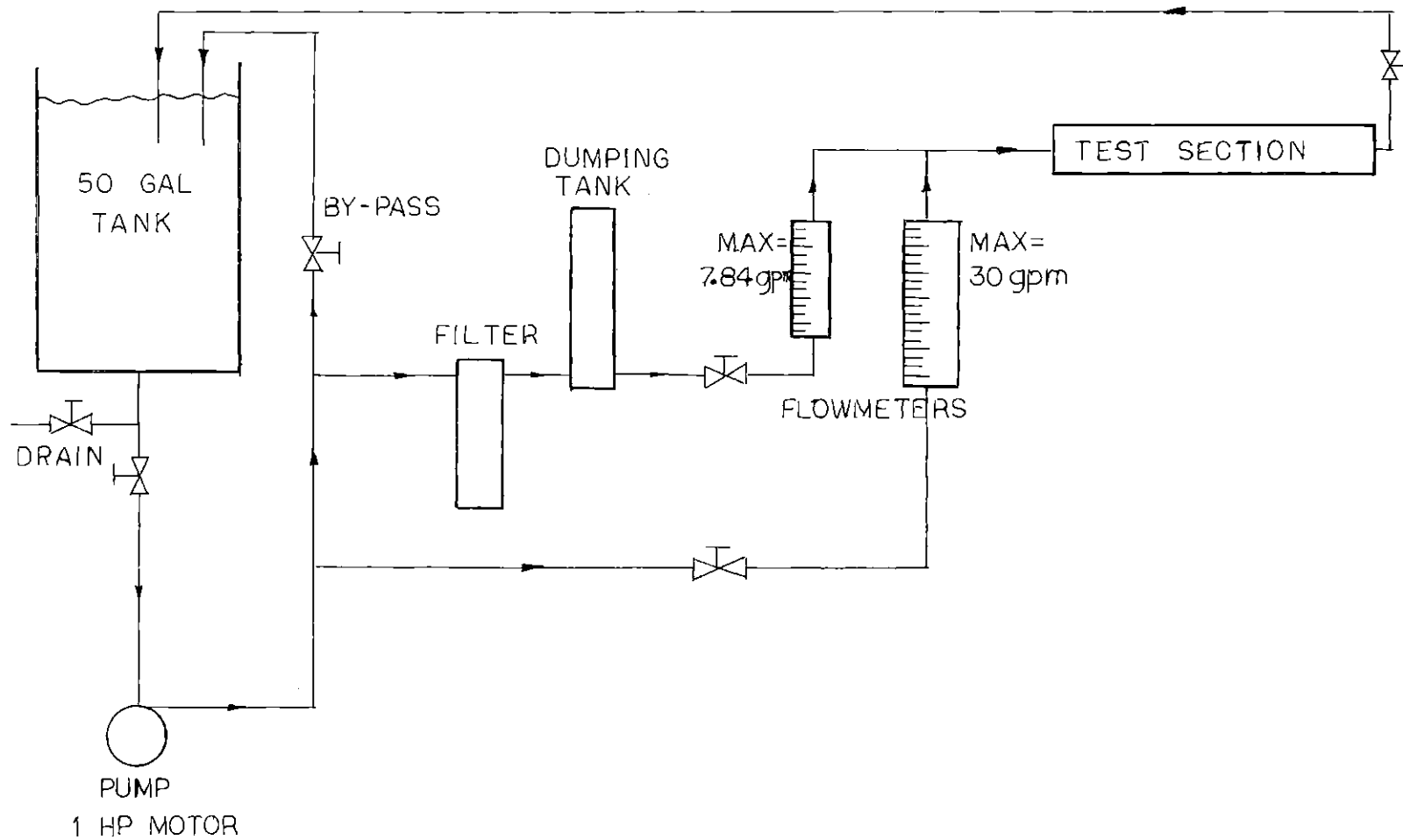


Fig. V.7. The Hydraulic Loop

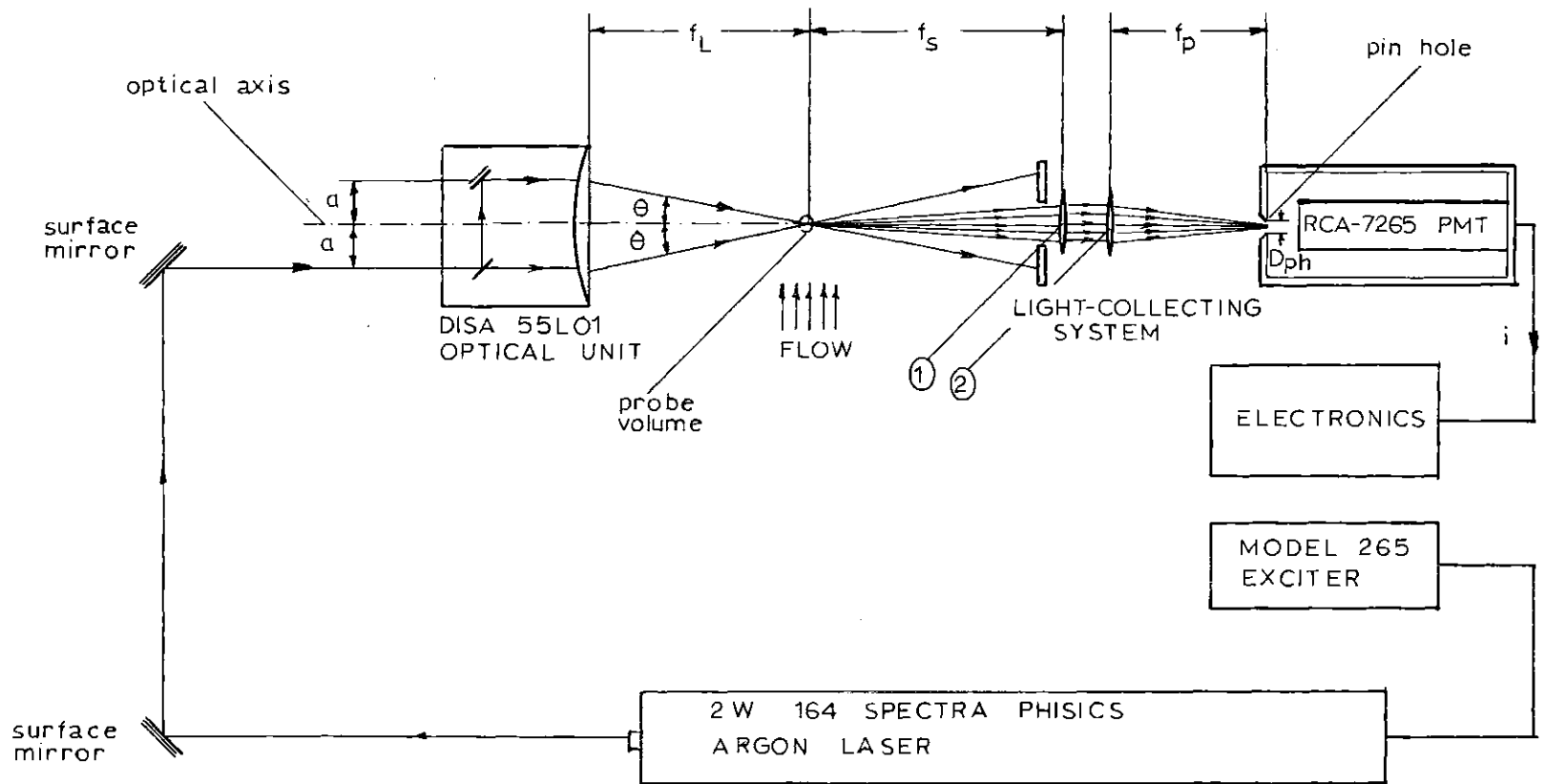


Fig. V.8. Laser Doppler Anemometer Set-up

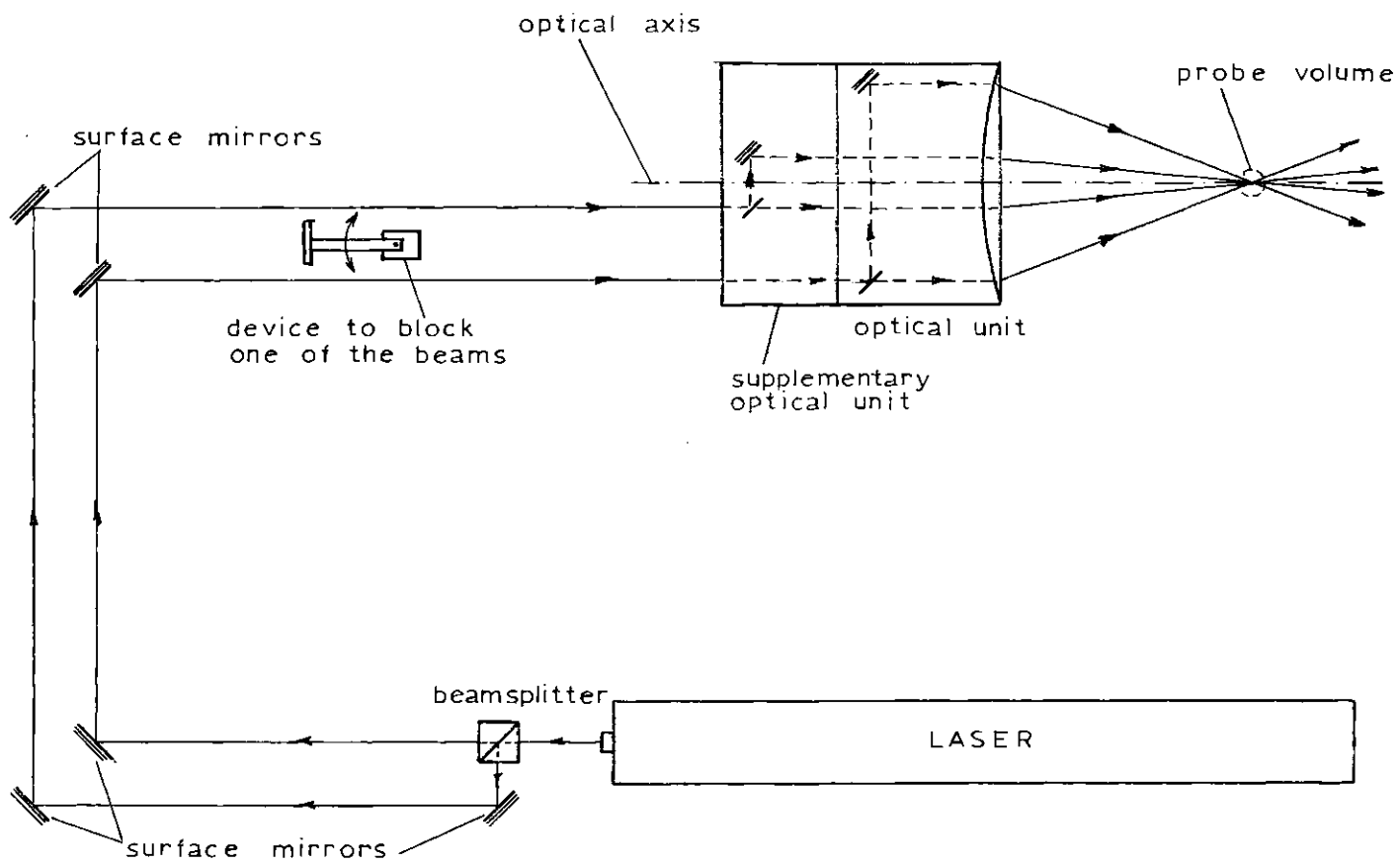


Fig. V.9. Sequential Method for Cross Correlation Measurements

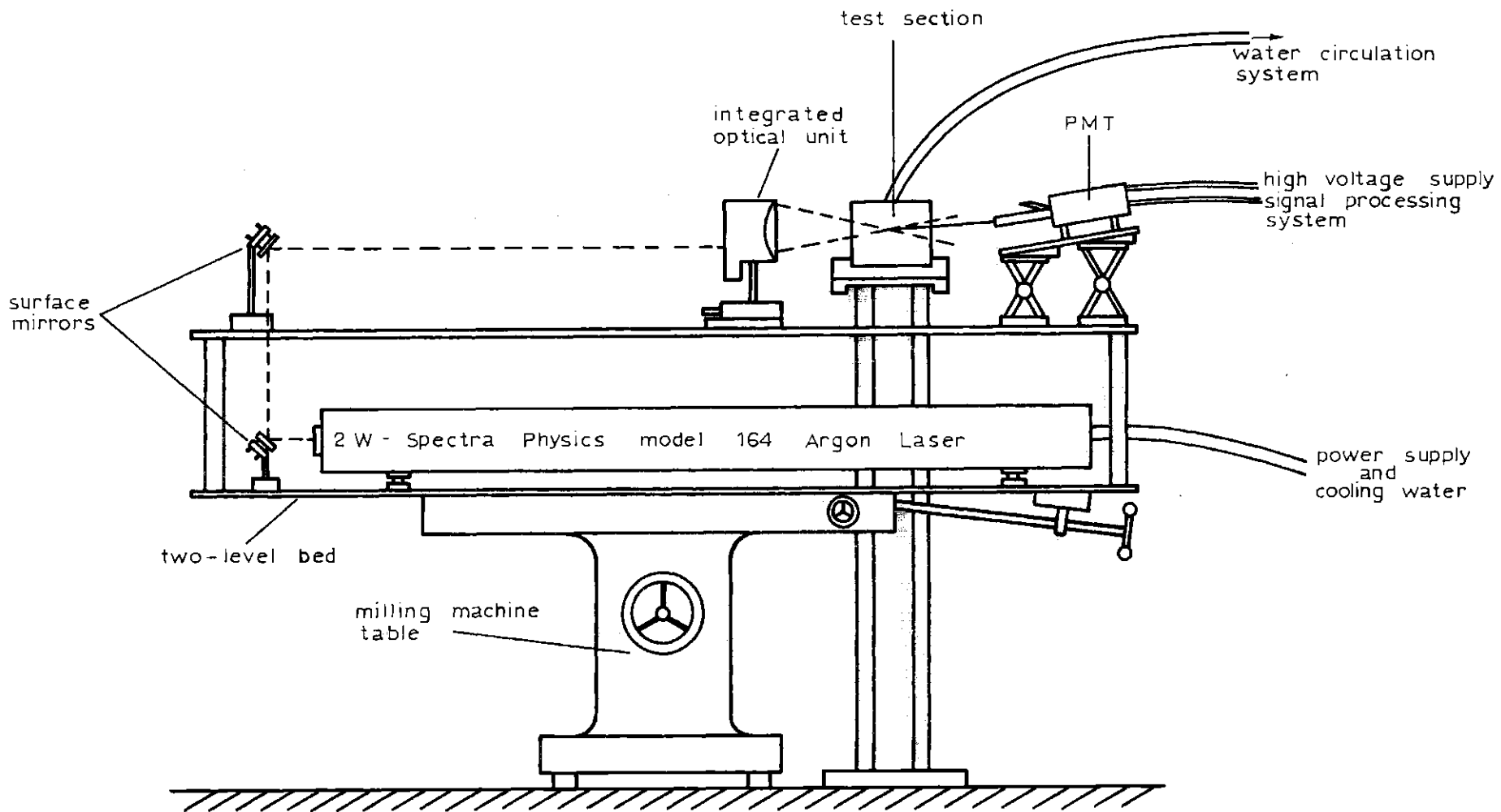


Fig. V.10. Experimental Set-up

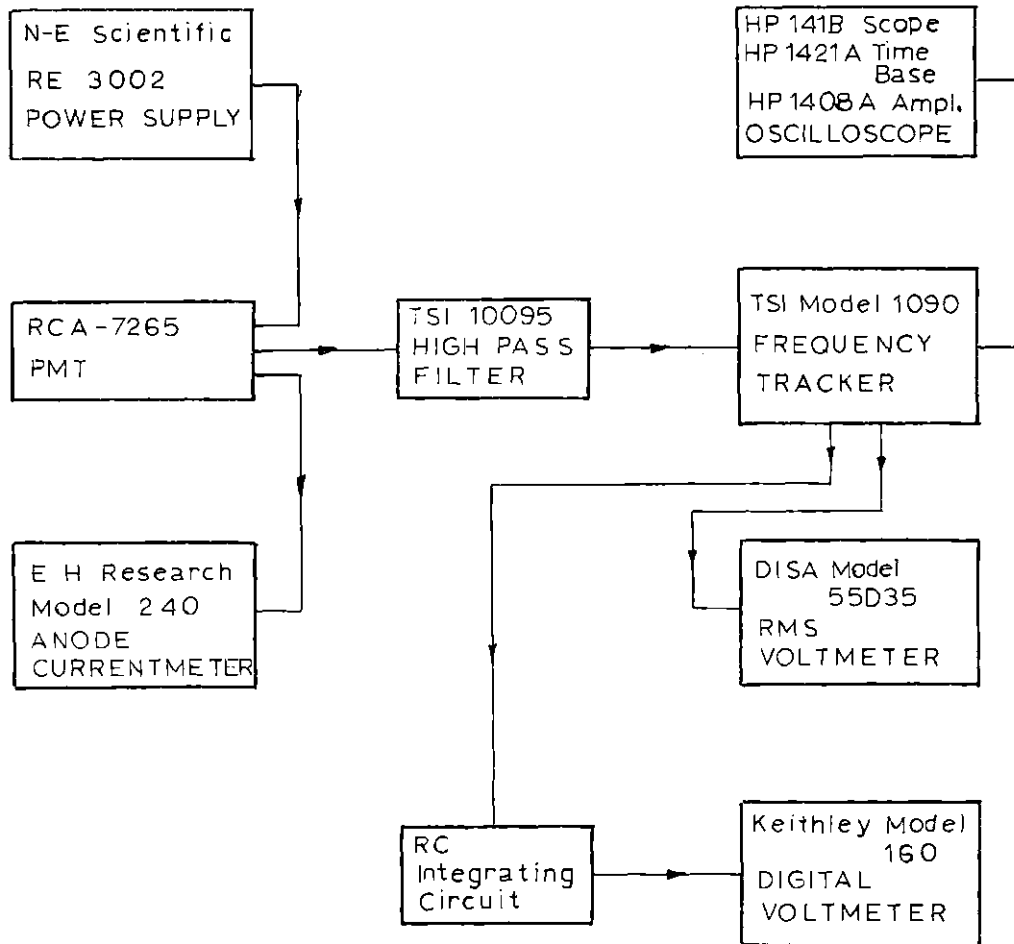


Fig. V.11. Signal Processing Electronics

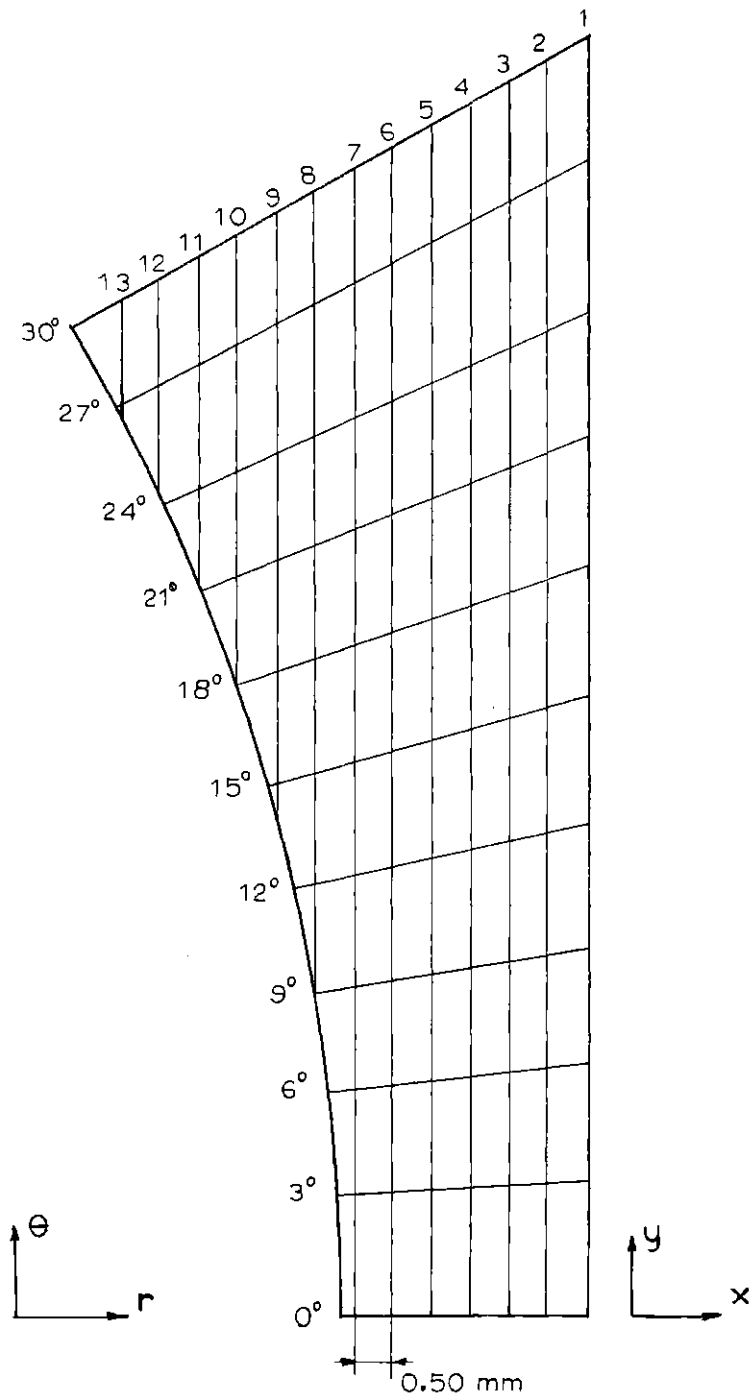


Fig. V.12. Mesh Grid for Experimental Measurements

REFERENCES

1. Tennekes, H. and Lumley, J.L., A First Course in Turbulence, The MIT Press, (1972)

CHAPTER VI

DISCUSSION OF RESULTS

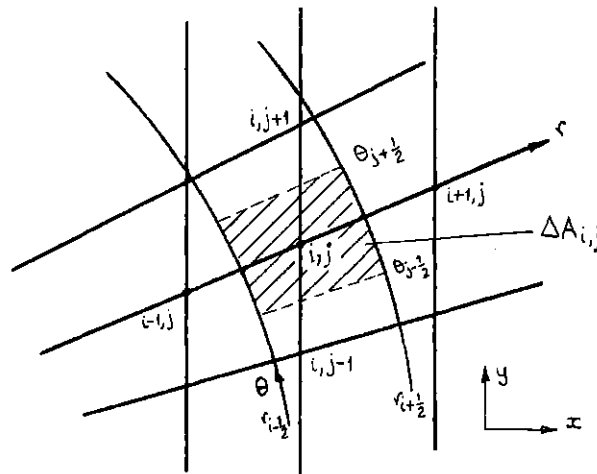
1. INTRODUCTION

Before performing the measurements at the maximum L/D_H position two preliminary tests were conducted: the first one, regarding the symmetry of the flow within the test section and the second one, related to the developing region of the flow. These tests are presented in detail in Appendix H. From the first test, it was observed that the flow, indeed, obeyed the symmetry lines of the cross section and that no assymetry was introduced in the flow by either the inlet nozzle or the fabrication of the test section. Regarding the development of the flow, it was observed that the differences between the velocity profiles for $L/D_H = 46$ and $L/D_H = 77$ were within the experimental error. However due to consistency of the deviations, it was concluded that, for values of L/D_H larger than 46, the flow was still in the developing region. Also it could not be concluded that the flow was fully developed at $L/D_H = 77$, since measurements for $L/D_H > 77$ were not permitted by the present test section. On the other hand, since the velocity profile did not change considerably in the range $L/D_H = [46, 77]$, there is no reason to believe that substantial modifications will occur for larger L/D_H .

Table VI.1 summarizes the measurements and conditions under which they were performed. The bulk velocity of the flow was calculated from the axial velocity measurements by numerically integrating the axial velocity over the area, i.e.,

$$v_b = \frac{1}{A_f} \sum_i \sum_j v_{i,j} \Delta A_{i,j} \quad (\text{VI.1})$$

where $v_{i,j}$ is the measured value of v_z at point i,j and $\Delta A_{i,j}$ can be observed from the sketch below.



$\Delta A_{i,j}$ is given by

$$\Delta A_{i,j} = \frac{1}{2} \Delta \theta (r_{i+1/2}^2 - r_{i-1/2}^2), \quad (\text{VI.2})$$

where $\Delta \theta$ is angular separation between two consecutive radial lines,

TABLE VI.1. Operational conditions for measurements
performed in rod bundle with P/D = 1.123

TEST	$\frac{L}{D_H}$	$Re \times 10^{-3}$	MEASURED PARAMETERS
A. PRELIMINARY TESTS			
I. Symmetry test	77	27	\bar{v}_z
II. Developing Region	15	26	\bar{v}_z
	46	27	\bar{v}_z
	77	27	\bar{v}_z
B. MEASUREMENTS			
I. Axial velocity	77	7.9	\bar{v}_z
	77	27	\bar{v}_z
II. Cross correlations:			
$\overline{v'_x v'_z}$	77	27	$\overline{v_1'^2}, \overline{v_2'^2}$
$\overline{v'_y v'_z}$	77	27	$\overline{v_3'^2}, \overline{v_4'^2}$
III. Turbulent intensities	77	27	$\overline{v_x'^2}, \overline{v_y'^2}, \overline{v_z'^2}$
IV. Secondary flow search	77	27	\bar{v}_x, \bar{v}_y
V. Pressure drop	15	26	Δp
	46	27	Δp
	77	27	Δp

$$r_{i+1/2} \equiv \frac{(r)_{i+1,j} + (r)_{i,j}}{2}, \quad (\text{VI.3})$$

and

$$r_{i-1/2} \equiv \frac{(r)_{i,j} + (r)_{i,j-1}}{2} \quad (\text{VI.4})$$

In order to check the consistency of the present measurements, for $P/D = 1.123$, of the axial velocity distribution, the results were compared to Eifler and Nijsing's⁽¹⁾ data for $P/D = 1.10$ and $P/D = 1.15$ and close values of Re . The present data were expected to be between those measurements which, in fact, occurred as can be observed in Figs. VI.1.(a), (b) and (c), for different values of θ .

From this point on, only measurements at $L/D = 77$ will be considered.

2. EXPERIMENTAL DATA OBTAINED IN THE PRESENT WORK

Figures VI.2.(a) and (b) show the velocity distribution maps (or isovels) for $Re = 7.9 \times 10^3$ (flow rate = 7.5 gpm) and $Re = 2.7 \times 10^4$ (flow rate = 22.5 gpm). The differences observed were larger than expected. The differences were attributed to the instability of DISA Model 55L20 frequency tracker utilized in the measurements for the lower Re , requiring very short integration time (1 sec) to get the time-averaged values of the velocity. Frequent loss of tracking made these results unreliable. After this fact was noticed, only the TSI Model 1090 frequency tracker was used since the DISA tracker was

being modified by the manufacturer.

The curvature of the isovels (see Fig. VI.2.(b)), for θ close to 30° , represents a clear indication of the existence of secondary flow moves in the direction of the subchannel symmetry line (MVL) for $\theta \sim 30^\circ$. The loop is closed with the flow moving toward the wall for $\theta \sim 15^\circ$. The center of the loop is probably in range $\theta \sim (20^\circ-25^\circ)$. The deformations of the isovels near the gap can be the result of either or both of the following speculations. The first one is that the isovels in this region are not affected by the secondary flow loop described above. Since such flow pushes the isovels in the wall direction in center of the channel, deformations are created by continuity of velocity distribution. The second one, is the possible existence of one more secondary flow swirl, in the gap region, with the flow moving in the opposite direction of the one described above. In any case, such observation is not in agreement with the secondary flow pattern suggested by Nijssing (described in Chapter II, Section 2.6). His proposed pattern leads to only one secondary flow loop with the center at, approximately, $\theta = 15^\circ$.

Figure VI.3 presents contours of constant turbulence kinetic energy.

Figure VI.4 shows the distribution of the Reynolds shear stress in the radial direction, $\overline{v'_r v'_z}$, compared to the linear distribution assumed by Nikuradse for pipe flow (see, for

example, Ref. 2, p. 568). An approximately linear behavior is also observed for the experimental points.

Due to the fact that, except for P/D approaching 1, the assymetry of the subchannel is not very large, the assymetry of the distribution of v'_θ is also small. So, the values of $\overline{v'_\theta v'_z}$, that are directly related to the distribution of v'_θ , should be very small. The experimental error, however, is large due to the fact that $\overline{v'_\theta v'_z}$ is calculated from measurements of large quantities (see Chapter V, Section 4.3). This led to very scattered experimental data as shown in Fig. VI.5. No attempt was made to interpret these results.

The experimental data for $Re = 2.7 \times 10^4$ are tabulated in Appendix I.

3. ERROR ANALYSIS

The expressions required for error analysis have been discussed in Chapter V, Section 5.

3.1 Axial velocity distribution

The bulk velocity, for $Re = 2.7 \times 10^4$, is $v_b = 1.35$ m/s. The error due to flow fluctuation, obtained from Eq. (V.27) is

$$\frac{\sigma_F}{v_b} \times 100 = \frac{30}{22.5} \cdot \frac{v_i}{400} \cdot \frac{100}{v_b} .$$

Hence, using a typical value of v_i/v_b equal to 1.0

$$\frac{\sigma_F}{v_b} \times 100 = 0.3\% .$$

The analog voltage error is given by Eq. (V.28)

$$\frac{\sigma_A}{v_b} \times 100 = \frac{0.04}{1.35} \times 100 = 3.0\% .$$

As will be seen, the largest value of v_T is of the order of 65v. For water, at 20°C (68°F), $\nu = 1.01 \times 10^{-6} \text{ m}^2/\text{s}$. So, from Eq. (V.39)

$$\frac{\sigma_T}{v_b} \times 100 = \left(\frac{2 \times 60 \times 1.01 \times 10^{-6}}{10} \right)^{1/2} \frac{100}{1.35} = 0.3\%$$

So, the analog voltage error is much larger than the others. The total error, in the axial velocity, is, then

$$\frac{\sigma}{v_b} \times 100 \approx 3.0\% \quad (\text{VI.5})$$

3.2 Turbulence kinetic energy

From Eq. (V.29), on average, taking $v_1 \equiv \sqrt{v_1'^2}$,

$$\frac{\sigma_{A'}}{v_1'} \times 100 = \frac{0.04}{1.35} \times 100 \approx 3.0\%$$

where v_1' was taken equal to v_b .

Close to the wall, where $v_1' < v_b$, the error is larger than the typical value above, while it decreases as the position moves away from the wall toward the center of the channel. The error introduced by the RMS voltmeter, for the range of voltage obtained, was estimated to be of the order of 5%. So, the

total error, on average, is approximately 6%, for each turbulent intensity. Table VI.2 shows the order of magnitude of turbulent intensities, near the wall and MVL.

TABLE VI.2
ORDER OF MAGNITUDE OF TURBULENT INTENSITIES AND ERRORS.

DIRECTION	TURBULENT INTENSITY (VOLTS)		ERROR (VOLTS)	
	MVL	CLOSE TO WALL	MVL	WALL
v'_x	.060	.100	.0036	.006
v'_y	.065	.110	.0039	.0066
v'_z	.115	.250	.0069	.015

From Eq. (V.44),

$$\sigma_k \sim (0.0013 - 0.0051) \text{ Volts}^2$$

or

$$\frac{\sigma_k}{K} \times 100 \approx 12\%$$

3.3 Cross correlations $\overline{v'_r v'_z}$ and $\overline{v'_\theta v'_z}$

The application of Eqs. (V.45-48) led to the conclusion that σ_{rz}/v_T^2 is in the range (0.35-0.52) as the angular position changes from $\theta = 0^\circ$ to $\theta = 30^\circ$.

Analogously, $\sigma_{\theta z}/v_{\tau}^2$ varies in the range (0.45-0.56) as θ goes from 0° to 30° .

4. SECONDARY FLOW SEARCH

A search was conducted in order to detect secondary flows, using the DISA Model 55L02 Flow Direction Adapter, however it was not successful. The reason was attributed to the error associated with the analog voltage produced by the frequency tracker. The frequency shift used in the search was 250 KHz and the tracker was operated in the range of 500 KHz. Since the analog voltage error is 1% f.s.d. of the range of operation, this error is of the order of 5 KHz. This means that, for the secondary flow be detected, it has to generate a frequency shift, at least, of the order of 5 KHz. Since this did not occur, it was concluded that secondary flows were smaller than the velocity corresponding to 5 KHz, that is, smaller than 0.009 m/s. This means that the secondary flow velocities are smaller than 0.67% of the bulk velocity.

5. DETERMINATION OF MIXING LENGTH AND CONSTANTS OF THE MODEL

From the discussion of Chapter III, one writes:

$$C_v \frac{\ell}{\hat{y}} = \frac{\overline{-v'_r v'_z}}{\hat{y} K^{1/2} (\partial v_z / \partial r)} \quad (\text{VI.7})$$

From the experimental data for $\overline{v'_r v'_z}$, K and v_z , the value of $C_v \ell / \hat{y}$ can be estimated. This was carried out and

the results, for $\theta=0^\circ$ and $\theta=30^\circ$, are shown in Fig. VI.6, compared to values given by Buleev's formula (Eq. III.17) with $C_v = 0.20$. The discrepancies between the estimated values and Buleev's occur, mainly, for values of y/\hat{y} larger than 0.5. The average curve shown in Fig. VI.6 represents the average radial distribution of the mixing length over all angular positions where measurements were performed. Assuming $l=y$ for points close to the wall, this average is closely represented by

$$\frac{l}{\hat{y}} = \frac{y}{\hat{y}} \quad , \quad \text{for } 0 \leq \frac{y}{\hat{y}} \leq 0.44,$$

(III.68)

$$\frac{l}{\hat{y}} = 0.44 + 0.066 \sin \left[\frac{\pi}{0.38} \left(\frac{y}{\hat{y}} - 0.44 \right) \right] ,$$

for $0.44 < \frac{y}{\hat{y}} \leq 1.0$, with C_v equal to 0.180. This distribution of the mixing length were used in the analytical analyses, although the utilization of Buleev's equation would not introduce appreciable error since the discrepancies occur only over a region where axial velocity gradients are not very large.

Now, to determine C_D , one observes, from Fig. VI.7, that close to the wall $K = 3.4 v_T^2$. From Eq. (III.46)

$$\frac{C_v}{C_D \kappa^2} = 3.4 \quad . \quad \text{(VI.8)}$$

Hence, $C_D \approx 0.30$. Better agreement, however, with measurement of the TKE distribution, were obtained for $C_D \approx 0.38$, as can be seen from Fig. VI.8, for $\theta=0^\circ$. Similar behavior occurs for other values of θ . So, the value of 0.38 was adopted for C_D .

The discussion of the other constants was already presented in Chapter III. Table VI.3 compares the constants used in the present work with those used in the past.

6. COMPARISON OF EXPERIMENTAL AND ANALYTICAL RESULTS

In this section, experimental and analytical results for P/D equal to 1.123 ($Re = 2.7 \times 10^4$) and 1.217 ($Re = 1.49 \times 10^5$) will be discussed. The experimental data for $P/D = 1.123$ are those obtained by the present author and for $P/D = 1.217$ are Kjellström's⁽⁶⁾. The axial velocity distributions, for sake of comparison, were also computed by the Ibragimov's method, described in Chapter II, Section 2.c. The predictions performed by the present one-equation model, for $P/D = 1.123$, were carried out, utilizing (a) $C_v = 0.180$ and $C_D = 0.38$, which are the values obtained by the author for those constants and (b) $C_v = 0.22$ and $C_D = 0.41$, which are the values for these constants most frequently recommended in the literature.

6.1 First case: $P/D = 1.123$

Figures VI.9.(a), (b) and (c) show the axial velocity distributions for $\theta=0^\circ$, 15° and 30° , respectively. It can be observed that the results obtained by the present method provide a closer agreement to the experimental data than those obtained by Ibragimov's method over most of the subchannel. The agreement was not satisfactory in the gap region, though. As discussed in Appendix G, Section 2, the experimental data may have been taken in the developing region where the tendency of velocity distribution in the gap region is to decrease. Since a small decrease in the gap region would not affect considerably the velocity distribution elsewhere due to the area and velocity magnitude relations, this could explain the behavior. The worst deviation, nevertheless, was less than 4%.

Figures VI.10.(a), (b) and (c) show the TKE distributions for $\theta=0^\circ$, 15° and 30° , respectively. The agreement between experimental and analytical results are within 10%.

The comparison between the predictions using the values of C_v and C_D suggested here and using the typical values for them is presented in Fig. VI.9 and 10. These results demonstrate the generality of the present one-equation model, in particular the fact that typical values of C_v and C_D can be utilized to handle an arbitrary rod bundle geometry without unacceptable error.

Figure VI.11 shows the streamlines of the secondary flow as predicted by the present model with $C_v = 0.180$ and $C_D = 0.38$. Two loops of secondary flow were obtained flowing in the directions indicated by the arrows. The strongest loop has its center at $\theta \approx 23^\circ$ and, as will be shown later in this chapter, the secondary flow velocity is always less than 0.6% of the bulk velocity. The weakest loop, near the gap, has its center at $\theta \approx 8^\circ$ and the secondary flow velocity is less than 0.2% of the bulk velocity. The present finding of two swirls of secondary flow as well as their position in the subchannel are in agreement with the discussion of Section 2. The order of magnitude of the secondary flow is within the expected range as described in Section 4.

6.2 Second case: $P/D = 1.217$

Figures VI.12.(a), (b) and (c) show the axial velocity distributions for $\theta = 0^\circ$, 15° and 30° . The results obtained by the present method are in closer agreement with the experimental data than those obtained by Ibragimov's method. The deviation is below 4% everywhere in the subchannel.

Figures VI.13.(a), (b) and (c) show the comparison between analytical and experimental TKE distributions for $\theta = 0^\circ$, 18° and 30° . The agreement is within 10%. Notice that, in this case, the experimental values of K were normalized by v_τ , instead of v_b in Figs. VI.10. v_b can be obtained with better

accuracy than v_τ , since v_b is obtained by integration of the axial velocity distribution given by a large number of velocity measurements over the subchannel area, while v_τ comes from single measurements of the local wall shear stress. So, errors in the value of v_τ may account for part of the deviation. Also, the analytical predictions, in this case, tend to give lower values than the experimental data, while, as can be observed from Figs. VI.10(a), (b) and (c), the predictions are usually larger than the experimental data. This may represent an indication that the constants C_v and C_D should be weak functions of P/D .

Figure VI.14 shows the predicted secondary flow streamlines. Here, again, two loops of secondary flow were observed with the difference that the strongest loop is spread over almost the entire subchannel with the weakest loop reduced to a small region near the gap and near the wall. However, the center of the strongest loop, when compared to the $P/D = 1.123$ case, has not moved considerably ($\theta \approx 21^\circ$, in this case). Kjellström attempted to measure the secondary flow velocity \bar{v}_θ and the experimental data that he obtained turned out to be very scattered. The present predictions were compared to these scattered data as shown in Fig. VI.15, for $\theta = 6^\circ, 12^\circ, 18^\circ, 24^\circ$. Although no definite conclusion can be drawn from this comparison, the analytical predictions are in agreement with the general trend of the experimental data.

7. APPLICATIONS OF THE THEORY

7.1 Wall shear stress distribution

Figures VI.16 and 17 show comparisons of experimental and analytical wall shear stress distributions for $P/D = 1.10$ and $P/D = 1.217$. The experimental data for $P/D = 1.10$ are those obtained by Subbotin and co-workers⁽⁷⁾ and for $P/D = 1.217$ are those obtained by Hall and Svenningsson⁽¹⁸⁾ and Kjellström⁽⁶⁾. The agreement between the experimental data and the predictions obtained by the present method is satisfactory, particularly for $P/D = 1.10$ (within 1%). For $P/D = 1.217$, the deviations were less than 2%, which is within the reported experimental error, and the experimental observation that, for this case, the maximum value of the wall shear stress does not occur at the angular position $\theta=30^\circ$ was also predicted. This feature is not predicted by Ibragimov's method.

7.2 Friction factor

The variation of the friction factor with the Reynolds number is shown in Fig. VI.18. For the same Re , the friction factors for rod bundle are larger than those for the smooth tube obtained by Blasius formula (Eq. II.8) and they increase as P/D increases.

7.3 Effect of Reynolds Number

The effect of the Reynolds number on the secondary flows and the wall shear stress distribution was studied for $P/D = 1.123$

Figure VI.19 shows the streamlines for $Re = 2 \times 10^5$. Comparing this figure to Fig. VI.11, it can be observed that the positions of the secondary flow loops do not change appreciably, but the loop closest to the gap becomes stronger as Re increases. Figure VI.20 shows a comparison between the predicted secondary flows for $Re = 2.7 \times 10^4$ and $Re = 2 \times 10^5$ for $\theta = 6^\circ, 12^\circ, 18^\circ, 24^\circ$. Observe that, for $\theta = 6^\circ$, which is within the weakest loop, the maximum value of v_θ/v_b goes from 0.15% to almost 0.4% while, for $\theta = 24^\circ$, within the strongest loop, the increase is only from 0.56% to 0.78%.

Since the secondary flows increase with Re , the wall shear stress distribution should be expected to become more uniform along the wall, which can be seen from Fig. VI.21. Due to the increase in the secondary flow rate wallward, near the center of the wall region, carrying high momentum flow, the position of the maximum value of the wall shear stress moves from $\theta = 30^\circ$ to lower values of θ .

7.4 Prediction of eddy diffusivities

Figure VI.22 shows a comparison between the turbulent viscosity distributions predicted analytically and the radial

eddy diffusivity estimated from the present experimental measurements, at different angular positions, for $P/D = 1.123$ and $Re = 2.7 \times 10^4$. The agreement is within 20%. As discussed in Section 3.3, the experimental error involved in the determination of $\overline{v_r'v_z'}$ is very large. Since $\epsilon_{m,r}$ is directly related to $\overline{v_r'v_z'}$ by the relation

$$\epsilon_{m,r} = - \frac{v_r'v_z'}{\left(\frac{\partial v_z}{\partial r}\right)}, \quad (\text{VI.9})$$

a deviation of 20% between predicted and experimental values is within the range of uncertainty due to experimental error.

8. FINAL NOTE

All the computations in this chapter were performed with the grid described in Chapter IV, Section 5. Sixteen angular positions, 2° apart, were used. The parameter λ , defined by the convergence criterion Eq. (IV.78), was taken as 0.0001. The computations were processed by an IBM Model 360/65. The average computation time, for each case, was of the order of 8 minutes.

TABLE VI.3

COMPARISON OF PRESENT VALUES OF CONSTANTS WITH VALUES IN THE LITERATURE

AUTHOR	C_v	C_D	σ_k	c_1	c_2	APPLICATION
Launder & Ying ⁽³⁾	0.22	0.39	1.5	2.6	0.365	Square duct
Wolfshtein ⁽⁴⁾	0.22	0.416	1.53			One-dimensional flow with turbulence augmentation and pressure gradient
Spalding ⁽⁵⁾	0.179	0.224	2.13			Heat transfer from turbulent separated flow
Present work	0.180	0.38	1.30	3.0	0.37	Rod bundle

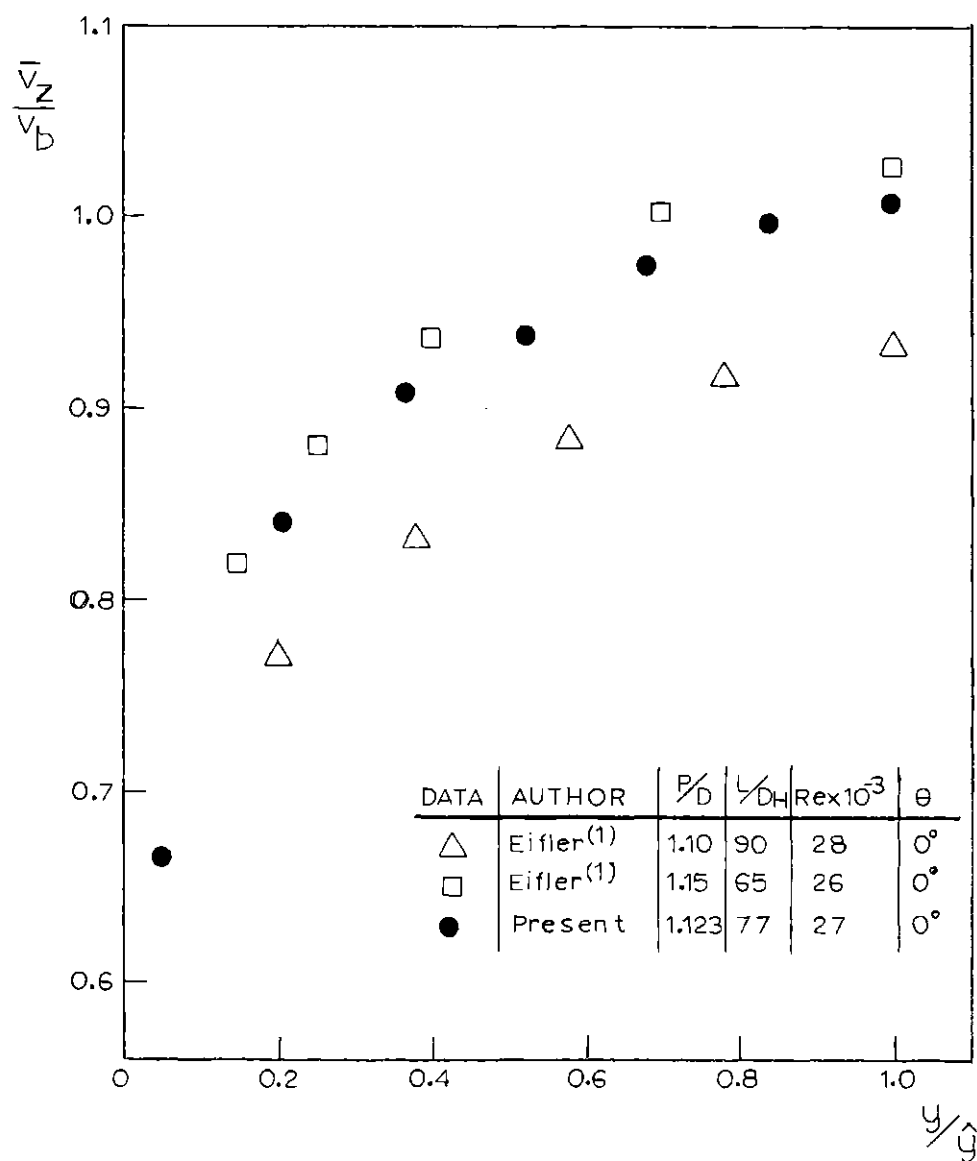


Fig. VI.1.(a) Comparison of Experimental Results for Axial Velocity

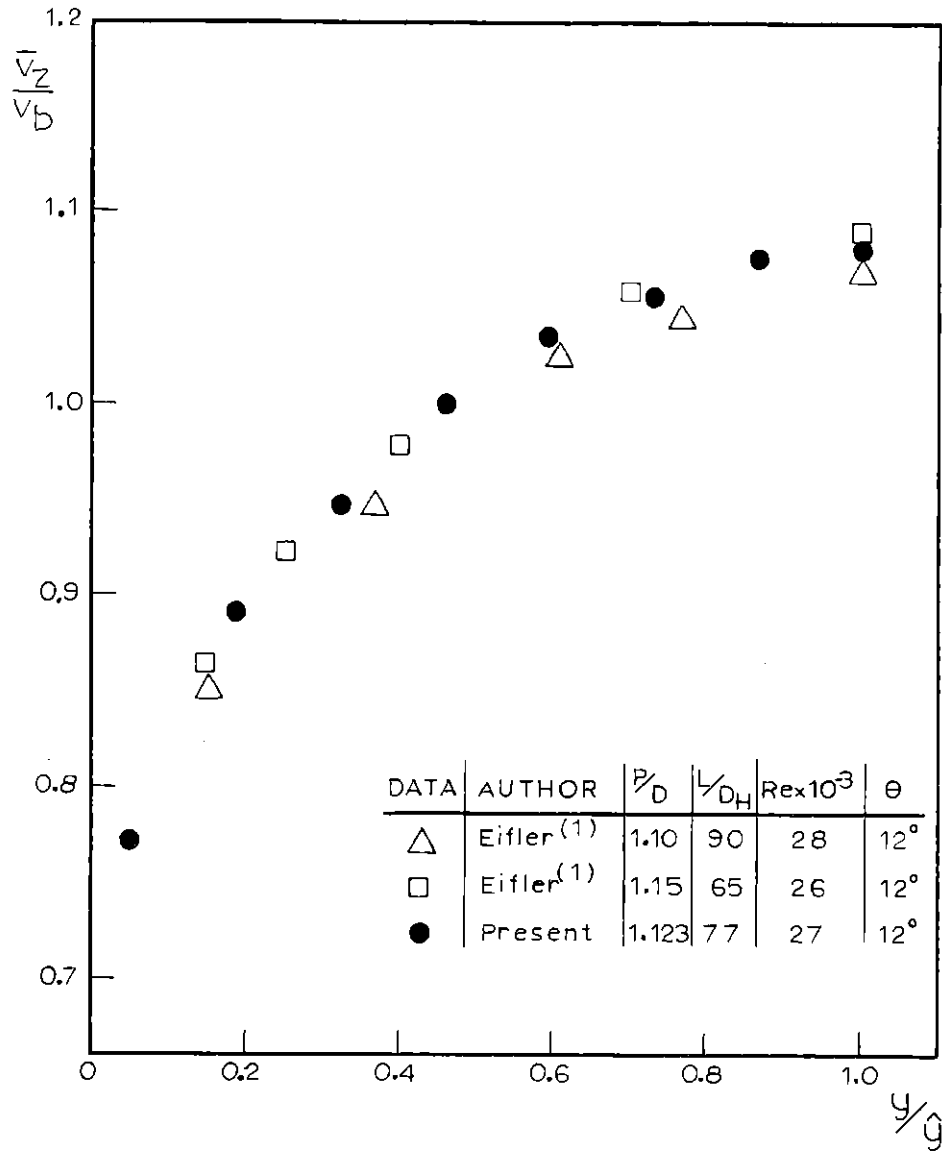


Fig. VI.1.(b) Comparison of Experimental Results for Axial Velocity

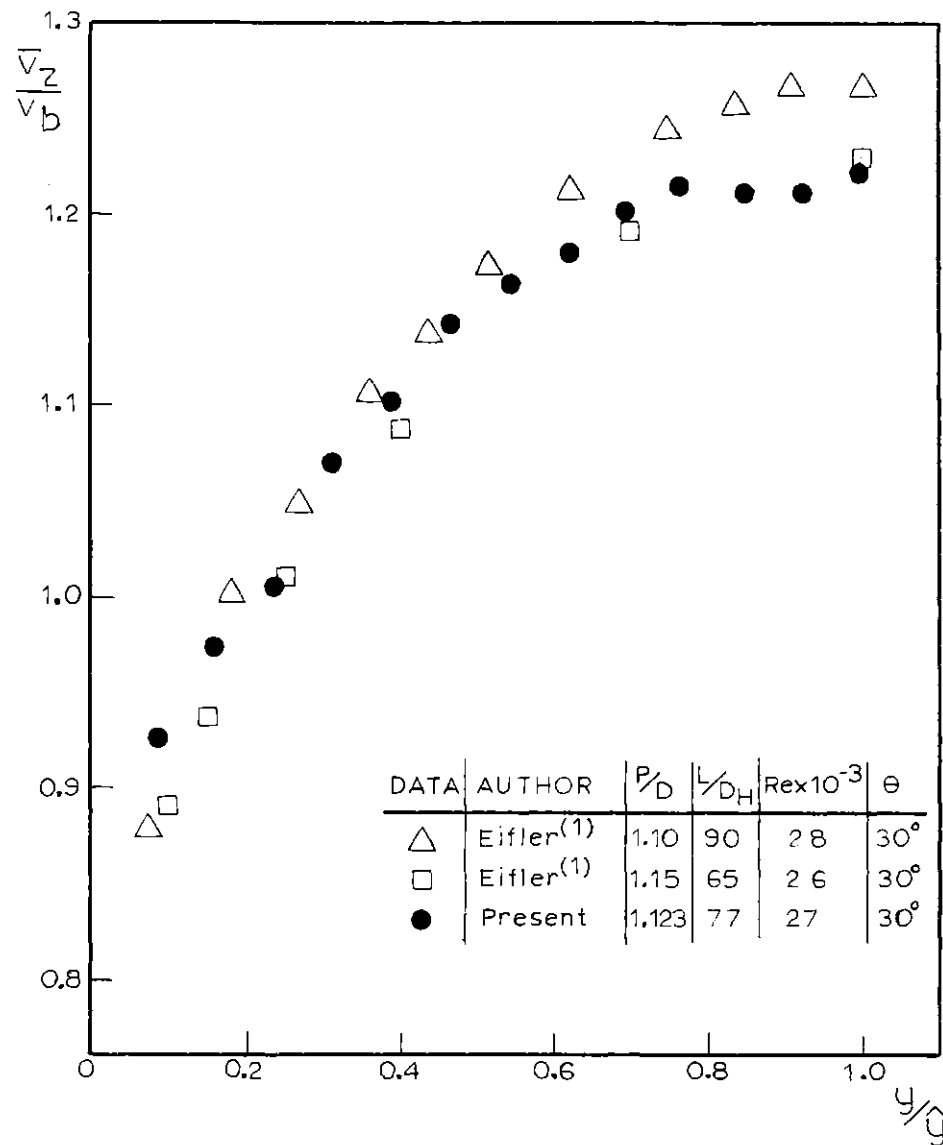


Fig. VI.1.(c) Comparison of Experimental Results for Axial Velocity

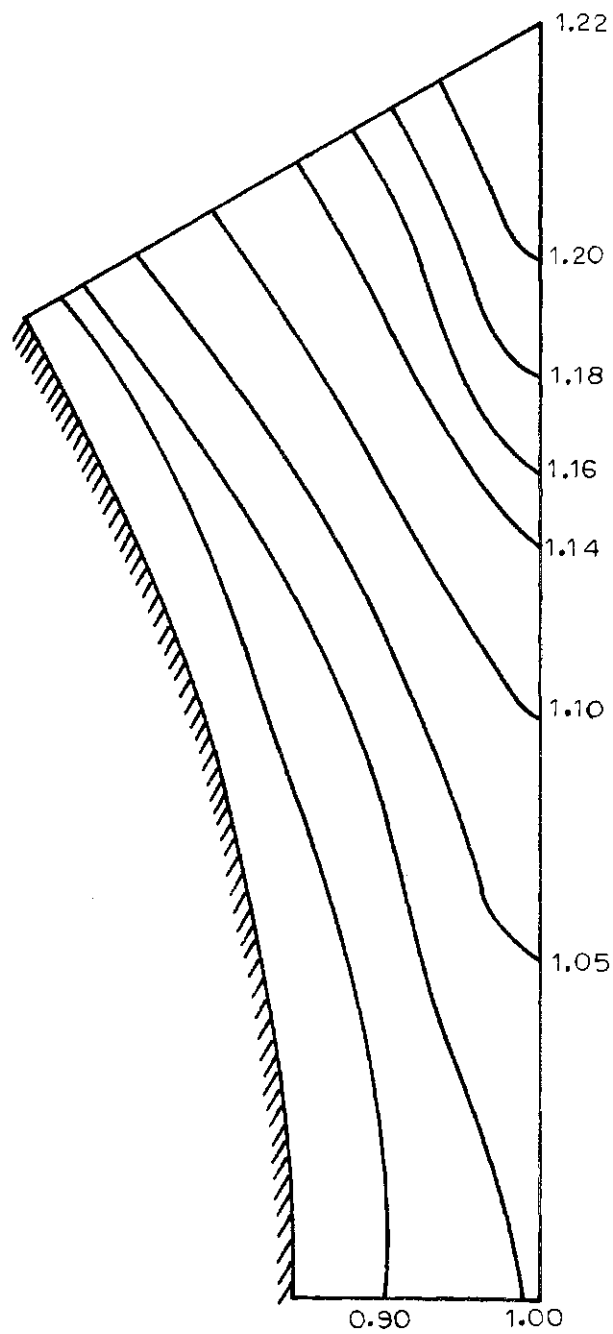
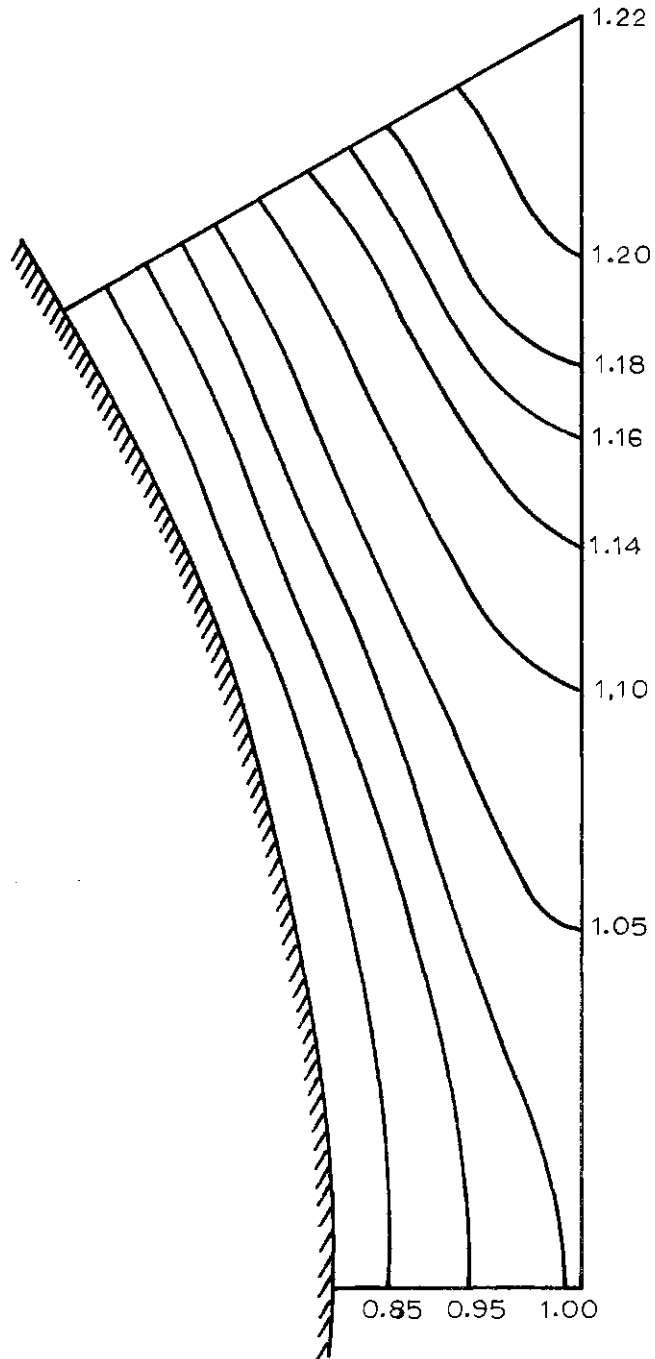


Fig. VI.2.(a) Isovel Plot for $\frac{L}{D_H} = 77$ and $\frac{P}{D} = 1.123$



Re = 27000

TSI Tracker

Fig. VI.2.(b) Isovel Plot for $\frac{L}{D_H} = 77$ and $\frac{P}{D} = 1.123$

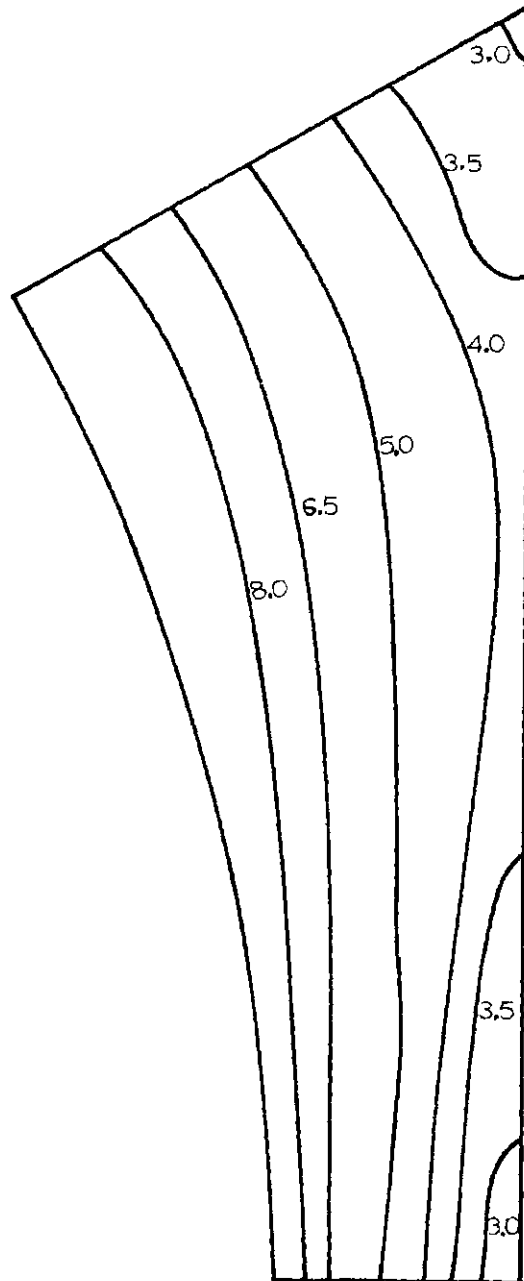


Fig. VI.3. Lines of Constant $\frac{K}{v_b} \times 10^3$ for $Re=27000$ and $\frac{P}{D}=1.123$

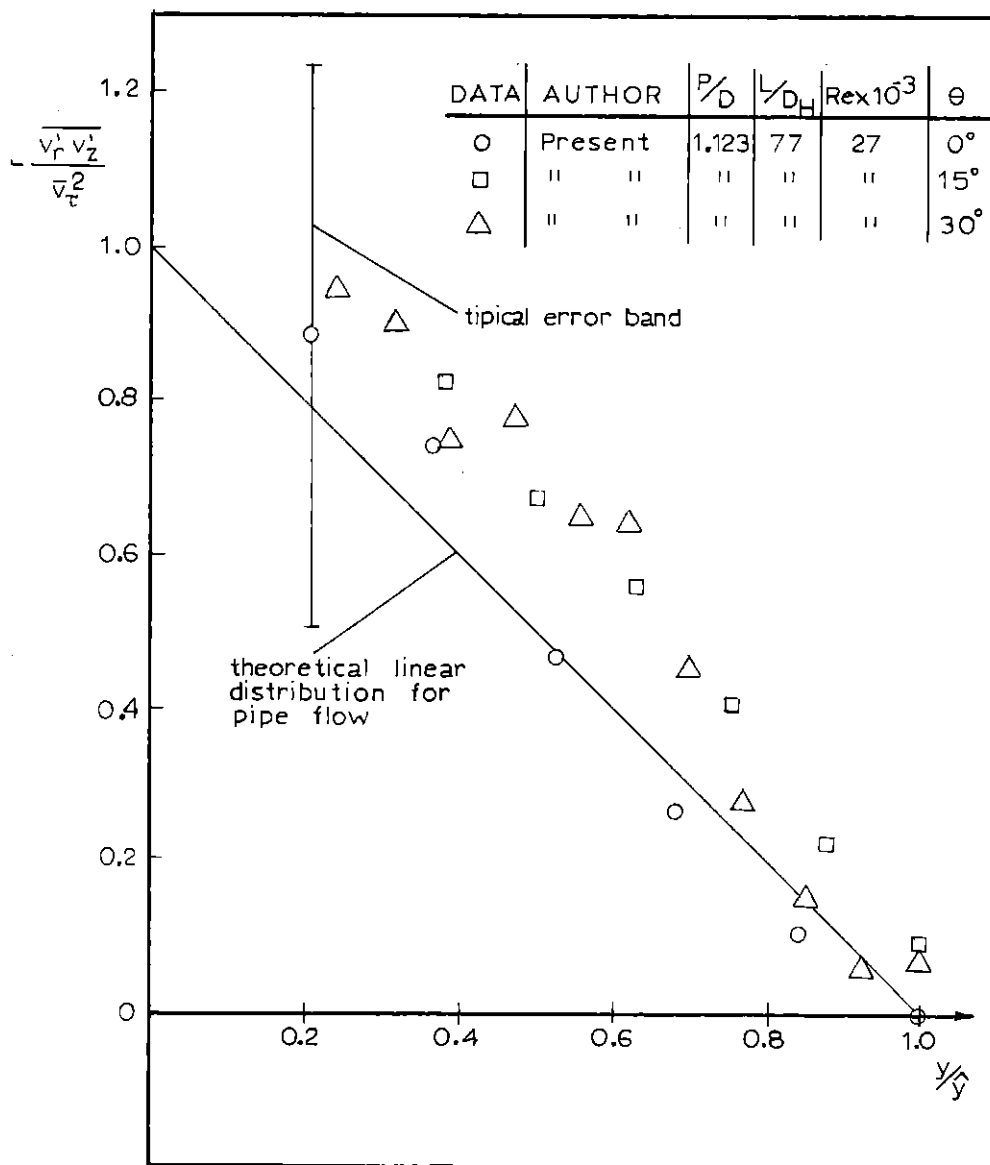


Fig. VI.4. Distribution of $-\frac{\overline{v_r'v_z'}}{\overline{v_\tau^2}}$

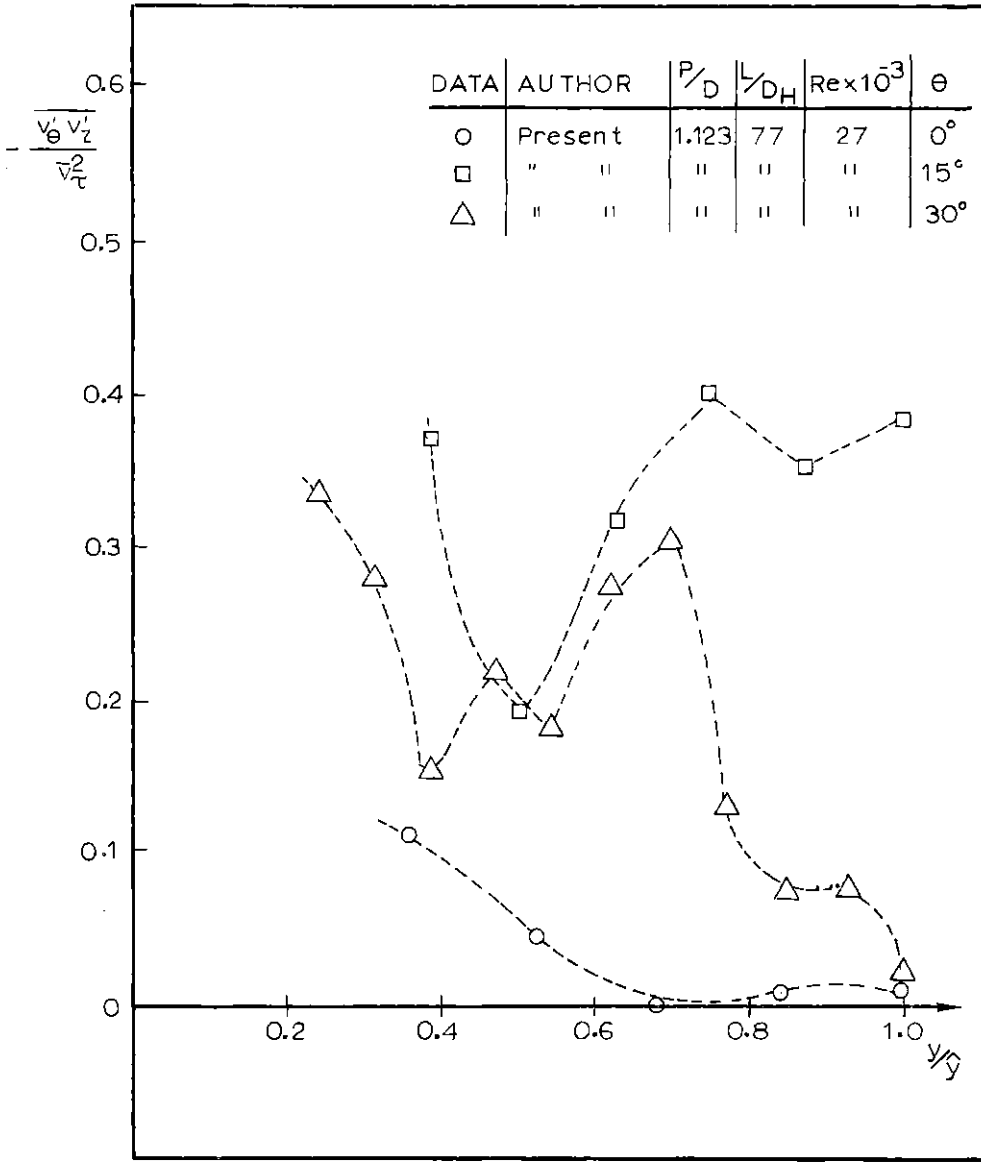


Fig. VI.5. Distribution of $-\frac{v'_\theta v'_z}{v_T^2}$

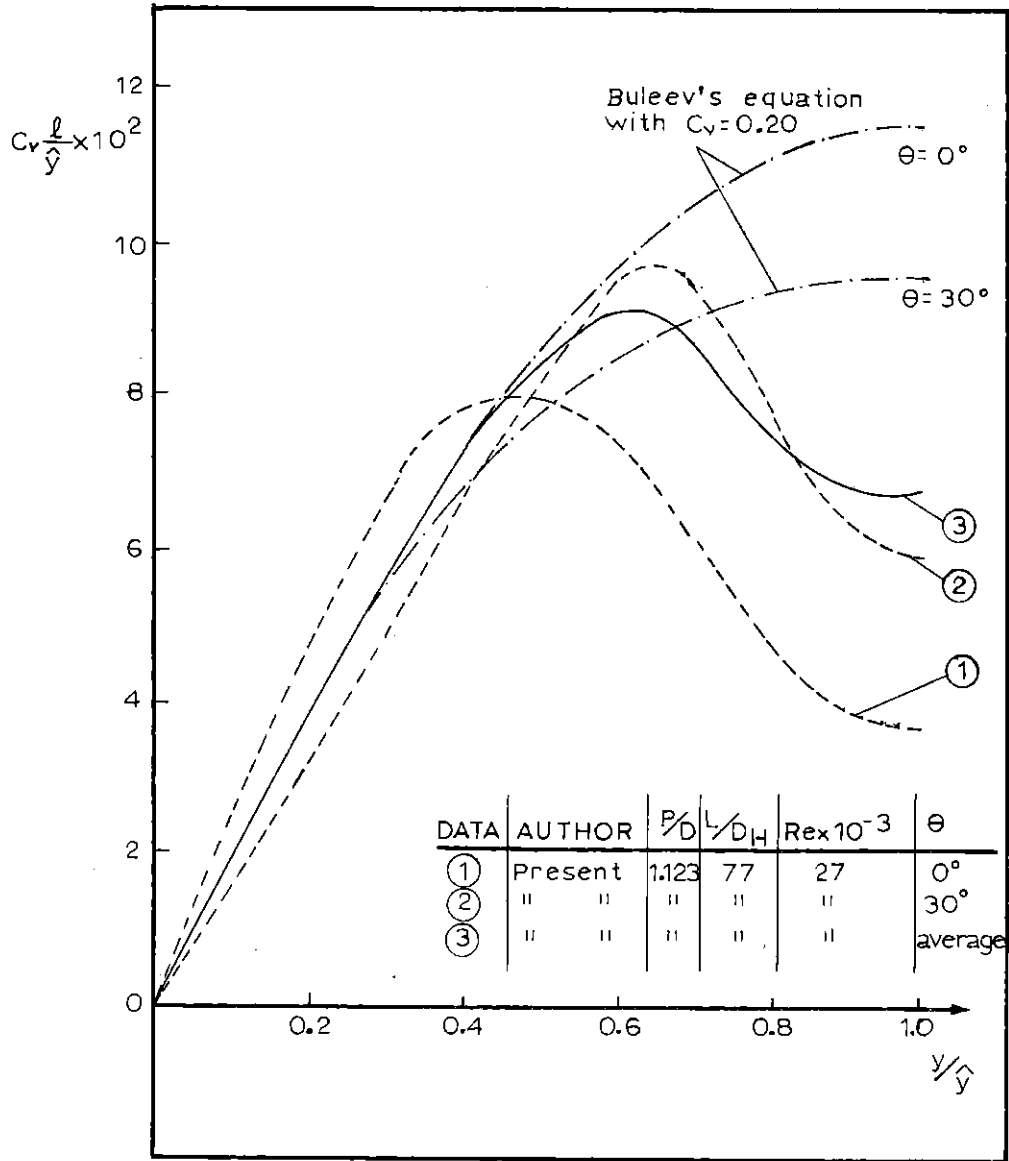


Fig. VI.6. Mixing Length Distribution

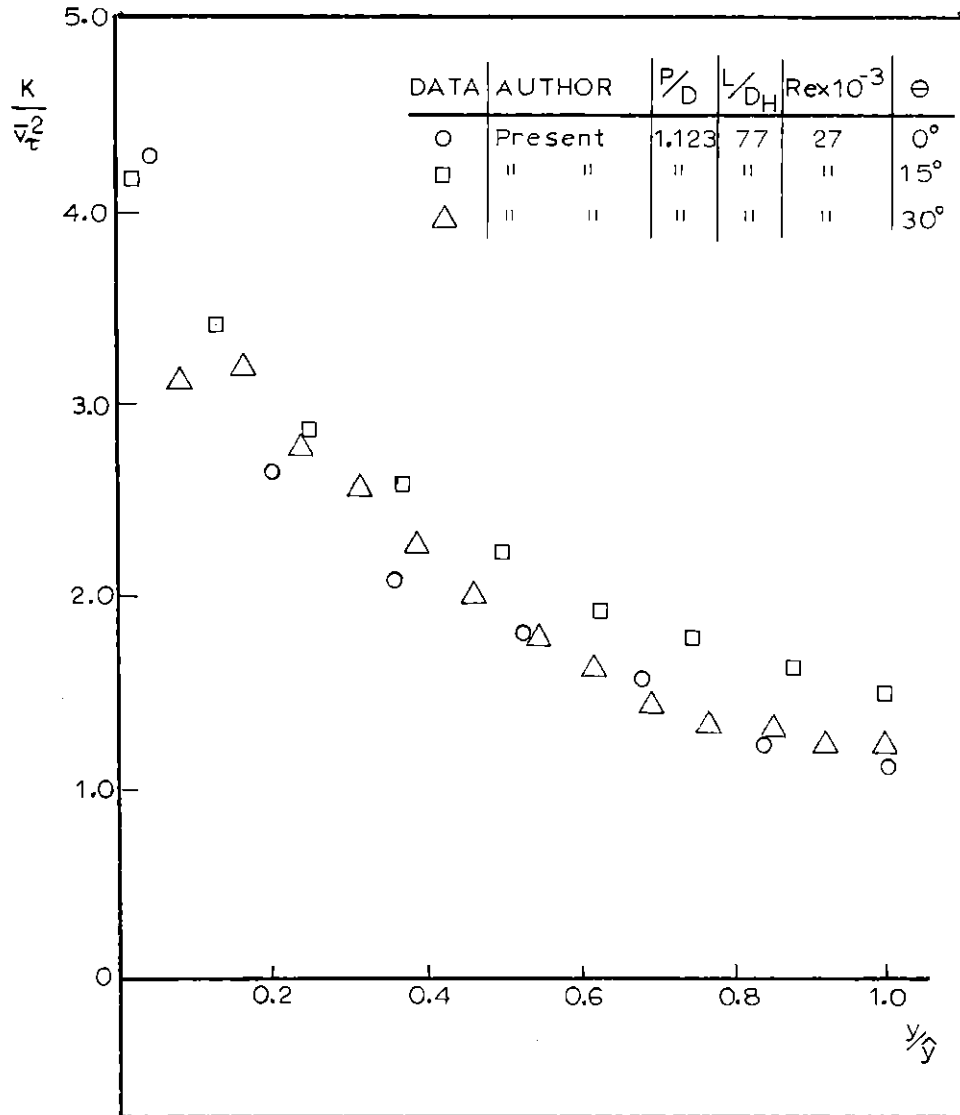


Fig. VI.7. The TKE Distribution

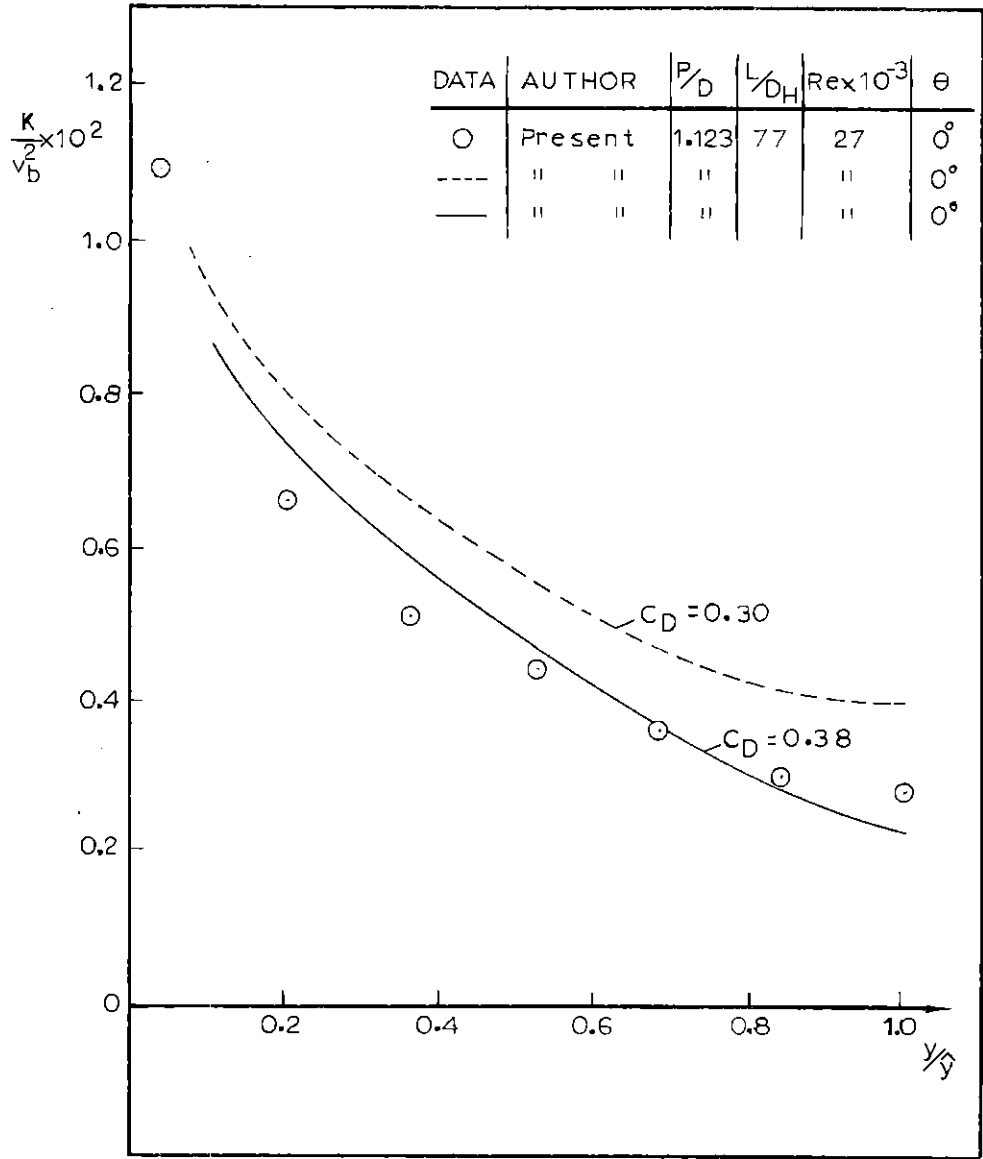


Fig. VI.8. Effect of the Value of C_D in the TKE Distribution

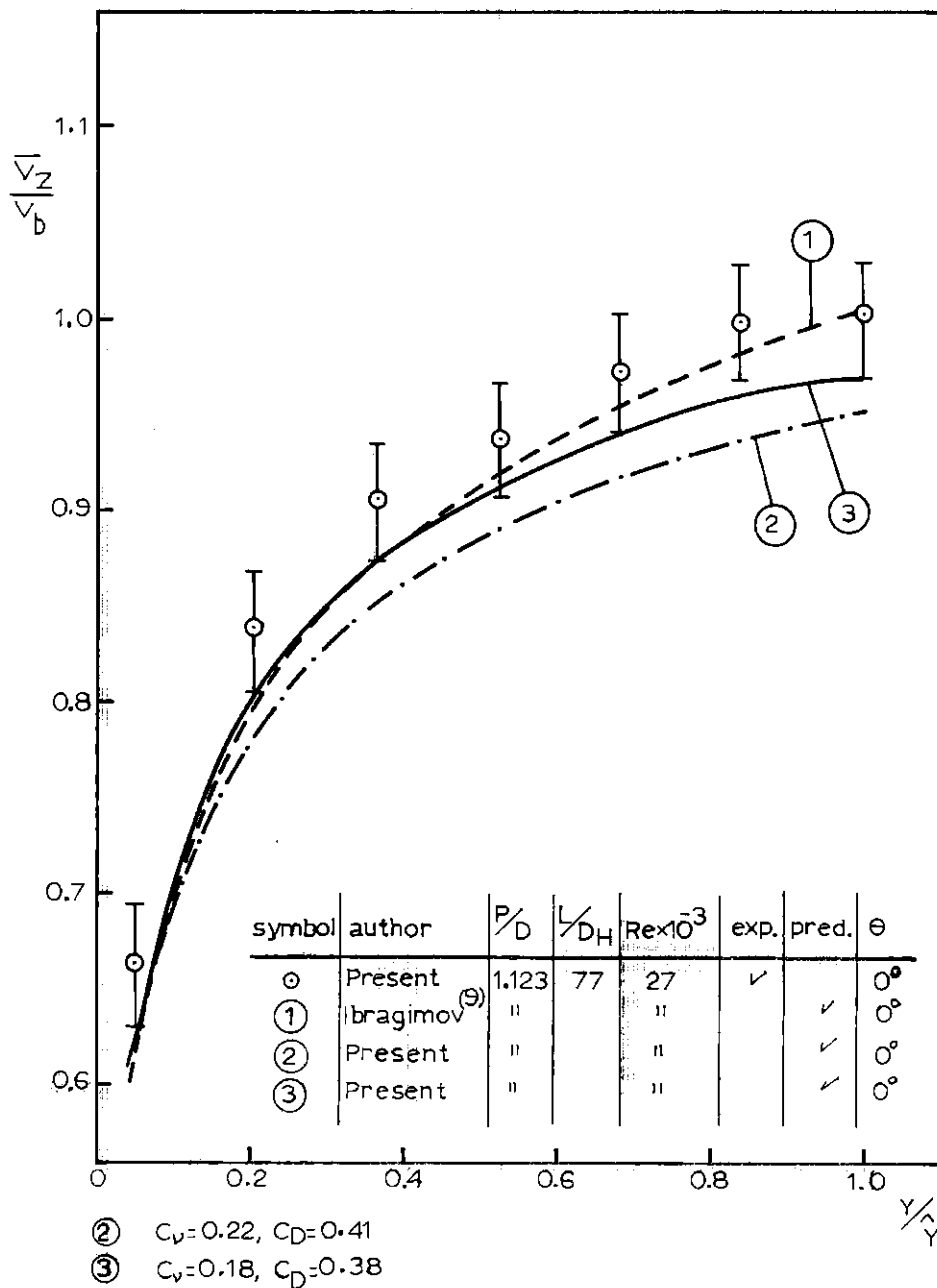


Fig. VI.9.(a) Comparison Between Experimental and Analytical Axial Velocity Distributions

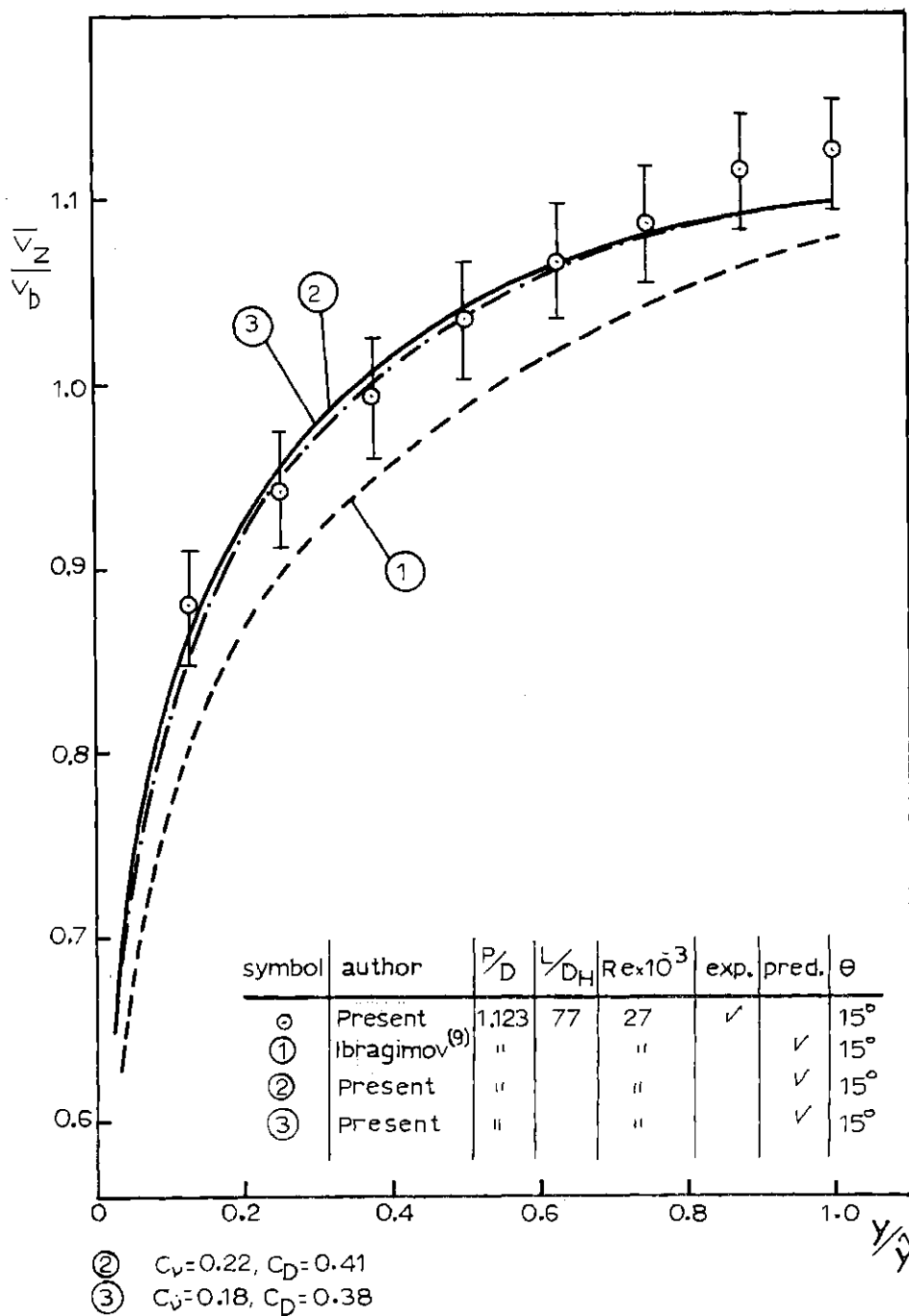


Fig. VI.9.(b) Comparison Between Experimental and Analytical Axial Velocity Distributions

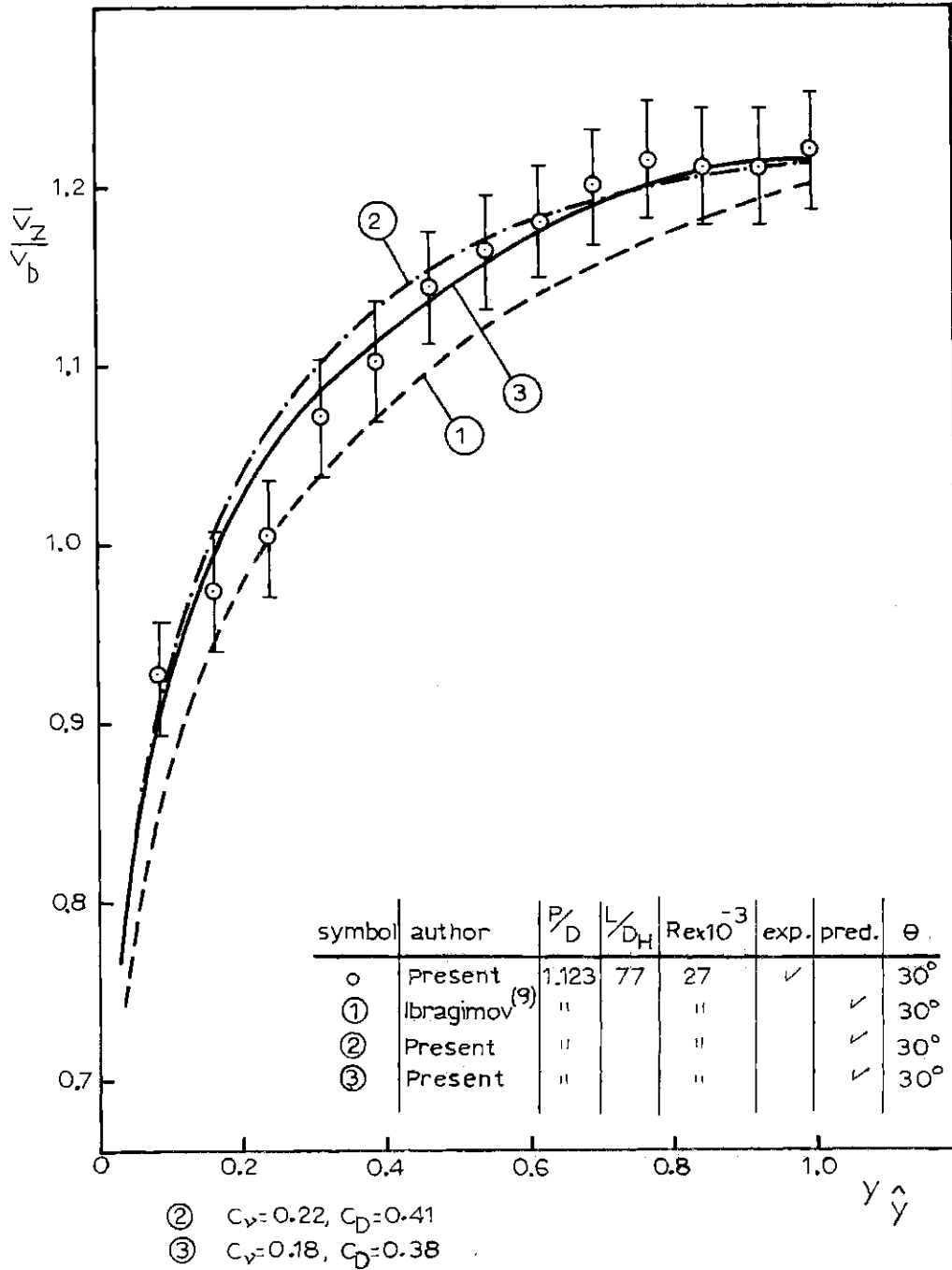


Fig. VI.9.(c) Comparison Between Experimental and Analytical Axial Velocity Distributions

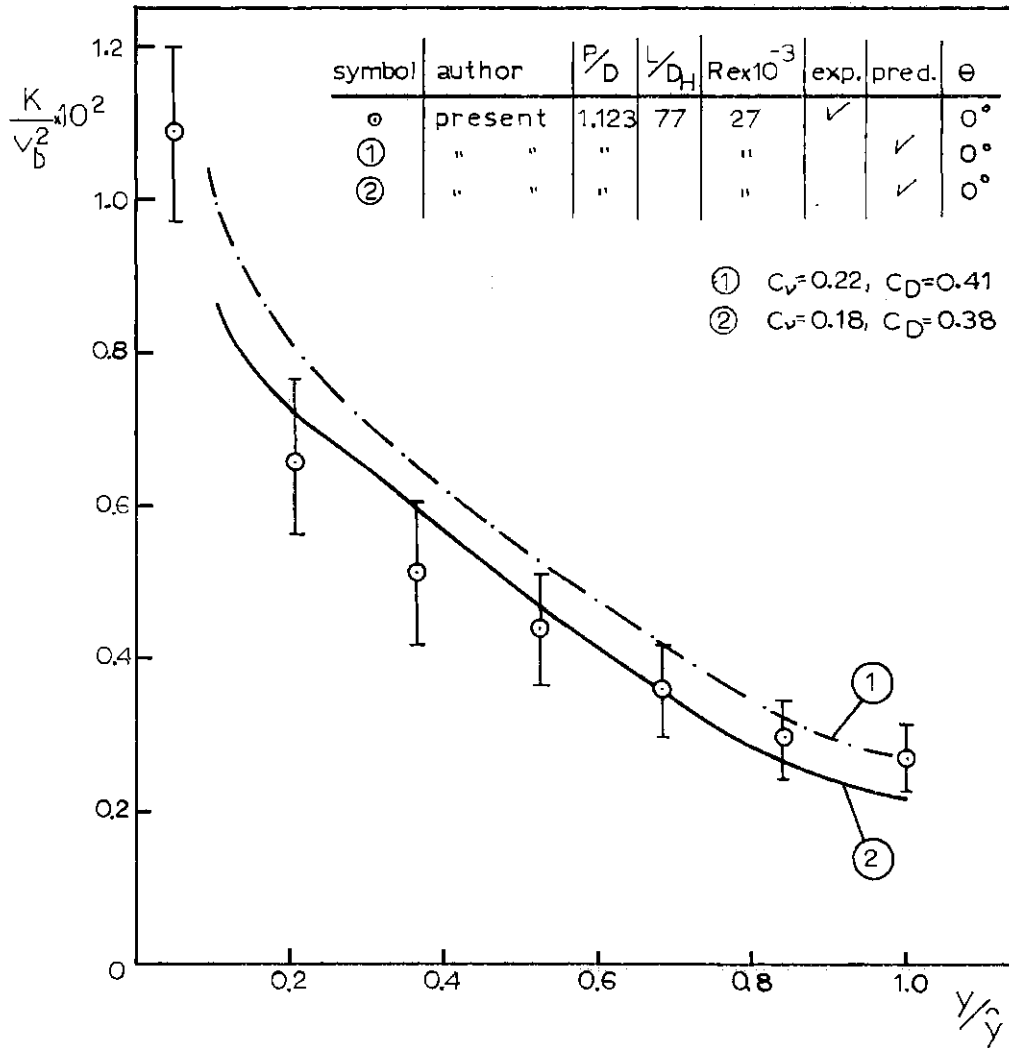


Fig. VI.10.(a) Comparison Between Experimental and Analytical TKE Distributions

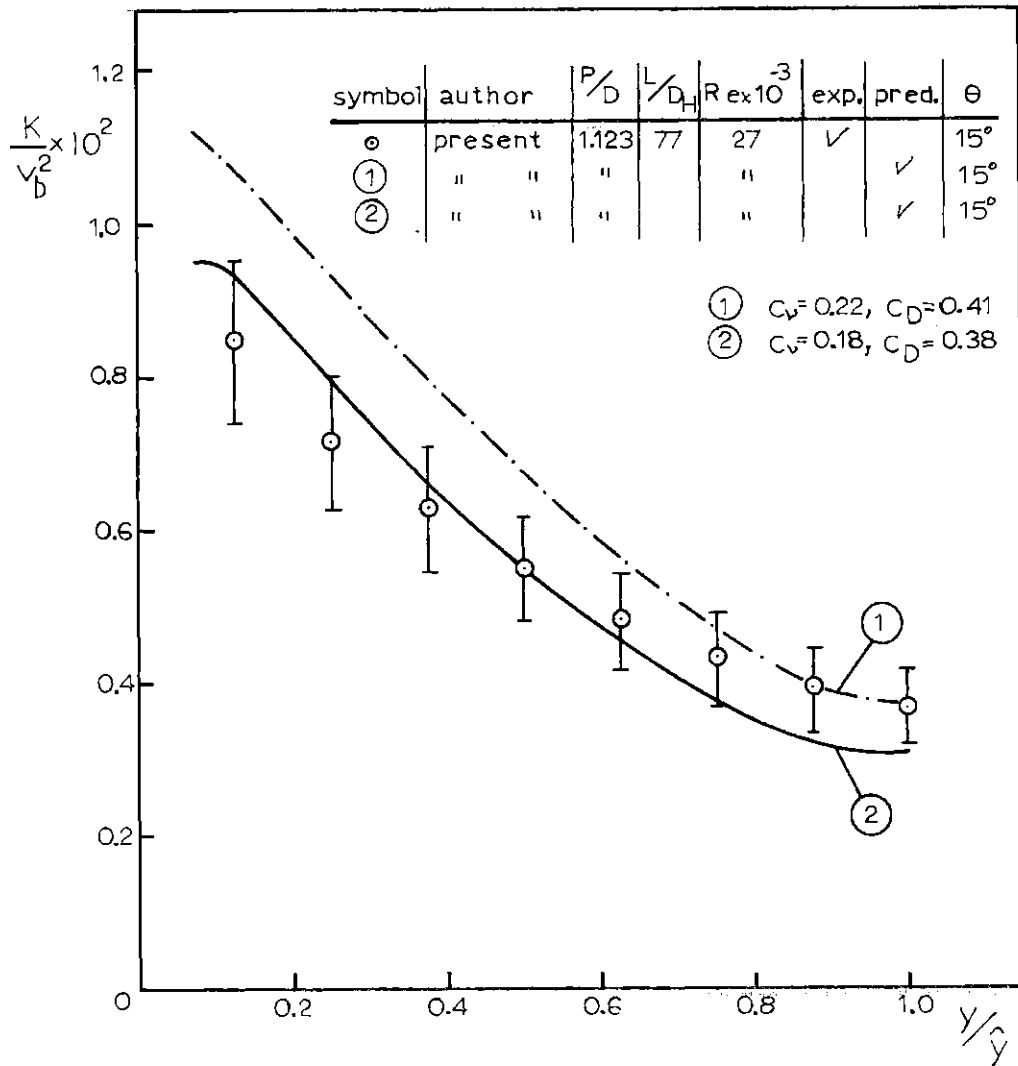


Fig. VI.10.(b) Comparison Between Experimental and Analytical TKE Distributions

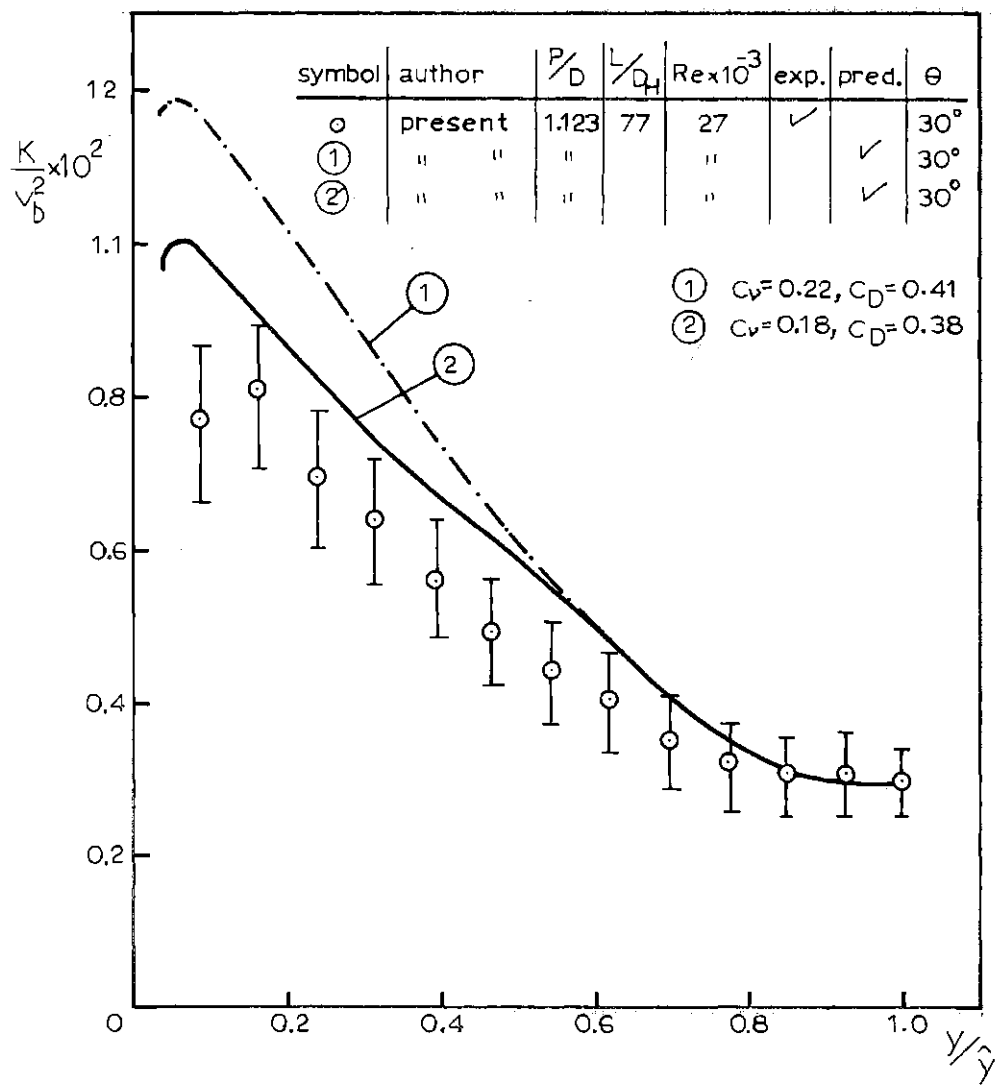


Fig. VI.10.(c) Comparison Between Experimental and Analytical TKE Distributions

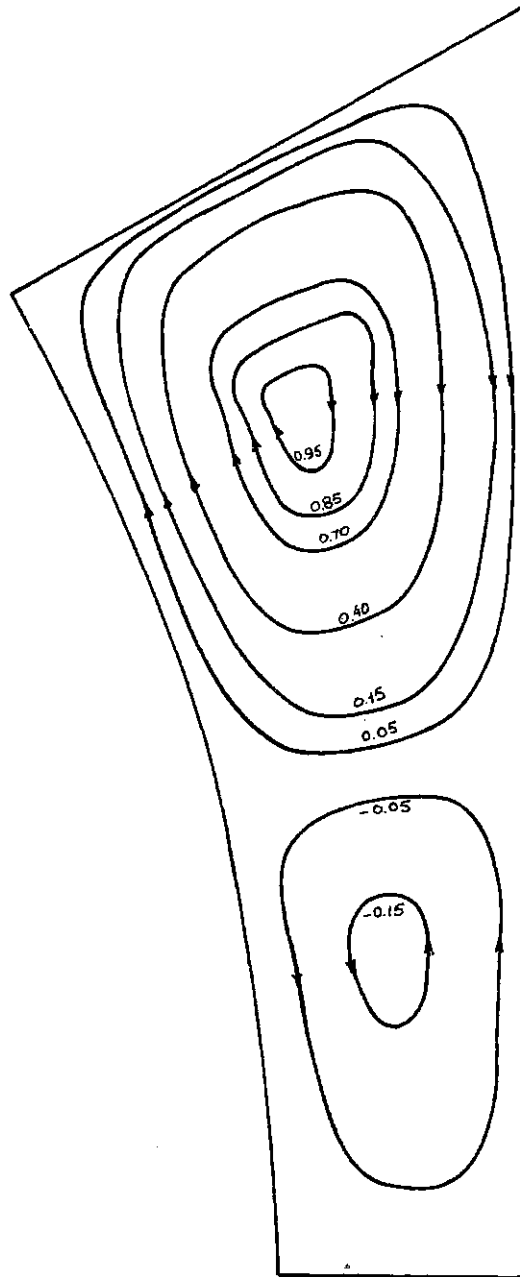


Fig. VI.11. Predicted Normalized Streamlines ($\frac{\psi}{\psi_{\max}}$) for
 $\frac{P}{D}=1.123$ and $Re=2.7 \times 10^4$

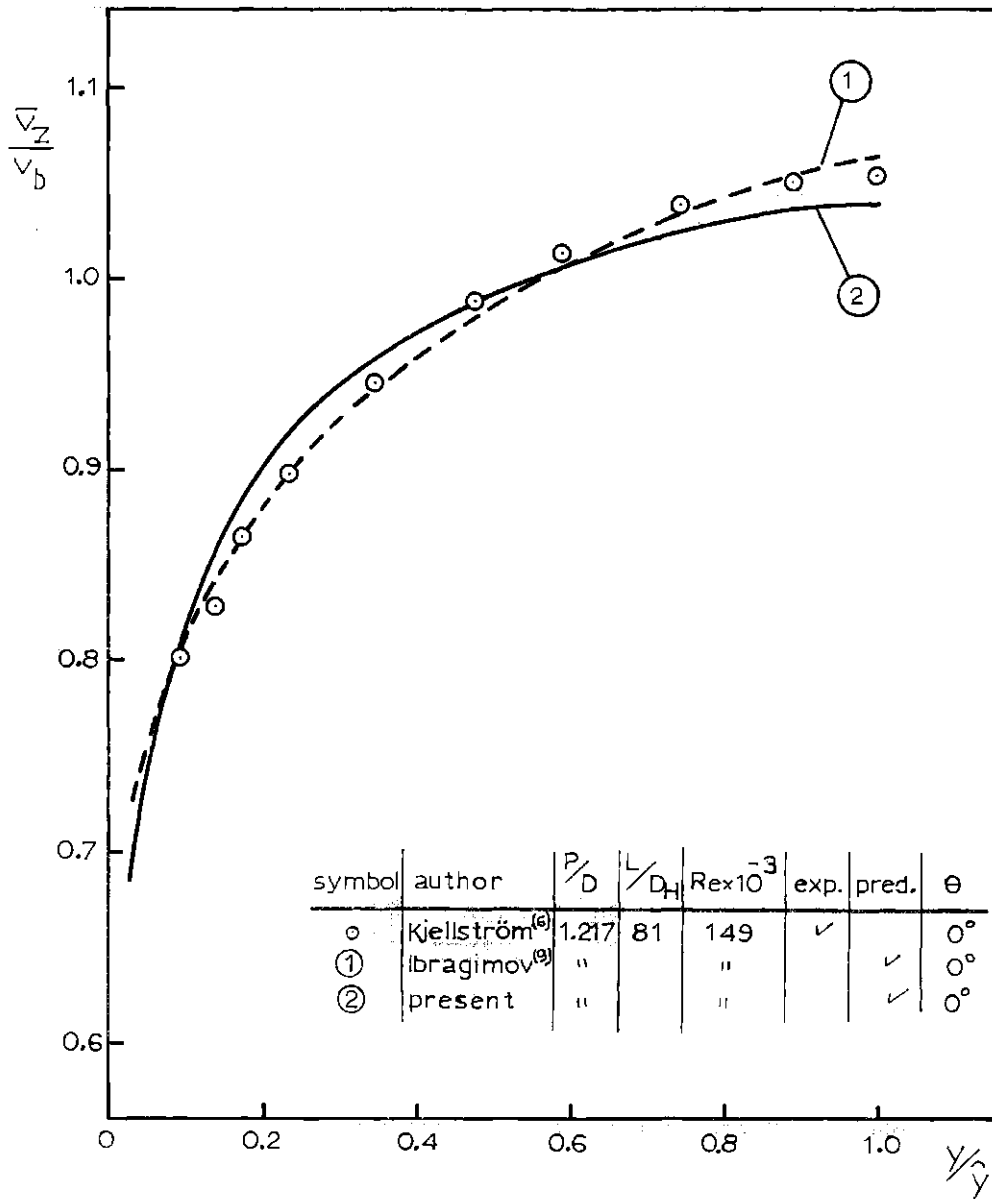


Fig. VI.12.(a) Comparison Between Experimental and Analytical Axial Velocity Distributions

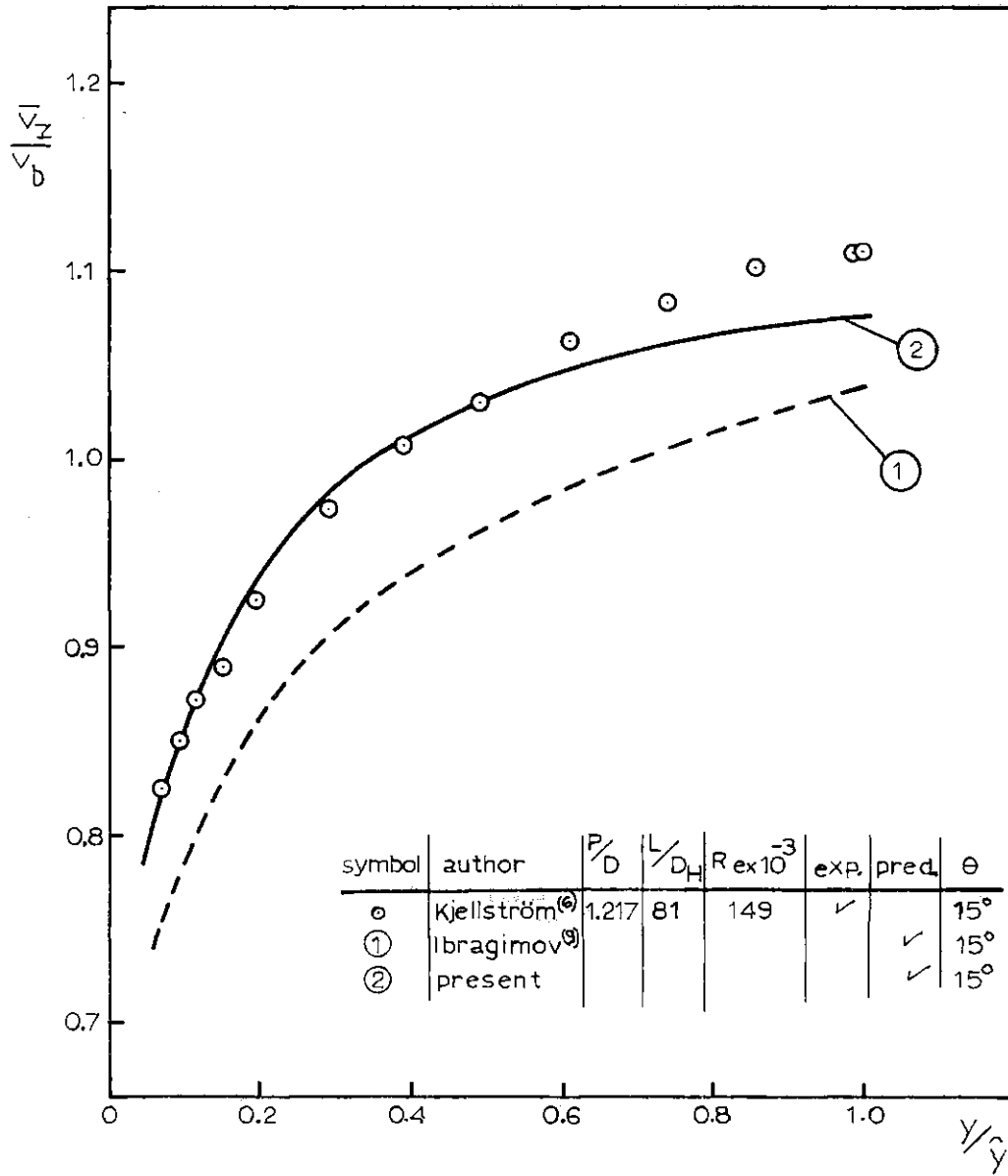


Fig. VI.12.(b) Comparison Between Experimental and Analytical Axial Velocity Distributions

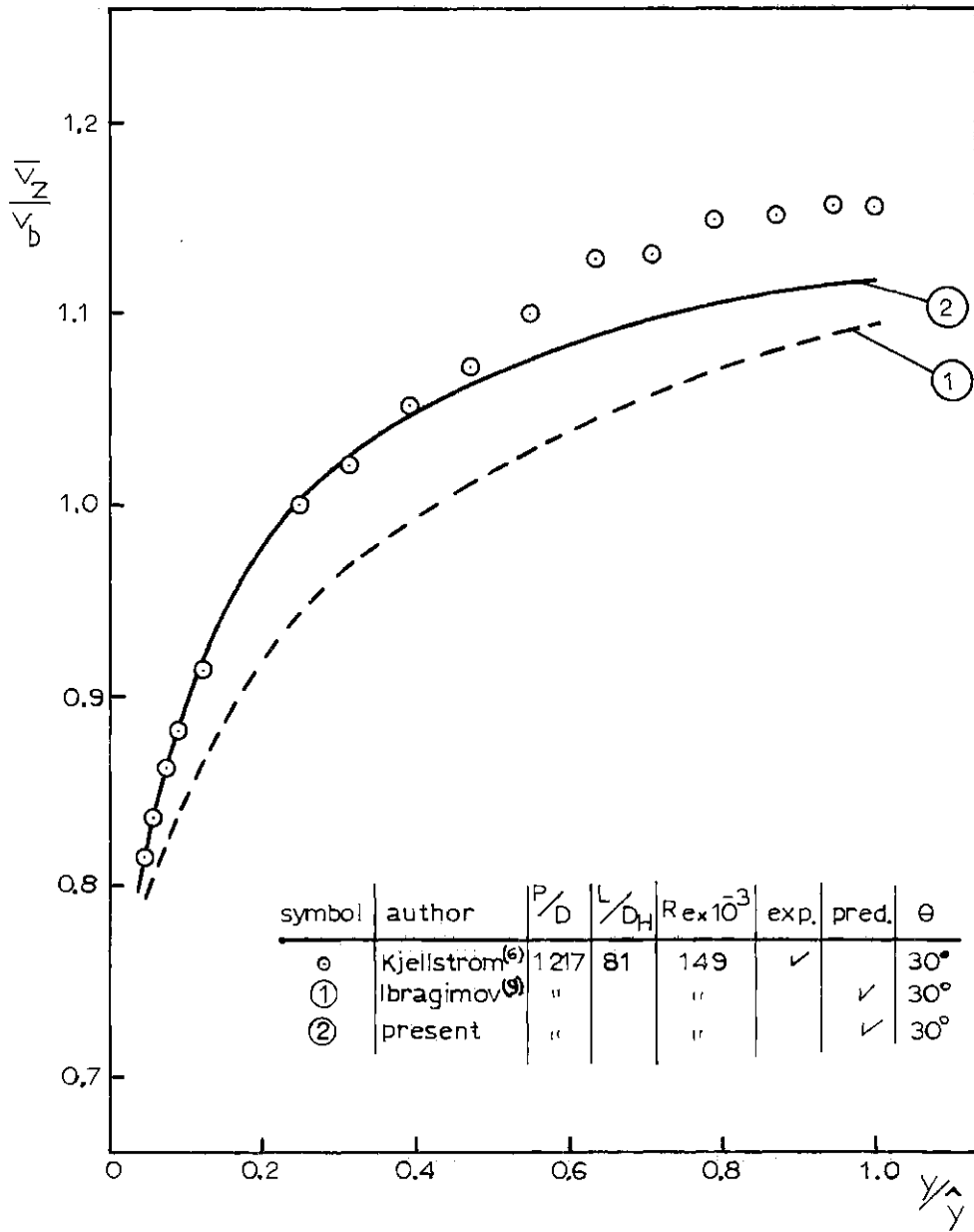


Fig. VI.12.(c) Comparison Between Experimental and Analytical Axial Velocity Distributions

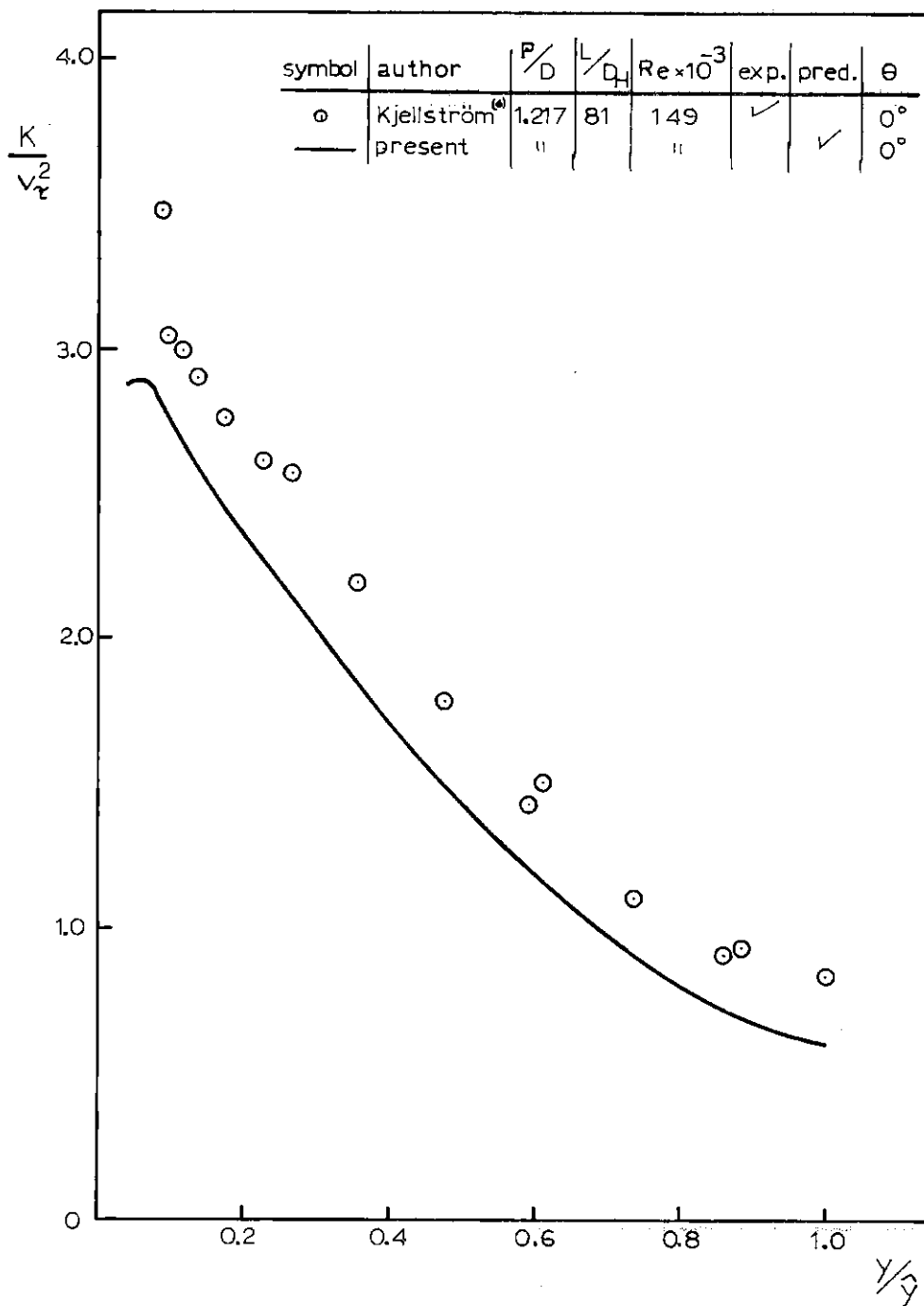


Fig. VI.13.(a) Comparison Between Experimental and Analytical TKE Distributions

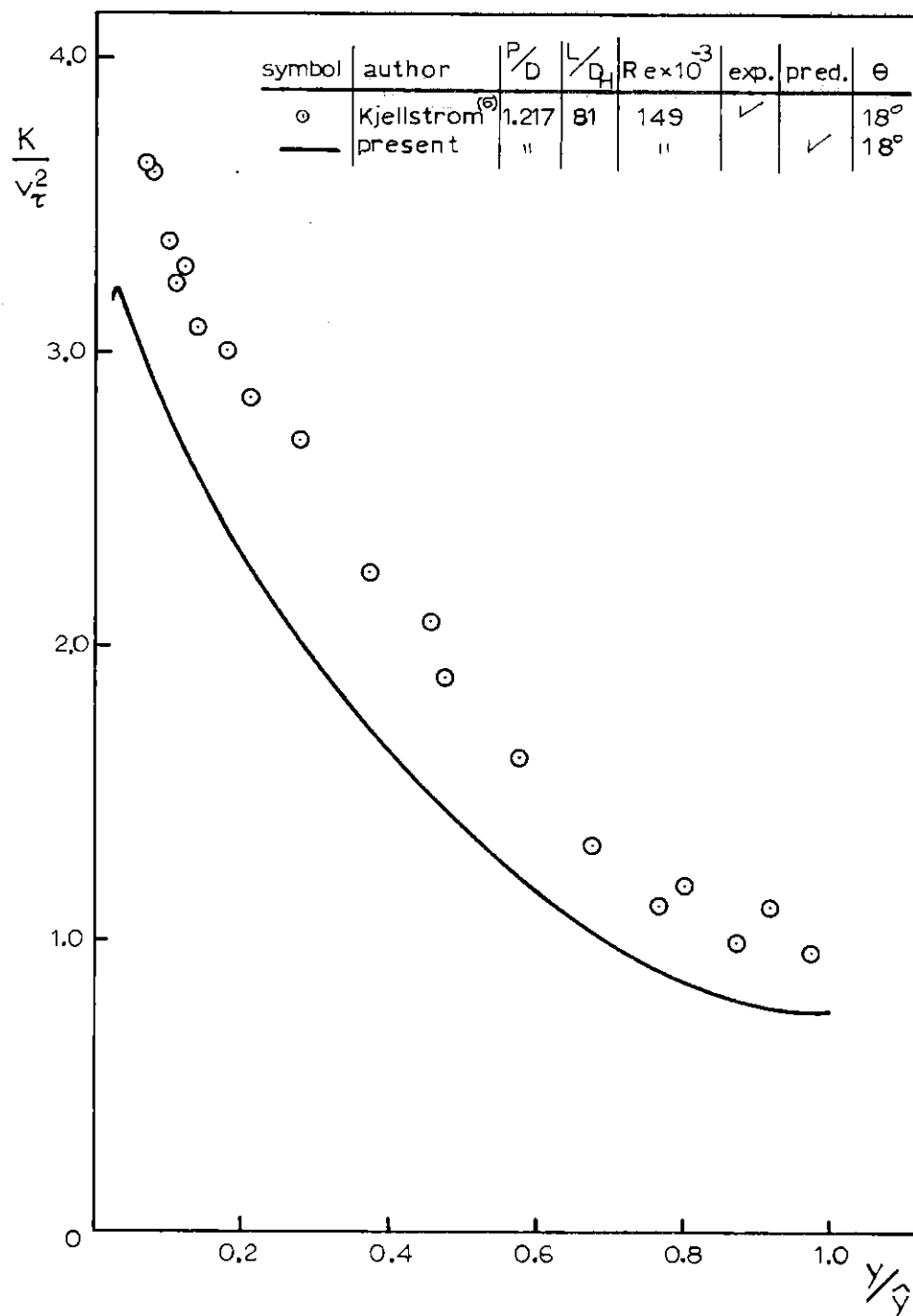


Fig. VI.13.(b) Comparison Between Experimental and Analytical TKE Distributions

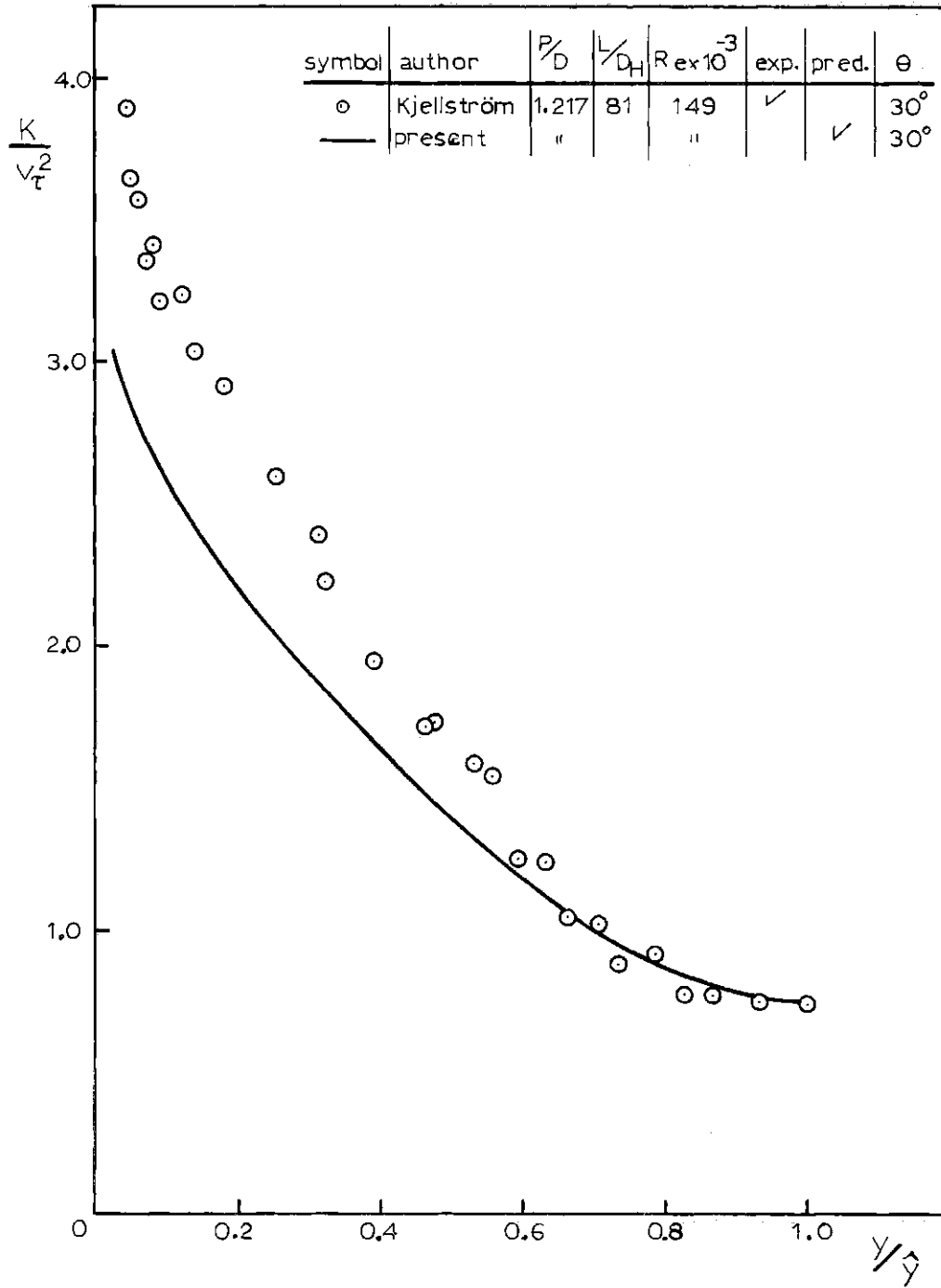


Fig. VI.13.(c) Comparison Between Experimental and Analytical TKE Distributions

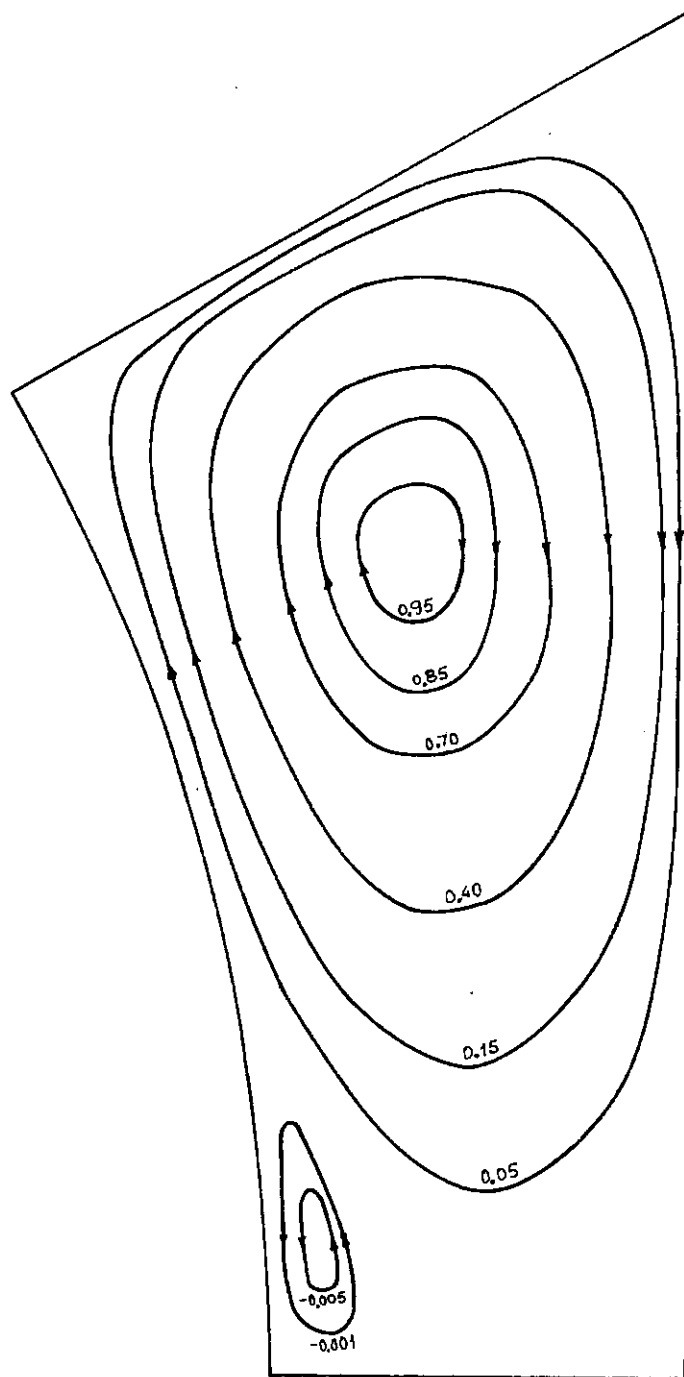


Fig. VI.14. Predicted Normalized Streamlines ($\frac{\psi}{\psi_{\max}}$) for $\frac{P}{D}=1.217$ and $Re=1.49 \times 10^5$

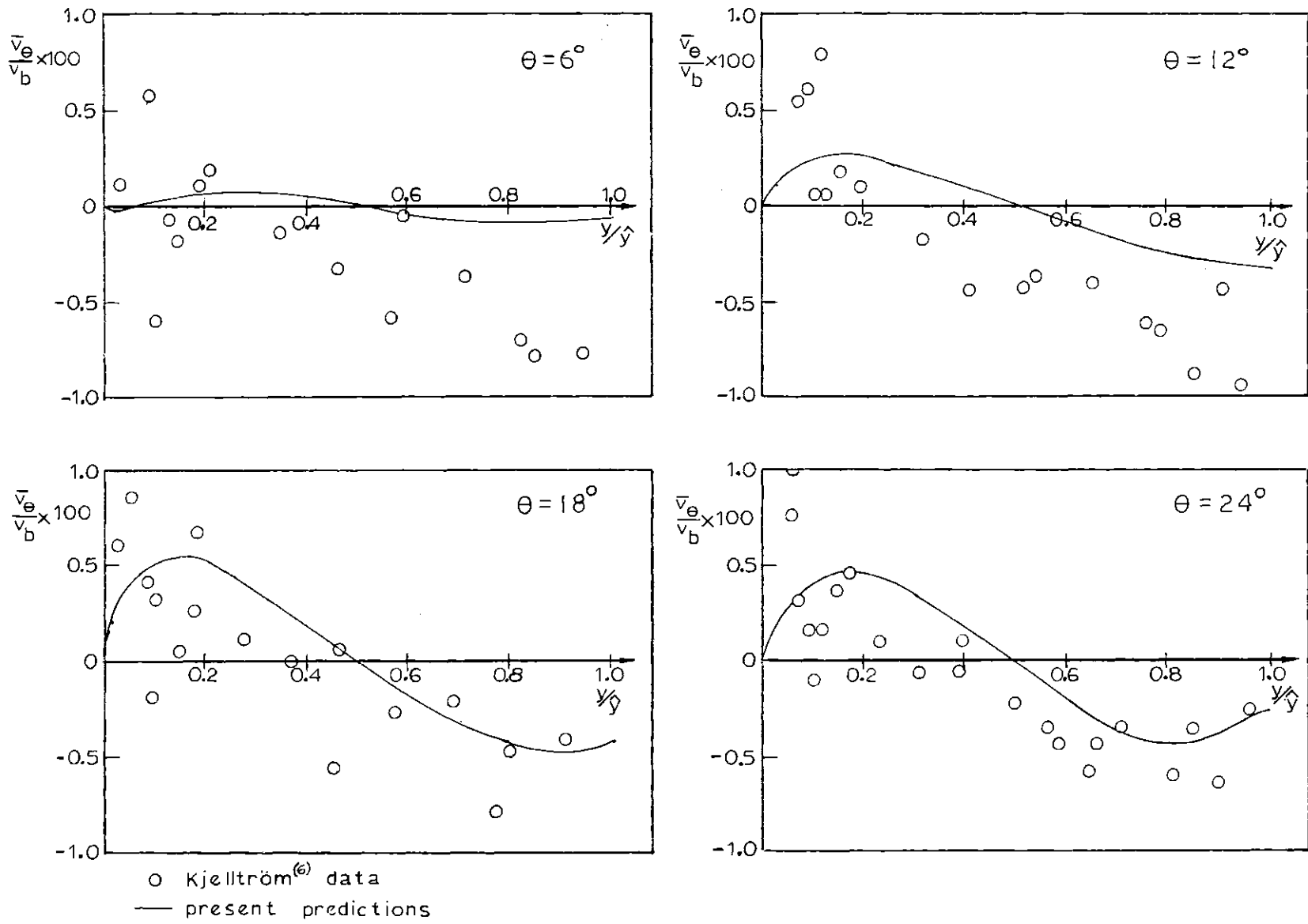


Fig. VI.15. Comparison of Predicted Secondary Flow with Experimental Data for $\frac{P}{D} = 1.217$

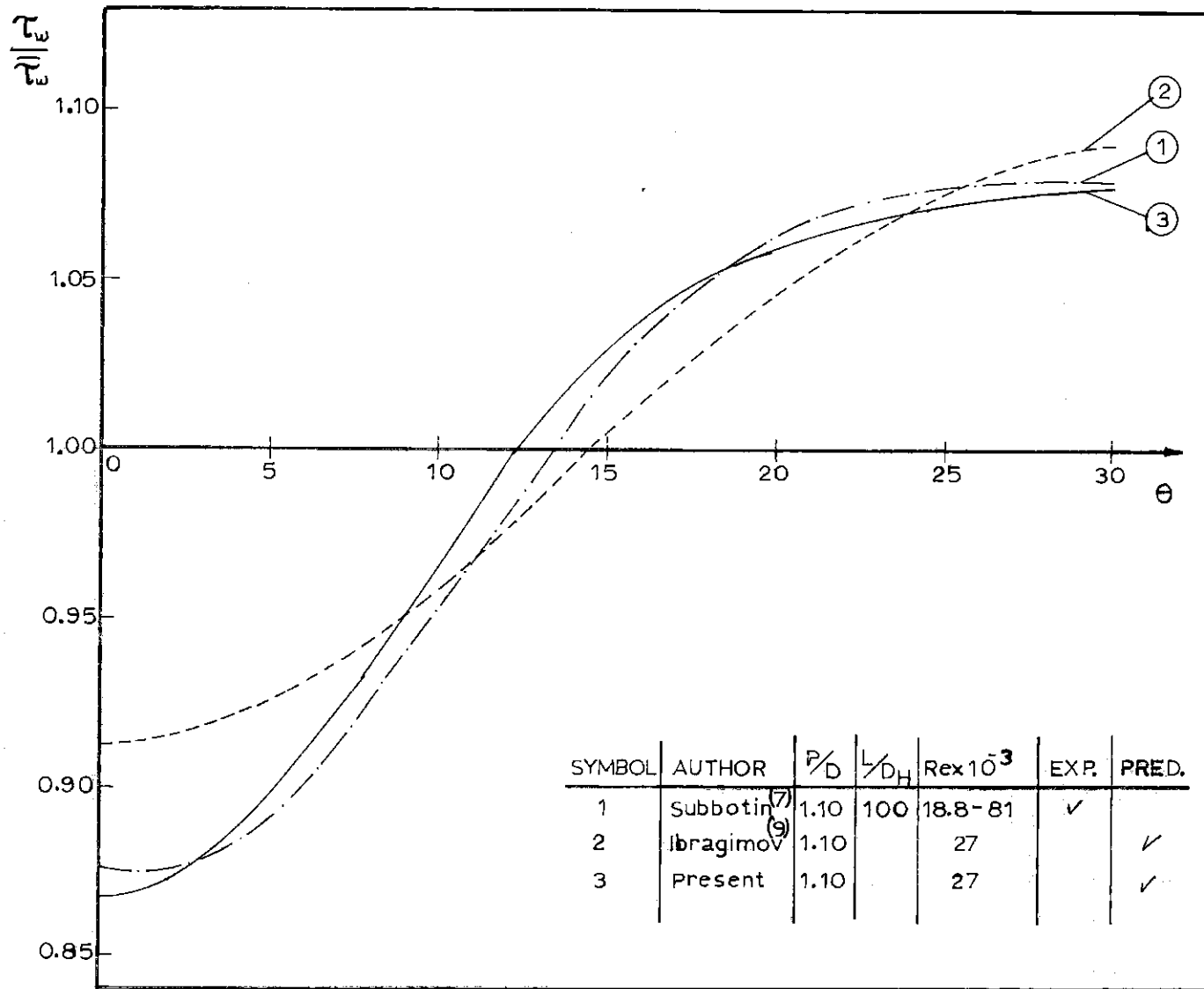


Fig. VI.16. Wall Shear Stress Distribution

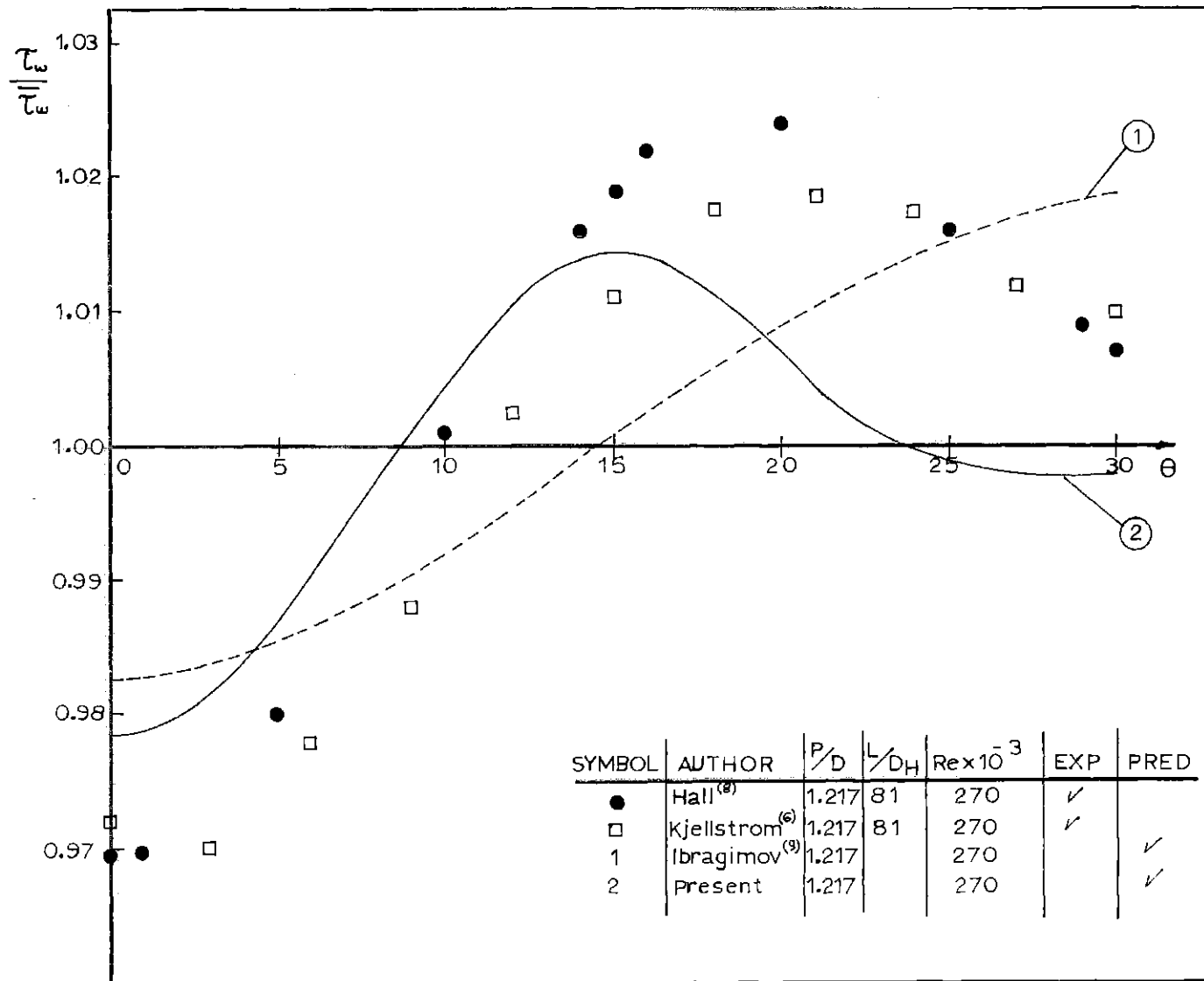


Fig. VI.17. Wall Shear Stress Distribution

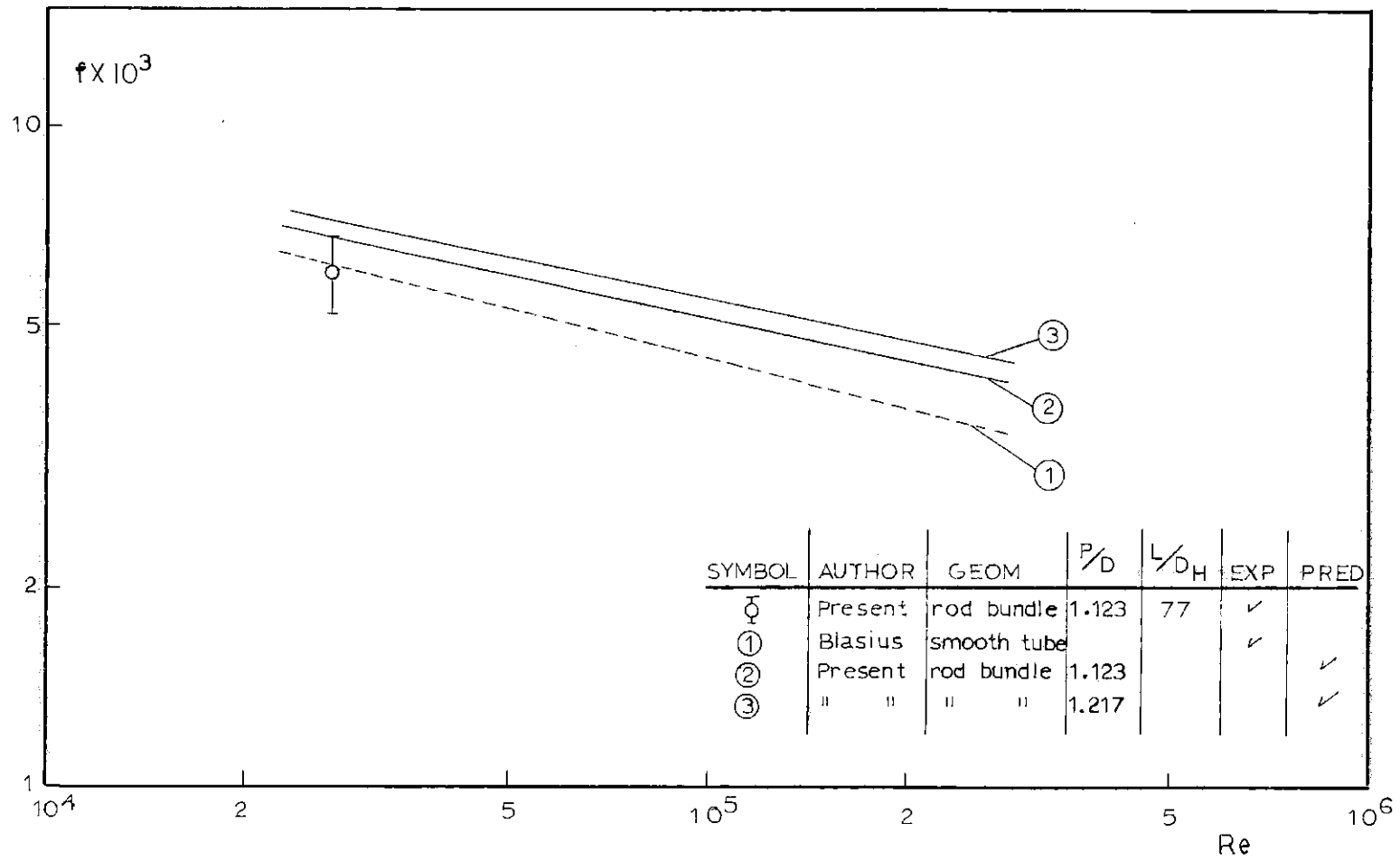


Fig. VI.18. Friction Factor vs Re

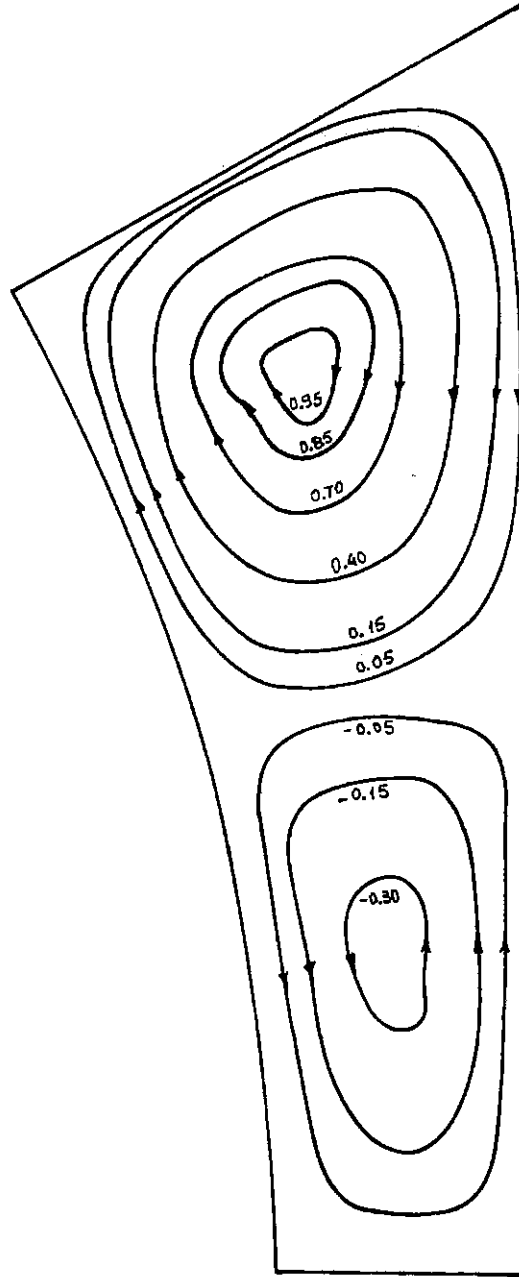


Fig. VI.19. Predicted Normalized Streamlines ($\frac{\psi}{\psi_{\max}}$) for $\frac{P}{D}=1.123$ and $Re=2 \times 10^5$

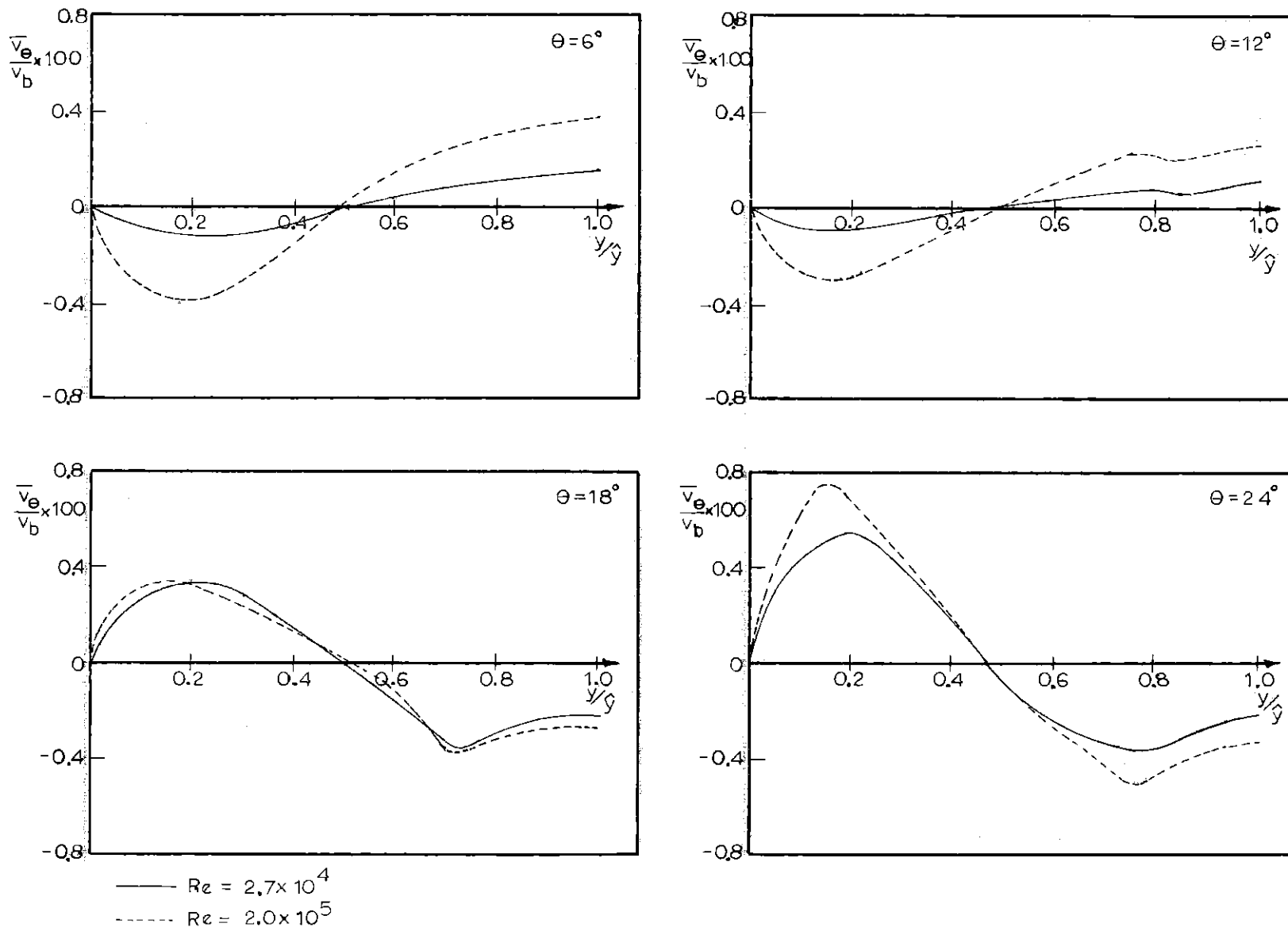


Fig. VI.20. Effect of Reynolds Number on Secondary Flow Distribution ($\frac{P}{D} = 1.123$)

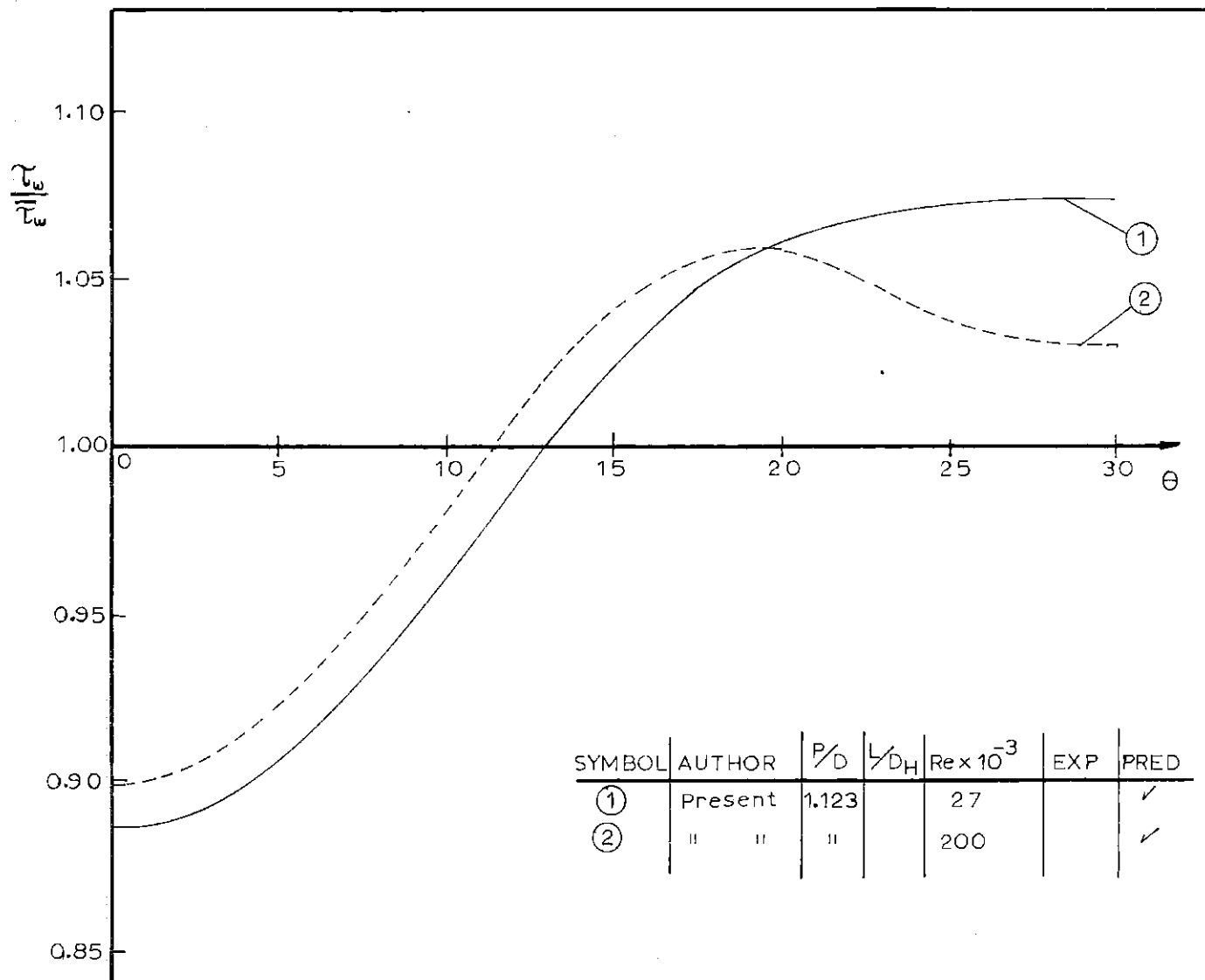


Fig. VI.21. Effect of Reynolds Number on the Wall Shear Stress Distribution ($\frac{P}{D}=1.123$)

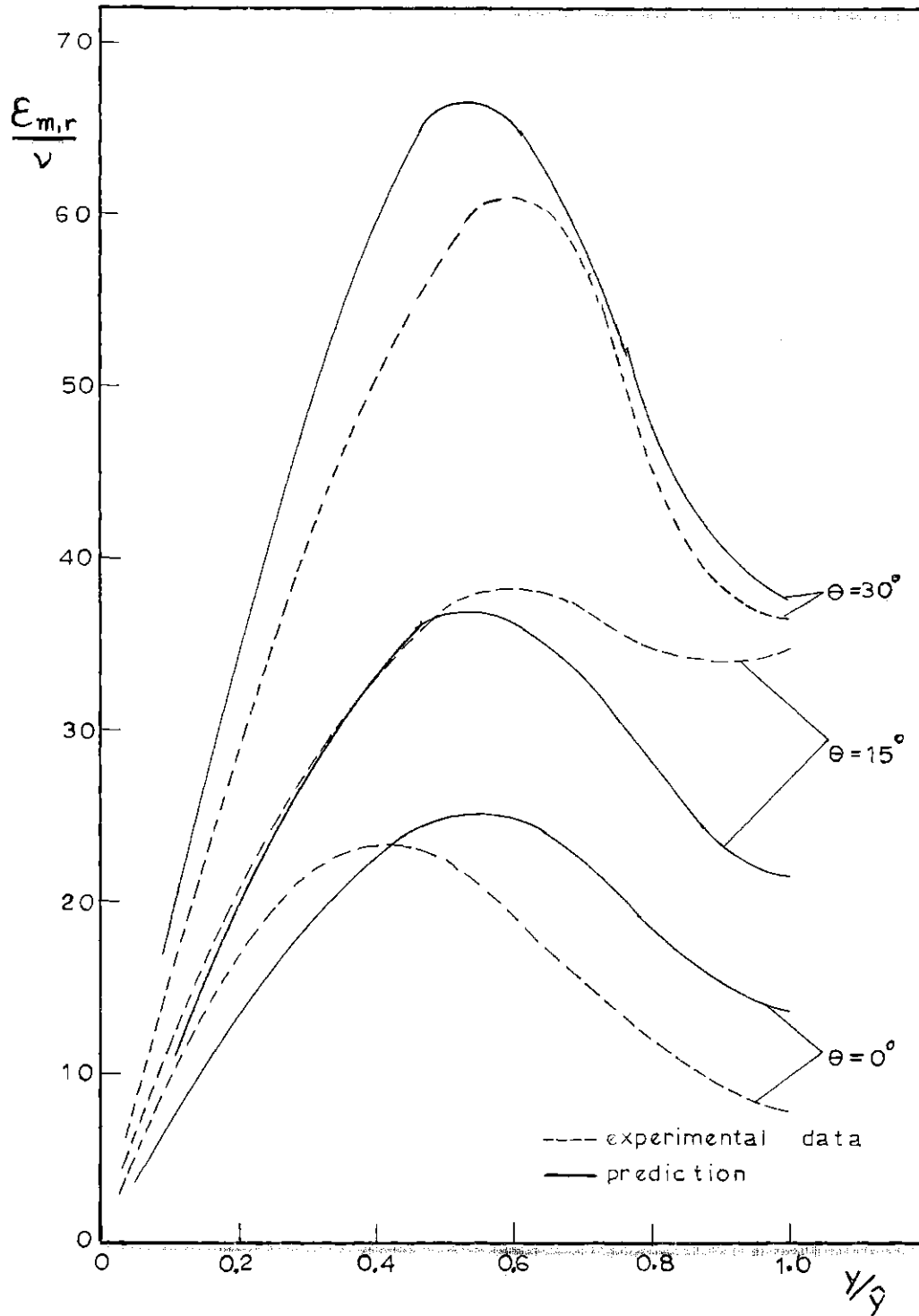


Fig. VI.22. Radial Eddy Diffusivity Distribution for $\frac{P}{D}=1.123$ and $Re=2.7 \times 10^4$

REFERENCES

1. Eifler, W. and Nijsing, R., Fundamental Studies of Fluid Flow and Heat Transfer in Fuel Element Geometries, Report EUR 2193.e, part II, (1965).
2. Schlichting, H., Boundary-Layer Theory, McGraw-Hill Book Co, 6th.ed., (1968)
3. Launder, B.E. and Ying, W.M., Prediction of Flow and Heat Transfer in Ducts of Square Cross-Section, The Inst. of Mech. Eng., Proceedings 1973, Vol. 187 37/73, pp. 455-461.
4. Wolfshtein, M., The Velocity and Temperature Distribution in One-dimensional Flow with Turbulence Augmentation and Pressure Gradient, Int. J. Heat Mass Transfer, Vol. 12, (1969), pp. 301-318.
5. Spalding, D.B., Heat Transfer from Turbulent Separated Flows, J. Fluid Mech. 27 (1967), pp. 97-109.
6. Kjellström, B., Studies of Turbulent Flow Parallel to a Rod Bundle of Triangular Array, Report AE-RV-196, AB Atomenergi, Sweden (1971).
7. Subbotin, V.I. et al., Velocity Field of Turbulent Fluid Flow in a Longitudinal Streamline of Clusters of Rods, AEC-tr-7189 (1971).
8. Hall, Ch. and Svenningsson, P.J., Secondary Flow Velocities in a Rod Bundle of Triangular Array, Report AE-RL-1326, AB Atomenergi, Sweden (1971).
9. Ibragimov, M. Kh. et al., Calculation of the Tangential Stresses at the Wall of a Channel and the Velocity Distribution in a Turbulent Flow of Liquid, Soviet Atomic Energy, Vol. 21, No. 2, (Aug. 1966), pp. 731-739.

CHAPTER VII

CONCLUSIONS AND RECOMMENDATIONS FOR FUTURE WORK

1. CONCLUSIONS

The present study has produced the following conclusions:

- a. Due to the small magnitude of the secondary flows (usually less than 0.5% of the bulk velocity) in rod bundles, methods that disturb the flow should not be expected to produce good results. However, even methods as the LDA, without a solid probe, will only be able to measure those velocities if a more accurate frequency tracking system is developed or if very high Reynolds number flows are investigated.
- b. The analytical predictions of the magnitude of the secondary flows are in agreement with the experimental limitation that secondary flow velocities should be less than 0.67% of v_b for $P/D = 1.123$ and $Re = 2.7 \times 10^4$.
- c. The analytical predictions of the secondary flows, for $P/D = 1.217$, are in qualitative agreement with the scattered data obtained by Kjellström.
- d. Two loops of secondary flows were predicted inside an

interior rod bundle subchannel, although one of them, located near the gap region, is very weak compared to the other one, and tends to disappear as the P/D increases. This pattern leads to good predictions of the wall shear stress distribution.

- e. The magnitude of the secondary flows relative to the bulk velocity increases with Re . The magnitude of the weakest secondary flow loop increases much faster than the magnitude of the other one. Regardless of this disproportional increase in magnitude, no significant change occurs in the secondary flow pattern.
- f. For the same Reynolds number, the maximum value of the secondary flow velocities decreases as P/D increases, as should be expected, since the assymetry of the subchannel also decreases.
- g. For the same P/D, the wall shear stress distribution becomes more uniform as Re increases. Due to the increase in the magnitude of the secondary flows with Re , the maximum value of this distribution moves from the angular position $\theta=30^\circ$ to lower values of θ .
- h. The axial velocity distributions predicted are in good agreement with experimental results.

2. RECOMMENDATIONS FOR FUTURE WORK

- a. It was observed that typical values for the constants C_v and C_D of the analytical model led to good predictions for the velocity field. Better agreement was obtained with the new values determined from the experimental data for $P/D = 1.123$. The model with these constants, however, when applied to the case $P/D = 1.217$, presented a deviation that probably could be reduced using slightly different values for C_v and C_D . So, an experimental study of the effect of P/D as well as Re on the constants could lead to an optimized set of constants for rod bundles.
- b. The law of the wall, assumed as the wall boundary condition for the axial momentum equation, was obtained in tube and flat plate flows. Measurements of the axial velocity distribution near the wall certainly could lead to even more accurate predictions of the velocity field.
- c. Measurements in test sections with larger values of L/D_H are necessary to put to rest the question of the length of the developing region in rod bundles.
- d. More accurate measurements of cross correlation $\overline{v'_r v'_z}$ are necessary for a better determination of the mixing length

distribution necessary for the one-equation models. This could, probably, be accomplished with the LDA operating with two colors: one for each component. The scattered light could be separated by interference filters or a dichroic mirror and the instantaneous signals generated by two photomultiplier tubes could be electronically multiplied leading to the cross correlation sought.

- e. Accurate cross correlation measurements, as proposed in item d, has the capability of producing good results for $\overline{v_{\theta}^i v_z^i}$. This piece of information is important to determine the degree of anisotropy of flows in rod bundles.
- f. With the existing tracking system, secondary flows can only be measured for very high Reynolds number and small P/D, even though the measurements would have a large experimental error. However, such measurements would probably show the secondary flow pattern and could be used as a check of the analytical method presented here. A digital voltmeter, with at least four digits, is required for these measurements.
- g. Expansion of the present method to handle different situations as lateral or corner subchannels, fuel rod spacers, etc., is required.
- h. Application of the method to predict temperature field

can also produce important information regarding the effect of the secondary flows on the wall temperature distribution and heat transfer coefficient.

- i. Measurements of $\overline{v_r'v_z'}/v_t^2$ obtained by Trupp and Azad for different P/D and Reynolds numbers, as well as those of the author, for P/D = 1.123 and Re = 2.7×10^4 , showed a linear behavior of this parameter with y/\hat{y} . In view of such behavior, it seems to the author that it is worth to investigate the possibility of correlating, for design purposes, the cross correlation $\overline{v_r'v_z'}$ directly, instead of associating it to axial velocity gradients by an eddy diffusivity. The behavior of $\overline{v_\theta'v_z'}$, within the subchannel, has still to be investigated, though.

3. CONCLUDING REMARKS

The author would like to point out that simple statistical turbulence models, such as the one presented here, adopting the algebraic stress model proposed by Launder and Ying, can provide good predictions of the axial velocity, wall shear stress and eddy diffusivity distributions as well as friction factors, for rod bundle subchannels. Also this model, compared to previous approaches, can take into account secondary flow effects without substantial increase in

complexity.

From the experimental point of view, one of the major limitations of the LDA is the presence of curved surfaces in the geometry to be studied. The technique introduced here can overcome this difficulty in many practical situations.

APPENDIX A

TRANSPORT EQUATIONS FOR COMPUTATION OF VELOCITY FIELD

Assuming temperature-independent properties, incompressible flow and neglecting any body forces, the momentum conservation equation known as Navier-Stokes equation, the derivation of which can be found in any fluid mechanics book (see, for ex., ref. 1). In vectorial form, this equation is

$$\frac{D\underline{V}}{Dt} = \frac{\partial \underline{V}}{\partial t} + \underline{\nabla} \cdot \underline{V}\underline{V} = -\frac{1}{\rho} \underline{\nabla} p + \nu \nabla^2 \underline{V} . \quad (\text{A.1})$$

This equation is valid for either laminar or turbulent flows. For turbulent flows, however, the point properties would be the instantaneous ones and the equation would be most difficult to treat analytical or numerically. So, the flow properties are written as a sum of time-average values and fluctuating components, that is,

$$\begin{aligned} \underline{V} &= \overline{\underline{V}} + \underline{v}' , \\ p &= \overline{p} + p' . \end{aligned} \quad (\text{A.2})$$

Applying (A.2) to equation (A.1), and averaging in time, one obtains:

$$\frac{\partial \bar{v}}{\partial t} + (\bar{v} \cdot \nabla) \bar{v} = -\frac{1}{\rho} \nabla \bar{p} + \nu \nabla^2 \bar{v} - (\nabla \cdot \overline{v'v'}) . \quad (\text{A.3})$$

This equation was first formulated by Reynolds (1895) and so bears his name. The term $\overline{v'v'}$ has nine components and is called the Reynolds, eddy or turbulent stress.

The mass conservation equation or continuity equation is

$$\nabla \cdot \underline{v} = 0 . \quad (\text{A.4})$$

Also applying (A.2) to (A.4), one gets

$$\nabla \cdot \bar{v} = 0 \quad (\text{A.5})$$

after time-averaging.

Equations (A.3) and (A.5) represent the basic tools available to handle computation of velocity fields in any geometry. In cylindrical coordinates, for steady state, fully developed flow, these equations are:

a) Continuity equation

$$\frac{1}{r} \frac{\partial}{\partial r} r \bar{u}_r + \frac{\partial}{\partial \theta} \bar{u}_\theta = 0 , \quad (\text{A.6})$$

since $\frac{\partial \bar{u}_z}{\partial z} = 0$ for fully developed flow.

b) Momentum-conservation equation

b.1. Axial direction

$$\bar{u}_r \frac{\partial \bar{u}_z}{\partial r} + \bar{u}_\theta \frac{\partial \bar{u}_z}{r \partial \theta} = -\frac{1}{\rho} \frac{\partial \bar{p}}{\partial z} + \nu \left(\frac{\partial^2 \bar{u}_z}{\partial r^2} + \frac{1}{r} \frac{\partial \bar{u}_z}{\partial r} + \frac{\partial^2 \bar{u}_z}{r^2 \partial \theta^2} \right) - \frac{1}{r} \frac{\partial}{\partial r} (r \overline{u_r' u_z'}) - \frac{\partial}{r \partial \theta} (\overline{u_\theta' u_z'}) ; \quad (\text{A.7})$$

b.2. Radial direction

$$\bar{u}_r \frac{\partial \bar{u}_r}{\partial r} + \bar{u}_\theta \frac{\partial \bar{u}_r}{r \partial \theta} - \frac{\bar{u}_\theta^2}{r} = -\frac{1}{\rho} \frac{\partial \bar{p}}{\partial r} + \nu \left(\frac{\partial^2 \bar{u}_r}{\partial r^2} + \frac{1}{r} \frac{\partial \bar{u}_r}{\partial r} - \frac{\bar{u}_r}{r^2} + \frac{\partial^2 \bar{u}_r}{r^2 \partial \theta^2} - \frac{2}{r} \frac{\partial \bar{u}_\theta}{r \partial \theta} \right) + \frac{1}{r} (\overline{u_\theta'^2} - \overline{u_r'^2}) - \frac{\partial \overline{u_r'^2}}{\partial r} - \frac{\partial}{r \partial \theta} (\overline{u_r' u_\theta'}) ; \quad (\text{A.8})$$

b.3. Tangential direction:

$$\begin{aligned}
\bar{u}_r \frac{\partial \bar{u}_\theta}{\partial r} + \bar{u}_\theta \frac{\partial \bar{u}_r}{r \partial \theta} + \frac{\bar{u}_r \bar{u}_\theta}{r} &= -\frac{1}{\rho} \frac{\partial \bar{p}}{r \partial \theta} + \nu \left(\frac{\partial^2 \bar{u}_\theta}{\partial r^2} + \right. \\
\left. \frac{1}{r} \frac{\partial \bar{u}_\theta}{\partial r} - \frac{\bar{u}_\theta}{r^2} + \frac{\partial^2 \bar{u}_\theta}{r^2 \partial \theta^2} + \frac{2}{r} \frac{\partial \bar{u}_r}{r \partial \theta} \right) - \frac{2}{r} (\overline{u_r' u_\theta'}) - \\
\frac{\partial}{\partial r} (\overline{u_r' u_\theta'}) - \frac{\partial \overline{u_\theta'^2}}{r \partial \theta} . & \quad (A.9)
\end{aligned}$$

In order to eliminate the gradients of \bar{p} in the radial and tangential directions, take $\frac{\partial}{\partial \theta}$ (eqn. A.8) and $\frac{\partial}{\partial r}$ (eqn. A.9) and subtract them. After tedious rearranging of the terms, the result can be written in the form:

$$I_c = \nu I_D + I_{\text{SOR}} \quad (A.10)$$

where

$$\begin{aligned}
I_c = \bar{u}_r \left[\frac{\partial \bar{u}_r}{r \partial \theta} - \frac{\partial \bar{u}_\theta}{\partial r} - \frac{\bar{u}_\theta}{r} \right] + \bar{u}_r \frac{\partial}{\partial r} r \left[\frac{\partial \bar{u}_\theta}{\partial r} + \frac{\bar{u}_\theta}{r} - \frac{\partial \bar{u}_r}{r \partial \theta} \right] \\
+ \bar{u}_\theta \frac{\partial}{\partial \theta} \left[\frac{\partial \bar{u}_\theta}{\partial r} + \frac{\bar{u}_\theta}{r} - \frac{\partial \bar{u}_r}{r \partial \theta} \right] , \quad (A.10-1)
\end{aligned}$$

$$\begin{aligned}
I_D = & \frac{\partial^2}{\partial r^2} r \left[\frac{\partial \bar{v}_\theta}{\partial r} + \frac{\bar{v}_\theta}{r} - \frac{\partial \bar{v}_r}{r \partial \theta} \right] - \frac{\partial}{\partial r} \left[\frac{\partial \bar{v}_\theta}{\partial r} + \frac{\bar{v}_\theta}{r} - \frac{\partial \bar{v}_r}{r \partial \theta} \right] \\
& + \frac{\partial^2}{r \partial \theta^2} \left[\frac{\partial \bar{v}_\theta}{\partial r} + \frac{\bar{v}_\theta}{r} - \frac{\partial \bar{v}_r}{r \partial \theta} \right], \quad (A.10-2)
\end{aligned}$$

$$\begin{aligned}
I_{scr} = & - \frac{\partial}{\partial \theta} \left[\frac{1}{r} \frac{\partial}{\partial r} r (\bar{v}_\theta^2 - \bar{v}_r^2) \right] - \left[\frac{\partial}{\partial r} \frac{1}{r} \frac{\partial}{\partial r} r - \frac{\partial^2}{r^2 \partial \theta^2} \right] (r \bar{v}_r' \bar{v}_\theta'). \quad (A.10-3)
\end{aligned}$$

At this point, the definition of vorticity is introduced as

$$\omega \equiv \frac{1}{r} \frac{\partial}{\partial r} r \bar{v}_\theta - \frac{\partial \bar{v}_r}{r \partial \theta}. \quad (A.11)$$

With the above definition, equation (A.10) takes the form:

$$\bar{v}_r \frac{\partial \omega}{\partial r} + \bar{v}_\theta \frac{\partial \omega}{r \partial \theta} = \nu \left[\frac{1}{r} \frac{\partial}{\partial r} r \frac{\partial \omega}{\partial r} + \frac{\partial^2 \omega}{r^2 \partial \theta^2} \right] + \frac{I_{scr}}{r}. \quad (A.12)$$

This is the transport equation for the vorticity. The term I_c represents convection of vorticity by the secondary flow and it tends to make the vorticity constant along the streamlines. Diffusion of vorticity by viscosity is given by I_D . It tends to make vorticity uniform over the duct cross-section by diffusing it from regions of high intensity to regions of low intensity. In laminar flow, these are the only terms in the equation since Reynolds stresses do not exist. Hence secondary flow cannot occur in a laminar flow because these flow mechanisms serve only to transport and not to generate vorticity. The last term, I_{sor} , represents production (or destruction) of vorticity. (It depends on the relative sense of this term to the vorticity).

In order to eliminate the need of working with the continuity equation (A.6), a stream function ψ is defined as

$$\bar{u}_\theta \equiv -\nu \frac{\partial \psi}{\partial r} ,$$

(A.13)

$$\bar{u}_r \equiv \nu \frac{\partial \psi}{r \partial \theta} .$$

Using this definition, equation (A.7), (A.11) and (A.12) are rewritten in the form below, after rearranging the terms.

Axial momentum equation:

$$\begin{aligned} \frac{1}{r} \frac{\partial}{\partial r} r \bar{u}_z \left(\frac{\partial \psi}{r \partial \theta} \right) - \frac{\partial}{r \partial \theta} \bar{u}_z \left(\frac{\partial \psi}{\partial r} \right) - \frac{1}{r} \frac{\partial}{\partial r} r \left(\frac{\partial \bar{u}_z}{\partial r} - \frac{\overline{u_r' u_z'}}{\nu} \right) \\ - \frac{\partial}{r \partial \theta} \left(\frac{\partial \bar{u}_z}{r \partial \theta} - \frac{\overline{u_\theta' u_z'}}{\nu} \right) = - \frac{1}{g \nu} \frac{\partial \bar{p}}{\partial z} . \end{aligned} \quad (\text{A.14})$$

Stream function equation [obtained directly from eqs. (A.11) and (A.13)]:

$$- \frac{1}{r} \frac{\partial}{\partial r} r \left(\frac{\partial \psi}{\partial r} \right) - \frac{\partial}{r \partial \theta} \left(\frac{\partial \psi}{r \partial \theta} \right) = \frac{\omega}{\nu} . \quad (\text{A.15})$$

Vorticity equation:

$$\begin{aligned} \frac{1}{r} \frac{\partial}{\partial r} r \omega \left(\frac{\partial \psi}{r \partial \theta} \right) - \frac{\partial}{r \partial \theta} \omega \left(\frac{\partial \psi}{\partial r} \right) - \frac{1}{r} \frac{\partial}{\partial r} r \left(\frac{\partial \omega}{\partial r} \right) \\ - \frac{\partial}{r \partial \theta} \left(\frac{\partial \omega}{r \partial \theta} \right) = \frac{I_{sor}}{\nu r} , \end{aligned} \quad (\text{A.16})$$

where I_{SOR} is given by equation (A.10-3).

These three last equations can only be solved with some knowledge of the Reynolds stresses. This represents the closure problem associated with the computation of a turbulent flow. Many turbulence models have been proposed to provide a closed system of equations. The most important models applied to rod bundle flows are discussed in the test.

APPENDIX B

TRANSPORT EQUATION FOR THE
TURBULENCE KINETIC ENERGY (TKE)

In order to provide a closed set of equations, the one-equation turbulence model requires the computation of the turbulence kinetic energy over the region of interest by solving its transport equation. The TKE transport equation is derived from the Navier-Stokes equation by multiplying the momentum equation for each direction by the corresponding fluctuating velocity component, averaging in time and then adding the three equations, that is:

a.1. axial direction:

$$\begin{aligned}
 & \overline{u'_3 \frac{\partial u'_3}{\partial t}} + \overline{u_r u'_3 \frac{\partial u'_3}{\partial r}} + \overline{u'_r u'_3 \frac{\partial \overline{u}_3}{\partial r}} + \overline{u'_r u'_3 \frac{\partial u'_3}{\partial r}} \\
 & + \overline{u_\theta u'_3 \frac{\partial u'_3}{r \partial \theta}} + \overline{u'_\theta u'_3 \frac{\partial \overline{u}_3}{r \partial \theta}} + \overline{u'_\theta u'_3 \frac{\partial u'_3}{r \partial \theta}} \\
 & + \overline{u'_3 \frac{\partial u'_3}{\partial z}} + \overline{u'_3{}^2 \frac{\partial \overline{u}_3}{\partial z}} + \overline{u'_3{}^2 \frac{\partial u'_3}{\partial z}} = -\frac{1}{\rho} \overline{u'_3 \frac{\partial p'}{\partial z}} \\
 & + \nu \overline{u'_3 \left[\frac{1}{r} \frac{\partial}{\partial r} r \frac{\partial u'_3}{\partial r} + \frac{\partial^2 u'_3}{r^2 \partial \theta^2} + \frac{\partial^2 u'_3}{\partial z^2} \right]}. \tag{B.1}
 \end{aligned}$$

a.2. peripheral direction:

$$\begin{aligned}
 & \overline{v'_\theta \frac{\partial v'_\theta}{\partial t}} + \overline{v_r v'_\theta \frac{\partial v'_\theta}{\partial r}} + \overline{v'_r v'_\theta \frac{\partial \bar{v}_\theta}{\partial r}} + \overline{v_r v'_\theta \frac{\partial v'_\theta}{\partial r}} + \\
 & \overline{v_\theta v'_\theta \frac{\partial v'_\theta}{r \partial \theta}} + \overline{v_\theta'^2 \frac{\partial \bar{v}_\theta}{r \partial \theta}} + \overline{v_\theta'^2 \frac{\partial v'_\theta}{r \partial \theta}} + \frac{\overline{v_r v_\theta'^2}}{r} + \\
 & \frac{\overline{v'_\theta v'_r v_\theta}}{r} + \frac{\overline{v'_r v_\theta'^2}}{r} + \overline{v'_\theta v'_\theta \frac{\partial v'_\theta}{\partial z}} + \overline{v'_\theta v'_\theta \frac{\partial \bar{v}_\theta}{\partial z}} + \\
 & \overline{v'_\theta v'_\theta \frac{\partial v'_\theta}{\partial z}} = - \frac{1}{\rho} \overline{v'_\theta \frac{\partial p'}{r \partial \theta}} + \\
 & \nu \overline{v'_\theta \left[\frac{1}{r} \frac{\partial}{\partial r} r \frac{\partial v'_\theta}{\partial r} - \frac{v'_\theta}{r^2} + \frac{\partial^2 v'_\theta}{r^2 \partial \theta^2} + \frac{2}{r} \frac{\partial v'_r}{r \partial \theta} + \frac{\partial^2 v'_\theta}{\partial z^2} \right]}.
 \end{aligned}$$

(B.2)

a.3. radial direction:

$$\begin{aligned}
 & \overline{v_r' \frac{\partial v_r'}{\partial t}} + \overline{v_r v_r' \frac{\partial v_r'}{\partial r}} + \overline{v_r'^2 \frac{\partial \bar{v}_r}{\partial r}} + \overline{v_r'^2 \frac{\partial v_r'}{\partial r}} + \\
 & \overline{v_\theta v_r' \frac{\partial v_r'}{r \partial \theta}} + \overline{v_r' v_\theta'} \frac{\partial \bar{v}_r}{r \partial \theta} + \overline{v_r' v_\theta' \frac{\partial v_r'}{r \partial \theta}} - 2 \frac{\overline{v_r' v_\theta' \bar{v}_\theta}}{r} \\
 & - \frac{\overline{v_r' v_\theta'^2}}{r} + \overline{v_z v_r' \frac{\partial v_r'}{\partial z}} + \overline{v_r' v_z'} \frac{\partial \bar{v}_r}{\partial z} + \\
 & \overline{v_r' v_z' \frac{\partial v_r'}{\partial z}} = - \frac{1}{\rho} \overline{v_r' \frac{\partial p'}{\partial r}} + \\
 & \nu v_r' \left[\frac{1}{r} \frac{\partial}{\partial r} r \frac{\partial v_r'}{\partial r} - \frac{v_r'}{r^2} + \frac{\partial^2 v_r'}{r^2 \partial \theta^2} - \frac{2}{r} \frac{\partial v_\theta'}{\partial \theta} + \frac{\partial^2 v_r'}{\partial z^2} \right].
 \end{aligned}$$

(B.3)

Equations (B.1), (B.2) and (B.3) are added, and use is made of the definition of TKE

$$k' \equiv \frac{1}{2} (u_z'^2 + u_r'^2 + u_\theta'^2) , \quad (\text{B.4})$$

and its time-averaged value

$$\bar{k} = \frac{1}{2} (\overline{u_z'^2} + \overline{u_r'^2} + \overline{u_\theta'^2}) . \quad (\text{B.5})$$

One obtains, using the continuity equation, after a very cumbersome rearranging of terms:

$$\begin{aligned} & \frac{\partial \bar{k}}{\partial t} + \frac{1}{r} \frac{\partial}{\partial r} r (\bar{u}_r \bar{k}) + \frac{\partial}{r \partial \theta} (\bar{u}_\theta \bar{k}) + \frac{\partial}{\partial z} (\bar{u}_z \bar{k}) \\ & - \left[\frac{1}{r} \frac{\partial}{\partial r} r \left(\nu \frac{\partial \bar{k}}{\partial r} - \overline{u_r' k'} \right) + \frac{\partial}{r \partial \theta} \left(\nu \frac{\partial \bar{k}}{r \partial \theta} - \overline{u_\theta' k'} \right) \right. \\ & \left. + \frac{\partial}{\partial z} \left(\nu \frac{\partial \bar{k}}{\partial z} - \overline{u_z' k'} \right) \right] = S_1 + S_2 + S_3 + S_4 , \quad (\text{B.6}) \end{aligned}$$

where

$$S_1 = -\frac{1}{\rho} \left[\frac{1}{r} \frac{\partial}{\partial r} r (\overline{u_r' p'}) + \frac{\partial}{r \partial \theta} (\overline{u_\theta' p'}) + \frac{\partial}{\partial z} (\overline{u_z' p'}) \right],$$

$$S_2 = -\nu \left\{ \left[\left(\frac{\partial \overline{u_r'}}{\partial r} \right)^2 + \left(\frac{\partial \overline{u_\theta'}}{\partial r} \right)^2 + \left(\frac{\partial \overline{u_z'}}{\partial r} \right)^2 \right] + \left[\left(\frac{\partial \overline{u_r'}}{r \partial \theta} \right)^2 + \left(\frac{\partial \overline{u_\theta'}}{r \partial \theta} \right)^2 + \left(\frac{\partial \overline{u_z'}}{r \partial \theta} \right)^2 \right] + \left[\left(\frac{\partial \overline{u_r'}}{\partial z} \right)^2 + \left(\frac{\partial \overline{u_\theta'}}{\partial z} \right)^2 + \left(\frac{\partial \overline{u_z'}}{\partial z} \right)^2 \right] \right\},$$

$$S_3 = - \left\{ \left[\overline{u_r'^2} \frac{\partial \overline{u_r}}{\partial r} + \overline{u_r' u_\theta'} \frac{\partial \overline{u_\theta}}{\partial r} + \overline{u_r' u_z'} \frac{\partial \overline{u_z}}{\partial r} \right] + \left[\overline{u_\theta' u_r'} \frac{\partial \overline{u_r}}{r \partial \theta} + \overline{u_\theta'^2} \frac{\partial \overline{u_\theta}}{r \partial \theta} + \overline{u_\theta' u_z'} \frac{\partial \overline{u_z}}{r \partial \theta} \right] + \left[\overline{u_z' u_r'} \frac{\partial \overline{u_r}}{\partial z} + \overline{u_z' u_\theta'} \frac{\partial \overline{u_\theta}}{\partial z} + \overline{u_z'^2} \frac{\partial \overline{u_z}}{\partial z} \right] + \left[\frac{\overline{u_\theta'^2} \overline{u_r}}{r} - \frac{\overline{u_r' u_\theta'} \overline{u_\theta}}{r} \right] \right\},$$

$$S_4 = -\frac{\nu}{r} \left[\frac{\overline{u_r'^2} + \overline{u_\theta'^2}}{r} + 2 \left(\overline{u_r' \frac{\partial u_\theta'}{r \partial \theta}} - \overline{u_\theta' \frac{\partial u_r'}{r \partial \theta}} \right) \right].$$

In order to transform this equation into a more workable form, a few approximations are necessary:

i. the term S_1 , which represents diffusion of K by fluctuating pressure effects, is assumed to be negligible;

ii. the terms S_2 and S_4 represent the rate of dissipation of K by molecular viscosity. Prandtl suggested, based on dimensional analysis, a simple form for these terms

$$S_2 + S_4 = - \frac{\bar{K}^{3/2}}{\ell_D} \equiv - D_K$$

where ℓ_D is the dissipation length scale of TKE.

D_K is associated with the mixing length and can be expressed as

$$D_K = C_D \frac{\bar{K}^{3/2}}{\ell} \quad , \quad (B.7)$$

where C_D is a function of the Reynolds number of turbulence, R_t . In fact, C_D is inversely proportional to R_t . For R_t large, however, C_D is expected to assume a constant value (see, for example, ref. 2, pg.287).

iii. The terms S_3 represents the rate of energy

transferred from the main flow to the turbulent eddies.

Gradients of the main velocity are predominant in affecting this transfer. Neglecting other velocity gradients and applying the fully developed flow condition, yields

$$S_3 = - \left[\overline{u_r' u_z'} \frac{\partial \bar{u}_z}{\partial r} + \overline{u_\theta' u_z'} \frac{\partial \bar{u}_z}{r \partial \theta} \right]. \quad (\text{B.8})$$

Making use of the definition of stream function given by equation (A.13) and the conditions of steady state, fully developed flow, equation (B.6) is reduced to

$$\begin{aligned} \frac{1}{r} \frac{\partial}{\partial r} r \bar{k} \left(\frac{\partial \psi}{r \partial \theta} \right) - \frac{\partial}{r \partial \theta} \bar{k} \left(\frac{\partial \psi}{\partial r} \right) - \frac{1}{r} \frac{\partial}{\partial r} r \left(\frac{\partial \bar{k}}{\partial r} - \frac{\overline{u_r' k'}}{\nu} \right) \\ - \frac{\partial}{r \partial \theta} \left(\frac{\partial \bar{k}}{r \partial \theta} - \frac{\overline{u_\theta' k'}}{\nu} \right) = - C_D \frac{\bar{k}^{-3/2}}{\ell} - \left[\overline{u_r' u_z'} \left(\frac{\partial \bar{u}_z}{\partial r} \right) + \overline{u_\theta' u_z'} \left(\frac{\partial \bar{u}_z}{r \partial \theta} \right) \right]. \end{aligned} \quad (\text{B.9})$$

This is the usual form of transport equation for the TKE used by one-equation turbulence models.

APPENDIX C

ANALYTICAL APPROACH FOR VORTICITY SOURCE TERM
BASED ON THE ALGEBRAIC STRESS MODEL⁽⁵⁾

As shown in chapter III, the vorticity source term, for rod bundle geometries, can be approximated by

$$I_{\text{SOR}} \simeq - \frac{\partial}{\partial \theta} \left[\frac{1}{r} \frac{\partial}{\partial r} r (\overline{u_\theta'^2} - \overline{u_r'^2}) \right] \quad (\text{C.1})$$

The starting point to obtain an analytical approximation for the difference $(\overline{v_\theta'^2} - \overline{v_r'^2})$ is the exact transport equations for the normal Reynolds stresses in the tangential and radial directions. They are equations (B.2) and (B.3) given in appendix B.

Take equation (B.3) in the form:

$$\underbrace{\left[\frac{\partial \overline{u_r'^2}}{\partial t} + \frac{1}{r} \frac{\partial}{\partial r} r \overline{u_r u_r'^2} + \frac{\partial}{r \partial \theta} \overline{u_\theta u_r'^2} + \frac{\partial}{\partial z} \overline{u_z u_r'^2} \right]}_{\text{Convection}} =$$

$$\underbrace{-2 \left[\overline{u_r'^2} \frac{\partial \overline{u_r}}{\partial r} + \overline{u_r' u_\theta'} \frac{\partial \overline{u_r}}{r \partial \theta} - 2 \overline{u_r' u_\theta'} \frac{\overline{u_\theta}}{r} + \overline{u_r' u_z'} \frac{\partial \overline{u_r}}{\partial z} \right]}_{\text{Generation}}$$

$$\begin{aligned}
& \underbrace{-2\nu \left[\overline{\left(\frac{\partial v_r'}{\partial r}\right)^2} + \overline{\left(\frac{\partial v_r'}{r\partial\theta}\right)^2} + \overline{\left(\frac{\partial v_r'}{\partial z}\right)^2} \right]}_{\text{Destruction}} + \underbrace{2 \frac{p'}{\rho} \frac{\partial v_r'}{\partial r}}_{\text{Redistribution}} \\
& - \underbrace{\left\{ \left[\frac{1}{r} \frac{\partial}{\partial r} r \overline{v_r'^3} + \frac{\partial}{r\partial\theta} \overline{v_\theta' v_r'^2} + \frac{\partial}{\partial z} \overline{v_z' v_r'^2} - \frac{\overline{v_\theta'^2 v_r'}}{r} \right] + 2 \frac{\partial}{\partial r} \frac{p' v_r'}{\rho} \right\}}_{\text{Diffusion}} \\
& - \underbrace{\nu \left\{ \left[\frac{1}{r} \frac{\partial}{\partial r} r \frac{\partial \overline{v_r'^2}}{\partial r} - \frac{\overline{v_r'^2}}{r^2} + \frac{\partial^2 \overline{v_r'^2}}{r^2 \partial\theta^2} + \frac{\partial^2 \overline{v_r'^2}}{\partial z^2} - 4 \frac{\overline{v_r'}}{r^2} \frac{\partial \overline{v_\theta'}}{\partial\theta} \right] \right\}}_{\text{Diffusion}}
\end{aligned} \tag{C.2}$$

Each one of the terms in the transport equation for $\overline{v_r'^2}$ can be identified as shown in equation (C.2).

The approximations involved in the algebraic stress model are:

(a) since vorticity is produced near solid walls and since only the distribution of $\overline{v_r'^2}$ in those regions is of interest, convection and diffusion terms are neglected as being very small in those regions;

(b) generation terms are negligible because gradients of secondary flows are very small compared to gradients of the axial flow, and thus are very small compared to the redistribution term; which as shown in equation (C.10)

is proportional to axial flow gradients. Note that the action of the redistribution term is to diminish the difference between the normal stress components⁽²⁾;

- (c) at high Re, dissipative motions should be isotropic. So, the destruction terms are approximated by $\frac{2}{3} \epsilon$, where ϵ is the dissipative rate of turbulence energy.

Using the above approximations, equation (C.2) is reduced to

$$\overline{\frac{p'}{\rho} \frac{\partial v_r'}{\partial r}} \approx \frac{\epsilon}{3} . \quad (C.3)$$

Analogous considerations can be applied to the tangential component of the normal Reynolds stresses, yielding

$$\overline{\frac{p'}{\rho} \frac{\partial v_\theta'}{r \partial \theta}} \approx \frac{\epsilon}{3} . \quad (C.4)$$

So, an approximate equation for $\overline{(v_\theta'^2 - v_r'^2)}$ can be written as

$$\overline{\frac{p'}{\rho} \left(\frac{\partial v_\theta'}{r \partial \theta} - \frac{\partial v_r'}{\partial r} \right)} = 0 . \quad (C.5)$$

Solution of equation (C.5) is next required to yield $\overline{(v_\theta'^2 - v_r'^2)}$. However, as quoted by Launder and Ying⁽⁵⁾, approximations of the correlations between pressure and velocity-gradient fluctuations are the least certain aspect

of closing the Reynolds stress equations.

It has been shown by Chou⁽⁶⁾ that the fluctuating component of the pressure obeys a Poisson equation and that the pressure fluctuation can be obtained by solving such equation. Take the divergence of the complete Navier-Stokes equation and apply the continuity equation in order to obtain the quantity $\frac{1}{\rho} \nabla^2(\bar{p} + p')$ in terms of velocity derivatives. The equation for p' is obtained observing that

$$\frac{1}{\rho} \nabla^2 p' = \frac{1}{\rho} \nabla^2(\bar{p} + p') - \overline{\frac{1}{\rho} \nabla^2(\bar{p} + p')} \quad (C.6)$$

Equation (C.6), in cylindrical coordinates, is

$$-\frac{1}{\rho} \nabla^2 p' = C_1 + C_2 + C_3, \quad (C.7)$$

where:

$$\begin{aligned} C_1 = & 2 \left[\left(\frac{\partial \bar{u}_r}{\partial r} \right) \left(\frac{\partial v_r'}{\partial r} \right) + \left(\frac{\partial \bar{v}_\theta}{r \partial \theta} \right) \left(\frac{\partial v_\theta'}{r \partial \theta} \right) + \left(\frac{\partial \bar{u}_z}{\partial z} \right) \left(\frac{\partial v_z'}{\partial z} \right) \right. \\ & + \left(\frac{\partial \bar{v}_r}{r \partial \theta} \right) \left(\frac{\partial v_\theta'}{\partial r} \right) + \left(\frac{\partial \bar{u}_r}{\partial z} \right) \left(\frac{\partial v_z'}{\partial r} \right) + \left(\frac{\partial \bar{v}_\theta}{\partial r} \right) \left(\frac{\partial v_r'}{r \partial \theta} \right) \\ & \left. + \left(\frac{\partial \bar{v}_\theta}{\partial z} \right) \left(\frac{\partial v_z'}{r \partial \theta} \right) + \left(\frac{\partial \bar{u}_z}{\partial r} \right) \left(\frac{\partial v_r'}{\partial z} \right) + \left(\frac{\partial \bar{u}_z}{r \partial \theta} \right) \left(\frac{\partial v_\theta'}{\partial z} \right) \right] \\ & + \frac{2}{r} \left[\frac{\bar{u}_r v_r'}{r} - \frac{\partial}{\partial r} (\bar{v}_\theta v_\theta') + \bar{u}_r \frac{\partial v_\theta'}{r \partial \theta} + v_r' \frac{\partial \bar{v}_\theta}{r \partial \theta} \right], \end{aligned}$$

$$\begin{aligned}
C_2 = & \frac{1}{r} \frac{\partial}{\partial r^2} r u_r'^2 + \frac{\partial^2 u_\theta'^2}{r^2 \partial \theta^2} + \frac{\partial^2 u_z'^2}{\partial z^2} + \left(\frac{1}{r} \frac{\partial}{\partial r} r \frac{\partial}{\partial \theta} + \frac{\partial}{r \partial \theta} \frac{1}{r} \frac{\partial}{\partial r} r \right) (u_\theta' u_r') \\
& + \left(\frac{1}{r} \frac{\partial}{\partial r} r \frac{\partial}{\partial z} + \frac{\partial}{\partial z} \frac{1}{r} \frac{\partial}{\partial r} \right) (u_r' u_z') + \left(\frac{\partial}{r \partial \theta} \frac{\partial}{\partial z} + \frac{\partial}{\partial z} \frac{\partial}{r \partial \theta} \right) (u_\theta' u_z') \\
& - \frac{1}{r} \left[\frac{\partial u_\theta'^2}{\partial r} + \frac{\partial}{\partial z} (u_z' u_r') \right],
\end{aligned}$$

$$\begin{aligned}
C_3 = & \frac{1}{r} \frac{\partial}{\partial r} r \left[\overline{u_r' \frac{\partial u_r'}{\partial r}} + \overline{u_\theta' \frac{\partial u_r'}{r \partial \theta}} - \frac{\overline{u_\theta'^2}}{r} + \overline{u_z' \frac{\partial u_r'}{\partial z}} \right] \\
& + \frac{\partial}{r \partial \theta} \left[\overline{u_r' \frac{\partial u_\theta'}{\partial r}} + \overline{u_\theta' \frac{\partial u_\theta'}{r \partial \theta}} + \frac{\overline{u_r' u_\theta'}}{r} + \overline{u_z' \frac{\partial u_\theta'}{\partial z}} \right] \\
& + \frac{\partial}{\partial z} \left[\overline{u_r' \frac{\partial u_z'}{\partial r}} + \overline{u_\theta' \frac{\partial u_z'}{r \partial \theta}} + \overline{u_z' \frac{\partial u_z'}{\partial z}} \right].
\end{aligned}$$

Observe that the term C_1 is mainly products of gradients of time-averaged and fluctuating velocity components. Term C_2 involves only derivatives of instantaneous Reynolds stresses. Term C_3 represents correlations and derivatives of correlations between velocity and velocity-gradient fluctuations.

The solution of equation (C.7) is obtained by application of Green's theorem given p' as an integral over all space⁽⁷⁾:

$$\begin{aligned}
 p'(\underline{r}) = & -\frac{1}{4\pi} \int_{\text{Volume}} \frac{1}{|\underline{r}-\underline{r}^*|} \nabla^2 p'(\underline{r}^*) d\text{Vol}(\underline{r}^*) \\
 & - \frac{1}{4\pi} \int_{\text{Surface}} p'(\underline{r}^*) \frac{\partial}{\partial n^*} \left(\frac{1}{|\underline{r}-\underline{r}^*|} \right) dS(\underline{r}^*) \\
 & + \frac{1}{4\pi} \int_{\text{Surface}} \frac{1}{|\underline{r}-\underline{r}^*|} \frac{\partial}{\partial n^*} p'(\underline{r}^*) dS(\underline{r}^*) . \quad (\text{C.8})
 \end{aligned}$$

Chou⁽⁶⁾ observed that "p' and gradients of p' at a point P are determined by the turbulent velocity fluctuations v'_i not only at P but everywhere within the fluid. Due to the factor $\frac{1}{|\underline{r}-\underline{r}^*|}$ in the integrands the effect of the velocity distribution at distant points P* on the pressure fluctuation at P gradually dies away as P* recedes farther and farther from P." Based on the above argument, Chou suggested that the surface integrals for points away from the immediate vicinity of a wall can be neglected, reducing equation (C.8) to

$$p'(\underline{r}) = -\frac{1}{4\pi} \int_{\text{Volume}} \nabla^2 p'(\underline{r}^*) \frac{d\text{Vol}(\underline{r}^*)}{|\underline{r} - \underline{r}^*|} . \quad (\text{C.9})$$

Now, the value of $\nabla^2 p'(\underline{r})$ given by equation (C.7) can be plugged into eq. (C.9). Multiply both sides of the resultant equation by $\frac{\partial v'_\theta}{r \partial \theta}$ and average in time. In tensor notation, equation (C.9) becomes:

$$\overline{\frac{p'}{\rho} \left(\frac{\partial v'_\theta}{r \partial \theta} \right)} \approx \frac{1}{2\pi} \int_{\text{Vol}} \left(\frac{\partial \bar{v}'_i}{\partial \xi'_j} \right)^* \overline{\left(\frac{\partial v'_j}{\partial \xi'_i} \right)^* \left(\frac{\partial v'_\theta}{r \partial \theta} \right)} \frac{d\text{Vol}}{|\underline{r} - \underline{r}^*|} + \frac{1}{4\pi} \int_{\text{Vol}} \frac{\partial}{\partial \eta'_i} \left(\frac{\partial}{\partial \eta'_j} v'_i v'_j \right)^* \left(\frac{\partial v'_\theta}{r \partial \theta} \right) \frac{d\text{Vol}}{|\underline{r} - \underline{r}^*|} , \quad (\text{C.10})$$

where

$$\frac{\partial}{\partial \xi'_r} \equiv \frac{\partial}{\partial r} , \quad \frac{\partial}{\partial \xi'_\theta} \equiv \frac{\partial}{r \partial \theta} , \quad \frac{\partial}{\partial \xi'_\phi} \equiv \frac{\partial}{\partial \phi} ,$$

$$\frac{\partial}{\partial \eta'_r} \equiv \frac{1}{r} \frac{\partial}{\partial r} r , \quad \frac{\partial}{\partial \eta'_\theta} \equiv \frac{\partial}{r \partial \theta} , \quad \frac{\partial}{\partial \eta'_\phi} \equiv \frac{\partial}{\partial \phi} .$$

An analogous equation can be obtained for the quantity $\overline{\frac{p'}{\rho} \frac{\partial v'_r}{\partial r}}$.

The above equation shows that the correlation between pressure and velocity-gradient fluctuations arises mainly from

two kinds of physical interactions. The first has its origin in the interaction between the main rate of strain and turbulence and the second from mutual interaction between turbulence components. So, in a general form, one writes

$$\overline{\frac{p'}{s} \frac{\partial v_i'}{\partial \xi_j'}} = \phi_{ij,1} + \phi_{ij,2} \quad (C.11)$$

where $\phi_{ij,1}$ and $\phi_{ij,2}$ represent the main rate of strain-turbulence and turbulence-turbulence interactions, respectively.

Utilizing the general form of eq. (C.11), equation (C.5) becomes:

$$\frac{p'}{s} \left(\frac{\partial v_\theta'}{\partial \theta} - \frac{\partial v_r'}{\partial r} \right) = (\phi_{\theta\theta} - \phi_{rr})_1 + (\phi_{\theta\theta} - \phi_{rr})_2 = 0. \quad (C.12)$$

The ϕ terms are next evaluated.

a. Interaction between the main rate of strain and turbulence.

As a first approximation, assuming that the mean velocity varies linearly over the volume that can contribute significantly to the pressure-velocity gradient correlation, the term $\phi_{ij,1}$ can be written as

$$\phi_{ij,1} \approx a_{lj}^{mi} \left(\frac{\partial \bar{v}_l}{\partial \xi_m} \right), \quad (C.13)$$

where

$$a_{ej}^{mi} \simeq \frac{1}{2\pi} \int_{V_{cl}} \overline{\left(\frac{\partial v_m'}{\partial \xi_e} \right)^* \left(\frac{\partial v_i'}{\partial \xi_j} \right)} \frac{dV_{cl}}{|r-r^*|} .$$

This approximation was first proposed by Chou⁽⁶⁾. Hanjalić⁽⁸⁾ proposed that the coefficients a_{ij}^{mi} could be satisfactorily approximated by a linear combination of Reynolds stresses involving one (or both) of the velocity components v_j' or v_i' . The expression proposed is

$$\begin{aligned} a_{ej}^{mi} = & \alpha \overline{v_m' v_i'} \delta_{ej} + \beta \left(\overline{v_m' v_e'} \delta_{ij} + \overline{v_m' v_j'} \delta_{ie} + \overline{v_i' v_j'} \delta_{me} \right. \\ & \left. + \overline{v_i' v_e'} \delta_{mj} \right) + \left(\gamma \delta_{mi} \delta_{ej} + \eta \left[\delta_{me} \delta_{ij} + \delta_{mj} \delta_{ie} \right] \right) K \\ & + \nu \left(\overline{v_m' v_j'} \overline{v_i' v_e'} + \overline{v_m' v_e'} \overline{v_i' v_j'} \right) / K + c_2 \left(\overline{v_m' v_i'} \overline{v_e' v_j'} \right) / K , \end{aligned} \quad (C.14)$$

where α , β , γ , η , ν and c_2 are constants. Conditions of symmetry and mass conservation enable five of them to be determined in terms of the sixth. The correlation $\overline{v_m' v_j'} \overline{v_i' v_e'}$ is to be replaced by $\overline{v_m' v_i'} K$ whenever it appears to ensure that ν and c_2 are non-zero.

For the present case, the following expressions for $\phi_{lm,1}$ are obtained:

$$\phi_{ee,1} \simeq a_{3e}^{re} \left(\frac{\partial \bar{U}_3}{\partial r} \right) + a_{3e}^{ee} \left(\frac{\partial \bar{U}_3}{r \partial e} \right) , \quad (C.15)$$

$$\phi_{r,i} \approx a_{3r}^{rr} \left(\frac{\partial \bar{u}_3}{\partial r} \right) + a_{3r}^{\theta\theta} \left(\frac{\partial \bar{u}_3}{r \partial \theta} \right). \quad (C.16)$$

Other velocity gradients were neglected as being much smaller than gradients of the axial velocity of the flow.

b. Mutual interaction between turbulence components.

In a non-isotropic homogeneous flow in conditions where the velocity gradients of the main flow are small or zero, only this part is significant in the turbulence redistribution process. This kind of flow decays to the more probable isotropic state and the process denoted by $\phi_{1m,2}$ must proceed to equalize the normal-stress components and to eliminate the shear stresses. Based on this reasoning, Rotta⁽⁹⁾ proposed and confirmed through analysis of experimental data that

$$(\phi_{ij} + \phi_{ji})_2 \approx -c_1 \left(\frac{\epsilon}{k} \right) (\overline{u_i' u_j'} - \frac{2}{3} k \delta_{ij}), \quad (C.17)$$

where ϵ is the dissipation rate of turbulence kinetic energy and c_1 , a constant with value between 2.5 and 3.0. This expression is generally accepted.

Using the expressions (C.15), (C.16) and (C.17), obtained in the previous sections, for the interaction terms,

equation (C.12) becomes:

$$\begin{aligned} & (a_{\partial\theta}^{r\theta} - a_{\partial r}^{rr}) \left(\frac{\partial \bar{u}_3}{\partial r} \right) + (a_{\partial\theta}^{\theta\theta} - a_{\partial r}^{\theta r}) \left(\frac{\partial \bar{u}_3}{r \partial \theta} \right) \\ & - \frac{c_1}{2} \left(\frac{\varepsilon}{k} \right) (\bar{u}_\theta'^2 - \bar{u}_r'^2) = 0. \end{aligned} \quad (C.18)$$

Using (C.14),

$$\begin{aligned} (a_{\partial\theta}^{r\theta} - a_{\partial r}^{rr}) &= -\beta \overline{u_r' u_\theta'} + \nu \left[\overline{u_r' u_\theta'} \overline{u_\theta' u_\theta'} + \overline{u_\theta' u_r'} (\bar{u}_\theta'^2 - 2\bar{u}_r'^2) \right] / k \\ &+ c_2 (\overline{u_r' u_\theta'} \overline{u_\theta' u_\theta'} - \bar{u}_r'^2 \overline{u_r' u_\theta'}) / k, \end{aligned} \quad (C.19)$$

$$\begin{aligned} (a_{\partial\theta}^{\theta\theta} - a_{\partial r}^{\theta r}) &= \beta \overline{u_\theta' u_\theta'} + \nu \left[\overline{u_\theta' u_\theta'} (2\bar{u}_\theta'^2 - \bar{u}_r'^2) - \overline{u_\theta' u_r'} \overline{u_\theta' u_r'} \right] / k \\ &+ c_2 (\overline{u_\theta' u_\theta'} \bar{u}_\theta'^2 - \overline{u_\theta' u_r'} \overline{u_\theta' u_r'}) / k. \end{aligned} \quad (C.20)$$

Hanjalić further showed that

$$\begin{aligned} \nu &= -c_2 \\ \beta &= -(2-6c_2)/11 \quad \text{and} \\ c_2 &= 0.4. \end{aligned}$$

Equation (C.18) can now be written as

$$\begin{aligned} & - \left[\frac{c_1}{2} \left(\frac{\varepsilon}{k} \right) + \frac{c_2}{k} \left(\overline{u_r' u_\theta'} \frac{\partial \bar{u}_3}{\partial r} + \overline{u_\theta' u_\theta'} \frac{\partial \bar{u}_3}{r \partial \theta} \right) \right] (\bar{u}_\theta'^2 - \bar{u}_r'^2) = \\ & \frac{(2-6c_2)}{11} \left[\overline{u_\theta' u_\theta'} \frac{\partial \bar{u}_3}{r \partial \theta} - \overline{u_r' u_\theta'} \frac{\partial \bar{u}_3}{\partial r} \right]. \end{aligned} \quad (C.21)$$

The terms $-\frac{\overline{v'_r v'_z}}{r} \frac{\partial \bar{v}_z}{\partial r}$ and $-\frac{\overline{v'_\theta v'_z}}{r} \frac{\partial \bar{v}_z}{r \partial \theta}$ denote the rate at which the longitudinal components gain energy by action of the velocity gradients when all other effects are assumed to be absent. Call it P_k , that is,

$$P_k \approx -\overline{v'_r v'_z} \frac{\partial \bar{v}_z}{\partial r} - \overline{v'_\theta v'_z} \frac{\partial \bar{v}_z}{r \partial \theta} . \quad (C.22)$$

Replacement of P_k by ϵ is consistent with the approximations made to obtain equation (C.5). Thus equation (C.21) is reduced to

$$(\overline{v_e'^2} - \overline{v_r'^2}) \approx c' \frac{k}{\epsilon} \left[\overline{v'_\theta v'_z} \left(\frac{\partial \bar{v}_z}{r \partial \theta} \right) - \overline{v'_r v'_z} \left(\frac{\partial \bar{v}_z}{\partial r} \right) \right] , \quad (C.23)$$

where

$$c' = -\frac{2(2-6c_2)}{11(c_1-2c_2)} .$$

It has been assumed that

$$\overline{v'_\theta v'_z} \approx -\nu_T \left(\frac{\partial \bar{v}_z}{r \partial \theta} \right) ,$$

$$\overline{v'_r v'_z} \approx -\nu_T \left(\frac{\partial \bar{v}_z}{\partial r} \right) , \quad \text{with}$$

$$\nu_T = c_\nu k^{1/2} l .$$

The rate of dissipation of turbulence kinetic energy, ϵ , is given by

$$\varepsilon = c_D \frac{k^{3/2}}{l} .$$

Taking these facts into account, equation (C.23) is finally reduced to

$$(\overline{v_\theta'^2} - \overline{v_r'^2}) \approx -c l^2 \left[\left(\frac{\partial \overline{v_z}}{r \partial \theta} \right)^2 - \left(\frac{\partial \overline{v_z}}{\partial r} \right)^2 \right] , \quad (\text{C.24})$$

with

$$c = c' \frac{C_v}{C_D} .$$

APPENDIX D

NUMERICAL PROCEDURE TO COMPUTE MIXING LENGTH USING BULEEV'S EQUATION

Buleev's equation, for the mixing length, ℓ , is⁽³⁾

$$\frac{1}{\ell} = \frac{1}{2} \int_0^{2\pi} \frac{d\psi}{s} \quad (D.1)$$

where s is the distance from the point being analysed to the solid walls, in the direction ϕ .

To numerically obtain ℓ , the contributions of the rods were divided into two groups: the first contribution is that of the rods in the immediate vicinity (i.e. rods 1,2, 3,4 in Fig.D.1) of the subchannel being studied; the second one is that coming from far away rods. The integral (D.1) is carried out only over the region of rods "seen" directly by the point P (see Fig. D.1).

In cylindrical coordinates, the point P is defined by (r_p, θ_p) . In order that all rods can be treated by the same numerical procedure, a cartesian coordinate system is utilized as shown in fig. D.1. The point P is, then, expressed by (x_p, y_p) where

$$x_p = \frac{P}{2} - r_p \cos \theta_p \quad , \quad (D.2)$$

$$y_p = r_p \sin \theta_p \quad .$$

The distance from P to the center of the rod "i" {say $C_i \equiv (x_i, y_i)$ }, is given by

$$d_i \equiv \left[(x_p - x_i)^2 + (y_p - y_i)^2 \right]^{1/2}, \quad (D.3)$$

and the angle formed by the line connecting the point P to C_i and the tangent to the corresponding rod, passing through P, is

$$\beta_i \equiv \text{Arc sin} \left(\frac{R}{d_i} \right). \quad (D.4)$$

The distance from P to the surface of the rod i, for a given angle $\beta \leq \beta_i$ is

$$s = d_i \cos \beta - \left[R^2 - d_i^2 \sin^2 \beta \right]^{1/2}. \quad (D.5)$$

If none of the other rods "projects a shadow" over rod i, as is shown in fig. D.2, its contribution is given by

$$\Sigma_i = \frac{1}{2} \int_{-\beta_i}^{+\beta_i} \frac{d\beta}{s}, \quad (D.6)$$

with s given by (D.5) and β_i by (D.4).

In order to determine whether or not a rod j is projecting a shadow over rod i, the angle β_{ij} given by the line connecting P to the center of rod i and the line tangent to rod j passing through P is calculated by simple geometry. If $\beta_{ij} \geq \beta_i$, no shadow is projected by rod j, hence β_i can be

used as one of the integration limits of equation (D.6).

On the other hand, if $\beta_{ij} < \beta_i$, the point P cannot see the rod i completely and so, β_{ij} will be one of the limits of the integration (D.6).

This procedure is followed for all rods, however, in the estimate of integral (D.6) regarding the contribution of far away rods, generically called rod "i" in this paragraph, s is assumed as being

$$s \approx d_i - R, \quad (D.7)$$

yielding

$$\Sigma_i \approx \frac{1}{2} \frac{\Delta\beta_i}{d_i - R}, \quad (D.8)$$

where $\Delta\beta_i$ limits the portion of that far away rod "i" seen by the point P. This approximation is reasonable because usually this Σ_i is very small compared to the contributions given by the closer rods and they are only included for mathematical rigor. This explains the reason for separating the contribution for the mixing length into two groups as mentioned previously.

The integral (D.6), in its most general form can be written as

$$\Sigma_i = \frac{1}{2} \int_{-\beta_s'}^{+\beta_s} \frac{d\beta}{\lambda}, \quad (D.9)$$

where β_s can be different from $\beta_{s'}$. Assume $\beta_s \geq \beta_{s'}$.

Σ_i can be written

$$\Sigma_i = \frac{1}{2} \int_{-\beta_{s'}}^{\beta_{s'}} \frac{d\beta}{\lambda} + \frac{1}{2} \int_{\beta_{s'}}^{\beta_s} \frac{d\beta}{\lambda}$$

or

$$\Sigma_i = \int_0^{\beta_{s'}} \frac{d\beta}{\lambda} + \frac{1}{2} \int_{\beta_{s'}}^{\beta_s} \frac{d\beta}{\lambda} \quad (D.10)$$

In the first term, $\beta_{s'}$ is divided into 10 parts and the following numerical expression ⁽⁴⁾ is applied:

$$\int_{x_0}^{x_{10}} f(x) dx \cong \frac{5h}{299376} \left\{ 16067 (f_0 + f_{10}) + 106300 (f_1 + f_9) \right. \\ \left. - 48525 (f_2 + f_8) + 272400 (f_3 - f_7) - 260550 (f_4 + f_6) + 427368 f_5 \right\}.$$

The second term is estimated by dividing $(\beta_s - \beta_{s'})$ into 5 parts and applying the expression ⁽⁴⁾:

$$\int_{x_0}^{x_5} f(x) dx \cong \frac{5h}{288} [19(f_0 + f_5) + 75(f_1 + f_3) + 50 f_2].$$

In these expressions, $h \equiv x_{i+1} - x_i$.

For the present case, $x \equiv \beta$ and $f(x) \equiv f(\beta) = \frac{1}{s}$,

where s is given by equation (D.5).

Although this numerical procedure differs from that used by Bender and co-workers ⁽¹⁰⁾, the results were the same.

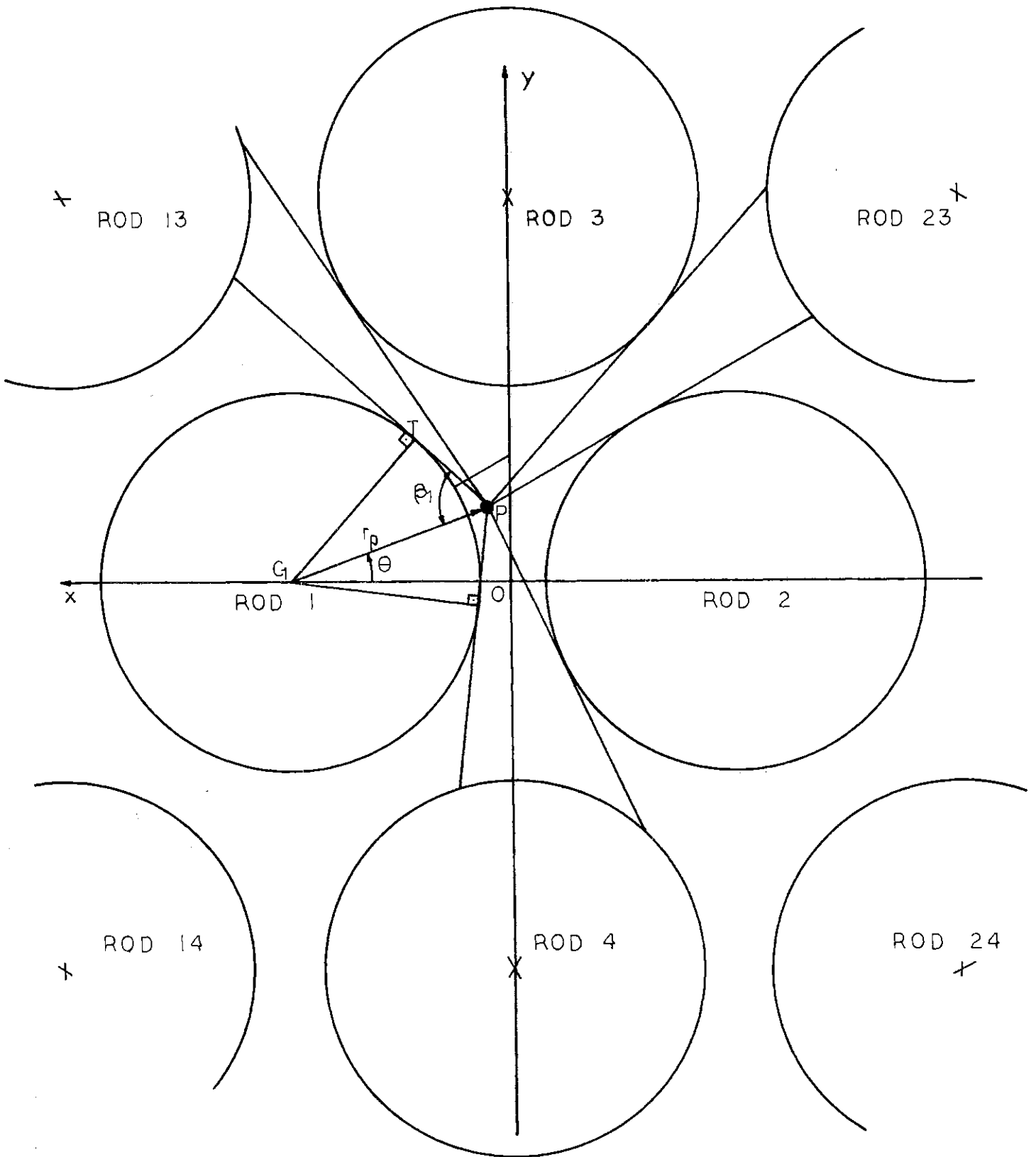


Fig. D.1. Computational Procedure of Buleev's Mixing Length

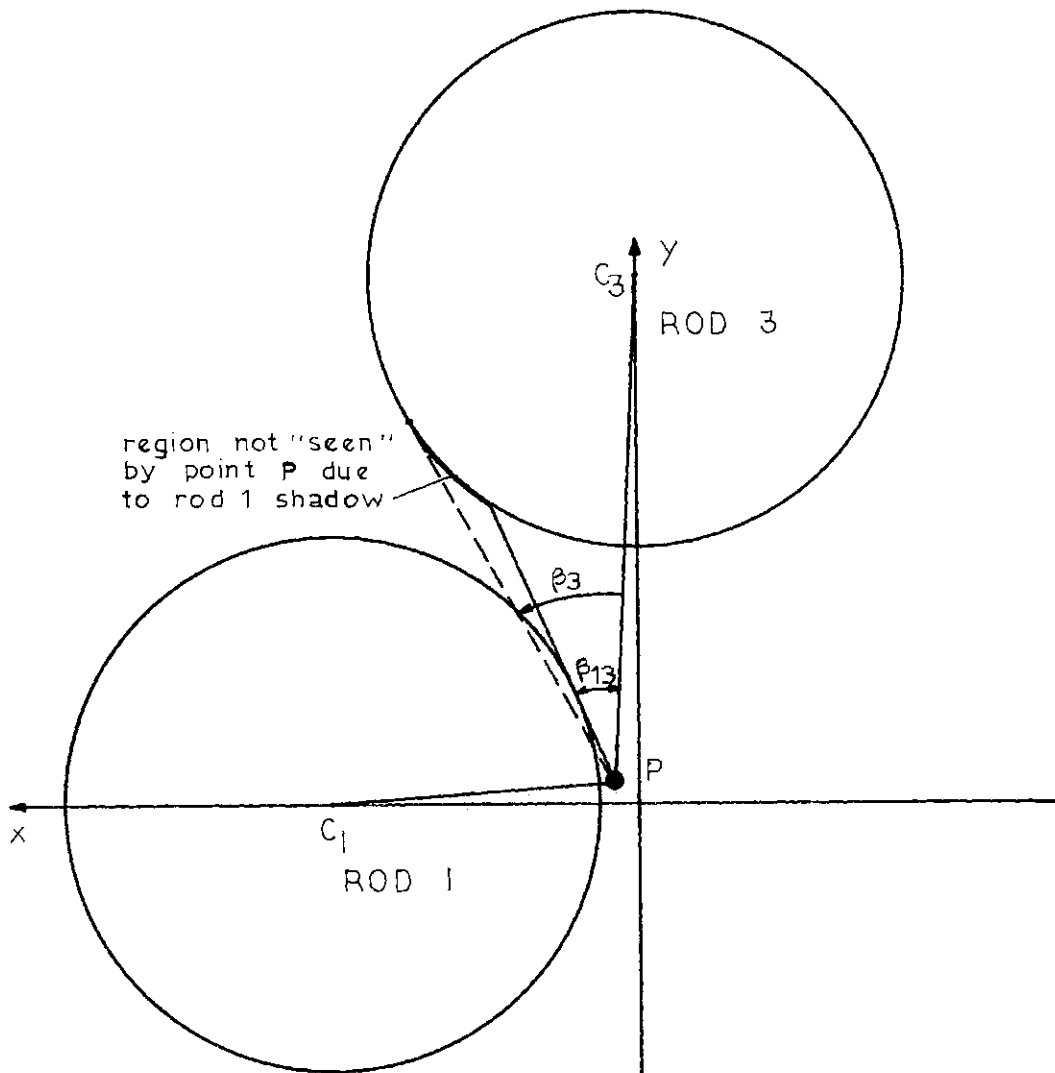


Fig. D.2. "Shadow" of Rod 1 over Rod 3 relative to Point P

APPENDIX E

COMMENT ON THE TURBULENT INTENSITY CORRELATIONS AS PROPOSED BY BOBKOV AND CO-WORKERS⁽¹¹⁾

Studying experimental data on the intensity of velocity fluctuations in turbulent flow in channels of different shape, Bobkov and co-workers found that the turbulent intensities could be correlated in form

$$v_i' \approx v_z \left[1 - \frac{v_b}{(v_z)_{\max}} \right] \cdot A_i e^{-B_i \frac{y}{y_0}} \quad (\text{E.1})$$

where

$$v_i' \equiv \sqrt{v_i'^2}$$

v_z = local axial velocity,

$(v_z)_{\max}$ = maximum axial velocity in the field,

v_b = bulk velocity,

A_i and B_i , constants function of the direction i .

They also pointed out that relation (E.1) was valid regardless of the existence of secondary flows in the plane of the cross section of the channels.

Since the turbulence kinetic energy is

$$k = \frac{1}{2} \left[\overline{v_z'^2} + \overline{v_\theta'^2} + \overline{v_r'^2} \right], \quad (\text{E.2})$$

the utilization of correlations to obtain y_1' would eliminate the necessity of solving a transport equation for k . So, correlations of the type (E.1) seemed very promising. However, from equations (E.1) and (E.2), it can be observed that

$$K \propto \left[1 - \frac{U_b}{(v_z)_{\max}} \right]^2 \quad (E.3)$$

Since $(v_z)_{\max}$ is obtained by a numerical procedure, a small deviation in its value would introduce a considerably large error in the calculated value of K . For example, for rod bundles with P/D in the range 1.1 - 1.25, it was observed experimentally that $(v_z)_{\max}/v_b$ is in the range 1.1 - 1.23. For illustration, take $(v_z)_{\max}/v_b$ equal to 1.15 as the actual value of this ratio.

$$\left(1 - \frac{1}{1.15} \right)^2 = 0.0170$$

If an error of 3% is committed in the determination of $(v_z)_{\max}$, say, to the lower side, $(v_z)_{\max}/v_b$ would be 1.127, and

$$\left(1 - \frac{1}{1.127} \right)^2 = 0.0127$$

The resulting error in the turbulence kinetic energy, k , would be

$$\frac{0.0170 - 0.0127}{0.0170} \times 100 = 25\% .$$

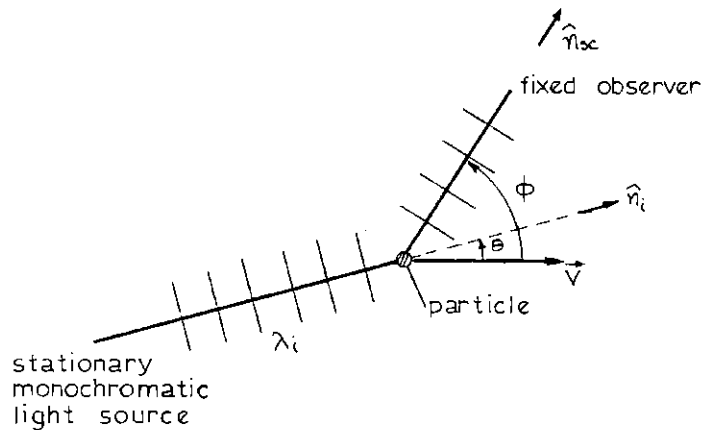
For this reason, this approach was not pursued.

APPENDIX F

LASER DOPPLER ANEMOMETER THEORY

1. PRINCIPLES

When an acoustic or electromagnetic wave, emitted by a fixed monochromatic source, is scattered by a moving body before reaching a fixed observer, its frequency as seen by the fixed observer is changed. This is known as the Doppler effect. The observed frequency shift can be related to the velocity of the body.



In the sketch above, the light beam is travelling in the direction defined by the unit vector \hat{n}_i with velocity c .

The number of wave fronts incident upon the particle per unit time is

$$\nu_p = \frac{(c - \vec{v} \cdot \hat{n}_i)}{\lambda_i}. \quad (\text{F.1})$$

This is also the number of wavefronts scattered by the particle. After scattering one wavefront in the unit direction vector \hat{n}_{sc} , the particle moves toward the wavefront with velocity $\vec{v} \cdot \hat{n}_{sc}$. Thus, when the next wavefront is scattered after a time interval $1/\nu_p$, the first wavefront is a distance λ_{sc} from the particle, where

$$\lambda_{sc} = \frac{c - \vec{v} \cdot \hat{n}_{sc}}{\nu_p} = \lambda_i \left(\frac{c - \vec{v} \cdot \hat{n}_{sc}}{c - \vec{v} \cdot \hat{n}_i} \right). \quad (\text{F.2})$$

λ_{sc} represents the wavelength of the scattered light in the direction of the fixed observer.

The Doppler shift is, then, given by

$$\nu_D = \nu_{sc} - \nu_i = \frac{c}{\lambda_{sc}} - \frac{c}{\lambda_i} = \frac{c}{\lambda_i} \left[\frac{\lambda_i}{\lambda_{sc}} - 1 \right]. \quad (\text{F.3})$$

From (F.2) and (F.3)

$$\nu_D = \frac{c}{\lambda_i} \left[\frac{c - \vec{v} \cdot \hat{n}_i}{c - \vec{v} \cdot \hat{n}_{sc}} - 1 \right] = \frac{c}{\lambda_i} \frac{\vec{v} \cdot (\hat{n}_{sc} - \hat{n}_i)}{1 - \frac{\vec{v} \cdot \hat{n}_{sc}}{c}} \quad (\text{F.4})$$

Since, for all practical applications of the LDA, $\vec{v} \ll c$,

$$\nu_D \approx \frac{1}{\lambda_i} \vec{V} \cdot (\hat{n}_{sc} - \hat{n}_i) . \quad (F.5)$$

This equation shows that the frequency shift is directly proportional to the particle velocity component in the direction defined by the vector difference $(\hat{n}_{sc} - \hat{n}_i)$.

The Doppler frequency is usually measured by an optical heterodyne technique. In the LDA, two laser beams are involved where either only one or both are scattered by particles in suspension in a fluid and moving with it. A photocathode mixes the scattered beam with a reference beam, in the first case, and both scattered beams in the second one, to generate a current whose a.c. component has a frequency equal to the difference frequency. Fig. F.1 shows the lay-out for both set-ups.

Take the first case, the two light beams of slightly different frequency may be represented by

$$E_1 = E_{10} \sin 2\pi\nu_0 t , \quad (F.6)$$

$$E_2 = E_{20} \sin 2\pi(\nu_0 + \nu_D) t . \quad (F.7)$$

The photocathode, being a square law detector, generates an output current i proportional to the square of the total electric field incident on it:

$$i \sim (E_1 + E_2)^2. \quad (\text{F.8})$$

Since the photodetector is only capable of following frequencies up to 10^8 Hz, since the laser frequency, ν_0 , is of the order of 10^{14} Hz, in the expansion of i , eq.(F.8), using eqs.(F.6) and (F.7), terms involving frequencies of the order of ν_0 will result in a d.c. current proportional to the time average of those terms. If ν_D is below the frequency limit of the photodetector, there will be an a.c. component which contains the Doppler shift as illustrated by equation (F.8).

$$i \sim \left[\frac{E_{10}^2 + E_{20}^2}{2} + E_{1c} E_{2c} \sin 2\pi (\nu_D t + \xi) \right], \quad (\text{F.9})$$

where ξ is a phase angle which is constant if the two beams are coherent.

This technique was first introduced by Yeh and Cummins⁽¹²⁾ and then applied to a wide range of cases by different investigators. References (13) and (14) give detailed description of design of a LDA.

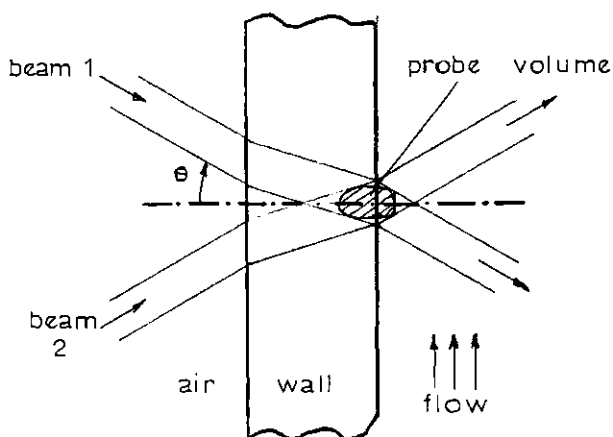
2. ADVANTAGES AND DISADVANTAGES OF LDA

The major advantages of the LDA are:

- i. since no solid probe is necessary, the flow is not disturbed during measurement;
- ii. probe volume can be made very small by correct selection of optical components thus high spacial resolution is obtained;
- iii. no calibration is required;
- iv. fluid velocity is directly proportional to frequency shift.

As disadvantages of this technique, it can be mentioned:

- i. difficulty of handling refractions introduced by curved surfaces;
- ii. determination of probe volume position is usually given by the distance from walls. This is accomplished by focusing the two beams on the wall and then moving the probe volume to the desired position. Since the dimensions of the probe volume are very small and due to light reflection by the wall, its position cannot be determined visually. So, in many cases, it has to be determined by the PMT signal (see Sketch).



Although the center of the probe volume is on the wall, part of it is still inside the flow which can be crossed by seeding particles yielding a Doppler signal which is detected by the PMT. Moving the probe volume further into the wall would give an incorrect wall position determination. Light reflection when the beams move from one region (wall) to the other (fluid) with different refractive indices decreases the signal-to-noise ratio (SNR), making this procedure be even more difficult. So, it can be concluded that the positioning error involved in the LDA is of the order of magnitude of the probe volume dimensions. This is a serious limitation when velocity profiles are to be determined in regions of size comparable to the probe volume dimensions.

3. THE DUAL SCATTERED BEAM MODE

The discussion that follows will be concentrated

on aspects of the dual scattered beam mode, Fig. F.1(b), since this is the operational mode used in the present work,

The dual scattered beam mode is also called "fringes mode" because interference fringes are formed in the probe volume. Fig. F.2 presents an enlarged view of the crossing region of the two gaussian beams showing how the interference fringes are created. By simple geometric consideration, it can be found that the distance between two consecutive fringes is

$$d_f = \frac{\lambda}{2 \sin \beta} \quad (\text{F.10})$$

Since the two incident beams are focused at the crossing point by a lens with focal length f_L , the beam radius at the waist is given by Airy disc⁽¹⁵⁾ from diffraction theory:

$$b_0 = 1.22 \frac{\lambda f_L}{D_0} \quad (\text{F.11})$$

where D_0 is beam diameter at the lens.

The dimensions of the probe volume, assuming crossing at waist as shown in Fig. F.2, are usually assumed as those of an ellipsoid with

$$l_v = \frac{\sqrt{2} b_o}{\sin \beta} , \quad (\text{F.12})$$

$$h_v = \frac{\sqrt{2} b_o}{\cos \beta} , \quad (\text{F.13})$$

$$\omega_v = 2 b_o \quad (\text{F.14})$$

Figure F.3 shows the light intensity radial distribution inside the probe volume. As a particle moves inside the probe volume, it scatters light with intensity proportional to light intensity along its path. Let $\Delta\tau$ be the time that a particle moving with velocity \vec{V} takes to go from one fringe to the next and \hat{n} , an unit vector normal to the fringes, then

$$\Delta\tau = \frac{d_f}{\vec{V} \cdot \hat{n}} \quad (\text{F.15})$$

The Doppler frequency shift is then given by

$$\nu_D = \frac{1}{\Delta\tau} = \frac{\vec{V} \cdot \hat{n}}{d_f} , \quad (\text{F.16})$$

or, from (F.10),

$$\nu_D = \frac{2 \sin \beta}{\lambda} (\vec{V} \cdot \hat{n}) . \quad (\text{F.17})$$

The product $(\vec{V} \cdot \hat{n})$ represents the particle velocity in the direction normal to the fringes.

The number of interference fringes inside the probe volume can be calculated by

$$N_f = \frac{h_v}{d_f} . \quad (\text{F.18})$$

3.1. Signal Analysis.

Fig. F.4 shows the typical signals generated by particles A and B (see Fig. F.3) crossing the probe volume at different positions. The signals have different modulations due to differences of the incident light beam intensities along their paths. Before the signal can be analysed, the "pedestals" are removed by a high-pass filter. The current signal generated by the photodetector is, then, transformed into a frequency signal by either a frequency tracker or a spectrum analyser. In general, for a turbulent flow, a broadening is observed around the Doppler frequency, ν_D , that can be attributed to three sources:

- (a) finite transit time broadening;
- (b) velocity gradient broadening;
- (c) fluctuating velocity component in the direction normal to the fringes.

3.1.a. Finite transit time broadening, $\Delta\nu_\tau$

The broadening attributable to finite transit time is obtained by analyzing the signal from a particle crossing the probe volume with uniform velocity. The signal after removing the pedestal can be represented by:

$$\frac{I_{sc}(t)}{I_0} = \cos(2\pi\nu_D t) e^{-8\left(\frac{t}{\tau}\right)^2}, \quad (\text{F.19})$$

where τ is the transit time that the particle takes to cross the probe volume. The Fourier transform of this signal is

$$\frac{P(\nu)}{P_0} = \frac{\pi}{2} \left(\frac{\tau}{2}\right)^2 e^{-\left(\frac{\pi\tau}{2}\right)^2 (\nu - \nu_D)^2}. \quad (\text{F.20})$$

Since the assumption of particles with uniform velocity was adopted the broadening in the signal $P(\nu)$ is only due to the finite transit time τ . The standard deviation of this gaussian broadening is obtained by taking

$$\left(\frac{\pi\tau}{2}\right)^2 (\Delta\nu_\tau)^2 = 1, \quad (\text{F.21})$$

directly from eq. (F.20). Hence

$$\Delta\nu_\tau = \frac{2}{\pi\tau}. \quad (\text{F.22})$$

Now the transit time τ can be written as

$$\tau = N_f \Delta\tau = \frac{N_f}{v_D} , \quad (\text{F.23})$$

then

$$\frac{\Delta v_\tau}{v_D} = \frac{2}{\pi N_f} . \quad (\text{F.24})$$

This last expression represents the finite transit time contribution to the frequency broadening of the signal.

3.1.b. Velocity gradient broadening, Δv_G

When velocity gradients are large over the probe volume, particles crossing this volume at different regions have different velocities and so generate signals with different Doppler frequency. This is the cause of the velocity gradient broadening. Assume a velocity gradient along the length of the probe volume, l_v (see Fig.F.2).

Calling $V_n \equiv \vec{V} \cdot \hat{n}$, equation (F.17) is reduced to

$$v_D = \frac{2 \sin \beta}{\lambda} V_n . \quad (\text{F.25})$$

Differentiating v_D in the direction of the probe volume length

$$\frac{\partial \nu_D}{\partial y} = \frac{2 \sin \beta}{\lambda} \left(\frac{\partial v_n}{\partial y} \right) \approx \frac{\Delta \nu_G}{\Delta y} . \quad (\text{F.26})$$

The probe volume length, ℓ_v , was calculated taking the beam radius as determined by a decrease of the light intensity by a factor of $1/e^2$ in the radial direction. To obtain $\Delta \nu_G$ corresponding to one standard deviation of the frequency broadening, Δy must correspond to a decrease of the light intensity by a factor of $1/e$. Then, $\Delta y = \ell_v/2$. Thus, from (F.25) and (F.26), one obtains:

$$\frac{\Delta \nu_G}{\nu_D} = \frac{\ell_v}{2 v_n} \left(\frac{\partial v_n}{\partial y} \right) . \quad (\text{F.27})$$

This is the Doppler frequency broadening due to velocity gradients over the probe volume. It can be seen that it decreases with a decrease in size of the probe volume in the direction of the velocity gradient.

3.1.c. Velocity fluctuation broadening, $\Delta \nu'$

Since the particles crossing the probe volume have different velocities due to turbulent fluctuations, they generate different frequency signals and so a broadening is observed in the frequency spectrum of the signal. This broadening represents the turbulent intensity of the velocity component normal to the interference fringes. If Δv is

the total broadening of the frequency spectrum, the turbulent intensity broadening $\Delta\nu'$ is obtained by

$$\left(\frac{\Delta\nu'}{\nu_D}\right)^2 = \left(\frac{\Delta\nu}{\nu_D}\right)^2 - \left[\left(\frac{\Delta\nu_t}{\nu_D}\right)^2 + \left(\frac{\Delta\nu_g}{\nu_D}\right)^2 \right], \quad (\text{F.28})$$

where $\left(\frac{\Delta\nu_t}{\nu_D}\right)$ and $\left(\frac{\Delta\nu_g}{\nu_D}\right)$ are given by eqs. (F.24) and (F.27), respectively.

3.2. Seeding particle constraints.

Since the scattered light comes from particles in suspension in the fluid, they have to be chosen such that their velocities are the same as the fluid velocity in every respect in order to permit the investigator to obtain all hydrodynamic parameters of the flow just by observing their behavior.

Three important things relative to the seeding particles have to be carefully examined:

- (a) density relative to the fluid whose flow is to be observed. The density should be as close to the fluid density as possible to eliminate velocity lags that might occur. For example, for a water flow, polystyrene ($\rho=1.0$) particles will follow the water at any velocity, however PVC ($\rho=1.54$) will follow the water flow, within 99%, only for

velocity fluctuations up to 10 KHz for particles with diameter of 5μ ⁽¹⁶⁾.

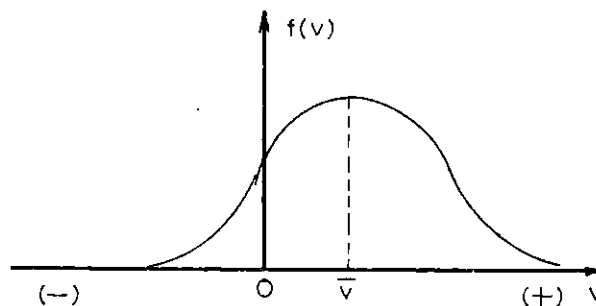
- (b) The diameter of the particles, d_p , should be small compared to the distance between fringes, d_f , for good signal modulation. It is usually recommended that

$$d_p \leq \frac{d_f}{4} . \quad (\text{F.29})$$

- (c) The concentration of the particles should be very small to avoid superimposing of signals due to a large number of particles in the probe volume. As a rough criterion, the concentration can be selected to yield no more than two or three particles inside the probe volume at the time.

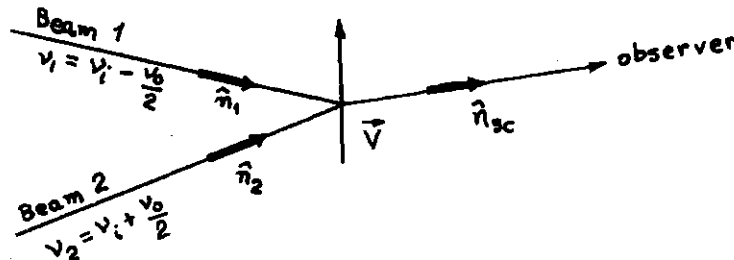
4. THE LDA DIRECTIONAL AMBIGUITY

Assume a velocity distribution where the time-averaged velocity is small compared to the turbulent fluctuations (see sketch below).



Since the LDA generates a frequency signal, the negative tail of this distribution would not be recognized as such and erroneous values for the average \bar{v} would be obtained. Another difficulty would be the removal of the signal pedestal, as discussed, since in the present case low frequencies represent an important part of the answer being sought. So, pedestal removal, with the frequency signal as it is, would also lead to wrong values for the turbulent intensity since part of the signal is cut off.

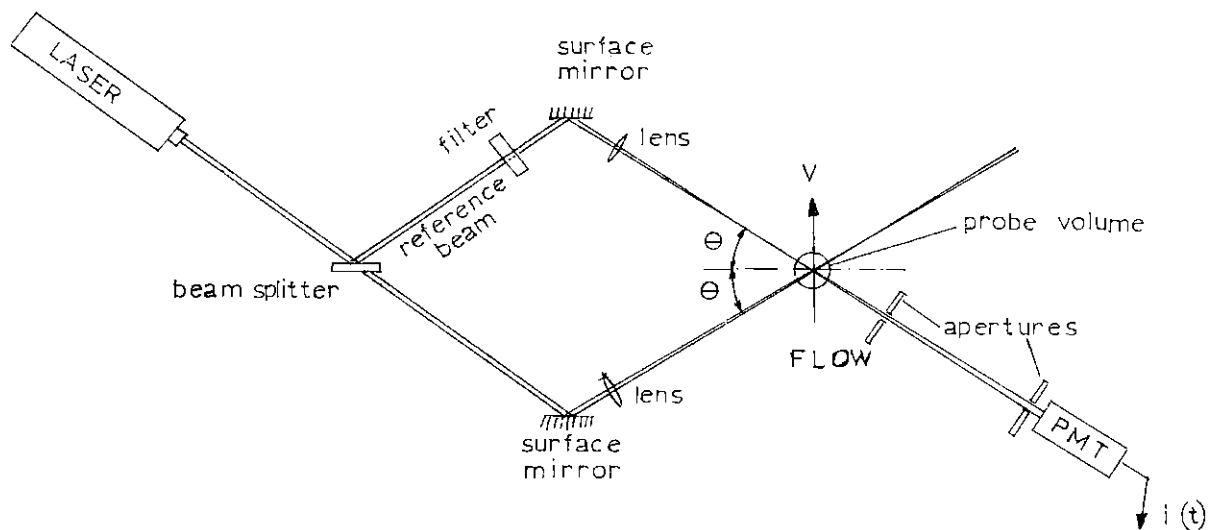
This difficulty, however, is eliminated by shifting the frequency of the incident beams using Bragg cells. One of the beams is shifted by $+\nu_0/2$ and the other by $-\nu_0/2$.



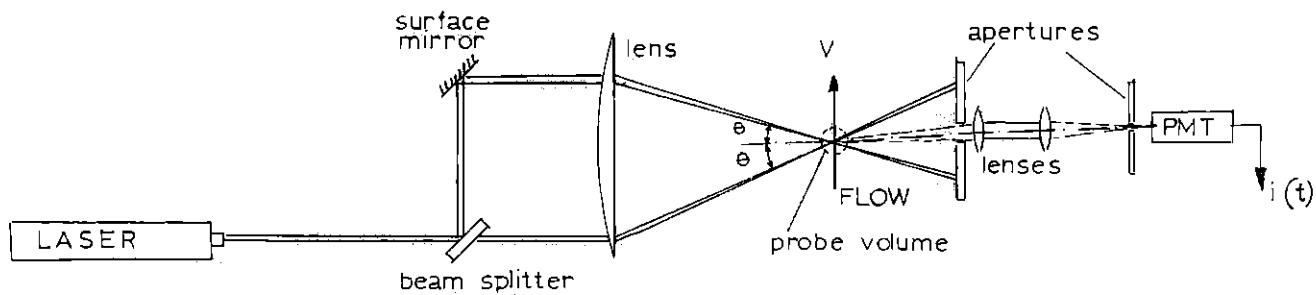
The discussion presented in section 1 of this appendix applies to the present case, leading to

$$\nu_D = \nu_0 + \frac{1}{\lambda_i} \bar{V} \cdot (\hat{n}_1 - \hat{n}_2) , \quad (\text{F.30})$$

for $v_0 \ll v_i$. After measuring v_D , with v_c known, the velocity can be easily obtained, as well as its turbulent fluctuation.



(a) Reference Beam Mode



(b) Dual Scattered Beam (Fringes) Mode

Fig. F.1. Basic LDA Set-ups

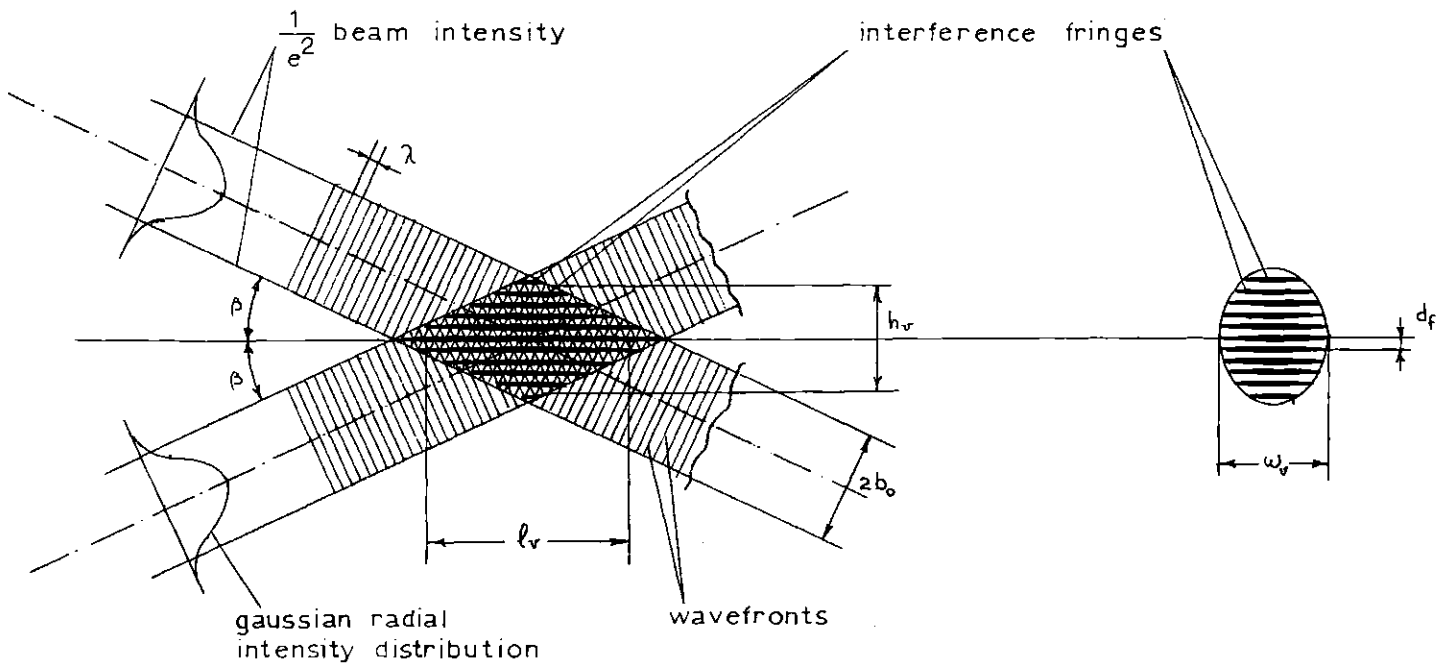


Fig. F.2. Enlarged View of Probe Volume

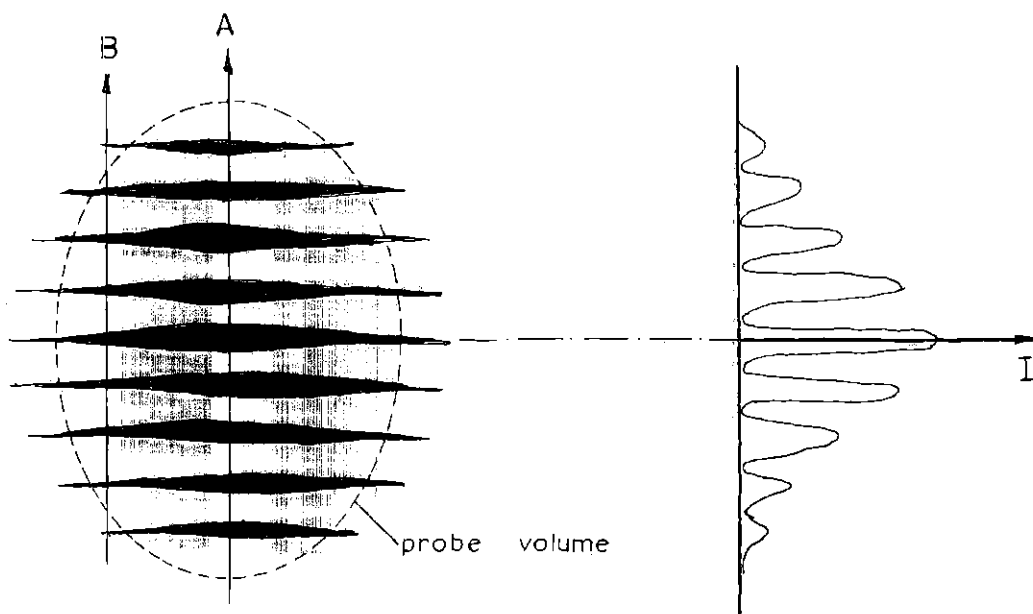


Fig. F.3. Light Intensity Radial Distribution in the Probe Volume

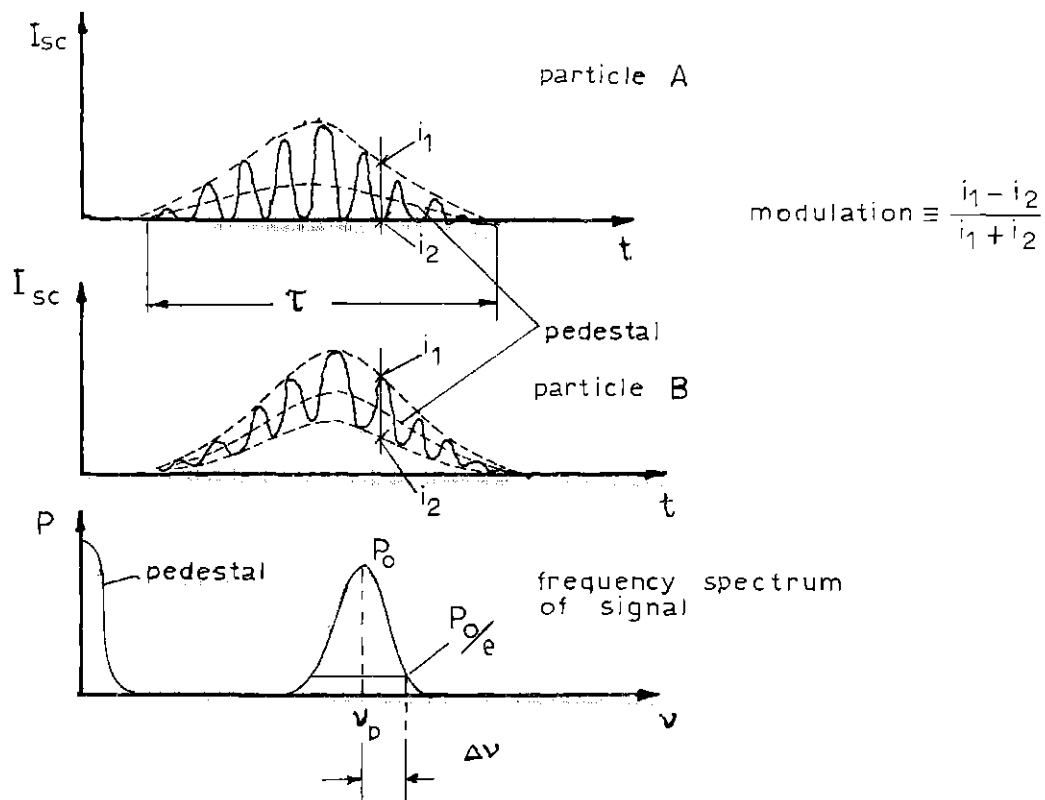


Fig. F.4. Typical Time and Frequency Signals Generated by Particles Crossing the Probe Volume

APPENDIX G

EFFECT OF DIFFERENT REFRACTIVE INDECES ON THE CROSSING POINT OF THE TWO BEAMS

In laser Doppler anemometry, when an integrated optical unit is used, the two light beams move parallel to the optical axis of the optical unit lens and are focused exactly at the focal length of the lens, if the medium is air. The crossing point will be exactly at the waist of the beams. However, when measurements are to be made of a water flow (index of refraction, $n_w=1.33$) separated from the air by a glass or plexiglas wall (index of refraction, $n_p=1.50$) the position where the two beams cross will change and the crossing can be off their waists.

From the LDA point of view, it is important to determine the distance from the center of the waist to the crossing point, since the spacial resolution of the system decreases as the crossing position moves far from the waist region due to the increase of the beam diameter. Another reason is the fact that, outside the waist region where the wavefronts are very nearly plane, the wavefronts of the beams are spherical. This leads to a deformation of the interference fringes which can result in a broadening in the frequency spectrum of the signal. Ultimately these facts

will represent errors in the velocity and its fluctuating component measurements.

Fig. G.1 shows the path of one of the beams in the situation where the center of the waist is off the optical axis. The optical axis of the lens is taken normal to the wall. The crossing point is characterized by the distance x_M from the inside surface of the wall. The waist position is determined by the coordinates (x_w, y_w) as defined in fig. G.1.

Start writing the refraction law for the interfaces:

i. interface (I)

$$\sin \alpha = \frac{n_c}{n_p} \sin \theta , \quad (\text{G.1})$$

ii. interface (II)

$$\sin \psi = \frac{n_p}{n_w} \sin \alpha = \frac{n_c}{n_w} \sin \theta \quad (\text{G.2})$$

From triangles PLO and ABO:

$$a_1 = (t + x_c) \left(\frac{a}{f_L} \right) . \quad (\text{G.3})$$

Now:

$$a_2 = a_1 - t \tan \alpha ,$$

or

$$a_2 = \left[\left(\frac{a}{f_L} \right) - \tan \alpha \right] t + \left(\frac{a}{f_L} \right) x_c . \quad (G.4)$$

The distance from the crossing point to the wall, x_M , is then obtained by

$$x_M = \frac{a_2}{\tan \varphi} , \quad (G.5)$$

where a_2 is given by eq. (G.4), and the angles α and φ are obtained directly from eqs. (G.1) and (G.2), respectively.

To find x_w and y_w , write equations (G.1) and (G.2) in the form

$$\alpha = \text{arc sin} \left[\left(\frac{n_c}{n_p} \right) \sin \theta \right] , \quad (G.6)$$

$$\varphi = \text{arc sin} \left[\left(\frac{n_c}{n_w} \right) \sin \theta \right] . \quad (G.7)$$

Differentiating α and φ as function of θ ,

$$d\alpha = \frac{\cos \theta}{\left[\left(\frac{n_p}{n_c} \right)^2 - \sin^2 \theta \right]^{1/2}} \delta \theta , \quad (G.8)$$

$$\delta\varphi = \frac{\cos \theta}{\left[\left(\frac{n_w}{n_c} \right)^2 - \sin^2 \theta \right]^{1/2}} \delta\theta . \quad (\text{G.9})$$

The deviation $\delta\theta$ is, then, written as

$$\delta\theta = \frac{D_0 \cos^2 \theta}{f_L} \quad (\text{G.10})$$

From triangles L_1L_2O and B_1B_2O , one obtains

$$D_1 = (t + x_c) \left(\frac{D_0}{f_L} \right) . \quad (\text{G.11})$$

Also from triangle B_1B_2O ,

$$\delta\alpha = \frac{D_1 \cos^2 \alpha}{x_p + t} = \frac{D_2 \cos^2 \alpha}{x_p} . \quad (\text{G.12})$$

From equation (G.12)

$$D_2 = \frac{x_p}{x_p + t} D_1 , \quad (\text{G.13})$$

with

$$x_p = \frac{D_1 \cos^2 \alpha}{\delta\alpha} - t . \quad (\text{G.14})$$

With the set of equations (G.8-14), the parameters

$\delta\alpha$, $\delta\varphi$, D_1 , D_2 , x_p , are obtained as function of D_0 , f_L , θ , t and x_0 . So, now, x_w can be calculated by

$$x_w = \frac{D_2 \cos^2 \varphi}{\delta\varphi}, \quad (\text{G.15})$$

and y_w ,

$$y_w = (x_M - x_w) \tan \varphi, \quad (\text{G.16})$$

with x_M given by eq. (G.5).

With the above analysis, the position of the crossing point was determined relative to the inside surface of the wall, as well as the coordinates of the center of the beam waist.

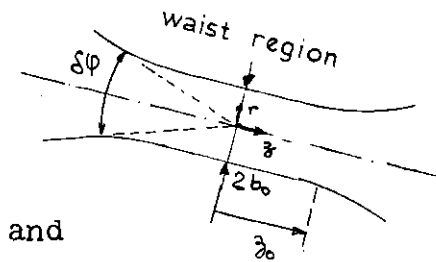
The distance between the center of the waist and the crossing point, Δz_M , is

$$\Delta z_M = \frac{x_M - x_w}{\cos \varphi} \quad (\text{G.16})$$

considering eqs. (G.5) and (G.15).

According to ref. (15), the beam intensity, near the focal plane, has an intensity distribution that presents radial minimum points due to diffraction. The first dark ring (radial minimum) is the so-called Airy disc and is

taken as the beam radius at the waist region. Defining, according to sketch below,



$$\xi \equiv \frac{\pi}{\lambda_w} (\delta\varphi) r \quad (\text{G.17})$$

$$\eta \equiv \frac{\pi}{2\lambda_w} (\delta\varphi)^2 z, \quad (\text{G.18})$$

where λ_w is the light wavelength in water. The Airy disc is given by⁽¹⁵⁾ $\xi_0 = 3.83$. It follows that the beam radius at the waist region, $r=b_0$, equals

$$b_0 = 1.22 \frac{\lambda_w}{\delta\varphi} = 1.22 \left(\frac{n_0}{n_w} \right) \frac{\lambda_i}{\delta\varphi}. \quad (\text{G.19})$$

Half of the waist length, z_0 , (also known as Rayleigh range) is defined by the condition $\eta_c = \xi_0 = 3.83$.

Hence

$$z_0 = \frac{2}{\delta\varphi} b_0 = 2.44 \left(\frac{n_0}{n_w} \right) \frac{\lambda_i}{(\delta\varphi)^2}. \quad (\text{G.20})$$

From the practical point of view, it is recommended that $|\Delta z_M| < z_0$.

This last criterion was applied to the set up used in the present work. The numerical values used are:

$$\lambda_1 = 0.5145 \mu,$$

$$D_0 = 1.5 \text{ mm},$$

$$a = 25 \text{ mm},$$

$$f_L = 130 \text{ mm},$$

$$t = 0.25 \text{ in.}$$

From Fig. G.2, it can be observed that the crossing point is always in the waist region, except for large values of x_0 , which does not occur in the present work. The curve x_M vs x_0 shows the variation of the measuring position with a variation in the focusing lens position relative to the wall.

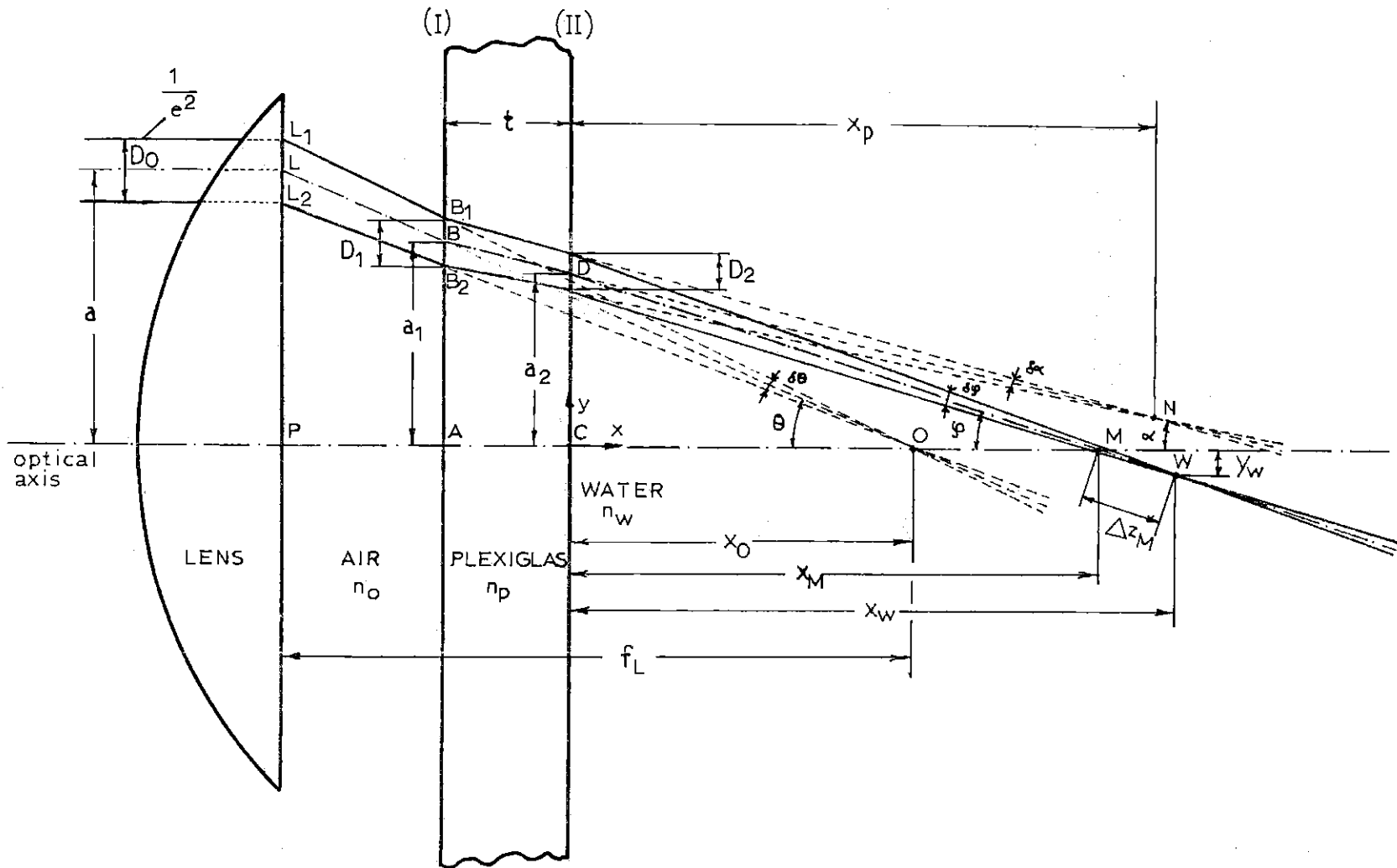


Fig. G.1. Laser Beam Path through Mediums with Different Refractive Indices when Focused by an Integrated Optical Unit Lens

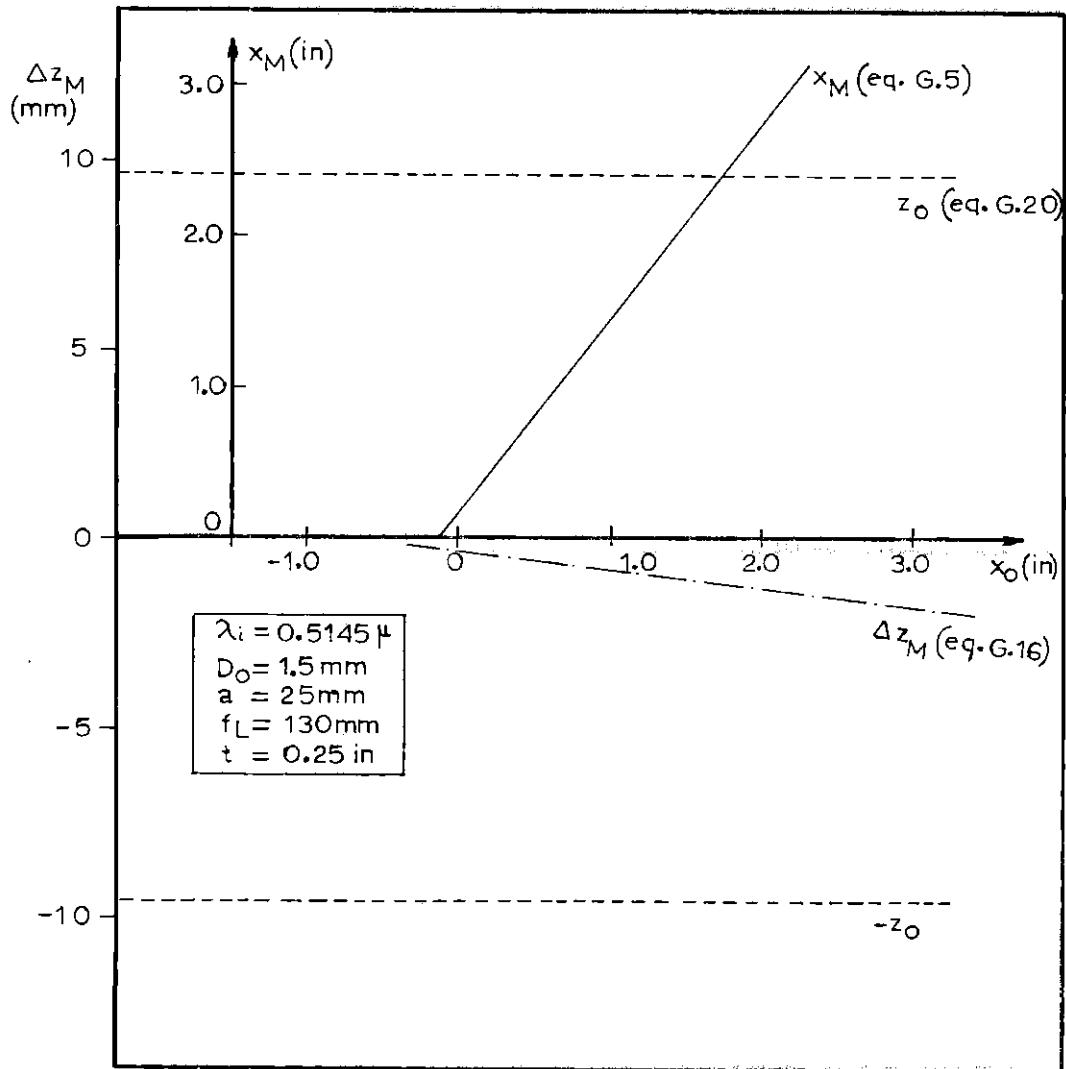


Fig. G.2. Determination of Measuring Region based on Crossing Point at Beam Waists

APPENDIX H

PRELIMINARY TEST OF TEST SECTION

Two preliminary tests were conducted over the test section: the first one, to determine the symmetry of flow over the cross section of the test section and the second one was an attempt to determine whether the flow was fully developed at the position $L/D_H=77$.

H.1. Symmetry test.

Axial velocities at symmetrical points of the cross section should be equal. So, the axial velocity distributions over 8 lines, as shown in fig. H.1., were measured. The results are presented in figs. H.2-6. The largest deviation observed was less than 0.5%, which is well within the 3% experimental error. It was concluded that the fabrication as well as the inlet section of the test section did not introduce any measurable assymetry in the flow.

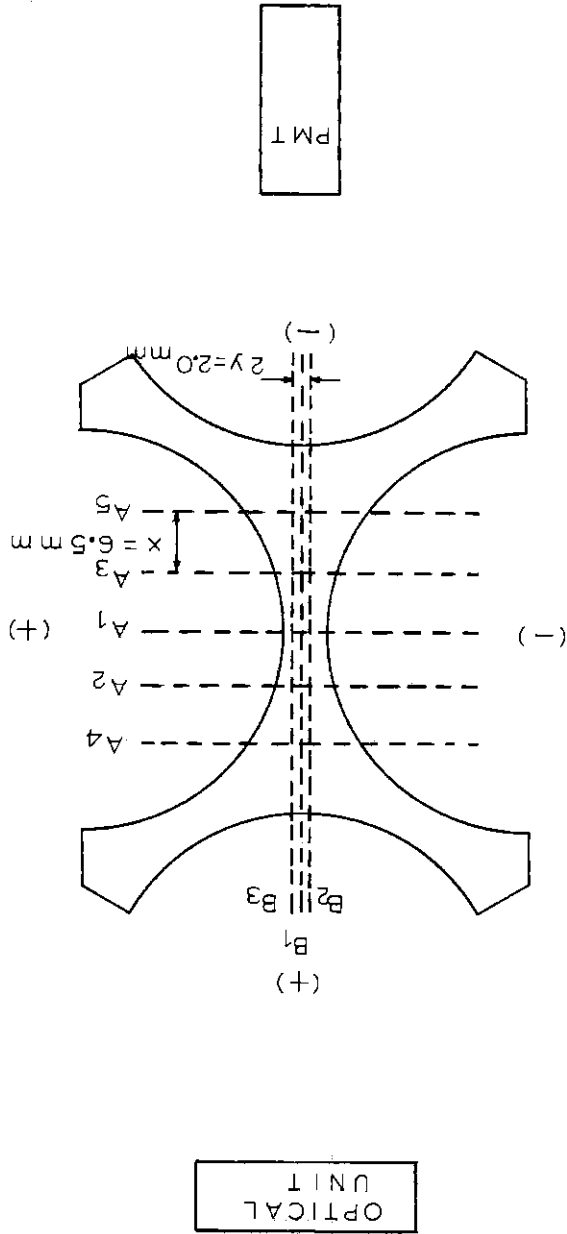
H.2. Development of the flow.

The velocity at the entrance of the test section can be considered uniform. As the flow progresses, a boundary layer forms and grows at the wall. Downstream, where the

velocity profile no longer changes along the flow path, the flow is said to be fully developed. To observe this flow development, axial velocity distributions were measured at $L/D_H = 15, 46, 77$. The isovels for $L/D_H = 15$ and $L/D_H = 46$ are shown in fig. H.7 and 8. The isovels for $L/D_H = 77$ are given in fig. VI.2. It can be observed that the isovels shown in fig. H.8 present most of the characteristics of those in fig. VI.2.(b). A comparison of the radial distributions, for $\theta = 0^\circ$ and $\theta = 30^\circ$, between the measurements at $L/D_H = 46$ and 77 is given by fig. H.9. Although the deviations are within the experimental error, values for $L/D_H = 77$ tend to be lower at $\theta = 0^\circ$ and higher at $\theta = 30^\circ$. This can be explained remembering that, due to largest effect of the wall shear stress in the gap region, the flow over that region is slowed down, while the flow, in the central region of the channel, is increased to maintain the same flow rate.

Since the variations in the axial velocity distribution, when the entrance length is increased from 46 to 77 hydraulic diameters is not very large, there is no reason to believe that very large changes will occur, from that point on, in the velocity profile. So, for practical purposes, the flow will be assumed fully developed at $L/D_H = 77$, although no conclusive evidence was obtained.

FIG. H.1. Test Section Symmetry Test



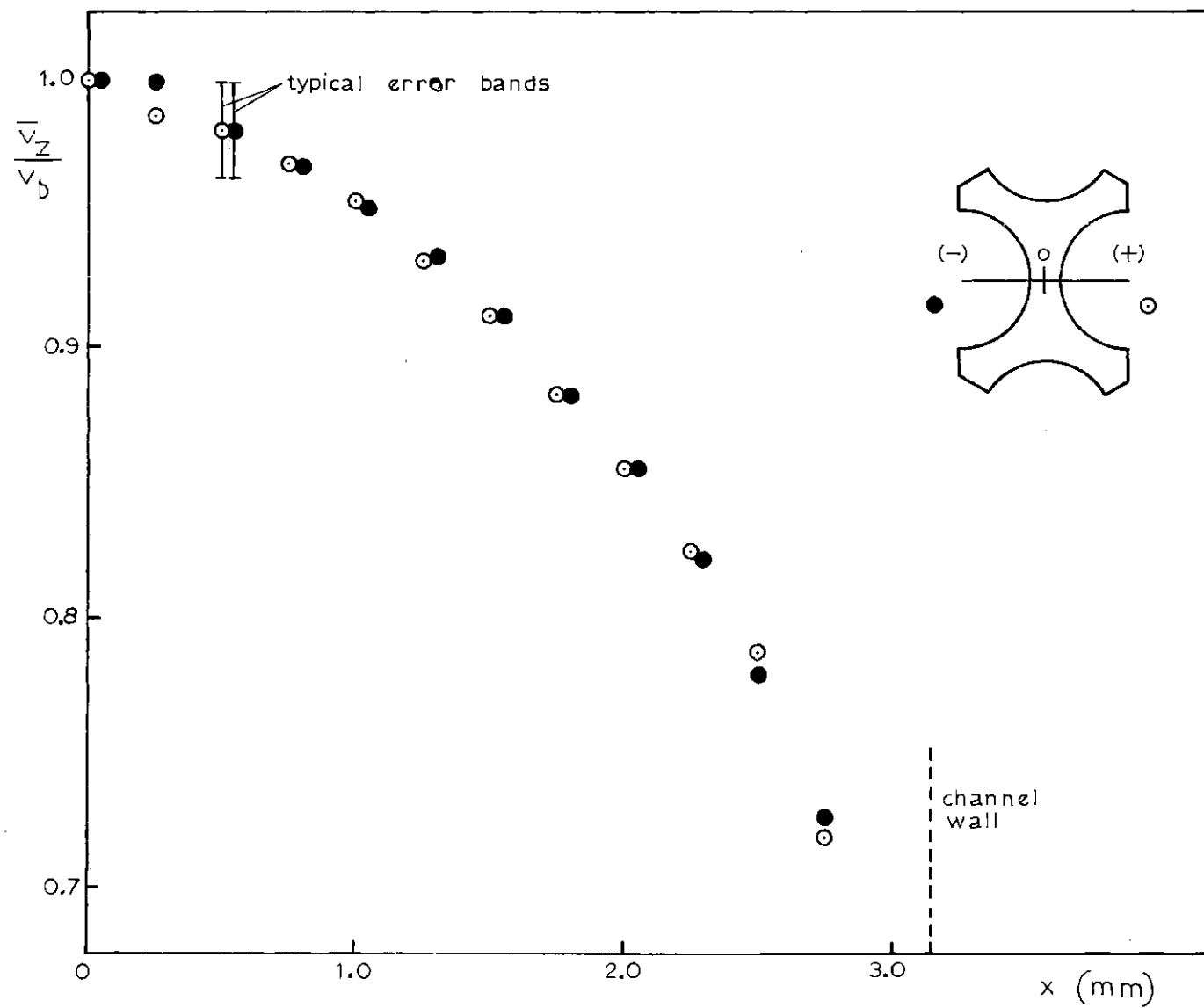


Fig. H.2. Symmetry Test of Test Section: line A_1

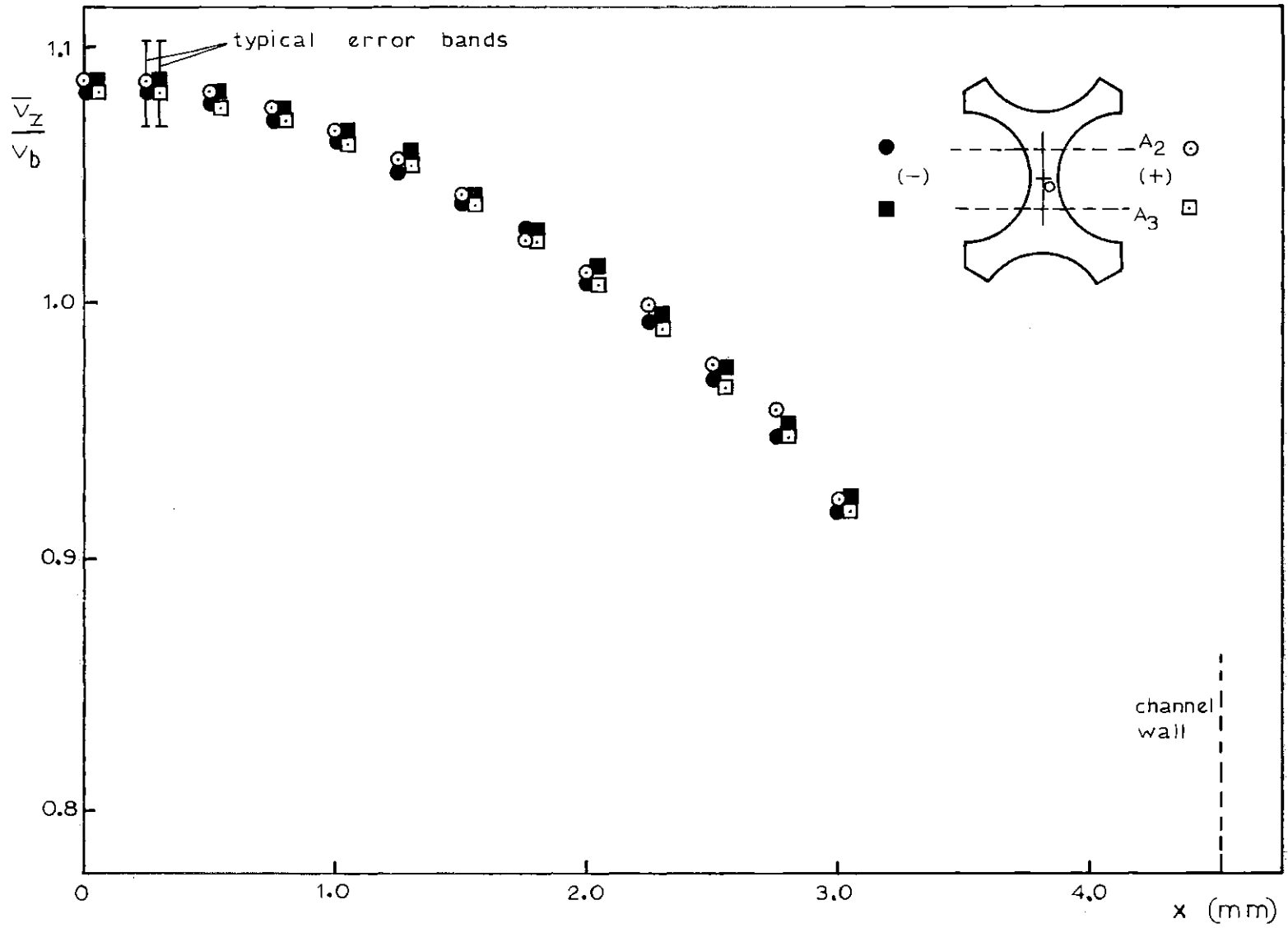


Fig. H.3. Symmetry Test of Test Section: lines A₂ and A₃

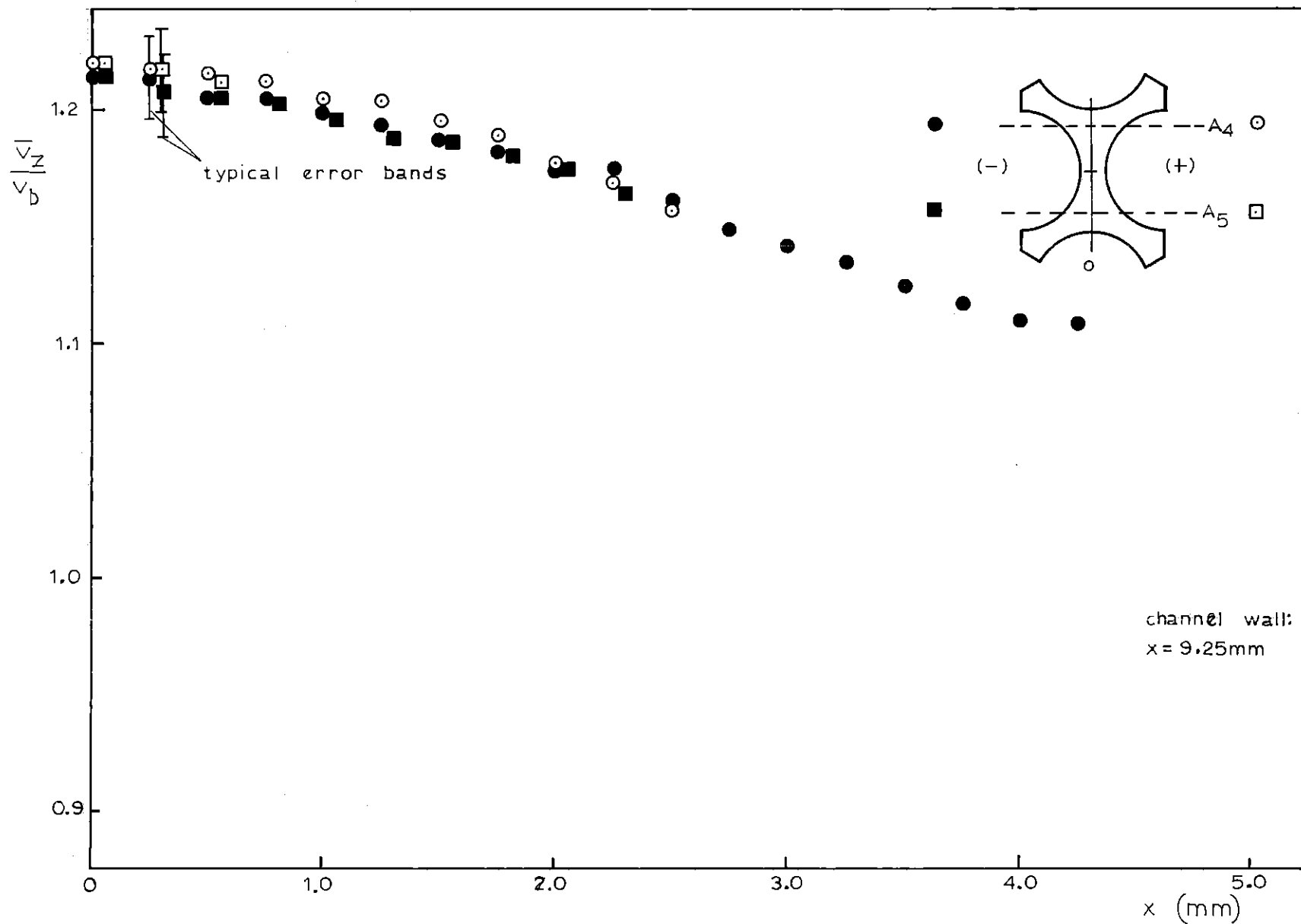


Fig. H.4. Symmetry Test of Test Section: lines A₄ and A₅

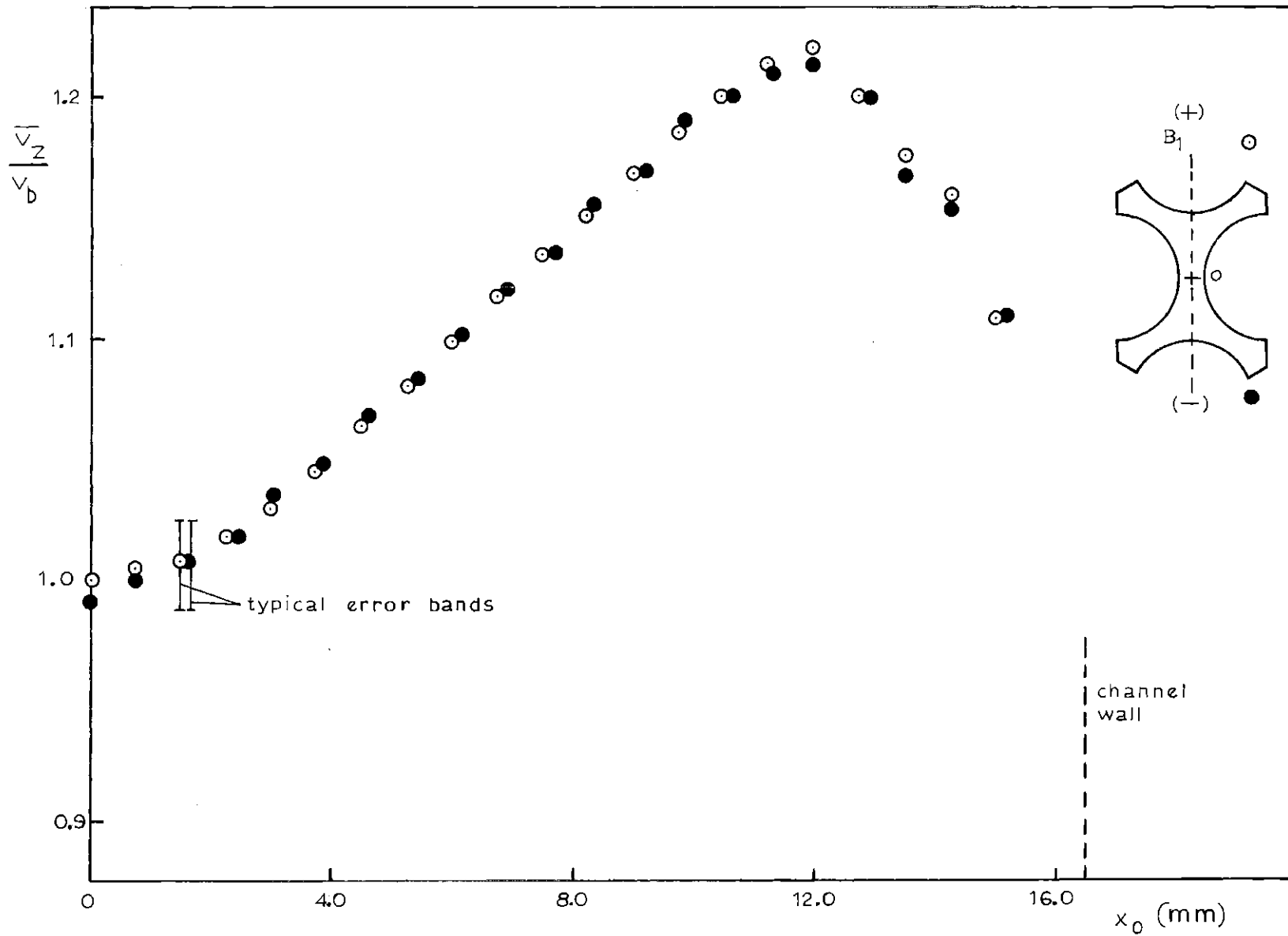
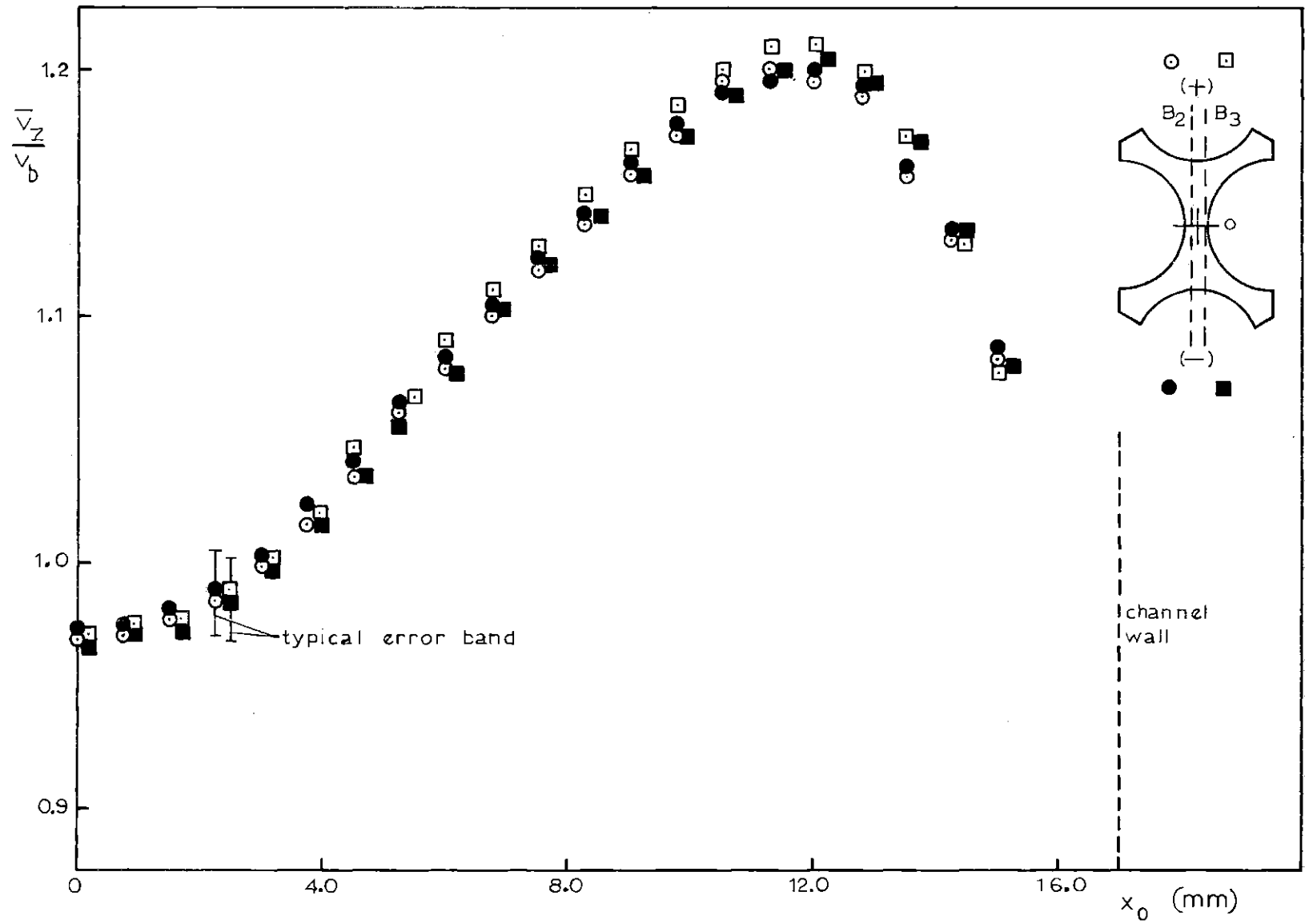


Fig. H.5. Symmetry Test of Test Section: Line B_1



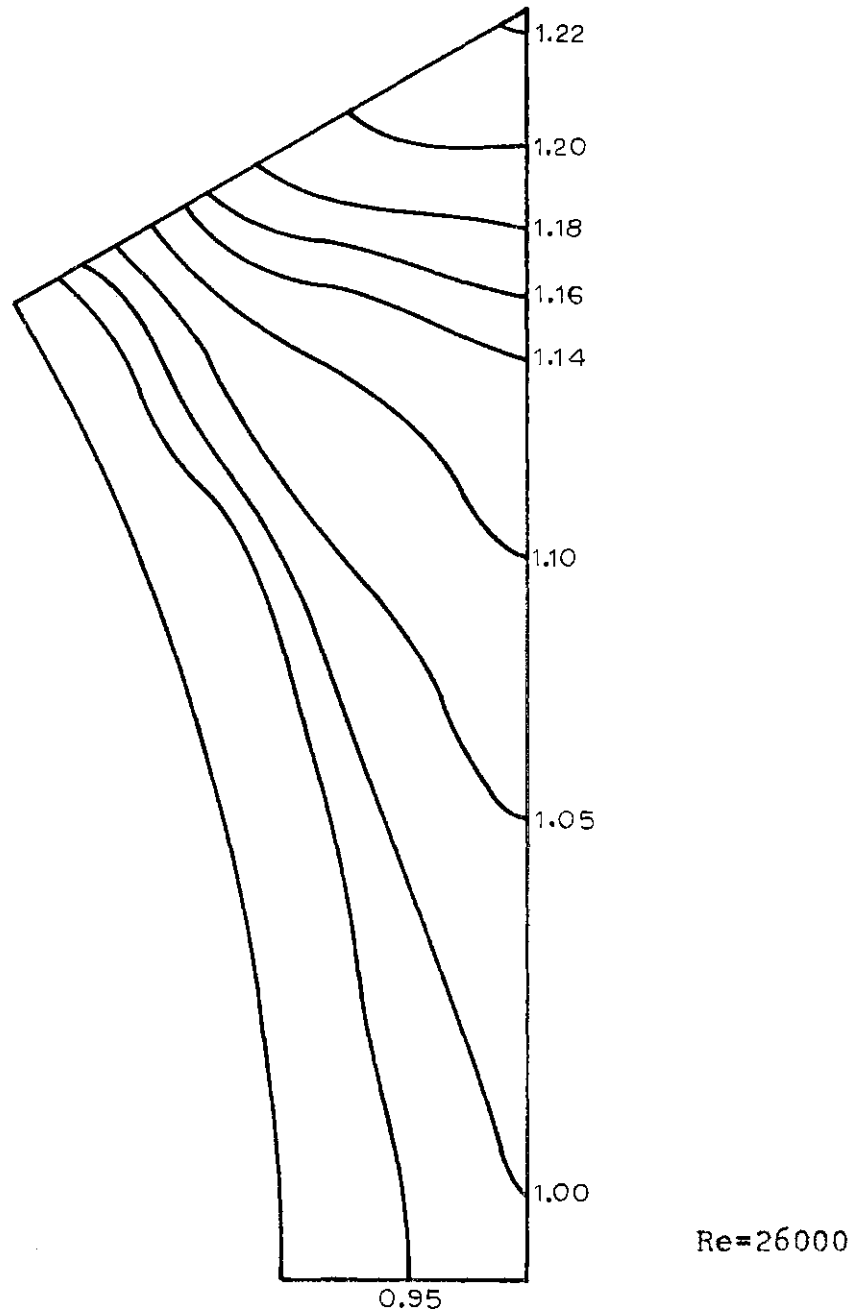
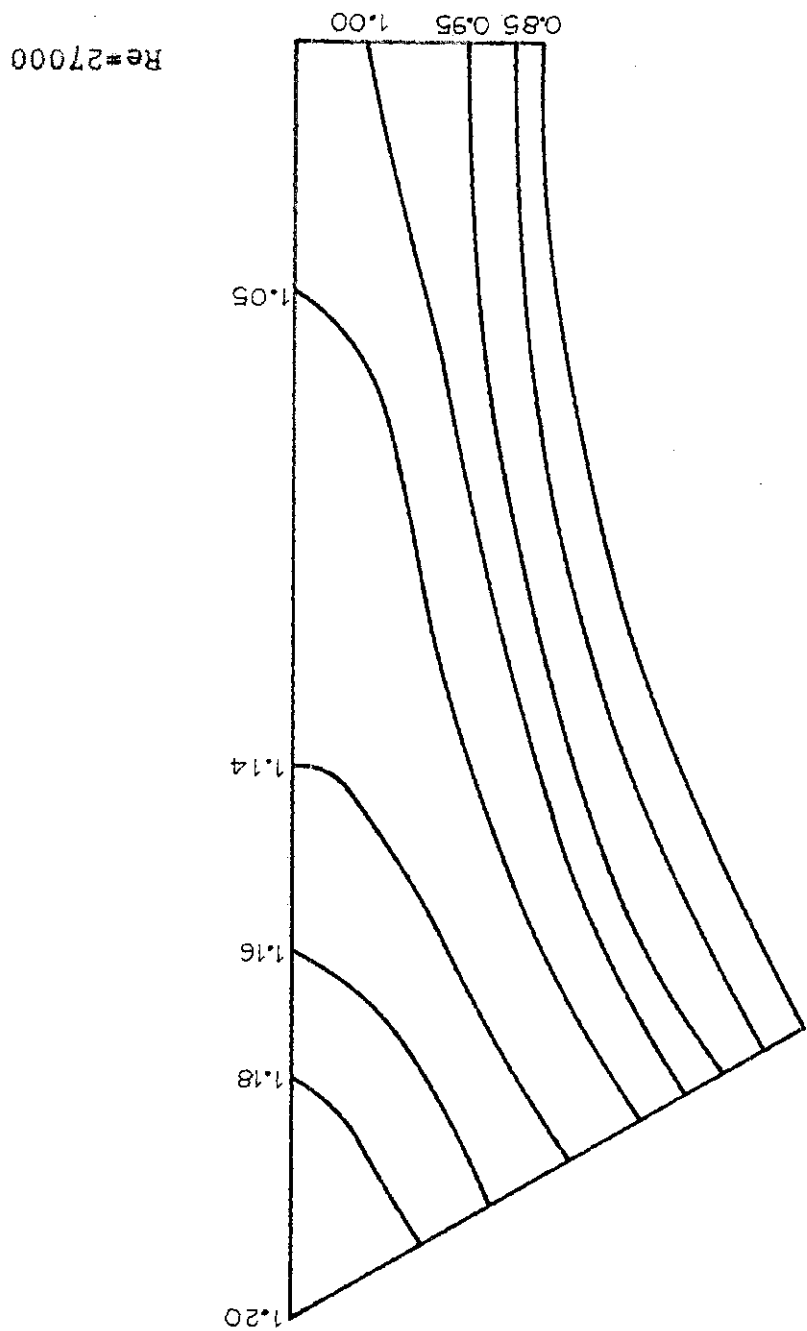


Fig. H.7. Isovel Plot for $\frac{L}{D_H} = 15$ and $\frac{P}{D} = 1.123$

FIG. H.8. Isovel Plot for $\frac{D}{L} = 46$ and $\frac{D}{P} = 1.123$



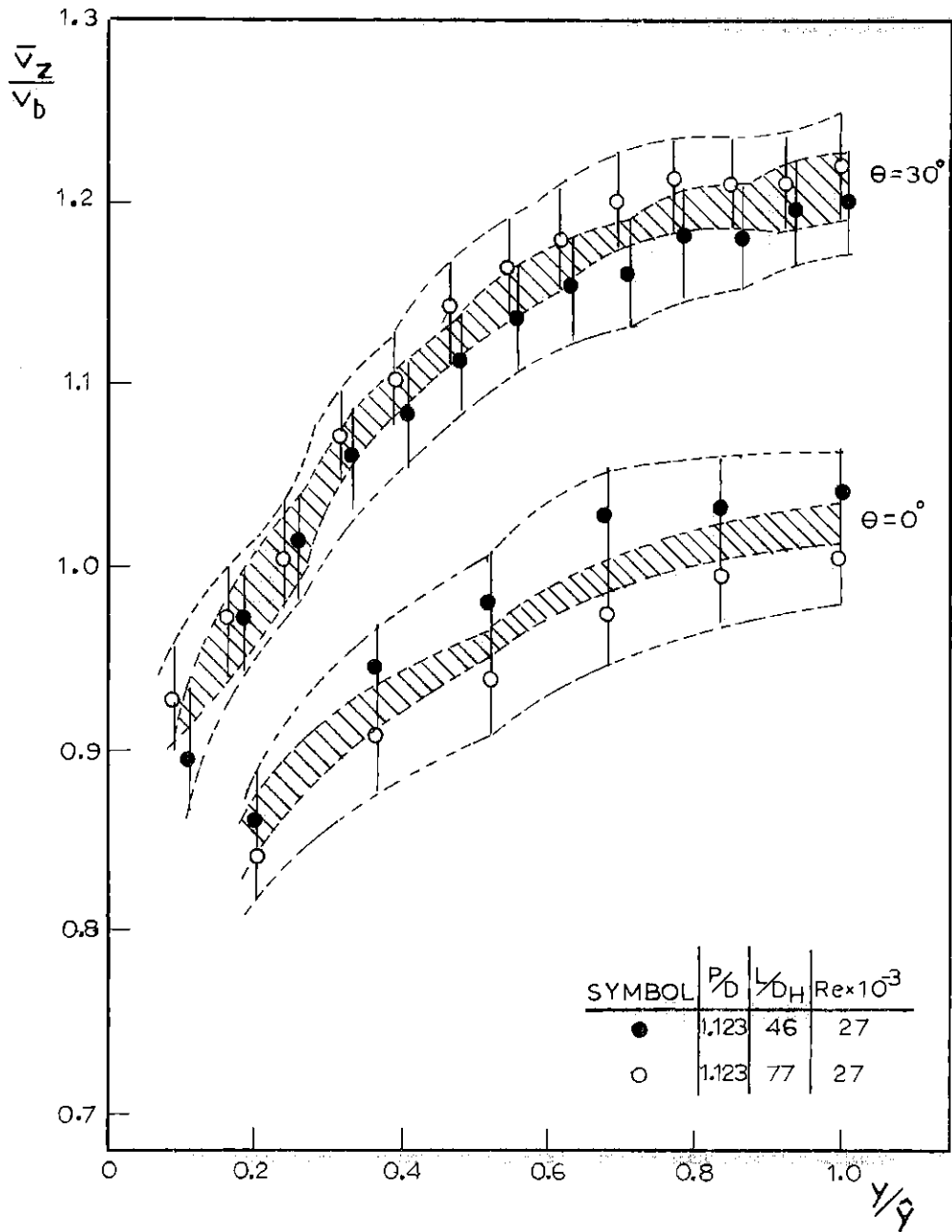


Fig. H.9. Developing Region Test

APPENDIX I

TABULATION OF EXPERIMENTAL DATA

In this appendix:

ΔH = inclined draft gage reading

$$v_i' = \sqrt{v_i'^2}$$

Table I.1. Pressure drop measurements

L/D_H	$R_e \times 10^{-3}$	ΔH (in)	$\bar{v}_c \times 10^2$ (m/s)	$f \times 10^3$
15	26	0.32	-	-
46	27	0.90 \pm 10%	6.7 \pm 1.3	5.0 \pm 0.5
77	27	1.08 \pm 10%	7.4 \pm 1.5	6.0 \pm 0.6

Table I.2. Measured distribution of parameters

θ	$\frac{y}{\hat{y}}$	$\frac{\bar{v}_z}{v_b}$	$\frac{v'_z}{v_b} \times 10$	$\frac{v'_e}{v_b} \times 10$	$\frac{v'_r}{v_b} \times 10$	$\frac{K}{v_b^2} \times 10^2$	$-\frac{\overline{v'_r v'_z}}{v_b^2} \times 10^2$
0	0.047	0.664	1.311	0.514	0.439	1.087	-
	0.205	0.839	0.918	0.544	0.418	0.657	0.219
	0.364	0.906	0.796	0.494	0.393	0.516	0.184
	0.523	0.937	0.740	0.459	0.363	0.445	0.115
	0.682	0.973	0.665	0.413	0.333	0.362	0.066
	0.841	0.999	0.585	0.398	0.313	0.299	0.027
	1.000	1.004	0.548	0.393	0.303	0.273	0
3	0.057	0.700	1.273	0.535	0.373	1.023	-
	0.214	0.855	0.936	0.550	0.428	0.681	-
	0.371	0.906	0.819	0.514	0.398	0.547	0.163
	0.529	0.947	0.763	0.479	0.368	0.474	0.134
	0.686	0.978	0.679	0.424	0.337	0.377	0.073
	0.843	1.004	0.613	0.403	0.317	0.320	0.032
	1.000	1.014	0.576	0.393	0.307	0.290	0.005
6	0.087	0.767	1.124	0.551	0.401	0.864	-
	0.239	0.875	0.918	0.541	0.432	0.660	-
	0.391	0.932	0.838	0.505	0.402	0.560	0.201
	0.544	0.968	0.777	0.490	0.372	0.491	0.130
	0.696	0.999	0.702	0.440	0.337	0.400	0.068
	0.848	1.020	0.627	0.414	0.322	0.334	0.026
	1.000	1.025	0.609	0.404	0.317	0.317	0.002
9	0.133	0.829	1.039	0.578	0.445	0.806	-
	0.278	0.906	0.913	0.572	0.445	0.680	-
	0.422	0.963	0.847	0.501	0.401	0.565	0.173
	0.567	0.999	0.777	0.486	0.384	0.494	0.141
	0.711	1.025	0.730	0.435	0.356	0.425	0.078
	0.856	1.045	0.655	0.415	0.336	0.357	0.040
	1.000	1.056	0.632	0.410	0.325	0.337	0.012
12	0.055	0.772	1.273	0.587	0.382	1.056	-
	0.190	0.891	1.007	0.564	0.443	0.764	-
	0.325	0.947	0.904	0.544	0.433	0.650	0.204
	0.460	0.999	0.843	0.493	0.399	0.556	0.179
	0.595	1.035	0.763	0.478	0.378	0.477	0.122
	0.730	1.056	0.735	0.431	0.360	0.428	0.096
	0.865	1.076	0.679	0.426	0.355	0.384	0.044
	1.000	1.081	0.655	0.416	0.350	0.363	0.017

θ	$\frac{y}{\hat{y}}$	$\frac{\bar{v}_z}{v_b}$	$\frac{v'_z}{v_b} \times 10$	$\frac{v'_e}{v_b} \times 10$	$\frac{v'_r}{v_b} \times 10$	$\frac{K}{v_b^2} \times 10^2$	$\frac{v'_r v'_z}{v_b^2} \times 10^2$
15	0.129	0.881	1.067	0.581	0.471	0.849	-
	0.253	0.942	0.955	0.556	0.457	0.715	-
	0.378	0.994	0.894	0.531	0.426	0.631	0.205
	0.502	1.035	0.833	0.489	0.407	0.550	0.166
	0.627	1.066	0.763	0.480	0.386	0.481	0.139
	0.751	1.087	0.730	0.443	0.368	0.432	0.100
	0.876	1.097	0.693	0.422	0.358	0.393	0.056
	1.000	1.107	0.655	0.422	0.358	0.368	0.021
18	0.091	0.814	1.212	0.602	0.464	1.024	-
	0.204	0.942	1.002	0.570	0.451	0.766	-
	0.318	0.994	0.936	0.532	0.445	0.679	0.226
	0.432	1.035	0.875	0.522	0.429	0.612	0.199
	0.545	1.071	0.810	0.481	0.400	0.524	0.169
	0.659	1.097	0.749	0.472	0.378	0.464	0.145
	0.773	1.117	0.730	0.440	0.371	0.432	0.101
	0.886	1.133	0.707	0.423	0.367	0.407	0.054
1.000	1.143	0.660	0.413	0.357	0.367	0.023	
21	0.071	0.834	1.194	0.661	0.477	1.045	-
	0.174	0.953	0.988	0.587	0.485	0.778	-
	0.278	0.994	0.941	0.548	0.474	0.705	0.258
	0.381	1.040	0.899	0.517	0.449	0.639	0.226
	0.484	1.081	0.838	0.503	0.428	0.569	0.200
	0.587	1.107	0.801	0.466	0.405	0.511	0.168
	0.690	1.128	0.740	0.457	0.389	0.454	0.140
	0.794	1.148	0.712	0.436	0.375	0.418	0.102
	0.897	1.159	0.702	0.413	0.373	0.401	0.059
1.000	1.169	0.660	0.410	0.356	0.365	0.034	
24	0.067	0.865	1.128	0.646	0.509	0.975	-
	0.160	0.932	1.039	0.644	0.485	0.865	-
	0.253	0.990	1.007	0.560	0.492	0.785	0.314
	0.347	1.051	0.932	0.525	0.457	0.676	0.245
	0.440	1.081	0.875	0.498	0.438	0.603	0.201
	0.533	1.123	0.815	0.496	0.420	0.543	0.204
	0.627	1.143	0.768	0.448	0.388	0.470	0.162
	0.720	1.159	0.721	0.432	0.379	0.425	0.128
	0.813	1.179	0.702	0.416	0.370	0.401	0.107
	0.907	1.184	0.679	0.404	0.367	0.379	0.040
1.000	1.195	0.651	0.406	0.354	0.357	0.025	

θ	$\frac{y}{\hat{y}}$	$\frac{\bar{v}_z}{v_b}$	$\frac{v'_z}{v_b} \times 10$	$\frac{v'_e}{v_b} \times 10$	$\frac{v'_r}{v_b} \times 10$	$\frac{K}{v_b^2} \times 10^2$	$\frac{v'_r v'_z}{v_b^2} \times 10^2$
27	0.073	0.860	1.053	0.651	0.341	0.824	-
	0.157	0.927	1.016	0.637	0.491	0.840	-
	0.242	1.014	0.978	0.598	0.477	0.771	0.283
	0.326	1.056	0.941	0.529	0.478	0.697	0.276
	0.410	1.097	0.857	0.501	0.441	0.589	0.225
	0.494	1.128	0.810	0.451	0.416	0.516	0.213
	0.579	1.148	0.768	0.444	0.392	0.470	0.195
	0.663	1.174	0.730	0.414	0.388	0.427	0.136
	0.747	1.190	0.674	0.415	0.355	0.376	0.112
	0.831	1.200	0.651	0.398	0.347	0.351	0.082
	0.916	1.210	0.637	0.420	0.299	0.336	0.049
	1.000	1.220	0.604	0.393	0.315	0.309	0.017
30	0.087	0.927	0.960	0.633	0.460	0.767	-
	0.163	0.973	0.993	0.592	0.521	0.803	-
	0.239	1.004	0.904	0.593	0.471	0.695	0.236
	0.315	1.071	0.890	0.556	0.414	0.636	0.224
	0.391	1.102	0.843	0.466	0.436	0.559	0.188
	0.468	1.143	0.791	0.433	0.413	0.492	0.195
	0.544	1.164	0.754	0.401	0.391	0.441	0.163
	0.620	1.179	0.712	0.410	0.360	0.402	0.160
	0.696	1.200	0.655	0.390	0.340	0.349	0.113
	0.772	1.215	0.623	0.399	0.308	0.321	0.070
	0.848	1.210	0.604	0.394	0.302	0.306	0.038
	0.924	1.210	0.609	0.396	0.294	0.307	0.015
1.000	1.220	0.590	0.394	0.302	0.297	0.002	

APPENDIX J

DESCRIPTION AND LISTING OF COMPUTER CODE "HYBBAC"

In order to solve the finite difference equations, presented in chapter IV, the computer code "HYBBAC" (HYdraulic Bare Bundle Analysis Code) was developed. Fig.J.1 shows the block diagram of the organization of the program. Presented below is a list of the subroutines related directly to the main program and their contribution to the computation. Numbers in parenthesis represent equation numbers as they appear in the text.

1. BLOCK DATA - Provides numerical input for the program:

- P, D, R_e, ν, ρ (flow)
- λ (IV.78), N_{\max} (max.# of iterations)
- I_n, J_n (Grid)

2. Inicialization Subroutines:

- IBRAG - f (II.9), $\tau_w/\bar{\tau}_w$ (II.6)
- COORD - $r_i, \theta_i, y_i=r_i-R, \eta_j$ (IV.56)
- GRID - $B_{i,j}$ (IV.19), $V_{i,j}$ (IV.25)
- FLOW - A_f (V.1), P_w (V.3), D_H (V.2), V_{bulk}
- INIT - Initial conditions (Ch.IV, section 9)
- MIXLEN - ℓ (III.18) or (III.17)
- STREAM - Ψ (IV.81)

3. VELDIS - $\bar{v}_\theta, \bar{v}_r$ (A.13)
4. NORM - normalization of initial conditions for v_z ,
for laminar flow.
5. NORM2 - normalization of output
- $$\frac{v_z}{v_b}, \frac{v_z}{v_\tau}, \frac{K}{v_b^2}, \frac{K}{v_\tau^2}, \frac{\psi}{\psi_{\max}}$$
6. Print-out subroutines
- PRINT - print-out of parameters distribution
- PRINT2 - print-out of general information:
 f, v_b, R_e, D_H , distribution of $(\tau_w/\bar{\tau}_w)$
7. CORE - Iterative Subroutine

Fig. J.2 shows the block diagram of the iterative subroutine CORE. Its related subroutines are listed below.

- VISCOS - (v_τ/ν) (III.11)
- MAXVAL - $\phi_{\max}^{(n-1)}$ (necessary for λ , IV.77)
- REYNU - Adjusts bulk velocity yielded by (n-1)
iteration to desired v_{bulk} .
- WALL - f (III.57), v_τ (III.67), $\bar{\tau}_w/\rho$ (III.60)
- WF - wall boundary conditions
 $\omega_{1,j}$ (IV.60), v_{im-1}^* (IV.71), K_{im-1}^* (IV.74)
- CONVEC - $A_{i,j}$ (IV.13.a)

STRESS - $(\Delta_{\omega})_{i,j}$ (IV,34)
SOURCE - Source terms (IV,26), (IV,29), (IV.40),
(IV.41)
BOUND - Boundary conditions except wall's.

The nomenclature followed in the program is the same used by Gosman et al⁽¹⁷⁾ in the ANSWER code.

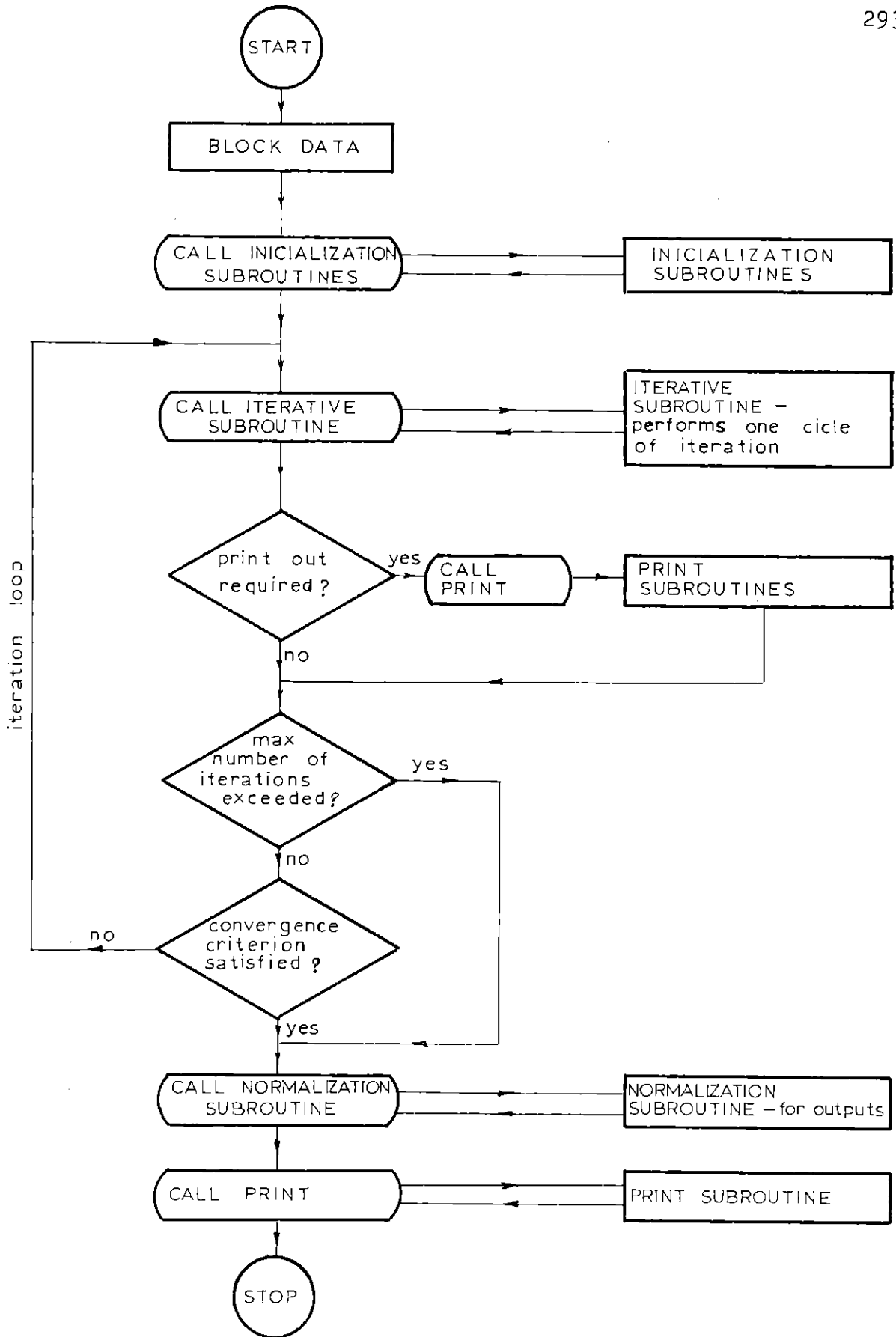


Fig. J.1. Block Diagram of Main Program

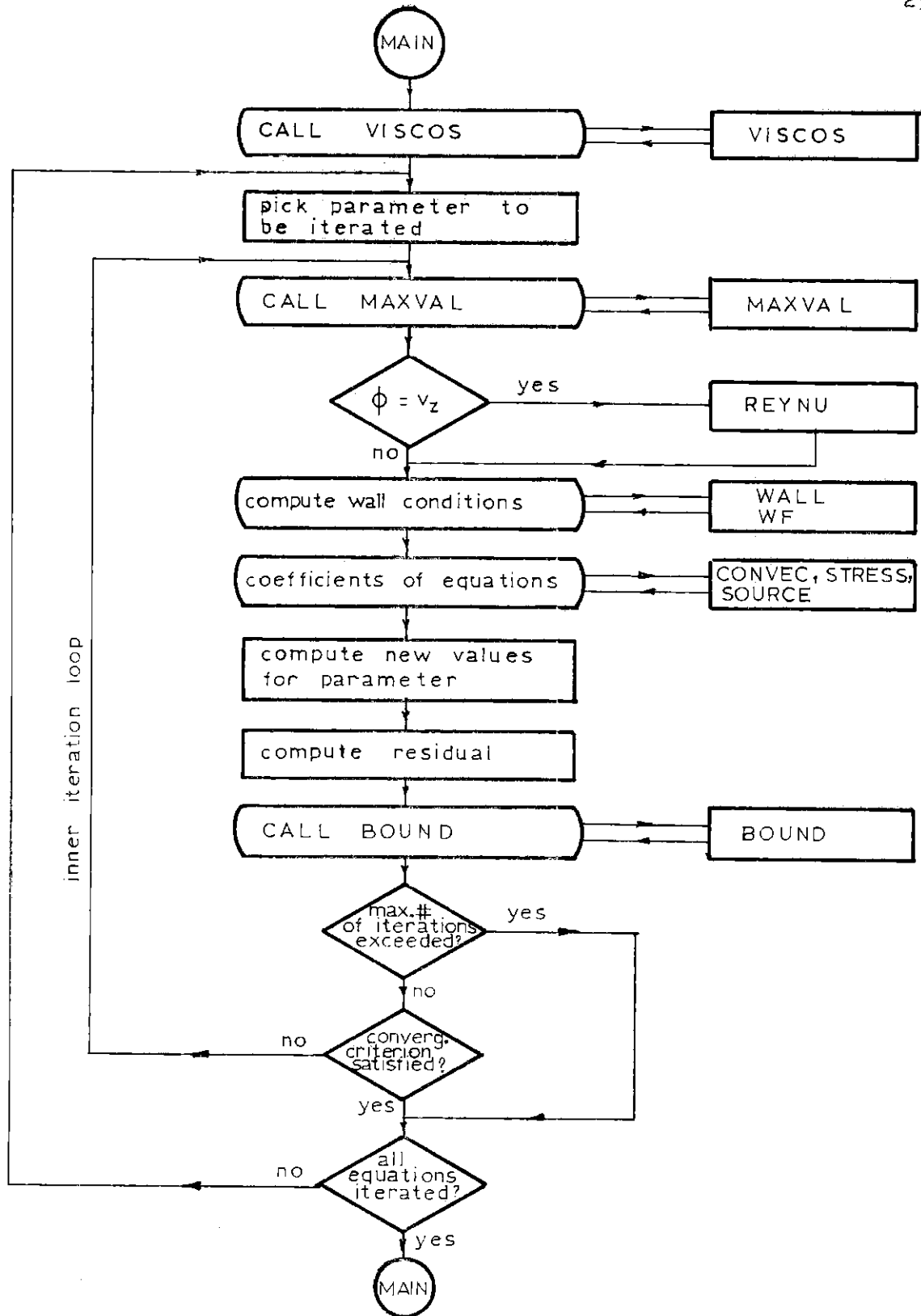


Fig. J.2. Block Diagram of Subroutine Core

```

DIMENSION A(41,21,8), ANAME(9,8), ASYMBL(9), BE(41), BW(41), BN(41),
2BS(41), ATITLE(27)
COMMON/CVRBLE/A, ANAME, ASYMBL
COMMON/CNUMBR/NW, NF, NV, NK, NL, NMO, NV1, MV2, II, IE, IV
COMMON/CGEO/IN, INM, JN, JN4, IMAX(21), ILIM(21), X1(41), X2(21),
2R(41), VP(41), ININ(4)
COMMON/CFLOW/PIT, DIA, DH, ATOT, RE, VAVG, KFLOW, BOREF, ZMUREF, VB
COMMON/CGEN/NMAX, INNER, NPRINT, IP, CC, PR(9), RP(9), RSDU(9)
COMMON/CWALL/TALAV, RTAL(21), USTAR(21), FR, YB(21)
COMMON/CBOUND/CB(21)
COMMON/CFUNC/PW(41,21)
COMMON/CCONST/CK, E, CVIS, CDIS, C1, C2
C*****
C  SUBROUTINE FOR INITIALISATION AND PROGRAM CONTROL
C*****
C
C***ENSURE THAT DIMENSIONS OF ARRAYS ABOVE CORRESPOND WITH VALUES
C  ASSIGNED TO N1, N2 AND N3 IN FOLLOWING DATA CARD
  DATA N1, N2, N3/41, 21, 8/
  INM=IN-1
  JNM=JN-1
C*** READ ALPHAMERIC INFORMATION FOR HEADINGS AND TITLES
  READ(5,200) ATITLE
  READ(5,200) ANAME, ASYMBL
C*** CALL INITIALISATION SUBROUTINES
  CALL FLOW
  CALL IBRAG
  CALL COORD
  CALL GRID (N1, N2, N3, BE, BW, BN, BS)
C*** WRITE PROBLEM-SPECIFICATION INFORMATION
  WRITE (6,301) ATITLE
  WRITE (6,310) (K, (ANAME(L,K), L=1,9), K=II, IF)
  WRITE (6,312) BOREF, ZMUREF, RE, (K, PR(K), K=1,4), (K, RP(K), K=1,4),
2NMAX, CC, IN, JN, (J, ILIM(J), IMAX(J), J=1, JN)
  CALL INIT (N1, N2, N3, A, ANAME)
  NITER=0

```

```

MAIN0001
MAIN0002
MAIN0003
MAIN0004
MAIN0005
MAIN0006
MAIN0007
MAIN0008
MAIN0009
MAIN0010
MAIN0011
MAIN0012
MAIN0013
MAIN0014
MAIN0015
MAIN0016
MAIN0017
MAIN0018
MAIN0019
MAIN0020
MAIN0021
MAIN0022
MAIN0023
MAIN0024
MAIN0025
MAIN0026
MAIN0027
MAIN0028
MAIN0029
MAIN0030
MAIN0031
MAIN0032
MAIN0033
MAIN0034
MAIN0035
MAIN0036

```


C*** ITERATION AND PRINTOUT CONTROL LOOP	MAIN0037
1 CONTINUE	MAIN0038
NITER=NITER+1	MAIN0039
C*** CAUSE ONE CYCLE OF ITERATION TO BE PERFORMED	MAIN0040
CALL CORE (N1,N2,N3,A,BE,BW,BN,BS,ANAME)	MAIN0041
C*** TEST IF PRINTOUT TO BE PRODUCED	MAIN0042
IF ((NITER+NPRINT-IP)/NPRINT.NE.NITER/NPRINT) GO TO 10	MAIN0043
CALL VELDIS (N1,N2,N3,A)	MAIN0044
CALL PRINT (N1,N2,N3,A)	MAIN0045
IF(KFLOW.EQ.1) GO TO 3	MAIN0046
CALL PRINT2	MAIN0047
3 CONTINUE	MAIN0048
WRITE (6,103) (ASYMBL(K),K=II,IE)	MAIN0049
10 WRITE (6,104) NITER,(RSDU(K),K=II,IE)	MAIN0050
C*** TEST IF MAXIMUM NUMBER OF ITERATIONS (NMAX) PERFORMED	MAIN0051
IF(NITER.EQ.NMAX) GO TO 8	MAIN0052
RES=0.	MAIN0053
DO 7 K=II,IE	MAIN0054
IF(ABS(RES).LT.ABS(RSDU(K))) RES=RSDU(K)	MAIN0055
7 RSDU(K)=0.	MAIN0056
C*** TEST IF CONVERGENCE CRITERION (CC) SATISFIED	MAIN0057
IF(ABS(RES).GT.CC.OR.NITER.LE.5) GO TO 1	MAIN0058
C*** END OF LOOP	MAIN0059
GO TO 9	MAIN0060
8 WRITE (6,106) NITER	MAIN0061
9 CONTINUE	MAIN0062
C*** OBTAIN VELOCITY DISTRIBUTIONS	MAIN0063
CALL VELDIS (N1,N2,N3,A)	MAIN0064
C*** FINAL PRINT-OUT	MAIN0065
CALL PRINT (N1,N2,N3,A)	MAIN0066
CALL PRINT2	MAIN0067
C*** NORMALIZE FINAL OUTPUT	MAIN0068
CALL NORM2 (N1,N2,N3,A)	MAIN0069
STOP	MAIN0070
103 FORMAT(35H0MAXIMUM RESIDUAL FOR EACH VARIABLE//6H NITER,2X,9(6X,	MAIN0071
1A4,2X)//)	MAIN0072

PAGE 2

104	FORMAT(1H ,I4,5X,9(1PE12.3))	MAIN0073
106	FORMAT (32H0THE PROCESS DID NOT CONVERGE IN,I5,13H ITERATIONS)	MAIN0074
200	FORMAT (9A4)	MAIN0075
301	FORMAT(1H124X,75HFINITE-DIFFERENCE ITERATIVE SOLUTION IS UNDER CON	MAIN0076
	2SIDERATION FOR THE CASE OF/ 25X,75H-----	MAIN0077
	2-----// 1X,27A4////	MAIN0078
	3 46H THE DEPENDENT VARIABLES BEING CONSIDERED ARE,)	MAIN0079
310	FORMAT(1HC 9X,I1,3H ,9A4)	MAIN0080
312	FORMAT(36H0THE INITIAL INFORMATION SUPPLIED IS//	MAIN0081
	310X,50HROREF, REFERENCE DENSITY FOR THE FLUID.....=,1PE15.6/	MAIN0082
	510X,50HZMUREF, REFERENCE VISCOSITY FOR THE FLUID.....=,1PE15.6/	MAIN0083
	510X,50HRE, REYNOLDS NUMBER.....=,1PE15.6/	MAIN0084
	310X,57HPR'S, RATIOS OF MOMENTUM AND PROPERTY DIFFUSIVITIES ARE//	MAIN0085
	5 18X,4(3HPR(,I1,2H)=,0PF5.2,2H,)/	MAIN0086
	510X,57HRP'S, RELAXATION PARAMETERS FOR DEPENDENT VARIABLES ARE//	MAIN0087
	5 18X,4(3HRP(,I1,2H)=,0PF5.2,2H,)/	MAIN0088
	110X,50HNMAX, THE MAXIMUM NUMBER OF ITERATIONS.....=,I6/	MAIN0089
	310X,50HCC, THE CONVERGENCY CRITERION.....=,1PE15.6/	MAIN0090
	310X,50HIN, THE NUMBER OF COLUMNS (DIRECTION-1).....=,I6/	MAIN0091
	410X,50HJN, THE NUMBER OF ROWS (DIRECTION-2).....=,I6//	MAIN0092
	511X,1HJ,10X,4HILIM, 9X,4HIMAX//(1H 9X,3(I2,11X))	MAIN0093
	END	MAIN0094

```

SUBROUTINE IBRAG
COMMON/CGEO/IN, INM, JN, JNM, IMAX (21), ILIM (21), X1 (41), X2 (21),
2R (41), VP (41), IMIN (4)
COMMON/CFLOW/PIT, DIA, DH, ATOT, RE, VAVG, KFLOW, ROREF, ZMUREF, VB
COMMON/CWALL/TALAV, RTAL (21), USTAR (21), FR, YB (21)
C*****
C SUBROUTINE FOR COMPUTATION OF WALL FRICTION BY IBRAGIMOV METHOD
C*****
C
C*** COMPUTE YAV
YAV=0.5*(3./3.1416*PIT*ALOG(3.)-DIA)
C*** COMPUTE FRICTION FACTOR, FR
X=ATOT/YAV**2
XK=X**0.25*PIT*(1./SQRT(3.)-0.5)/YAV
XX=-0.021*XK**3
RFR=(.58+.42*EXP(XX))*(1+.1*(2.*YAV/DIA+1.))**(4./3.)
FCIP=0.046*RFR**(-.2)
IF(KFLOW.EQ.1) FCIP=16./RE
FR=RFR*FCIP
C*** COMPUTE DISTRIBUTION OF TAL AND USTAR
TALAV=0.5*FR*VAVG**2
AC=3.85*PIT/(X**0.8*YAV)
CC=(AC/2.)**0.5*3.1416/6.
C=1.-6./3.1416*(3.1416/2./AC)**0.5*EXP(-AC)*ERF(CC)
C=1./C
B=7.7/(X**0.8*YAV)
CC=3.1416/6.*(0.25*B*PIT)**0.5
CD=-0.5*B*(PIT-DIA)
CI=6./(3.1416*B*PIT)**0.5*EXP(CD)*ERF(CC)
C=1./(1.-CI)
DTETA=3.1416/6./FLOAT(JNM)
DO 1 J=1, JN
TETA=DTETA*FLOAT(J-1)
YT=0.5*(PIT/COS(TETA)-DIA)
BY=-E*YT
RTAL(J)=C*(1.-EXP(BY))

```

```

IBRA0001
IBRA0002
IBRA0003
IBRA0004
IBRA0005
IBRA0006
IBRA0007
IBRA0008
IBRA0009
IBRA0010
IBRA0011
IBRA0012
IBRA0013
IBRA0014
IBRA0015
IBRA0016
IBRA0017
IBRA0018
IBRA0019
IBRA0020
IBRA0021
IBRA0022
IBRA0023
IBRA0024
IBRA0025
IBRA0026
IBRA0027
IBRA0028
IBRA0029
IBRA0030
IBRA0031
IBRA0032
IBRA0033
IBRA0034
IBRA0035
IBRA0036

```

```
1  USTAR(J) = (TALAV*RTAL(J))**0.5  
   RETURN  
   END
```

```
IBRA0037  
IBRA0038  
IBRA0039
```

COORD001
 COORD002
 COORD003
 COORD004
 COORD005
 COORD006
 COORD007
 COORD008
 COORD009
 COORD010
 COORD011
 COORD012
 COORD013
 COORD014
 COORD015
 COORD016
 COORD017
 COORD018
 COORD019
 COORD020
 COORD021
 COORD022
 COORD023
 COORD024
 COORD025
 COORD026
 COORD027
 COORD028
 COORD029
 COORD030
 COORD031
 COORD032
 COORD033
 COORD034
 COORD035
 COORD036

```

SUBROUTINE COORD
COMMON/CNUMBR/NM,NF,NV,NK,NL,NMU,NV1,NV2,II,IE,IV
COMMON/CGEO/IN,INM,JN,JNM,IMAX(21),ILIM(21),XI(41),X2(21),
ZR(41),VP(41),IMIN(4)
COMMON/CFLOW/PII,DIA,DH,ATOT,RE,VAVG,KFLOW,RORF,ZMUREF,VB
COMMON/CWALL/TALAV,RTAL(21),USTAR(21),FR,YB(21)
COMMON/CBOUND/CB(21)
*****
C SUBROUTINE TO COMPUTE THE GRID COORDINATES
*****
C
C*** CIRCUMFERENTIAL COORDINATES, X2(J)
      DELTA=3.14159/6./FLOAT(JNM)
      X2(1)=0.
      DO 1 J=2,JN
        X2(J)=X2(J-1)+DELTA
      X1(1)=0.0
      C*** RADIAL COORDINATES, X1(I)
        GAP=0.5*(PI-DIA)
      C*** RADIAL COORDINATES NEAR SOLID WALL
        M=IN-JNM
        MN=M-1
      C*** DETERMINE WALL SUBLAYER THICKNESS
        XB=30.*ZMUREF/SQRT(TALAV)
      C*** DETERMINATION OF AVERAGE THICKNESS OF SUBLAYER
        DO 20 J=1,JN
          YB(J)=XB
          X1(M)=GAP
          YBAR=GAP/LOAT(M-1)
          DO 2 I=1,IN
            DR=XB/(LOAT(I)+0.5)
            IB=I+Z
            IF(YBAR.GE.DR) GO TO 6
          CONTINUE
        DO 11 I=2,IB
          X1(I)=X1(I-1)+DR
  11

```

C*** STRETCHED GRID	COOR0037
L=(M-IB)*(M-IB+1)/2	COOR0038
DR=(X1(M)-X1(1B)-FLOAT(M-1B)*X1(2))/FLOAT(L)	COOR0039
IL=IB+1	COOR0040
DO 15 I=IL,MN	COOR0041
15 X1(I)=X1(I-1)+X1(2)+FLOAT(I-IL+1)*DR	COOR0042
DO 3 J=1,JN	COOR0043
TETA=X2(J)	COOR0044
3 X1(M+J-1)=PI*2./COS(TETA)-DIA/2.	COOR0045
C*** RADIAL DISTANCES, R(I)	COOR0046
DO 4 I=1,IN	COOR0047
4 R(I)=0.5*DIA+X1(I)	COOR0048
C*** DETERMINATION OF IMIN	COOR0049
IMIN(NW)=2	COOR0050
IMIN(NF)=2	COOR0051
IMIN(NV)=IB	COOR0052
IF(KFLOW.EQ.1) IMIN(NV)=2	COOR0053
IMIN(NK)=IB	COOR0054
C*** DETERMINATION OF ILIM AND IMAX	COOR0055
DO 5 J=1,JN	COOR0056
IMAX(J)=M+J-2	COOR0057
5 ILIM(J)=M+J-1	COOR0058
C*** FIND EAST BOUNDARY PARAMETERS, CB(J)	COOR0059
DO 10 J=2,JNM	COOR0060
IB=ILIM(J)	COOR0061
TETA=X2(J)	COOR0062
10 CB(J)=(R(1B)-R(1B-1))/R(1B)/(X2(J+1)-X2(J))*TAN(TETA)	COOR0063
C*** PRINT OUT COORDINATES, ILIM AND IMAX	COOR0064
WRITE(6,101) (X1(I),I=1,IN)	COOR0065
WRITE(6,102) (X2(J),J=1,JN)	COOR0066
WRITE(6,103) ((ILIM(L),IMAX(L)),L=1,JN)	COOR0067
RETURN	COOR0068
101 FORMAT(25HODISTANCES IN DIRECTION-1/(1H 4E25.8))	COOR0069
102 FORMAT(25HODISTANCES IN DIRECTION-2/(1H 4E25.8))	COOR0070
103 FORMAT(24H0VALUES OF ILIM AND IMAX/(1H 4(5X,I4,7X,I4,5X)))	COOR0071
END	COOR0072

```

SUBROUTINE GRID (N1,N2,N3,BE,BW,BN,BS)
DIMENSION BE(N1),BW(N1),BN(N1),BS(N1)
COMMON/CNUMBER/NW,NF,NV,NK,NL,NMU,NV1,NV2,II,IE,IV
COMMON/CGEO/IN,INM,JN,JMM,IMAX(21),ILIM(21),X1(41),X2(21),
2R(41),VP(41),IMIN(4)
C*****
C SUBROUTINE FOR CALCULATION OF BE,BW,BN,BS AND VP
C*****
DTETA=X2(2)
C*** COMPUTE BE,BW,BN,BS AND VP
VP(1)=DTETA*R(1)*(R(2)-R(1))
VP(IN)=DTETA*R(IN)*(R(IN)-R(INM))
DO 21 I=2,INM
BE(I)=.25*DTETA*(R(I+1)+R(I))/(R(I+1)-R(I))
BW(I)=.25*DTETA*(R(I-1)+R(I))/(R(I)-R(I-1))
BN(I)=.25*(R(I+1)-R(I-1))/R(I)/DTETA
BS(I)=BN(I)
21 VP(I)=DTETA*(R(I+1)-R(I-1))*(R(I+1)+2.*R(I)+R(I-1))/8.
RETURN
END

```

```

GRID0001
GRID0002
GRID0003
GRID0004
GRID0005
GRID0006
GRID0007
GRID0008
GRID0009
GRID0010
GRID0011
GRID0012
GRID0013
GRID0014
GRID0015
GRID0016
GRID0017
GRID0018
GRID0019
GRID0020

```

```

SUBROUTINE FLOW
COMMON/CNUMBER/NW,NF,NV,NK,NL,NMU,NV1,NV2,LI,IF,IV
COMMON/CGFO/IN,INM,JN,JNM,IMAX(21),ILIM(21),X1(41),X2(21),
2R(41),VP(41),IMIN(4)
COMMON/CFLOW/PIT,DIA,DH,ATOT,RE,VAVG,KFLOW,ROPEF,ZMUREF,VB
C*****
C SUBROUTINE TO COMPUTE HYDRAULIC PARAMETERS OF THE FLOW
C*****
C
C*** COMPUTE CHANNEL AREA
ATOT=PIT*PIT/8./SQRT(3.)-DIA*DIA*3.14159/48.
C*** WETTED PERIMETER
PW=DIA*3.14159/12.
C*** HYDRAULIC DIAMETER
DH=4.*ATOT/PW
C*** AVERAGE VELOCITY
VAVG=ZMUREF*RE/DH
RETURN
END

```

```

FLOW0001
FLOW0002
FLOW0003
FLOW0004
FLOW0005
FLOW0006
FLOW0007
FLOW0008
FLOW0009
FLOW0010
FLOW0011
FLOW0012
FLOW0013
FLOW0014
FLOW0015
FLOW0016
FLOW0017
FLOW0018
FLOW0019

```



```

SUBROUTINE INIT (N1,N2,N3,A,ANAME)
DIMENSION A(N1,N2,N3),ANAME(9,N3)
COMMON/CNUMBER/NW,NP,NV,NK,NL,NMU,NV1,NV2,II,IE,IV
COMMON/CGEO/IN,INM,JN,JNM,IMAX(21),ILIM(21),X1(41),X2(21),
2R(41),VP(41),IMIN(4)
COMMON/CFLOW/PIT,DIA,DH,ATOT,RE,VAVG,KFLOW,ROREF,ZMUREF,VB
COMMON/CWALL/TALAV,ETAL(21),USTAR(21),FR,YE(21)
COMMON/CCONST/CK,E,CVIS,CDIS,C1,C2
C*****
C SUBROUTINE FOR COMPUTATION OF INITIAL CONDITIONS
C*****
C
C*** SET VALUES IN STORE TO ZERO
      DO 30 K=1,N3
      DO 30 J=1,JN
      DO 30 I=1,IN
30    A(I,J,K)=0.0
C*** INITIAL CONDITIONS FOR AXIAL VELOCITY
C*** ASSUMING KARMAN'S LINEAR APPROXIMATION AND
C*** IBRAGIMOV WALL SHEAR STRESS DISTRIBUTION
      DO 55 J=1,JN
      IL=ILIM(J)
      DO 55 I=2,IL
      XS=USTAR(J)*X1(I)/ZMUREF
      Y=ALOG(XS)
55    A(I,J,NV)=USTAR(J)*(2.5*Y+5.5)
C*** COMPUTE BULK VELOCITY
      CALL REYNU (N1,N2,N3,A)
      IF(KFLOW.EQ.1) GO TO 65
C*** COMPUTE MIXING LENGTH
      CALL MIXLEN (N1,N2,N3,A)
C*** INITIAL CONDITIONS FOR TKE ASSUMING ROBKOV'S CORRELATION
      FV=1.-VAVG/A(IN,JN,NV)
      DO 10 J=1,JN
      IL=IMIN(NK)-1
      IM=ILIM(J)

```

```

INIT0001
INIT0002
INIT0003
INIT0004
INIT0005
INIT0006
INIT0007
INIT0008
INIT0009
INIT0010
INIT0011
INIT0012
INIT0013
INIT0014
INIT0015
INIT0016
INIT0017
INIT0018
INIT0019
INIT0020
INIT0021
INIT0022
INIT0023
INIT0024
INIT0025
INIT0026
INIT0027
INIT0028
INIT0029
INIT0030
INIT0031
INIT0032
INIT0033
INIT0034
INIT0035
INIT0036

```

DO 10 I=IL,IM	INIT0037
ETA=X1(I)/X1(IM)	INIT0038
YZ=-1.48*ETA	INIT0039
YT=-1.17*ETA	INIT0040
YR=-0.77*ETA	INIT0041
FZ=0.95*EXP(YZ)	INIT0042
FT=0.60*EXP(YT)	INIT0043
FD=0.40*EXP(YR)	INIT0044
FK=0.5*(FZ**2+FT**2+FD**2)	INIT0045
10 A(I,J,NK)=FK*(FV*A(I,J,NV))**2	INIT0046
C*** INITIAL CONDITIONS FOR STREAM FUNCTION	INIT0047
IF(KFLOW.EQ.2) GO TO 50	INIT0048
IF(KFLOW.NE.3.AND.II.EQ.3) GO TO 50	INIT0049
CALL STREAM (N1,N2,N3,A)	INIT0050
CALL VELDISE (N1,N2,N3,A)	INIT0051
GO TO 50	INIT0052
C*** NORMALIZE INPUT FOR LAMINAR CASE	INIT0053
65 CALL NORM (N1,N2,N3,A)	INIT0054
C*** PRINT INITIAL CONDITIONS	INIT0055
50 CALL PRINT (N1,N2,N3,A)	INIT0056
CALL PRINT2	INIT0057
IF(KFLOW.LT.4) RETURN	INIT0058
C*** FICTITIOUS VALUES AT WALL FOR VELOCITY AND TKE	INIT0059
CALL WF (N1,N2,N3,A,NV)	INIT0060
CALL WF (N1,N2,N3,A,NK)	INIT0061
RETURN	INIT0062
END	INIT0063

SUBROUTINE MIXLEN (N1,N2,N3,A)	MIXL0001
DIMENSION A(N1,N2,N3)	MIXL0002
COMMON/CNUMBR/NW,NF,NV,NK,NL,NMU,NV1,NV2,II,IE,IV	MIXL0003
COMMON/CGEO/IN,INN,JN,JNM,IMAX(21),ILIM(21),X1(41),X2(21),	MIXL0004
2R(41),VP(41),IMIN(4)	MIXL0005
COMMON/CFLOW/PIT,DIA,DH,ATOT,RE,VAVG,KFLOW,ROREF,ZMUREF,VB	MIXL0006
C*****	MIXL0007
C SUBROUTINE TO COMPUTE THE MIXING LENGTH	MIXL0008
C*****	MIXL0009
DO 10 J=1,JN	MIXL0010
IH=ILIM(J)	MIXL0011
DO 10 I=2,IH	MIXL0012
ETA=X1(I)/X1(IH)	MIXL0013
IF(ETA.GT.0.44) GO TO 15	MIXL0014
A(I,J,NL)=X1(I)	MIXL0015
GO TO 10	MIXL0016
15 CT=3.14159/.38*(ETA-0.44)	MIXL0017
A(I,J,NL)=(0.44+0.066*SIN(CT))*X1(IH)	MIXL0018
10 CONTINUE	MIXL0019
RETURN	MIXL0020
END	MIXL0021

SUBROUTINE CORE (N1,N2,N3,A,BE,BW,EN,BS,ANAME)	CORE0001
DIMENSION ANAME(9,N3)	CORE0002
DIMENSION A (N1,N2,N3),BE(N1),RW(N1),BN(N1),BS(N1)	CORE0003
DIMENSION BAE(41,21),BAW(41,21),BAN(41,21),BAS(41,21),SORCE(41,21)	CORE0004
COMMON/CNUMPR/NW,NF,NV,NK,NL,NMU,NV1,NV2,II,IE,IV	CORE0005
COMMON/CGEO/IN,INN,JN,JNM,IMAX(21),ILIM(21),X1(41),X2(21),	CORE0006
2R(41),VP(41),IMIN(4)	CORE0007
COMMON/CFLOW/PIT,DIA,DH,ATOT,RE,VAVG,KFLOW,ROREF,ZMUREF,VB	CORE0008
COMMON/CGEN/NMAX,INNER,NPRINT,IP,CC,PR(9),RP(9),RSDU(9)	CORE0009
COMMON/CWALL/TALAV,RTAL(21),USTAR(21),FR,YB(21)	CORE0010
COMMON/CBOUND/CB(21)	CORE0011
COMMON/CFUNC/FW(41,21)	CORE0012
COMMON/CCONST/CK,E,CVIS,CDIS,C1,C2	CORE0013
C*****	CORE0014
C ITERATION SUBROUTINE	CORE0015
C*****	CORE0016
C	CORE0017
C*** CHECK KIND OF FLOW	CORE0018
IF(KFLOW.EQ.1) GO TO 1	CORE0019
C*** OBTAIN TURBULENT VISCOSITY	CORE0020
CALL VISCOS (N1,N2,N3,A)	CORE0021
C*** OBTAIN FW(I,J) FOR STRESS MODEL	CORE0022
IF(KFLOW.NE.4) GO TO 1	CORE0023
CALL STRESS (N1,N2,N3,A)	CORE0024
C*** ITERATION CYCLES	CORE0025
1 DO 90 K=II,IE	CORE0026
IF(K.EQ.NW) AF=-3.*ZMUREF/X1(2)**2	CORE0027
IG=IMIN(K)	CORE0028
C*** COMPUTE DIFFUSION,CONVECTION AND SOURCE TERMS	CORE0029
DO 10 J=2,JNM	CORE0030
IH=IMAX(J)	CORE0031
DO 10 I=IG,IH	CORE0032
C*** OBTAIN CONVECTION COEFFICIENTS	CORE0033
CALL CONVEC (N1,N2,N3,A,AF,AW,AN,AS,I,J,K)	CORE0034
C*** COMPUTE DIFFUSION+CONVECTION COEFFICIENTS	CORE0035
IF(K.EQ.NW.OR.K.EQ.NF) GO TO 5	CORE0036

C*** AXIAL VELOCITY AND TKE EQUATIONS	CORE0037
BAE(I,J)=BE(I)*(2.+(A(I+1,J,NMU)+A(I,J,NMU))/PR(K))+AE	CORE0038
BAW(I,J)=BW(I)*(2.+(A(I-1,J,NMU)+A(I,J,NMU))/PR(K))+AW	CORE0039
BAN(I,J)=BN(I)*(2.+(A(I,J+1,NMU)+A(I,J,NMU))/PR(K))+AN	CORE0040
BAS(I,J)=BS(I)*(2.+(A(I,J-1,NMU)+A(I,J,NMU))/PR(K))+AS	CORE0041
GO TO 10	CORE0042
C*** VORTICITY AND STREAM FUNCTION EQUATIONS	CORE0043
5 BAE(I,J)=2.*BE(I)+AE	CORE0044
BAW(I,J)=2.*BW(I)+AW	CORE0045
BAN(I,J)=2.*BN(I)+AN	CORE0046
PAS(I,J)=2.*BS(I)+AS	CORE0047
C*** COMPUTE SOURCE TERMS FOR VORTICITY AND STREAM FUNCTION	CORE0048
CALL SOURCE (N1,N2,N3,A,SORCE,I,J,K)	CORE0049
10 CONTINUE	CORE0050
C*** INNER ITERATIONS	CORE0051
DO 80 IT=1,INNER	CORE0052
IF(K.NE.NV.OR.KFLOW.EQ.1) GO TO 20	CORE0053
C*** ADJUST USTAR(J) AND FRICTION FACTOR, FR	CORE0054
CALL WALL (N1,N2,N3,A)	CORE0055
20 CONTINUE	CORE0056
C*** PARAMETER AT WALL	CORE0057
CALL WF (N1,N2,N3,A,K)	CORE0058
C*** COMPUTE MAXIMUM VALUE OF PARAMETER OVER FIELD	CORE0059
CALL MAXVAL (N1,N2,N3,A,K,AMAX)	CORE0060
DO 70 J=2,JNM	CORE0061
C*** INTERNAL POINTS	CORE0062
IH=IMAX(J)	CORE0063
DO 70 I=IG,IH	CORE0064
C*** COMPUTE SOURCE TERM FOR AXIAL VELOCITY AND TKE	CORE0065
IF(K.NE.NV.AND.K.NE.NK) GO TO 15	COPE0066
CALL SOURCE (N1,N2,N3,A,SORCE,I,J,K)	CORE0067
15 CONTINUE	CORE0068
C*** COMPUTE FINITE DIFFERENCE EQUATION	CORE0069
IF(K.EQ.NW.AND.I.EQ.2) GO TO 30	CORE0070
ANUM=BAE(I,J)*A(I+1,J,K)+BAW(I,J)*A(I-1,J,K)+BAN(I,J)*A(I,J+1,K)	CORE0071
/+BAS(I,J)*A(I,J-1,K)+SORCE(I,J)	CORE0072

ADNM=BAE(I,J)+BAW(I,J)+EAN(I,J)+BAS(I,J)	CORE0073
GO TO 35	CORE0074
C*** FINITE DIFFERENCE EQUATION FOR VORTICITY NEAR WALL	CORE0075
30 ANUM=BAE(2,J)*A(3,J,K)+BAW(2,J)*AF*A(2,J,NF)+BAN(2,J)*A(2,J+1,K)+	CORE0076
/BAS(2,J)*A(2,J-1,K)+SORCE(2,J)	CORE0077
ADNM=BAE(2,J)+(0.5+BAW(2,J))+BAN(2,J)+BAS(2,J)	CORE0078
35 CONTINUE	CORE0079
IF(ADNM.EQ.0.) GO TO 70	CORE0080
C*** STORE OLD VALUE OF PARAMETER	CORE0081
Z=A(I,J,K)	CORE0082
C*** CALCULATE NEW VALUE	CORE0083
A(I,J,K)=ANUM/ADNM	CORE0084
C*** CALCULATE RESIDUAL	CORE0085
IF(AMAX.EQ.0.) GO TO 70	CORE0086
RL=(A(I,J,K)-Z)/AMAX	CORE0087
C*** UNDER- OR OVER-RELAX, IF SPECIFIED	CORE0088
A(I,J,K)=Z+RP(K)*(A(I,J,K)-Z)	CORE0089
IF(ABS(RL).GT.ABS(RSDU(K))) RSDU(K)=RL	CORE0090
70 CONTINUE	CORE0091
C*** COMPUTE PARAMETER AT BOUNDARIES	CORE0092
CALL BOUND(N1,N2,N3,A,K)	CORE0093
C*** TEST IF CONVERGENCE CRITERION (CC) SATISFIED	CORE0094
IF(ABS(RSDU(K)).LT.CC) GO TO 90	CORE0095
80 CONTINUE	CORE0096
90 CONTINUE	CORE0097
IF(KFLOW.NE.3) GO TO 300	CORE0098
C*** COMPUTE STREAM FUNCTION USING NIJSING'S APPROXIMATION	CORE0099
CALL STREAM(N1,N2,N3,A)	CORE0100
300 CONTINUE	CORE0101
RETURN	CORE0102
END	CORE0103

```

SUBROUTINE MAXVAL (N1,N2,N3,A,K,AMAX)
DIMENSION A (N1,N2,N3)
COMMON/CNUMBR/NW,NF,NV,NK,NL,NMU,NV1,NV2,IE,IV
COMMON/CGEO/IN,INN,JN,JNM,IMAX (21),ILIM (21),X1 (41),X2 (21),
2R (41),VP (41),IMIN (4)
C*****
C SUBROUTINE TO FIND MAXIMUM VALUE OF VARIABLES OVER THE FIELD
C*****
    AMAX=0.0
    DO 15 J=1,JN
    IH=ILIM (J)
    DO 15 I=1,IH
    IF (ABS (A (I,J,K)) .GT. ABS (AMAX)) AMAX=A (I,J,K)
15 CONTINUE
RETURN
END

```

```

MAXV0001
MAXV0002
MAXV0003
MAXV0004
MAXV0005
MAXV0006
MAXV0007
MAXV0008
MAXV0009
MAXV0010
MAXV0011
MAXV0012
MAXV0013
MAXV0014
MAXV0015
MAXV0016

```

SUBROUTINE STREAM (N1,N2,N3,A)	STRE0001
DIMENSION A(N1,N2,N3)	STRE0002
COMMON/CNUMBER/NW,NF,NV,NK,NL,NMU,NV1,NV2,II,IE,IV	STRE0003
COMMON/CGEO/IN,INM,JN,JNM,IMAX(21),ILIM(21),X1(41),X2(21),	STRE0004
2R(41),VP(41),IMIN(4)	STRE0005
COMMON/CFLOW/PIT,DIA,DH,ATOT,RE,VAVG,KFLOW,ROREF,ZMUREF,VB	STRE0006
COMMON/CWALL/TALAV,RTAL(21),USTAR(21),FR,YB(21)	STRE0007
C*****	STRE0008
C SUBROUTINE TO COMPUTE STREAM FUNCTION USING NIJSING APPROXIMATION	STRE0009
C*****	STRE0010
C=-0.19*TALAV**2/ZMUREF	STRE0011
DO 100 J=2,JNM	STRE0012
TETA=X2(J)	STRE0013
DU=(RTAL(J+1)-RTAL(J-1))/(X2(J+1)-X2(J-1))	STRE0014
IH=IMAX(J)	STRE0015
CR=C*X1(IH+1)	STRE0016
DO 100 I=2,IH	STRE0017
ANGLE=3.14159*X1(I)/X1(IH+1)	STRE0018
100 A(I,J,NF)=CR*DU*SIN(ANGLE)	STRE0019
RETURN	STRE0020
END	STRE0021

SUBROUTINE STRESS (N1,N2,N3,A)	TRES0001
DIMENSION A (N1,N2,N3)	TRES0002
COMMON/CNUMBER/NW,NF,NV,NK,NL,NMU,NV1,NV2,II,IE,IV	TRES0003
COMMON/CGEO/IN,INM,JN,JNM,IMAX(21),ILIM(21),X1(41),X2(21),	TRES0004
2R(41),VP(41),IMIN(4)	TRES0005
COMMON/CFLOW/PIT,DIA,DH,ATOT,RE,VAVG,KFLOW,ROREF,ZMUREF,VB	TRES0006
COMMON/CFUNC/FW(41,21)	TRES0007
COMMON/CCONST/CK,E,CVIS,CDIS,C1,C2	TRES0008
C*****	TRES0009
C STRESS MODEL FOR COMPUTATION OF VORTICITY SOURCE TERM	TRES0010
C*****	TRES0011
C	TRES0012
C*** COMPUTE CONSTANT C	TRES0013
CB=-2.*(6.*C2-2.)/11./(C1-2.*C2)	TRES0014
C=CB*CVIS/CDIS	TRES0015
DO 100 J=1,JN	TRES0016
IH=ILIM(J)	TRES0017
DO 100 I=1,IH	TRES0018
FW(I,J)=0.0	TRES0019
IL=IMIN(NV)-1	TRES0020
IF(I.LE.IL) GO TO 100	TRES0021
C*** COMPUTE TANGENTIAL VELOCITY GRADIENT, DVT	TRES0022
DVT=0.0	TRES0023
IF(J.EQ.1.OR.J.EQ.JN) GO TO 5	TRES0024
IF(I.GT.ILIM(J-1)) GO TO 4	TRES0025
C*** INTERNAL POINTS	TRES0026
DVT=(A(I,J+1,NV)-A(I,J-1,NV))/(2.*X2(2)*R(I))	TRES0027
GO TO 5	TRES0028
C*** FAST BOUNDARY	TRES0029
4 DVT=(A(I,J+1,NV)-A(J,J,NV))/(X2(2)*R(I))	TRES0030
5 DVT5=DVT*DVT	TRES0031
C*** COMPUTE RADIAL VELOCITY GRADIENT, DVR	TRES0032
DVR=0.0	TRES0033
IF(I.EQ.ILIM(J)) GO TO 6	TRES0034
C*** INTERNAL POINTS	TRES0035
RQ=(R(I)-R(I-1))/(R(I+1)-R(I))	TRES0036

	DVR=(RQ*(A(I+1,J,NV)-A(I,J,NV))+A(I,J,NV)-A(I-1,J,NV))/RQ)/	TRES0037
	/(R(I+1)-R(I-1))	TRES0038
	GO TO 10	TRES0039
C***	POINTS AT EAST BOUNDARY	TRES0040
6	DVR=(A(I,J,NV)-A(I-1,J,NV))/(R(I)-R(I-1))	TRES0041
10	DVRS=DVR*DVR	TRES0042
	XL=A(I,J,NL)**2	TRES0043
C***	COMPUTE FUNCTION FW(I,J)	TRES0044
	IF(A(I,J,NK).EQ.0.0) GO TO 100	TRES0045
	FW(I,J)=C*XL*(DVTS-DVRS)/A(I,J,NK)	TRES0046
100	CONTINUE	TRES0047
	RETURN	TRES0048
	END	TRES0049

SUBROUTINE SOURCE (N1,N2,N3,A,SORCE,I,J,K)	SOUR0001
DIMENSION A(N1,N2,N3),SORCE(N1,N2)	SOUR0002
COMMON/CNUMBER/NW,NF,NV,NK,NL,NMU,NV1,NV2,II,IE,IV	SOUR0003
COMMON/CGEO/IN,INM,JN,JNC,IMAX(21),ILIM(21),X1(41),X2(21),	SOUR0004
2R(41),VP(41),IMIN(4)	SOUR0005
COMMON/CFLOW/PIT,DIA,DH,ATOT,RE,VAVG,KFLOW,ROREF,ZMUREF,VE	SOUR0006
COMMON/CWALL/TALAV,RTAL(21),USTAR(21),FR,YB(21)	SOUR0007
COMMON/CFUNC/FW(41,21)	SOUR0008
COMMON/CCONST/CK,E,CVIS,CDIS,C1,C2	SOUR0009
C*****	SOUR0010
C SUBROUTINE FOR CALCULATION OF SOURCE TERMS	SOUR0011
C*****	SOUR0012
GO TO (1,2,3,4),K	SOUR0013
C*** FOR VORTICITY EQUATION	SOUR0014
C*** TURBULENT FLOW WITH RECIRCULATION	SOUR0015
1 SORCE(I,J)=0.0	SOUR0016
IF(I.LT.IMIN(NV)) RETURN	SOUR0017
C=0.25/ZMUREF	SOUR0018
D=(R(I+1)-R(I-1))/R(I)	SOUR0019
DF=FW(I+1,J+1)*A(I+1,J+1,NK)+FW(I-1,J-1)*A(I-1,J-1,NK)-	SOUR0020
/FW(I-1,J+1)*A(I-1,J+1,NK)-FW(I+1,J-1)*A(I+1,J-1,NK)-D*(SOUR0021
/FW(I,J+1)*A(I,J+1,NK)-FW(I,J-1)*A(I,J-1,NK))	SOUR0022
SORCE(I,J)=-C*DF	SOUR0023
RETURN	SOUR0024
C*** FOR STREAM FUNCTION EQUATION	SOUR0025
2 C=.125*R(I)*X2(2)/ZMUREF	SOUR0026
DF=(R(I+1)-R(I-1))*(A(I,J,NW)+A(I,J+1,NW)+A(I,J-1,NW))+	SOUR0027
/(R(I+1)-R(I))*A(I+1,J,NW)+(R(I)-R(I-1))*A(I-1,J,NW)	SOUR0028
SORCE(I,J)=C*DF	SOUR0029
RETURN	SOUR0030
C*** FOR AXIAL VELOCITY EQUATION	SOUR0031
3 IF(KFLOW.GT.1) GO TO 30	SOUR0032
C*** LAMINAR FLOW	SOUR0033
SORCE(I,J)=4./(DIA*DIA)*VP(I)	SOUR0034
RETURN	SOUR0035
C*** TURBULENT FLOW	SOUR0036

30	SORCE(I,J)=2.*FR*VAVG**2/ZMUREF/DH*VP(I)	SOUR0037
	RETURN	SOUR0038
C***	FOR TURBULENCE KINETIC ENERGY EQUATION	SOUR0039
4	DTETA=X2(2)	SOUR0040
C***	COMPUTE SORCE1	SOUR0041
	DV1=(A(I+1,J,NV)-A(I,J,NV))*(R(I)-R(I-1))/(R(I+1)-R(I))	SOUR0042
	/+(A(I,J,NV)-A(I-1,J,NV))*(R(I+1)-R(I))/(R(I)-R(I-1))/(R(I+1)-	SOUR0043
	/R(I-1))	SOUR0044
	DV2=(A(I,J+1,NV)-A(I,J-1,NV))/(2.*R(I)*DTETA)	SOUR0045
	DF=(R(I+1)-R(I-1))*(A(I,J-1,NMU)+A(I,J+1,NMU))+2.*(R(I)-R(I-1))*	SOUR0046
	/A(I-1,J,NMU)+2.*(R(I+1)-R(I))*A(I+1,J,NMU)	SOUR0047
	SORCE1=DTETA*R(I)/8.*DF*(DV1**2+DV2**2)	SOUR0048
C***	COMPUTE SORCE2	SOUR0049
	XK1=A(I,J+1,NK)**1.5/A(I,J+1,NL)	SOUR0050
	XK2=A(I,J-1,NK)**1.5/A(I,J-1,NL)	SOUR0051
	XK3=A(I+1,J,NK)**1.5/A(I+1,J,NL)	SOUR0052
	IF(I.EQ.2) GO TO 41	SOUR0053
	XK4=A(I-1,J,NK)**1.5/A(I-1,J,NL)	SOUR0054
	GO TO 42	SOUR0055
41	XKH=2.*(A(I,J,NK)+A(I-1,J,NK))/2.**1.5/A(I,J,NL)	SOUR0056
	XK0=A(I,J,NK)**1.5/A(I,J,NL)	SOUR0057
	XK4=2.*XKH-XK0	SOUR0058
42	DK=(R(I+1)-R(I-1))*(XK1+XK2)+2.*(R(I)-R(I-1))*XK4+	SOUR0059
	/2.*(R(I+1)-R(I))*XK3	SOUR0060
	SORCE2=-CDIS*DTETA*R(I)/8.*DK/ZMUREF	SOUR0061
	SORCE(I,J)=SORCE1+SORCE2	SOUR0062
	RETURN	SOUR0063
	END	SOUR0064

SUBROUTINE VISCOS (N1,N2,N3,A)	VISC0001
DIMENSION A(N1,N2,N3)	VISC0002
COMMON/CNUMBER/NW,NF,NV,NK,NL,NMU,NV1,NV2,II,IE,IV	VISC0003
COMMON/CGEO/IN,INM,JN,JNM,IMAX(21),ILIM(21),X1(41),X2(21),	VISC0004
2R(41),VP(41),IMIN(4)	VISC0005
COMMON/CFLOW/PIT,DIA,DH,ATOT,RE,VAVG,KFLOW,ROREF,ZMUREF,VB	VISC0006
COMMON/CWALL/TALAV,RTAL(21),USTAR(21),FR,YE(21)	VISC0007
COMMON/CCONST/CK,E,CVIS,CDIS,C1,C2	VISC0008
C*****	VISC0009
C SUBROUTINE FOR CALCULATION OF THE TURBULENT VISCOSITY	VISC0010
C*****	VISC0011
DO 10 J=1,JN	VISC0012
IL=IMIN(NK)-1	VISC0013
IN=ILIM(J)	VISC0014
DO 10 I=IL,IN	VISC0015
XK=A(I,J,NK)	VISC0016
10 A(I,J,NMU)=CVIS*A(I,J,NL)*SQRT(XK)/ZMUREF	VISC0017
RETURN	VISC0018
END	VISC0019

```

SUBROUTINE CONVEC (N1,N2,N3,A,AE,AW,AN,AS,I,J,K)
DIMENSION A(N1,N2,N3)
COMMON/CNUMBR/NW,NP,NV,NK,NL,NMU,NV1,NV2,II,IE,IV
COMMON/CGEO/IN,INM,JN,JNM,IMAX(21),ILIM(21),X1(41),X2(21),
2R(41),VP(41),IMIM(4)
C*****
C SUBROUTINE FOR CALCULATION OF AE,AW,AN,AS
C*****
C
C*** SET COEFFICIENTS TO ZERO
    AE=0.0
    AW=0.0
    AN=0.0
    AS=0.0
C*** STREAM FUNCTION EQUATION
    IF(K.EQ.NP) RETURN
    IF(I.EQ.IMAX(J)) GO TO 5
C*** COMPUTE AE,AW,AN,AS FOR THE OTHER EQUATIONS
    GE=A(I+1,J-1,NP)+A(I,J-1,NP)-A(I+1,J+1,NP)-A(I,J+1,NP)
    GW=A(I-1,J+1,NP)+A(I,J+1,NP)-A(I-1,J-1,NP)-A(I,J-1,NP)
    GN=A(I+1,J+1,NP)+A(I+1,J,NP)-A(I-1,J+1,NP)-A(I-1,J,NP)
    GS=A(I-1,J-1,NP)+A(I-1,J,NP)-A(I+1,J-1,NP)-A(I+1,J,NP)
    GO TO 10
C*** COEFFICIENTS NEAR EAST BOUNDARY
5    GE=-A(I+1,J+1,NP)-A(I,J+1,NP)-A(I,J,NP)
    GW=A(I-1,J+1,NP)-A(I-1,J-1,NP)+A(I,J+1,NP)
    GN=A(I+1,J+1,NP)-A(I-1,J+1,NP)-A(I-1,J,NP)
    GS=A(I-1,J-1,NP)+A(I-1,J,NP)+A(I,J,NP)
10   AE=0.125*(GE+ABS(GE))
    AW=0.125*(GW+ABS(GW))
    AN=0.125*(GN+ABS(GN))
    AS=0.125*(GS+ABS(GS))
    RETURN
END

```

```

CONV0001
CONV0002
CONV0003
CONV0004
CONV0005
CONV0006
CONV0007
CONV0008
CONV0009
CONV0010
CONV0011
CONV0012
CONV0013
CONV0014
CONV0015
CONV0016
CONV0017
CONV0018
CONV0019
CONV0020
CONV0021
CONV0022
CONV0023
CONV0024
CONV0025
CONV0026
CONV0027
CONV0028
CONV0029
CONV0030
CONV0031
CONV0032
CONV0033
CONV0034

```

SUBROUTINE BOUND (N1,N2,N3,A,K)	BOUN0001
DIMENSION A(N1,N2,N3)	BOUN0002
COMMON/CNUMBER/NW,NF,NV,NK,NL,NMU,NV1,NV2,II,IE,IV	BOUN0003
COMMON/CGEO/IN,IMM,JN,JNM,IMAX(21),ILIM(21),X1(41),X2(21),	BOUN0004
2R(41),VP(41),IMIN(4)	BOUN0005
COMMON/CFLOW/PIT,DIA,DH,ATOT,RE,VAVG,KFLOW,ROREF,ZMURF,VB	BOUN0006
COMMON/CBOUND/CB(21)	BOUN0007
C*****	BOUN0008
C SUBROUTINE FOR CALCULATION OF PARAMETERS AT BOUNDARIES	BOUN0009
C*****	BOUN0010
IF(K.EQ.NW.OR.K.EQ.NF) RETURN	BOUN0011
C*** SOUTH BOUNDARY	BOUN0012
IH=ILIM(1)	BOUN0013
DO 31 I=2,IH	BOUN0014
31 A(I,1,K)=1.33*A(I,2,K)-.33*A(I,3,K)	BOUN0015
C*** NORTH BOUNDARY	BOUN0016
IH=ILIM(JN-2)	BOUN0017
DO 32 I=2,IH	BOUN0018
32 A(I,JN,K)=1.33*A(I,JN-1,K)-.33*A(I,JN-2,K)	BOUN0019
IF(IH.LT.ILIM(JN-1)) A(IH+1,JN,K)=1.33*A(IH,JN,K)-.33*A(IH-1,	BOUN0020
/JN,K)	BOUN0021
A(IN,JN,K)=1.33*A(IN-1,JN,K)-.33*A(IN-2,JN,K)	BOUN0022
C*** EAST BOUNDARY	BOUN0023
DO 20 J=2,JNM	BOUN0024
I=ILIM(J)	BOUN0025
20 A(I,J,K)=(A(I-1,J,K)+CB(J)*A(I,J+1,K))/(1.+CB(J))	BOUN0026
RETURN	BOUN0027
END	BOUN0028

SUBROUTINE VELDIS (N1,N2,N3,A)	VELD0001
DIMENSION A(N1,N2,N3)	VELD0002
COMMON/CNUMBER/NW,NF,NV,NK,NL,NMU,NV1,NV2,II,IE,IV	VELD0003
COMMON/CGEO/IN,INM,JN,JNM,IMAX(21),ILIM(21),X1(41),X2(21),	VELD0004
2R(41),VP(41),IMIN(4)	VELD0005
COMMON/CFLOW/PIT,DIA,DH,ATOT,RE,VAVG,KFLOW,ROREF,ZMUREF,VB	VELD0006
C*****	VELD0007
C SUBROUTINE FOR CALCULATION OF SECONDARY FLOW	VELD0008
C*****	VELD0009
DTETA=3.14159/6./FLOAT(JNM)	VELD0010
C*** INTERIOR NODES	VELD0011
DO 10 J=2,JNM	VELD0012
IH=ILIM(J)-1	VELD0013
DO 10 I=2,IH	VELD0014
H=(R(I-1)-R(I))/(R(I+1)-R(I))	VELD0015
A(I,J,NV1)=0.5*(A(I,J+1,NF)-A(I,J-1,NF))/(R(I)*DTETA)*ZMUREF/VAVG	VELD0016
10 A(I,J,NV2)=((A(I+1,J,NF)-A(I,J,NF))*H+(A(I,J,NF)-A(I-1,J,NF))/H)/(VELD0017
2R(I+1)-R(I-1))*ZMUREF/VAVG	VELD0018
C*** SOUTH SIDE	VELD0019
IH=ILIM(1)-1	VELD0020
DO 20 I=2,IH	VELD0021
20 A(I,1,NV1)=A(I,2,NF)/(R(I)*DTETA)*ZMUREF/VAVG	VELD0022
C*** NORTH SIDE	VELD0023
IH=ILIM(JN)-1	VELD0024
DO 30 I=2,IH	VELD0025
30 A(I,JN,NV1)=-A(I,JN-1,NF)/(R(I)*DTETA)*ZMUREF/VAVG	VELD0026
C*** EAST SIDE	VELD0027
DO 40 J=2,JNM	VELD0028
IH=ILIM(J)	VELD0029
A(IH,J,NV1)=A(IH,J+1,NF)/(R(IH)*DTETA)*ZMUREF/VAVG	VELD0030
40 A(IH,J,NV2)=A(IH-1,J,NF)/(R(IH)-R(IH-1))*ZMUREF/VAVG	VELD0031
RETURN	VELD0032
END	VELD0033

SUBROUTINE REYNU (N1,N2,N3,A)	REYN0001
DIMENSION A(N1,N2,N3)	REYN0002
COMMON/CNUMBER/NW,NF,NV,NK,NL,NMU,NV1,NV2,II,IE,IV	REYN0003
COMMON/CGEO/IN,INM,JN,JNM,IMAX(21),ILIM(21),X1(41),X2(21),	REYN0004
2R(41),VP(41),IMIN(4)	REYN0005
COMMON/CFLOW/PIT,DIA,DH,ATOT,RE,VAVG,KFLOW,ROREF,ZMUREF,VB	REYN0006
COMMON/CCONST/CK,E,CVIS,CDIS,C1,C2	REYN0007
C*****	REYN0008
C SUBROUTINE FOR COMPUTATION OF BULK VELOCITY, VB	REYN0009
C*****	REYN0010
C	REYN0011
AV=0.0	REYN0012
DTETA=X2(2)	REYN0013
DO 20 J=1,JN	REYN0014
C*** INTERNAL POINTS	REYN0015
TAV=0.0	REYN0016
IH=ILIM(J)	REYN0017
DO 10 I=2,IH	REYN0018
DAV=DTETA/6.*(R(I)-R(I-1))*(A(I-1,J,NV)*(R(I)+2.*R(I-1))+	REYN0019
/A(I,J,NV)*(2.*R(I)+R(I-1)))	REYN0020
IF(I.EQ.IN) DAV=0.75*DAV	REYN0021
10 TAV=TAV+DAV	REYN0022
IF(J.EQ.1.OR.J.EQ.JN) TAV=0.5*TAV	REYN0023
20 AV=AV+TAV	REYN0024
C*** CALCULATE BULK VELOCITY	REYN0025
VB=AV/ATOT	REYN0026
C*** NORMALIZ5 VELOCITY DISTRIBUTION	REYN0027
F=VAVG/VB	REYN0028
DO 30 J=1,JN	REYN0029
IL=ILIM(J)	REYN0030
DO 30 I=1,IL	REYN0031
30 A(I,J,NV)=F*A(I,J,NV)	REYN0032
RETURN	REYN0033
END	REYN0034

SUBROUTINE WALL (N1,N2,N3,A)	WALL0001
DIMENSION A(N1,N2,N3)	WALL0002
COMMON/CNUMBR/NW,NF,NV,NK,NL,NMU,NV1,NV2,II,IE,IV	WALL0003
COMMON/CGEO/IN,IMM,JN,JNM,IMAX(21),ILIM(21),X1(41),X2(21),	WALL0004
2R(41),VF(41),IMIN(4)	WALL0005
COMMON/CFLOW/PIT,DIA,DH,ATOT,RE,VAVG,KFLOW,ROREF,ZMUREF,VB	WALL0006
COMMON/CWALL/TALAV,RTAL(21),USTAR(21),FR,YB(21)	WALL0007
COMMON/CCONST/CK,E,CVIS,CDIS,C1,C2	WALL0008
C*****	WALL0009
C SUBROUTINE FOR COMPUTATION OF USTAR(J) AND FRICTION FACTOR,FR	WALL0010
C*****	WALL0011
C	WALL0012
C*** NORMALIZE VELOCITY TO VAVG	WALL0013
CALL REYNU (N1,N2,N3,A)	WALL0014
C*** COMPUTE NEW VALUE OF USTAR(J)	WALL0015
IM=IMIN(NV)	WALL0016
CE=30.*E	WALL0017
QSI=15.*ZMUREF*(ALOG(CE)-1.)/X1(IM)	WALL0018
ETA=30.*ZMUREF*CK/K1(IM)	WALL0019
DO 10 J=1,JN	WALL0020
10 USTAR(J)=(QSI**2+ETA*A(IM,J,NV))**0.5-QSI	WALL0021
C*** COMPUTE NEW FRICTION FACTOR	WALL0022
S=0.5*(USTAR(1)**2+USTAR(JN)**2)	WALL0023
DO 20 J=2,JNM	WALL0024
20 S=S+USTAR(J)**2	WALL0025
TALAV=S/FLOAT(JNM)	WALL0026
FR=2.*TALAV/VAVG**2	WALL0027
C*** WALL SHEAR STRESS DISTRIBUTION	WALL0028
DO 30 J=1,JN	WALL0029
30 RTAL(J)=USTAR(J)**2/TALAV	WALL0030
C*** COMPUTE NEW VALUES FOR YB(J)	WALL0031
DO 40 J=1,JN	WALL0032
40 YB(J)=30.*ZMUREF/USTAR(J)	WALL0033
RETURN	WALL0034
END	WALL0035

SUBROUTINE WF (N1,N2,N3,A,K)	WF 0001
DIMENSION A(N1,N2,N3)	WF 0002
COMMON/CNUMBER/NW,NF,NV,NK,NL,NMU,NV1,NV2,II,IE,IV	WF 0003
COMMON/CGEO/IN,INN,JN,JNM,IMAX(21),ILIM(21),X1(41),X2(21),	WF 0004
2R(41),VP(41),IMIN(4)	WF 0005
COMMON/CFLOW/PIT,DIA,DH,ATOT,RE,VAVG,KFLOW,ROREF,ZMUREF,VB	WF 0006
COMMON/CWALL/TALAV,RTAL(21),USTAR(21),FR,YB(21)	WF 0007
COMMON/CCONST/CK,E,CVIS,CDIS,C1,C2	WF 0008
C*****	WF 0009
C SUBROUTINE FOR COMPUTATION OF FICTITIOUS VALUES AT SOLID WALL	WF 0010
C*****	WF 0011
GO TO (1,2,3,4), K	WF 0012
C*** VORTICITY AT WALL	WF 0013
1 AF=3.*ZMUREF/X1(2)**2	WF 0014
DO 10 J=2,JNM	WF 0015
10 A(1,J,NW)=-AF*A(2,J,NF)-0.5*A(2,J,NW)	WF 0016
RETURN	WF 0017
C*** STREAM FUNCTION AT WALL	WF 0018
2 DO 20 J=1,JN	WF 0019
20 A(1,J,NF)=0.0	WF 0020
RETURN	WF 0021
C*** FICTITIOUS VELOCITY AT WALL	WF 0022
3 IL=IMIN(NV)-1	WF 0023
CE=30.*E	WF 0024
DO 30 J=1,JN	WF 0025
BV=USTAR(J)/CK*A LOG(CE)	WF 0026
H=(X1(IL+1)-X1(IL))/(X1(IL+1)-YB(J))	WF 0027
30 A(IL,J,NV)=(1.-H)*A(IL+1,J,NV)+H*BV	WF 0028
RETURN	WF 0029
C*** FICTITIOUS TKE AT WALL	WF 0030
4 AK=CVIS/(CDIS*CK**2)	WF 0031
IL=IMIN(NK)-1	WF 0032
DO 40 J=1,JN	WF 0033
BK=AK*USTAR(J)**2	WF 0034
H=(X1(IL+1)-X1(IL))/(X1(IL+1)-YB(J))	WF 0035
40 A(IL,J,NK)=(1.-H)*A(IL+1,J,NK)+H*BK	WF 0036

RETURN
END

WF 0037
WF 0038

SUBROUTINE NORM (N1,N2,N3,A)	NORM0001
DIMENSION A(N1,N2,N3)	NORM0002
COMMON/CNUMBER/NW,NF,NV,NK,NL,NMU,NV1,NV2,II,IE,IV	NORM0003
COMMON/CGEO/IN,INM,JN,JNM,IMAX(21),ILIM(21),X1(41),X2(21),	NORM0004
2R(41),VP(41),IMIN(4)	NORM0005
COMMON/CFLOW/PIT,DIA,DH,ATCT,RE,VAVG,KFLOW,ROREF,ZMUREF,VB	NORM0006
C*****	NORM0007
C SUBROUTINE FOR NORMALIZATION OF INPUT FOR LAMINAR CASE	NORM0008
C*****	NORM0009
U2=0.0	NORM0010
U3=0.0	NORM0011
DO 30 L=2,JNM	NORM0012
U2=U2+A(2,L,NV)	NORM0013
30 U3=U3+A(3,L,NV)	NORM0014
U2BAR=(0.5*(A(2,1,NV)+A(2,JN,NV))+U2)/FLOAT(JN)	NORM0015
U3BAR=(0.5*(A(3,1,NV)+A(3,JN,NV))+U3)/FLOAT(JN)	NORM0016
GRADV=(U2BAR*X1(3)/X1(2)-U3BAR*X1(2)/X1(3))/(X1(3)-X1(2))	NORM0017
SORCE1=-4.*GRADV/DH	NORM0018
PDR=-4./(SORCE1*DIA**2)	NORM0019
DO 10 J=1,JN	NORM0020
IH=ILIM(J)	NORM0021
DO 10 I=1,IH	NORM0022
10 A(I,J,NV)=PDR*A(I,J,NV)	NORM0023
RETURN	NORM0024
END	NORM0025

SUBROUTINE NORM2 (N1,N2,N3,A)	NOR20001
DIMENSION A(N1,N2,N3)	NOR20002
COMMON/CNUMBR/NW,NF,NV,NK,NL,NNU,NV1,NV2,IL,IE,IV	NOR20003
COMMON/CGEO/IN,INM,JN,JNM,IMAX(21),ILIM(21),X1(41),X2(21),	NOR20004
2R(41),VP(41),IMIN(4)	NOR20005
COMMON/CFLOW/PIT,DIA,DH,ATOT,RE,VAVG,KELOW,ROREF,ZMUREF,VB	NOR20006
COMMON/CWALL/TALAV,RTAL(21),USTAR(21),FR,YB(21)	NOR20007
COMMON/CCONST/CK,E,CVIS,CDIS,C1,C2	NOR20008
C*****	NOR20009
C SUBROUTINE FOR NORMALIZATION OF OUTPUT	NOR20010
C*****	NOR20011
C	NOR20012
C*** COMPUTE VELOCITY NEAR WALL	NOR20013
IL=IMIN(NV)-1	NOR20014
DO 1 J=1,JN	NOR20015
DO 1 I=2,IL	NOR20016
C=E*USTAR(J)*X1(I)/ZMUREF	NOR20017
1 A(I,J,NV)=USTAR(J)/CK*ALOG(C)	NOR20018
C*** CASE 1: VELOCITY AND TKE NORMALIZED BY VAVG	NOR20019
F=1./VAVG	NOR20020
FF=1./VAVG**2	NOR20021
DO 2 J=1,JN	NOR20022
IH=ILIM(J)	NOR20023
DO 2 I=2,IH	NOR20024
A(I,J,NK)=FF*A(I,J,NK)	NOR20025
2 A(I,J,NV)=F*A(I,J,NV)	NOR20026
C*** NORMALIZE STREAM FUNCTION BY MAXIMUM VALUE	NOR20027
CALL MAXVAL (N1,N2,N3,A,NF,AMAX)	NOR20028
IF(AMAX.EQ.0.0) GO TO 20	NOR20029
DO 15 J=2,JNM	NOR20030
IH=IMAX(J)	NOR20031
DO 15 I=2,IH	NOR20032
15 A(I,J,NF)=A(I,J,NF)/AMAX	NOR20033
20 CONTINUE	NOR20034
WRITE(6,100)	NOR20035
CALL PRINT (N1,N2,N3,A)	NOR20036

	IF(KFLOW.GT.1) GO TO 10	NOR20037
	DO 5 J=1,JN	NOR20038
5	USTAR(J)=(ZMUREF*A(2,J,NV)*VAVG/X1(2))**0.5	NOR20039
	TALAV=0.5*(USTAR(1)**2+USTAR(JN)**2)	NOR20040
	DO 6 J=2,JNM	NOR20041
6	TALAV=TALAV+USTAR(J)**2	NOR20042
	TALAV=TALAV/FLOAT(JNM)	NOR20043
	DO 7 J=1,JN	NOR20044
7	RTAL(J)=USTAR(J)**2/TALAV	NOR20045
	FR=2.*TALAV/VAVG**2	NOR20046
	CALL PRINT2	NOR20047
	RETURN	NOR20048
C***	CASE 2: VELOCITY AND TKE NORMALIZED BY USTAR	NOR20049
10	DO 3 J=1,JN	NOR20050
	RVL=VAVG/USTAR(J)	NOR20051
	RKE=VAVG**2/TALAV	NOR20052
	IH=ILIM(J)	NOR20053
	DO 3 I=2,IH	NOR20054
	A(I,J,NV)=A(I,J,NV)*RVL	NOR20055
3	A(I,J,NK)=A(I,J,NK)*RKE	NOR20056
	WRITE(6,200)	NOR20057
	CALL PRINT(N1,N2,N3,A)	NOR20058
	RETURN	NOR20059
100	FORMAT(44H1CASE 1: VELOCITY AND TKE NORMALIZED BY VAVG//)	NOR20060
200	FORMAT(45H1CASE 2: VELOCITY AND TKE NORMALIZED BY USTAR//)	NOR20061
	END	NOR20062

OUT1	SUBROUTINE PRINT (N1,N2,N3,A)	SUBE0001
	DIMENSION A (N1,N2,N3)	SUBE0002
	COMMON/CNUMBR/NW,NF,NV,NK,NL,NMU,NV1,NV2,II,IE,IV	SUBE0003
	COMMON/CGEO/IN,INM,JN,JNM,IMAX(21),ILIM(21),X1(41),X2(21),	SUBE0004
	2R(41),VP(41),IMIN(4)	SUBE0005
	C*****	SUBE0006
	C OUTPUT SUBROUTINE	SUBE0007
	C*****	SUBE0008
	WRITE(6,100)	SUBE0009
	DTETA=30./FLOAT(JNM)	SUBE0010
	DO 50 J=1,JN	SUBE0011
	TETA=DTETA*FLOAT(J-1)	SUBE0012
	WRITE(6,101) TETA	SUBE0013
	WRITE(6,102)	SUBE0014
	IH=ILIM(J)	SUBE0015
	DO 50 I=1,IH	SUBE0016
	QSI=X1(I)/X1(IH)	SUBE0017
	ETA=X1(I)/X1(IN)	SUBE0018
	WRITE(6,103) I,QSI,ETA,(A(I,J,K),K=1,N3)	SUBE0019
50	CONTINUE	SUBE0020
	RETURN	SUBE0021
100	FORMAT(1H140X,26HDISTRIBUTION OF PARAMETERS/ /41X,26H-----//)	SUBE0022
101	FORMAT(1H0,10X,19HTETA (IN DEGREES) =,F7.2//)	SUBE0023
102	FORMAT(3X,1HI,6X,3HQSI,5X,3HETA,3X,9HVORTICITY,2X,8HSTREAM F,4X,7H /AXIAL V,6X,3HTKE,6X,7HMIX LEN,3X,9HTURB VISC,3X,5HRAD V,6X,6HTANG /V//)	SUBE0024
103	FORMAT(1X,I3,2X,2(F8.3),8(1PE11.3))	SUBE0025
	END	SUBE0026
		SUBE0027
		SUBE0028
		SUBE0029
		SUBE0030

SUBROUTINE PRINT2	OUT20001
COMMON/CGEO/IN, INM, JN, JNM, IMAX (21), ILIM (21), X1 (41), X2 (21),	OUT20002
2R (41), VP (41), IMIN (4)	OUT20003
COMMON/CFLOW/PIT, DIA, DH, ATOT, RE, VAVG, KFLOW, ROREF, ZMUREF, VB	OUT20004
COMMON/CWALL/TALAV, RTAL (21), USTAR (21), FR, YB (21)	OUT20005
C*****	OUT20006
C SUBROUTINE FOR PRINTING OF WALL SHEAR STRESS DISTRIBUTION	OUT20007
C*****	OUT20008
WRITE (6,100) FR, TALAV, DH, VAVG, VB	OUT20009
WRITE (6,200)	OUT20010
DO 10 J=1, JN	OUT20011
WRITE (6,300) J, RTAL (J), USTAR (J)	OUT20012
10 CONTINUE	OUT20013
RETURN	OUT20014
100 FORMAT (31HOFLOW INFORMATION CALCULATED IS//	OUT20015
110X, 50HFR, FRICTION FACTOR.....=, 1PE15.6/	OUT20016
210X, 50HTALAV, AVERAGE WALL SHEAR STRESS/ROREF.....=, 1PE15.6/	OUT20017
310X, 50HDI, HYDRAULIC DIAMETER.....=, 1PE15.6/	OUT20018
410X, 50HVAVG, BULK VELOCITY.....=, 1PE15.6/	OUT20019
510X, 50HVS, COMPUTED BULK VELOCITY.....=, 1PE15.6)	OUT20020
200 FORMAT (1H130X, 35HDISTRIBUTION OF WALL SHEAR STRESSES//	OUT20021
/5X, 1HJ, 10X, 9HTAL/TALAV, 10X, 5HUSTAR//)	OUT20022
300 FORMAT (4X, I2, 8X, E11.4, 6X, 1PE11.3/)	OUT20023
END	OUT20024

BLOCK DATA	BDAT0001
COMMON/CNUMBER/NW,NF,NV,NK,NL,NMU,NV1,NV2,II,IE,IV	BDAT0002
COMMON/CGEO/IN,INN,JN,JNM,IMAX(21),ILIM(21),X1(41),X2(21),	BDAT0003
2R(41),VP(41),IMIN(4)	BDAT0004
COMMON/CFLOW/PIT,DIA,DH,ATOT,RE,VAVG,KFLOW,ROREF,ZMUREF,VB	BDAT0005
COMMON/CGEN/NMAX,INNER,NPRINT,IP,CC,PR(9),RP(9),RSDU(9)	BDAT0006
COMMON/CWALL/TALAV,RTAL(21),USTAR(21),FR,YB(21)	BDAT0007
COMMON/CBOUND/CF(21)	BDAT0008
COMMON/CFUNC/FW(41,21)	BDAT0009
COMMON/CCONST/CK,E,CVIS,CDIS,C1,C2	BDAT0010
C*****	BDAT0011
C INPUT OF NUMERICAL DATA FOR THE PROBLEM	BDAT0012
C*****	BDAT0013
C	BDAT0014
C*** PROGRAM AND PRINTOUT CONTROL DATA	BDAT0015
DATA NW,NF,NV,NK,NL,NMU,NV1,NV2,IV/1,2,3,4,5,6,7,8,8/	BDAT0016
1,NMAX,INNER,NPRINT,IP,CC/250,1,500,1,1.0E-03/	BDAT0017
2,RP/2*1.00,7*1.0/	BDAT0018
3,RSDU/9*0.0/	BDAT0019
C*** PHYSICAL DATA	BDAT0020
DATA ROREF,ZMUREF/1.205,1.516E-05/	BDAT0021
1,PR/3*1.0,1.30,5*1.0/	BDAT0022
2,PIT,DIA/.044,.040/	BDAT0023
C*** CONSTANTS OF MODEL	BDAT0024
DATA CK,E,CVIS,CDIS,C1,C2/0.419,9.8,0.180,0.38,3.0,0.360/	BDAT0025
C*** FLOW DATA	BDAT0026
DATA II,IE,KFLOW,RE/1,4,4,2.7E+04/	BDAT0027
C*** GRID DATA	BDAT0028
DATA IN,JN/30,16/	BDAT0029
END	BDAT0030

**** TEST CASE **** BARE ROD
BUNDLE * FULLY DEVELOPED, TURBULENT
FLOW *** STRETCHED COORDINATES ****
VORTICITY
STREAM FUNCTION
AXIAL VELOCITY
TURBULENCE KINETIC ENERGY
MIXING LENGTH
TURBULENT VISCOSITY
RADIAL VELOCITY
TANGENTIAL VELOCITY
RSVORSSTRSAVRSKE

INPC0001
INPC0002
INPC0003
INPC0004
INPC0005
INPC0006
INPC0007
INPC0008
INPC0009
INPC0010
INPC0011
INPC0012

REFERENCES FOR APPENDICES

1. Brodkey, R.S., The Phenomena of Fluid Motions, Addison-Wesley Publishing Co., (1967).
2. Hinze, J.O., Turbulence, McGraw-Hill Book Co., (1959).
3. Buleev, N.I., Theoretical Model of the Mechanism of Turbulent Exchange in Fluid Flows, (1963) (United Kingdom Atomic Energy Authority, AERE-Trans 957).
4. Handbook of Mathematical Functions with Formulas, Graphs, and Mathematical Tables, U.S. Dept. Commerce, Natl. Bureau Stand. (1964), Applied Math. Series 55, pp. 886-887.
5. Launder, B.E. and Ying, W.M., Prediction of Flow and Heat Transfer in Ducts of Square Cross-Section, The Inst. Mech. Eng., Proceedings 1973, Vol. 187 37/73, pp. 455-461.
6. Chou, P.Y., On Velocity Correlations and the Solutions of the Equations of Turbulent Fluctuation, Quart. Appl. Math. 3, 31 (1945).
7. Mathematical Handbook for Scientists and Engineers, ed. Korn and Korn, MacGraw-Hill (1961).
8. Hanjalic, K. and Launder, B.E., A Reynolds Stress Model of Turbulence and its Application to Thin Shear Flows, J. Fluid. Mech., Vol. 52, part 4, (1972), pp. 609-638.
9. Rotta, J., Turbulent Boundary Layers in Incompressible Flow, In Progress in Aeronautical Sciences, Vol. 2 (ed. A. Ferri, D. Kuchemann and L.H.G. Sterne), Macmillan (1962).
10. Bender, D.J., Switick, D.M. and Field, J.H., Turbulent Velocity Distribution in a Rod Bundle, GEAP-5411, (1967).
11. Bobkov, V.P. et al., Correlation of Experimental Data on the Pulsation Velocity Intensity for Turbulent Fluid Flow in Channels of Different Form, Fluid Dynamics, Vol. 3, No. 3, (1968), pp. 111-113.
12. Yeh, Y. and Cummins, H., Localized Fluid Flow Measurements with a He-Ne Laser Spectrometer, Appl. Phys. Letters, Vol. 4, No. 10 (1964), p. 176.

13. Goldstein,R.J.and Kreid,D.K., Fluid Velocity Measurement from the Doppler Shift of Scattered Laser Radiation, HTL TR No. 85, Uniy.Minnesota, Minneapolis (1968).
14. Durst,F. and Whitelaw,J.H., Light Source and Geometrical Requirements for the Optimization of Optical Anemometry Signals, Opto-electronics 5 (1973),pp.137-151.
15. Linfoot,E.H.and Wolf,E., Phase Distribution near Focus in an Aberration-free Diffraction Image, Proc.Phys.Soc. B, Vol.69 (1956), pp.823-832.
16. Melling, A., Scattering Particles I -Specification, Lecture 6, Intern.Short Course on Laser Velocimetry, Purdue University, (March 1974).
17. Gosman, A.D.et al., Heat and Mass Transfer in Recirculating Flows, Academic Press (1969).

BIOGRAPHICAL NOTE

The author was born May 30, 1945 in São Paulo, S.P., Brazil. After graduation from High School, he entered the ITA, Instituto Tecnológico de Aeronáutica, Brazil, where he received his B.S. in Mechanical Engineering. He entered the Nuclear Engineering Department of the Massachusetts Institute of Technology in the Fall of 1970 and received his M.S. in November 1972.

The author is a member of the Society of Sigma Xi and student member of the American Nuclear Society.

The author is married to the former Terezinha Stokino and has a daughter Tatiana.

Publication: (co-author, Neil E. Todreas)

"Expansion of the Method of Correlated Temperatures to Clad and Fuel Design Analyses," Nucl. Eng. Des.30 (1974).